LEABHARLANN CHOLÁISTE NA TRÍONÓIDE, BAILE ÁTHA CLIATH | TRINITY COLLEGE LIBRARY DUBLIN
Ollscoil Átha Cliath | The University of Dublin

Terms and Conditions of Use of Digitised Theses from Trinity College Library Dublin

Copyright statement

All material supplied by Trinity College Library is protected by copyright (under the Copyright and Related Rights Act, 2000 as amended) and other relevant Intellectual Property Rights. By accessing and using a Digitised Thesis from Trinity College Library you acknowledge that all Intellectual Property Rights in any Works supplied are the sole and exclusive property of the copyright and/or other IPR holder. Specific copyright holders may not be explicitly identified. Use of materials from other sources within a thesis should not be construed as a claim over them.

A non-exclusive, non-transferable licence is hereby granted to those using or reproducing, in whole or in part, the material for valid purposes, providing the copyright owners are acknowledged using the normal conventions. Where specific permission to use material is required, this is identified and such permission must be sought from the copyright holder or agency cited.

Liability statement

By using a Digitised Thesis, I accept that Trinity College Dublin bears no legal responsibility for the accuracy, legality or comprehensiveness of materials contained within the thesis, and that Trinity College Dublin accepts no liability for indirect, consequential, or incidental, damages or losses arising from use of the thesis for whatever reason. Information located in a thesis may be subject to specific use constraints, details of which may not be explicitly described. It is the responsibility of potential and actual users to be aware of such constraints and to abide by them. By making use of material from a digitised thesis, you accept these copyright and disclaimer provisions. Where it is brought to the attention of Trinity College Library that there may be a breach of copyright or other restraint, it is the policy to withdraw or take down access to a thesis while the issue is being resolved.

Access Agreement

By using a Digitised Thesis from Trinity College Library you are bound by the following Terms & Conditions. Please read them carefully.

I have read and I understand the following statement: All material supplied via a Digitised Thesis from Trinity College Library is protected by copyright and other intellectual property rights, and duplication or sale of all or part of any of a thesis is not permitted, except that material may be duplicated by you for your research use or for educational purposes in electronic or print form providing the copyright owners are acknowledged using the normal conventions. You must obtain permission for any other use. Electronic or print copies may not be offered, whether for sale or otherwise to anyone. This copy has been supplied on the understanding that it is copyright material and that no quotation from the thesis may be published without proper acknowledgement.

ESTIMATING THE GROUND DEFORMATIONS ASSOCIATED WITH EARTHWORKS AND FOUNDATIONS IN BOULDER CLAY

Myles Lawler

Baccalaureus in Arte & *Baccalaureus in Arte Ingenaria* 1998

LIBRARY DUBLIN

Thesis submitted in partial fulfilment of the requirements for the degree of

Doctor of Philosophy in Civil Engineering

UNIVERSITY OF DUBLIN, TRINITY COLLEGE, 2002

TRINITY COLLEGE
0 3 JUL 2003
LIBRARY DUBLIN
THESIS
7432
7343

DECLARATION

Except where accredited, I declare that this is my own work and has not been submitted for a degree before this time. The library may copy or lend this thesis.

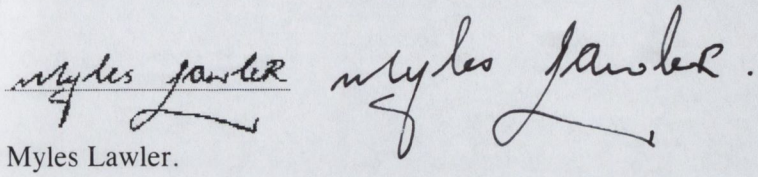

Myles Lawler.

ABSTRACT

Accurate estimates of the ground deformations associated with earthworks and foundations in boulder clay necessitate the validation of an appropriate soil model within a simplified ground model. Recent advances in numerical and analytical methods in soil mechanics, and boulder clay soil testing in the city of Dublin (Ireland), have given rise to the possibility of the development of such a model within the finite element (FE) method.

Estimating the ground movements of boulder clay is made difficult, however, by the non-linearity of the soil response, by problems associated with obtaining the relevant soil parameters from either field or laboratory tests and by deposits unique to these ground conditions, such as boulders and sand lenses. Together, these problems have led to the apparent inapplicability of intricate numerical models to boulder clay.

To be of value to geotechnical practice, the FE model should be commercially available and the input parameters assessable from standard tests. Ideally, the model should incorporate the decisive features of soil behaviour, including stiffness, stiffness non-linearity, the in situ stress-state and soil strength and dilatancy. In conjunction with this, the accurate measurement of these soil properties is essential, as is the placement of the numerical model in the correct geological context.

In the numerical analysis of geotechnical problems, advanced soil models potentially have considerable advantages over the use of simpler models, in that the deformations over a variety of stress paths can be more correctly simulated. Simple models of soil behaviour should not be discounted, however, as the parameters are obtainable with standard testing and the predictions more easily analysed.

This thesis applies the results of a comprehensive research project, covering the decisive features of boulder clay behaviour, to predict the observed ground deformation associated with a foundation, an excavation and a bored pile in Dublin. Primarily, the analysis shows that the FE method is applicable to Dublin till conditions and that, at least for these straightforward cases, numerical models of boulder clay behaviour can be very accurate.

Key words: earthworks; foundations; glaciation; numerical methods; stiffness; strength.

ACKNOWLEDGEMENT

This thesis is the result of fieldwork, laboratory study and theoretical research in soil mechanics at the University of Dublin, Trinity College (1998 – 2002).

These investigations were under the supervision of Dr. E. Farrell, Senior Lecturer in soil mechanics & hydraulics at the University of Dublin.

Mr. M. Carney assisted the author with soil testing in the Soils Laboratory.

The cost of field tests was met by May Gurney Ltd., Precision Monitoring & Control Ltd., Irish Geotechnical Services Ltd. and Davies Site Investigation Ltd.. Geoconsult Consortium (Dublin Port Tunnel contractor) and B.M.A. Ltd. provided soil test data.

Sponsorship for laboratory and theoretical research was from the Department of Civil Engineering (under the late Professor S. H. Perry), the Geotechnical Trust Fund of the Institution of Engineers of Ireland and the Dublin University Travel Fund.

Bennett Construction Ltd., N.M.I. Consortium, T.J. O'Connor Ltd. and Walls Ltd. facilitated access to sites.

The assistance, through the use of specialised machinery and equipment, of the Civil, Electronic and Mechanical Engineering Faculties of the University of Dublin, is acknowledged; Mr. D. McCauley assisted in the machining of laboratory apparatuses.

Dr. D. Doff, of the Department of Geochemistry, and Dr. S. Hillier, of the McCauley Land Research Institute, conducted X-ray diffraction tests.

The writer acknowledges the constructive criticism of manuscripts of Dr. T. Orr, Senior Lecturer in soil mechanics at the University of Dublin, Dr. G. Milligan, of the University of Oxford/Geotechnical Consulting Group, and Dr. B. Lehane, Associate Professor in soil mechanics at the University of Western Australia.

The author's parents, Mr. Brendan Lawler & Mrs. Eileen Lawler, and Brian A. Lawler Esq. are duly acknowledged.

ABSTRACT iii
ACKNOWLEDGEMENT iv
LIST OF TABLES x
LIST OF FIGURES xi

1.0 INTRODUCTION 1
1.1 Background 1
1.2 Objectives 1
1.3 Thesis Outline 4

2.0 LITERATURE REVIEW 5
2.1 Introduction 5
2.2 Geology 5
2.2.1 Land Area of Interest 5
2.2.2 The Last Glaciation of Europe 5
2.2.3 Glacial Events over Dublin Based on the Literature 6
2.2.4 Glacial Action 7
2.2.5 Soils 8
2.2.6 Rock 15
2.3 Sampling 20
2.3.1 Representative Sampling of Boulder Clay 20
2.3.2 Soil Disturbance 20
2.3.3 Reconstituted Soil Testing 22
2.4 Stress-History 26
2.4.1 Soil Overconsolidation 26
2.4.2 Coefficient of Earth Pressure, K_0 28
2.5 Stiffness and Stress-Strain 34
2.5.1 Introduction 34
2.5.2 Stress-Strain 34
2.5.3 Factors affecting Soil Stiffness 35
2.5.4 Strain Measurement 40
2.5.5 Stiffness Moduli 41
2.5.5.1 Static Stiffness 41
2.5.5.2 Dynamic Stiffness 42
2.6 Strength 61
2.6.1 Introduction 61
2.6.2 Effective Strength of Dublin Boulder Clay 62
2.6.3 Undrained Shear Strength 63
2.6.4 Soil Structural Strength 64
2.7 Dilatancy 69
2.8 Suction 76

2.9 Soil Modelling 81
2.9.1 Soil Models 81
2.9.1.1 Elasticity 81
2.9.1.2 Elastic-Perfect Plasticity 81
2.9.1.3 Hyperbolic (Konder, 1963) 83
2.9.1.4 Duncan and Chang (1970) 84
2.9.1.5 Modified Cam-Clay 85
2.9.1.6 Kinematic Models 86
2.9.2 Examination of Soil Model Predictions in Boulder Clay 87
2.10 Conventional Methods of Ground Deformation Analysis 96
2.10.1 Introduction 96
2.10.2 Excavations 96
2.10.2.1 Stability 96
2.10.2.2 Ground Movements 97
2.10.3 Footings 100
2.10.4 Piles 101
2.10.4.1 Pile Design Methods 101
2.10.4.2 Pile Capacity and Settlement in Boulder Clay 103

3.0 GLACIAL HISTORY - RELATED GEOLOGY AND TILL PROPERTIES 113
3.1 Glacial Advance 113
3.2 Glacial Consolidation 116
3.2.1 The Glacial Consolidation Equation 116
3.2.2 Importance of the Glacial Consolidation Equation 120
3.3 Glacial Retreat 122
3.4 Post-Glaciation 123
3.5 Implementation of Dublin Geology in FE Analysis 124

4.0 FIELD AND LABORATORY WORK - MATERIALS AND METHODS 128
4.1 Description of Soils Tested 128
4.2 Sampling Method: Geobor S 132
4.3 One-Dimensional Consolidation 134
4.3.1 Introduction 134
4.3.2 Design and Operation of New Oedometer 134
4.3.2.1 Components 134
4.3.2.2 Calibration 135
4.3.2.3 Soil Bedding Effects 136
4.3.2.4 Procedures Followed in Oedometer Tests 137
4.3.2.5 Reconstituted Test 137
4.3.2.6 Testing 138
4.4 Triaxial Testing 141
4.4.1 Introduction 141
4.4.2 Apparatus 141
4.4.3 Bender Element Testing 142
4.4.3.1 Apparatus Description 142
4.4.3.2 Set-Up of Soil Sample 144
4.4.3.3 Calibration 144
4.4.3.4 Testing Method 145
4.4.4 K_0 Consolidation Method 147

4.4.5 General Triaxial Testing 149
4.4.5.1 Definitions and Calculations 149
4.4.5.2 Triaxial Test Procedure 150
4.4.5.3 Corrections Applied 152
4.4.5.4 Reconstituted Sample Preparation for Triaxial Testing 152
4.4.5.5 LVDTs 153
4.5 Soil Suction 156
4.5.1 Introduction 156
4.5.2 Filter Paper Method 156
4.6 Microscopic and Mineralogical Studies 157
4.6.1 Introduction 157
4.6.2 X-Ray Diffraction 157
4.6.3 Scanning Electron Microscopy 158
4.6.3.1 Introduction 158
4.6.3.2 Apparatus 158
4.6.3.3 Test Method 159
4.7 In Situ Soil Testing: Pressuremeter and Seismic Tests 160
4.7.1 Pressuremeter Tests 160
4.7.1.1 Apparatus 160
4.7.1.2 Test Procedure 160
4.7.1.3 Test Interpretation Methods 161
4.7.1.4 Determination of In Situ Stresses 162
4.7.1.5 Stiffness 162
4.7.1.6 Strength 162
4.7.2 Seismic Tests 162

5.0 FIELD AND LABORATORY WORK - DISCUSSION 164
5.1 Introduction 164
5.2 Sampling 164
5.3 One-Dimensional Consolidation 165
5.3.1 Yield Stress, σ_{vy}' 165
5.3.1.1 Methods of Determination and Laboratory Estimate 165
5.3.1.2 Semi-Empirical Prediction of Yield Stress 166
5.3.2 Soil Stiffness in One-Dimensional Compression 167
5.3.3 Soil Structural Strength 169
5.3.3.1 Soil Structural Strength Measurements 169
5.3.3.2 The Origin of Structural Strength 170
5.3.3.3 Importance of Structural Strength 171
5.3.4 Primary and Secondary Consolidation and Consolidation Characteristics 171
5.3.4.1 Analysis of Consolidation Data 171
5.3.4.2 The Coefficient of Consolidation, c_v 171
5.3.4.3 Coefficient of Permeability, k 172
5.4 Triaxial Testing 176
5.4.1 General Behaviour 176
5.4.2 Soil Stiffness 180
5.4.2.1 Stiffness Parameters 180
5.4.2.2 The Threshold Effect 182
5.4.2.3 Local versus External Strain Measurement 182

5.4.3 Effective Strength Parameters 183
5.4.4 K_0 184
5.4.5 Angle of Soil Dilation 185
5.4.6 Poisson's Ratio 186
5.4.7 Behaviour of Reconstituted Soil 186
5.5 Soil Suction 193
5.5.1 Filter-Paper Measurement of Soil Suction 193
5.5.2 Soil Suction Paradox 193
5.5.3 Importance of Cohesive Forces (other than Clay Mineral Aggregation) 194
5.6 Microscopic and Mineralogical Studies 197
5.6.1 Introduction 197
5.6.2 Qualitative X-Ray Diffraction (XRD) 197
5.6.3 SEM 198
5.6.3.1 Introduction 198
5.6.3.2 Mottled Brown Lodgement Till 198
5.6.3.3 Brown Deformation Till 200
5.6.3.4 Black Boulder Clay 201
5.6.4 Quantitative XRD (QXRD) 201
5.7 In Situ Soil Testing: Pressuremeter and Seismic Tests 204
5.7.1 Pressuremeter 204
5.7.1.1 In Situ Stresses (K_0) 204
5.7.1.2 Stiffness 204
5.7.1.3 Strength 205
5.7.2 Seismic 205

6.0 NUMERICAL MODELLING 206
6.1 Introduction 206
6.2 Hardening Soil 207
6.2.1 Hardening Soil Formulation 207
6.2.2 Soil Model Parameters 211
6.2.3 Modelling In Situ Soil Stresses 213
6.2.4 Validation of the HS Model 213
6.2.4.1 Drained Tests 214
6.2.4.2 Undrained Tests 215
6.3 Predictions of Field Trials with the HS Model 221
6.3.1 Footing 221
6.3.2 Trial Excavation 222
6.3.3 Pile Tests 224
6.3.3.1 CFA Pile FE Model 224
6.3.3.2 Pile Design by the FE Method 226
6.4 Elastic-Perfectly Plastic Soil Model 235
6.4.1 Introduction 235
6.4.2 Elastic-Perfectly Plastic Predictions 235
6.4.2.1 Selection of Parameters 235
6.4.2.2 Laboratory Test Predictions 238
6.4.2.3 Footing 238
6.4.2.4 Trial Excavation 239
6.4.2.5 Pile Tests 239

7.0 CONCLUSIONS 244
7.1 Introduction 244
7.2 Soil Modelling 244
7.2.1 HS Model 244
7.2.2 Elastic-Perfectly Plastic Soil Model 246
7.2.3 Comparison of FE Methods with other Methods 246
7.3 Geology 247
7.4 Sampling 249
7.5 Stress-History 249
7.6 Stiffness and Stress-Strain 250
7.7 Strength 253
7.8 Dilatancy 254
7.9 Soil Suction 254
7.10 Suggestions for Further Research 254

APPENDICES 256
A Field and Laboratory Work- Test Results 256
A.1 One-Dimensional Consolidation 256
A.1.1 Oedometer Test O 256
A.1.2 Oedometer Test E 257
A.1.3 Oedometer Test R 258
A.2 Triaxial Testing 265
A.2.1 Triaxial Test BE1 (CIRD) 265
A.2.2 Triaxial Test BE4 (CK_0RD) 267
A.2.3 Triaxial Test T1 (CK_0RD – reconstituted) 269
A.2.4 Triaxial Test SS1 (CK_0RD) 270
A.3 Soil Suction 283
A.3.1 Test S1 283
A.3.2 Test S2 283
A.4 Microscopic and Mineralogical Studies 285
A.4.1 Qualitative XRD 285
A.4.2 Scanning Electron Microscope 285
A.4.3 Quantitative XRD 286
A.5 In Situ Soil Testing: Pressuremeter and Seismic Tests 304
A.5.1 Pressuremeter 304
A.5.2 Seismic 304
B Pile Tests 310
B.1 Materials and Methods 310
B.2 Results 318
C Apparatus Design Drawings and Photographs 326

REFERENCES 336

LIST OF TABLES AND FIGURES

LIST OF TABLES

2.2.1(a). Database of the index and state properties of stiff tills 13
2.2.1(b). Database of the strength properties of stiff tills 14
2.8.1. Methods of measurement of suction, adapted from Ridley and Wray (1995) 77

4.1.1. Mean consistency indices and standard deviation (SD) about the mean 128
4.4.1. Waveforms generated routinely in the BE tests 147
4.4.2. Table of typical triaxial test procedure 151

5.3.1. Measured σ_{vy}' and OCR 166
5.4.1. Small strain secant modulus, E_s', values in tests 178
5.4.2. Summary of soil behaviour measured in the triaxial tests 179

6.2.1. Lodgement till soil model parameters for use in the HS model 211
6.2.2. Deformation till soil model parameters for use in the HS model 211
6.2.3(a). Summary of how stiffness related parameters were obtained 212
6.2.3(b). Summary of how strength and dilation parameters were obtained 212
6.2.3(c). Summary of how stress-history and in situ stress-state parameters were obtained 212
6.2.3(d). Summary of how auxiliary parameters were obtained 213
6.4.1(a). Parameters used in the elastic-perfectly plastic prediction: lodgement till 237
6.4.1(b). Parameters used in the elastic-perfectly plastic prediction: deformation till 237

A.1.1. Oedometer compression, recompression and swelling indeces 257
A.3.1. Suction test results: unsaturated till 283
A.3.2. Suction test results: lodgement till 284
A.4.1. Soils tested in XRD analysis 285
A.4.2(a). Results of quantitative analyses (percentage of mineral by weight) using the RIR method (Hillier, 2002) 286
A.4.2(b). Relative percentage of clay minerals in the sub-2 micron fraction 286
A.5.1. Seismic test data 305

B.2.1. Pile test summary 318

LIST OF FIGURES

2.2.1. The Europe-wide extent of the Last Glaciation, after Steenfelt (1997) 16
2.2.2. X-ray diffraction trace for Dublin boulder clay, after Farrell et al. (1995b) 16
2.2.3. Typical plasticity chart for Dublin boulder clay, after Farrell et al. (1995b) 17
2.2.4. Scanning electron micrograph showing the angularity of the soil grains, after Farrell et al. (1988) 17
2.2.5. Typical PSD plot for Dublin boulder clay 18
2.2.6. Typical water contents of Dublin boulder clay, after Farrell et al. (1995b) 18
2.2.7. Fissured soil underlying Dublin boulder clay at Griffith Ave., Marino 19
2.2.8. Typical sand lens in Dublin boulder clay (Griffith Avenue, Marino) 19
2.3.1. Influence of the ratio of sample size to fissure spacing on the strength of London clay, after Simpson et al. (1979) 24
2.3.2. The adverse effects of fissuring on the stress-strain characteristics of stiff clay, after Simpson et al. (1979) 24
2.3.3. Stress-path taken by soil when sampled, adapted from Hight et al. (1985) 25
2.3.4. SHANSEP method of removing sample disturbance effects, adapted from Ladd and Foott (1974) 25
2.4.1. Oedometer tests on Dublin black boulder clay, after Lehane and Simpson (2000) 32
2.4.2. Typical relationship between vertical and horizontal effective stresses in, initially normally consolidated, clay, after Brooker and Ireland (1965) 32
2.4.3. 'Brick' estimates of K_0 for Dublin boulder clay, after Lehane and Simpson (2000) 33
2.5.1. Stress-strain behaviour of Dublin boulder clay in CID tests 49
2.5.2. Non-linearity of the response of foundations in glacial till, after DeJong and Harris (1971) 49
2.5.3. Non-linearity of the response of a foundation in Dublin boulder clay 50
2.5.4. Variation of stiffness due to definition, after Atkinson and Salfors (1991) 50
2.5.5. Dependence of reconstituted boulder clay on overconsolidation, after Atkinson (1993) 51
2.5.6. Effect of 'recent' stress-history on the soil stiffness of reconstituted stiff clay, after Atkinson and Salfors (1991) 51
2.5.7. Classical 'S'-shape curve 52
2.5.8. Very small strain stiffness and the elastic threshold of Dublin boulder clay, adapted from a test by O'Shea (1996) 52
2.5.9. Typical strains associated with foundations and excavations, after Atkinson (2000) 53
2.5.10. Dependence of Dublin boulder clay on strain level, recent stress-history and stress-level, after Lehane and Simpson (2000) 53
2.5.11. Definition of E_{oed}, after Schanz and Vermeer (1998) 54
2.5.12. Definition of E_{ur}, after Duncan and Chang (1970) 54
2.5.13. Comparison of stiffness measured in standard oedometer test with other methods of measurement in stiff clay, after Matthews et al. (2000) 55
2.5.14. Approximate linear relationship between E_{ur} and σ_1' measured in the oedometer on stiff till, after Steenfelt (1997) 55
2.5.15. Coefficient of consolidation of boulder clay against vertical effective stress, adapted from McKinlay et al. (1978) 56
2.5.16. Permeability of boulder clay against vertical effective stress, adapted from McKinlay et al. (1978) 56
2.5.17. Stiffness degradation of reconstituted Dublin boulder clay measured locally and externally, after Faulkner (1998) 57

2.5.18. Early indication of the discrepancy between standard laboratory test stiffness and stiffness back-analysed from the field, after DeJong and Harris (1971) 57
2.5.19. Evidence of small strains at working loads in stiff clay and boulder clay, after Burghignoli et al. (1991) 58
2.5.20. Variability of stiffness modulus in till depending on method of measurement, after Weltman and Healy (1978) 58
2.5.21. Typical volume change-compression curve in the pressuremeter test 59
2.5.22. Bender element detail, after Brignoli et al. (1996) 59
2.5.23. Typical response of a bender element to a square wave input, after Viggiani and Atkinson (1995) 60
2.6.1. Stress-paths and peak/failure conditions in undrained and drained triaxial tests 67
2.6.2. Effective angle of friction in CID tests on Dublin black boulder clay 67
2.6.3. Variation in c_u of boulder clay with moisture content, after Weltman and Healy (1978) 68
2.7.1. Mobilisation of the angle of dilation in CID triaxial tests in Dublin boulder clay, adapted from tests conducted by O'Shea (1996) 73
2.7.2. Dilatancy behaviour of dense soil in triaxial shearing 73
2.7.3. Saw-tooth model of soil dilation 74
2.7.4. Rowe's model of soil dilation, after Houlsby (1991) 74
2.7.5. Comparison of flow rules, after Houlsby (1991) 75
2.7.6. Comparison of Rowe's stress-dilatancy theory with CID test data adapted from tests conducted by O'Shea (1996) (see Fig. 2.7.1) 75
2.8.1. Soil-water characteristic curve, after Fredlund et al. (2001) 79
2.8.2. Capillary rise model of soil suction 79
2.8.3. Soil suction in stiff till, after Jacobsen (1970) 80
2.9.1. Mohr-Coulomb total yield contour in principal stress space 90
2.9.1. Elastic-perfectly plastic representation of soil stress-strain behaviour 90
2.9.3. Geometry of the rectangular hyperbola, after Konder (1963) 91
2.9.4. v-logp' relations in Cam-clay 91
2.9.5. Cam-clay yield contour in q-p' space 92
2.9.6. Very advanced soil model, after Robertson and Ferreira (1993) 92
2.9.7. Graphical depiction of the 'Brick' soil model, after Simpson (1992) 93
2.9.8. Brick prediction of the settlement of a footing, after Lehane and Simpson (2000) 93
2.9.9. FE prediction of ground movements in heavily OC clay, after Hird and Pierpoint (1998) 94
2.9.10. Prediction of the deflection of a retaining wall in boulder clay, after Eisenstein and Medeiros (1983) 94
2.9.11. Foundation settlement prediction in stiff till, after Kristensen et al. (1995) 95
2.9.12. Non-linear prediction of footing settlement with the Atkinson (2000) method 95
2.10.1. Typical excavation practice and slope angles in Dublin boulder clay (Griffith Avenue) 105
2.10.2. Stiffness in plate bearing tests on very stiff clay; E_u/c_u = 1000 represents the stiffness of excavations, after Simpson et al. (1979) 105
2.10.3. Evidence of small strains in excavations in stiff clay, after Jardine et al. (1986) 106
2.10.4. The development of inward wall deflection with increasing depth of excavation in boulder clay, after Eisenstein and Medeiros (1983) 106
2.10.5. Surface settlement of boulder clay at distance perpendicular to a supported excavation, after Eisenstein and Medeiros (1983) 107
2.10.6(a). Vertical surface settlement in Dublin boulder clay, adapted from Treacy (1995) 107

2.10.6(b). Horizontal surface settlement in Dublin boulder clay, adapted from Treacy (1995) 108
2.10.7. Fig. 2.10.6(a) replotted with a normalising procedure and compared to data on stiff clays and till given by O'Rourke (1981) 108
2.10.8. Foundation details in Edmonton till (CN tower), after DeJong and Harris (1971) 109
2.10.9. Load and settlement history of foundations shown in Fig. 2.10.8, after DeJong and Harris (1971) 109
2.10.10. Non-linear stiffness of foundations in Edmonton till, after DeJong and Harris (1971) 110
2.10.11. Driven pile tests in Dublin boulder clay, adapted from Farrell et al. (1995a) 110
2.10.12. Settlement of pile groups in stiff till, after DeJong and Harris (1971) 111-112

3.1.1. Ice flow patterns over Ireland 115
3.5.1. Dublin boulder clay stratigraphy 126
3.5.2(a). Typical stratigraphic sequence in Dublin boulder clay 126
3.5.2(b). Simplified stratigraphic sequence for use in FE analysis 127

4.1.1. Natural water contents of soils tested 130
4.1.2. Atterberg limits of soils tested 130
4.1.3. Particle size distributions of soils tested 131
4.3.1. Radial strains in stainless steel rings subjected to internal pressure 140
4.4.1. Flow diagram of triaxial test set-up 154
4.4.2. Calibration of bender elements 155
4.4.3. Stresses in triaxial K_0 consolidation 155

5.3.1. Isotropic overconsolidation ratio prediction 174
5.3.2. Consolidation curve including unload-reload loops 174
5.3.3. Comparison of the behaviour of reconstituted and intact till 175
5.3.4. Comparison of intact and reconstituted oedometer tests 175
5.4.1. Overall behaviour of Dublin boulder clay in the CD triaxial test 187
5.4.2. Depiction of overall behaviour of Dublin boulder clay shown in Fig. 5.4.1 188
5.4.3. Detail of the bender element tests of Tests BE1 and BE4 188
5.4.4. Shear modulus versus logarithm shear strain curves: CK_0RD tests 189
5.4.5. Very small strain stiffness tests: comparison with theoretical value 189
5.4.6. Plot of stiffnesses measured in all laboratory tests 190
5.4.7. Deviator stress against axial small strain of various test types in the region of small strain showing high threshold to initial yield 190
5.4.8. Comparison of N_{60} and c_u measured in CIU tests 191
5.4.9. Comparison of K_0 measurements in the laboratory and field with predictions 191
5.4.10. Comparison of Rowe's stress-dilatancy theory with measured data 192
5.4.11. Comparison of the stress-strain behaviour of intact (Test BE4) and reconstituted (Test T1) lodgement till 192
5.5.1. Theoretical capillary attraction stresses in soils, after Doran et al. (1995) 196

6.2.1. Total yield contour of HS model 217
6.2.2. Essential features of the HS model in q-p′ space 217
6.2.3. FE mesh, loads and boundary conditions for triaxial test prediction 218
6.2.4. Comparison of predicted (HS) and measured (Test BE4) triaxial tests 218
6.2.5. FE mesh, loads and boundary conditions for oedometer test prediction 219

6.2.6. Comparison of predicted and measured (Test E) oedometer tests 219
6.2.7(a). Comparison of predicted and measured CIU triaxial test stress paths 220
6.2.7(b). Comparison of predicted and measured CIU triaxial test excess pore water pressure against axial strain 220
6.3.1. FE mesh, loads and boundary conditions for footing prediction 228
6.3.2. Comparison of predicted (HS) and measured footing settlement 228
6.3.3. HS prediction of the ultimate footing bearing stress and settlement condition 229
6.3.4. FE mesh, loads and boundary conditions for excavation prediction 229
6.3.5(a). Comparison of predicted (HS) and measured vertical ground movement of soil adjacent to an excavation 230
6.3.5(b). Comparison of predicted (HS) and measured horizontal ground movement of soil adjacent to an excavation 230
6.3.6(a). Comparison of measured vertical ground movements with the movements predicted with very small strain stiffness 231
6.3.6(b). Comparison of measured horizontal ground movements with the movements predicted with very small strain stiffness 231
6.3.7. FE mesh, loads and boundary conditions for pile prediction 232
6.3.8. Comparison of predicted and measured (Pile 600) pile head load against pile head settlement 232
6.3.9. Comparison of K_0 at the pile-soil interface and K_0 in the soil 233
6.3.10. Comparison of predicted and measured (Pile 600) pile head load against pile head settlement 233
6.3.11. Comparison of predicted and measured load distribution and the development of load distribution in Pile 600, including installation effects (note that lines without symbols are the predictions) 234
6.3.12. Pile design procedure validation (note that the curves overlap) 234
6.4.1. Elastic-perfectly plastic prediction of CK_0RD test (Test BE4) 240
6.4.2. Stiffness degradation prediction by elastic-perfectly plasticity 240
6.4.3. Elastic-perfectly plastic prediction of oedometer test 241
6.4.4. Elastic-perfectly plastic prediction of footing settlement 241
6.4.5(a). Elastic-perfectly plastic prediction of the vertical deformation adjacent to an excavation 242
6.4.5(b). Elastic-perfectly plastic prediction of the horizontal deformation of the ground adjacent to an excavation 242
6.4.6. Elastic-perfectly plastic prediction of Pile 600 head settlement 243

A.1.1. Consolidation curves of undisturbed oedometer tests (note that the unload-reload loops of Test E are not plotted) 259
A.1.2. Stiffness parameters 259
A.1.3(a). Methods of measuring σ_{vy}': (a) Tavenas et al. (1979) 260
A.1.3(b). Methods of measuring σ_{vy}': (b) Butterfield (1979) 260
A.1.3(c). Methods of measuring σ_{vy}': (c) Janbu (1991) 261
A.1.4. Coefficient of consolidation 261
A.1.5. Coefficient of permeability change with vertical effective stress 262
A.1.6. Typical time-settlement plots 262
A.1.7. Detail of unload-reload curves of Test E (note that the loops have been separated out for clarity; i.e. the curves do not show creep settlement) 263
A.1.8. Reconstituted oedometer Test R (note unload-reload loops have been removed) 263

A.1.9. Typical time-settlement curves for reconstituted soil 264
A.2.1. G_{max} versus isotropic effective stress: Test BE1 273
A.2.2. Isotropic consolidation: Test BE1 273
A.2.3. Deviator stress against axial strain for Test BE1 274
A.2.4. Stiffness data from triaxial Test BE1 274
A.2.5. Stiffness data and stiffness degradation for Test BE1 275
A.2.6. Shear strength data 275
A.2.7. Volumetric strain (dilative) against shear strain for Test BE1 276
A.2.8. K_0 consolidation stress-path in Test BE4 276
A.2.9. Radial strain measured in K_0 consolidation stage of Test BE4 277
A.2.10. G_{max} against vertical effective stress in K_0 consolidation/swelling stage: Test BE4 277
A.2.11. Deviator stress against axial strain curve of Test BE4 278
A.2.12. Stiffness degradation curves for Test BE4 278
A.2.13. Shear strain against volumetric strain for Test BE4 279
A.2.14. K_0 data measured in the triaxial tests 279
A.2.15. Radial effective stress against vertical effective stress for K_0 load stage of reconstituted Test T1 280
A.2.16. Stress-strain curve of reconstituted Test T1 280
A.2.17. Shear strain against volumetric strain for Test T1 281
A.2.18. Stress-strain curve of Test SS 281
A.2.19. Comparison of methods of strain measurement in the triaxial test (Test SS1) 282
A.2.20. Compression-dilation characteristics measured in Test SS1 282
A.4.1. X-ray diffraction trace, Test XRD1 287
A.4.2. X-ray diffraction trace, Test XRD2 287
A.4.3. EM1: stiff mottled brown till 288
A.4.4. EM1: stiff mottled brown till 289
A.4.5. EM1: stiff mottled brown till 290
A.4.6. EM1: stiff mottled brown till 291
A.4.7. Calcite cementation, after Knudsen et al. (1995) 292
A.4.8. EM2: firm brown till 293
A.4.9. EM2: firm brown till 294
A.4.10. EM2: firm brown till 295
A.4.11. EM2: firm brown till 296
A.4.12. EM2: firm brown till 297
A.4.13. EM2: firm brown till 298
A.4.14. EM3: stiff black till 299
A.4.15. EM3: stiff black till 300
A.4.16. EM3: stiff black till 301
A.4.17. EM4: stiff black till 302
A.4.18. Influence of inactive minerals on the plasticity of a soil, after Moon (1978) 303
A.5.1. A good pressuremeter test in the boulder clay, after Geoconsult-Arup (1997) 306
A.5.2. K_0 determined from the pressuremeter tests (closed symbols indicate tests with very distinct yield points and open symbols indicate that the yield point was less well defined) 307
A.5.3(a). Secant stiffness measured on reload in pressuremeter test loop 307
A.5.3(b). Secant stiffness measured on reload in pressuremeter test loop 308
A.5.4(a). Borehole records in the vicinity of the Scholarstown seismic refraction study 308
A.5.4(b). Borehole records in the vicinity of the Dublin Port seismic refraction study 309
A.5.5. Comparison of stiffness measured in situ and in the laboratory dynamic tests 309

B.1.1(a). Stratigraphy relevant to Pile 450 315
B.1.1(b). Stratigraphy relevant to Pile 600 315
B.1.2. Standard Penetration Test results at Saint James's St. 316
B.1.3(a). Pile 450 dimensions and instrumentation 316
B.1.3(b). Pile 600 dimensions and instrumentation 317
B.1.4. Pile section indicating forces and dimensions for load and strain calculations 317
B.2.1(a). Pile 450 calibration curve 320
B.2.1(b). Pile 600 calibration curve 320
B.2.2(a). Strain distribution against depth for Pile 450 321
B.2.2(b). Strain distribution against depth for Pile 600 321
B.2.3. Strains in Pile 450 due to curing 322
B.2.4. Temperature variation in Pile 450 due to curing 322
B.2.5(a). Load distribution in Pile 450 323
B.2.5(b). Load distribution in Pile 600 323
B.2.6(a). Gauge level load against gauge level deflection for Pile 450 324
B.2.6(b). Gauge level load against gauge level deflection for Pile 600 324
B.2.7(a). Shaft friction distribution/mobilisation in Pile 450 325
B.2.7(b). Shaft friction distribution/mobilisation in Pile 600 325

C.1. Special oedometer design drawings 326
C.2. Special oedometer: cell, load cap and LVDTs: with and without ring 328
C.2 cont'd.... Oedometer load frame 329
C.3. Diamond bladed drop saw used for slicing oedometer specimens 329
C.4. Triaxial test set-up: bender element top cap and radial and axial LVDTs 330
C.5. (a) Typical square wave; (b) typical sine wave (note near field effect) 331
C.5. cont'd.... (c) arbitrary sine wave (near-field effect removed – see Fig. D.2(b)); (d) typical resonance test (note that the instability, evident in the previous traces, is resolved) 332
C.6. Geobor S rig, wire-line and polymer gel flush 333
C.7. Pile testing equipment: Pile test reaction frame 333
C.8. Pile testing equipment: Pile test: load cell, displacement transducers and pile cap 334
C.9. Pile testing equipment: CFA rig immediately prior to construction of 11 m length Pile 600 334
C.10. Pile testing equipment: VWSG spot-welded to rebar 335
C.11. Pile testing equipment: Diametrically opposite VWSGs in housing, pile cage and spacers 335

CHAPTER 1

INTRODUCTION

CHAPTER 1

INTRODUCTION

1.1 Background.

The upcoming series of tunnels, tall building foundations and deep excavations in Dublin will induce in the city's glacial soils a wide range of strain levels and stress-paths. Estimating the effect the resulting ground movements will have on the many historical and important buildings in the capital requires an accurate model of how the soil will behave. Owing to the recent advances in high speed, low cost computers and the development of the FE method, it is considered that the greatest potential value of this research lies in the application of the FE method to geotechnical practice.

Estimating the ground movements of boulder clay is made difficult, however, by the non-linearity of the soil response, by problems associated with obtaining the relevant soil parameters from either field or laboratory tests and by deposits unique to these ground conditions, such as boulders and sand lenses. As well as these, other questions need to be systematically addressed in order that the difficulties in the application of the FE method to boulder clay are overcome. These include the formation of the brown till, the precise mechanisms of glacial lodgement and the high strength, in excess of that due purely to inter-particle friction, of the subsequent till.

Recently, however, there have been advanced developments in the area of FE modelling and, allied to these advances, there have been encouraging developments in the testing of boulder clay in Dublin and in methods of analysis. Despite this, the key problem remains, which is the validation and calibration of an appropriate soil model within a simplified ground model.

1.2 Work Conducted in this Study.

The assessment and validation of FE models that would be of use to routine geotechnical design in boulder clay required an accurate assessment of a wide range of decisive soil properties and soil mechanical behaviour including stiffness, strength and stress-strain properties following various stress-paths, in situ conditions and stress-history. If the potential of the FE method is to

be realised, however, it is of uppermost importance that the observed behaviour of the soil be correctly incorporated. Therefore, the validation of the FE method also required knowledge of the soil behaviour in the field, i.e. foundation and excavation behaviour. Furthermore, although advanced soil models do have considerable advantages over the use of simpler models, simple models of soil behaviour were not discounted by the author, as these too were of considerable potential value, in that the parameters were obtainable with standard testing and the predictions more easily analysed.

Geological aspects must be incorporated correctly in numerical models if a reasonable prediction of ground movements around structures or excavations is to be made. It was therefore necessary to implement a soil stratigraphy that was possible to include in routine design yet was based on a sound understanding of the geology of a site. However, glacial deposits, such as lodgement tills, are generally regarded as being too variable and unpredictable to attempt the complex numerical modelling that is required of an estimate of ground movements. To address this, a simplified model is developed by systematically examining the glaciations and the processes of glacial consolidation, glacier retreat and post-glaciation.

Following this, an assessment was made of a wide range of very simple soil models and design methods through to very advanced soil models, including those for footings, excavations and piles.

All available laboratory and field data on the properties of the till, including very valuable tests resulting from the Dublin Port Tunnel works, were reviewed. These tests included trial footings and excavations and pressuremeter, seismic and triaxial tests, all of which yielded important information on stress-strain behaviour and the strength, stiffness and in situ stress-state of the soil. The review of previous work identified areas that required further research; investigations into state-of-the-art practice in laboratory testing were subsequently undertaken.

As a result of these preliminary investigations, experimental tests and methods were designed and conducted by the author in the field and in the laboratory. The purpose of these tests was to examine in a very detailed way the behaviour of the boulder clay, to measure the required soil model parameters and to provide essential data for validation and verification of the soil models.

As soils are now known to be highly non-linear, in terms of stress and strain and stiffness, and because boulder clay is a particularly difficult soil to test, the following series of special laboratory and field tests were necessary.

Initially, the high stiffness of the till and the gravel and boulder inclusions within the till made sampling and testing of representative, undisturbed samples difficult. To overcome this, an assessment of sampling disturbance and sampling, handling and storage techniques was made. As a result, a new sampling technique called Geobor S was employed and various methods developed to ensure that test samples of the boulder clay were as undisturbed as possible. Disturbed samples of till were also obtained from different sites around Dublin, including the Dublin Port Tunnel works.

A special oedometer apparatus, capable of resisting very high test pressures without developing significant vertical and radial strains, was designed to measure the very high apparent preconsolidation stress and the one-dimensional consolidation and stiffness characteristics of the soil.

Next, a triaxial test set-up was developed that included software capable of K_0 and isotropic consolidation and very small strain measurement with local axial, local radial and bender element measurement of soil stiffness. Best practice was followed, based on a comprehensive review of the methods of measurement.

Reconstituted soil testing was conducted in the oedometer and triaxial cells, which provided invaluable information on the fundamental behaviour of the soil and contributed to the understanding of the intact soil behaviour.

The mineralogy of a soil, particularly that of the clay fraction, has a deterministic effect on many of the properties of interest to the soil engineer. The latest developments in scanning electron micrography and X-Ray diffraction were, therefore, employed, which proved to be effective techniques in the accurate determination of the composition and origin of the till fabric.

In the course of the research, full-scale field tests on bored piles were conducted. These tests, along with previous full-scale field trials, including a footing and an excavation, provided a range of field structures, with which it was possible to verify the soil models comprehensively against actual field conditions, as well as under laboratory conditions. Taken together, these cases involve the wide-range of stress and strain levels and directions of loading commonly imposed on the Dublin till.

Routine soil tests were conducted throughout on the soils tested in the field (standard penetration test) and laboratory (particle sizes, Atterberg limits and density). Furthermore, the results of the soil tests were compared to well-established soil frameworks and, in the course of the research, the author visited and examined numerous sites and excavations around Dublin.

1.3 Thesis Outline.

In the chapter that follows, a review is undertaken of the soils research and the methods of measurement of interest to this thesis. This literature review is, as a result, very broad.

In Chapter 3, 'Glacial history - related geology and till properties', a research study into the glacial history of Dublin is detailed. Glacial advance, retreat and post-glacial processes are proposed which explain the geotechnical properties and ground conditions measured today.

The apparatuses that have been developed and the methods of measurement adopted in the laboratory and field tests are explained in detail in Chapter 4. The raw results of these tests are given in Appendix A but are referred to in Chapter 5, where these are placed in the context of the parameters and features involved in soil modelling.

Chapter 6 is an assessment of new soil modelling methods for use in routine work in boulder clay. The laboratory and field tests are used to verify the models.

Finally, in Chapter 7, the main findings of the research are given and recommendations for future research suggested. Appendices, including the results of pile tests, are presented at the end of the report, followed by the references. Figures are presented at the end of each section.

CHAPTER 2

LITERATURE REVIEW

CHAPTER 2

LITERATURE REVIEW

2.1 Introduction to the Review.

Soil models single out and make available for intensive investigation those areas which are decisive (Muir-Wood, 1990). The decisive areas include soil stiffness and stiffness non-linearity, strength, dilatancy and stress-history. These soil properties, and their measurement, therefore form the basis of this literature review. Furthermore, owing to the particular difficulties of sampling boulder clay, a review of sampling methods is undertaken, as is a review of soil suction. Soil models are also examined in detail; however, as these are not intended to be an exact replica of soil behaviour, it is of utmost importance that the models be validated against actual measured till behaviour, in the laboratory and, importantly, in the field.

2.2 Geology.

2.2.1 Land Area of Interest.

Lodgement till is found throughout Ireland. However, owing to the relative importance of the Dublin area, emphasis is placed on the tills found in the area to the west as far as the Tallaght/Rathfarnham axis, to the north as far as Meakstown (Northern Cross) and to the south as far as the Wicklow mountains (see Fig. **3.1.1**).

2.2.2 The Last Glaciation of Europe.

Different nomenclature has developed for the last glaciation that affected Ireland, Great Britain and Europe. Ehlers et al. (1991) and Farrell and Wall (1990) give comparative glaciations. From these, it can be deduced that the Midlandian glaciation that affected Ireland corresponds to the North Europe wide Weichsel glaciation, which is shown in Fig. **2.2.1**. In Britain, these events are termed the Late Devensian.

2.2.3 Glacial Events over Dublin Based on the Literature.

The southern limit of Midlandian ice of northern provenance is delineated by the Southern Irish End Moraine (SIEM) (Charlesworth, 1928). The SIEM forms an arcuate line from the Shannon estuary to Wicklow Head.

Hoare (1975) suggested that the Midlandian glaciation was responsible for tills west of Rathfarnham and the Munsterian glaciation (of N/NE provenance) for tills east of there. The latter glaciation is referred to as Irish Sea ice. Furthermore, the author believed that the distinctive fines content of the tills indicated unique ice advance and retreat phases and that for much of the early and middle stages, of the Midlandian epoch, Ireland was ice-free.

Evidence of erratic distribution suggests that Irish Sea ('Scottish') ice covered a greater part of County Dublin and that this ice may have come in contact with inland ice (Hoare, 1975). The ice sheet did not overwhelm the Wicklow Mountains, which is suggested by erratics found at a maximum 610 m OD on northern slopes. Furthermore, there are features associated with a glacier dammed up against the mountain range, e.g. the 'Scalp' valley, which is a V-shaped, pro-glacial valley (Hanrahan, 1977) on the northern side of the mountains.

Synge (1987) suggested that Irish Sea ('Saale') ice of N and NE provenance protruded about 20 miles inland over Dublin. This was followed by the Weichsel glaciation of several Irish centres and delineated by the SIEM, which in turn was followed by a regular recession of the margins in deglacial times. Each instance of ice accumulation was believed to have been preceded by local ice, e.g. valley glaciers in the Wicklow Mountains (see Fig. **3.1.1**).

Warren (1991a) thought that there were four general ice sheets: a Midlandian ('Fenitian') Irish ice sheet, one that occupied the Irish Sea basin partly fed through the Firth of Clyde (Ailsa Craig) and an extended ice cap centred around the Cork and Kerry mountains. Localised glaciers in the Wicklow Mountains were also believed to be significant. The Midlandian and Irish Sea sheets are believed to have affected Dublin, though the succession is debatable.

Bowen (1991) suggested a large Irish Sea ('Eastern General') ice sheet composed of several different ice centres during the Late Devensian Substage.

Hoare (1991) describes a Midlandian (General) sheet that went E then SE across eastern Ireland. Late Midlandian age till has been dated at 30,500 BP and the limestone rich deposits are associated with this movement, overlying deposits of Irish Sea provenance.

2.2.4 Glacial Action.

Lodgement occurs when the force of moving ice on debris in traction over the glacier bed is not sufficient to overcome the frictional drag of the debris at the glacier-bed interface (Boulton, 1975). In a glacier the processes of erosion, transport, and deposition are linked, as follows. Basal shear stress is mobilised as a result of drag against the glacial bed and once sufficient frictional resistance is mobilised, initial deposition of eroded basal debris in traction with the interface is initiated[1]. This initial deposition acts as the trigger that allows further deposition by providing an obstruction to other particles, which forms the lodgement till exposed on glacier retreat. The lodgement process involves a continuous mixing and kneading action and the till may undergo deformation and shearing of the upper zones (Boulton et al., 1974), resulting in a remoulded, and therefore softer, deposit, termed deformation till (Boulton, 1996). The presence of a till of this type has been recognised in Edmonton, Alberta (inter alia De Jong and Harris (1971)), where typical blow counts for the top 0.6-0.9 metre are about half that of the lodgement till below.

Boulders are likely to be nucleated in boulder clusters due to the difficulty a boulder has in moving over another boulder lodged in the bed. Cavities can form in these clusters (Boulton and Paul, 1976), as was observed in a tunnel in Dublin boulder clay by Bevan and Parkes (1975)). The boulders generally lie horizontally; the extent of any one boulder is, therefore, greater than the thickness from borehole logs would suggest.

Glaciers can be temperate, sub-polar or cold based (Boulton, 1972). The difference is due to the relation of the ice to the pressure melting point: temperate glaciers are glaciers where the ice is at the pressure melting point and cold glaciers are glaciers where the ice is below the

[1] The reader is referred to Boulton (1975).

pressure melting point[2]. Temperate based glaciers transport till in a thin layer of regelation ice immediately over the bed; sub-polar glaciers have mechanisms which allow basal debris to be lifted up, giving a greater distribution through the ice and cold-based glaciers give rise to a varied sequence, associated with out-wash. This latter sequence is not found in Dublin and, it follows that, the ice sheet over Dublin was either temperate or sub-polar. However, as the till sheet in Dublin is relatively thick, a requirement of the temperate/sub-polar theory is that the main glacial event was of long duration and probably longer than previously assumed (by Synge (1987), for example, in the previous section). This would be in keeping with the more recent theory of climate systems, which suggests that glacial events occur on a continental, Europe-wide scale (Bowen, 1991), and not on a local level, as previously assumed. This theory is discussed in detail in the next chapter.

2.2.5 Soils.

Dublin till is typically separated into upper brown boulder clay and lower black boulder clay; the former is the weathered mantle of the latter (Farrell et al., 1995b). However, the upper metre or so of the brown till also reflects subglacial shearing of the lodgement till immediately underlying the ice (Boulton et al., 1974). Hence, a distinction is drawn between deformation till (Boulton, 1996) and lodgement till. This important point is expanded upon in the next chapter.

The predominant subglacial deposit is lodgement till, which is an unsorted, well-graded, material containing boulder clusters, gravel, sand, silt and clay. The general black shade, which lends the soil its name, is derived from the mudstone and shale intrusions in the limestone bedrock. Depending on the concentration of these intrusions the limestone, and consequently the till, are occasionally lighter in shade, often grey. The formation of the brown boulder clay layer has been attributed in the past to a separate glacial event. However, Farrell et al. (1995b) have shown that the brown till is oxidised black till, the mechanisms of which are discussed in the following chapter.

---

[2] Sub-polar glaciers are glaciers where the ice is at the pressure melting point internally and less than the pressure melting point marginally. Pressure melting occurs where high pressure, on the up-glacier side of an immovable obstacle on the glacier bed, causes a lowering of the ice melting point (Weertman, 1957). This allows the glacier to move around immovable obstacles.

Dublin boulder clay consists of limestone, sandstone, mudstone, metamorphic rock, vein quartz and chert (Farrell et al., 1995b). Quartz, chlorite, calcite with some feldspar, illite and mica have been identified by X-ray diffractometry, shown in Fig. **2.2.2**. This wide-range of rocks and minerals is due to the combined mechanisms of glacial erosion and transport, which occur over a very wide area prior to deposition. Significantly, there is a substantial calcium carbonate component ($CaCO_3$) (Farrell et al., cited), which is derived from the limestone.

The glacial formation of the soil has produced a certain set of characteristics, which can be summarised by the following:

(a) The soil lies on the T-line (till line) (Boulton and Paul, 1976) on the plasticity chart. This line is above Skempton's A-line (which is for sedimentary clays of low carbonate and organic content). A typical plasticity chart is shown in Fig. **2.2.3**, indicating that the soil lies in the low to intermediate plasticity zone (CL to CI), with the deformation till also lying near the T-line but of higher plasticity.

(b) Ice erosion has powdered and scored the rock to produce rock flour (Hartford, 1987) and angular soil grains, which is demonstrated in the scanning electron micrograph of Fig. **2.2.4**.

(c) Ice transport has produced a very well graded, highly mixed soil. Particle size distribution (PSD) is affected by all the glacial processes and has, therefore, a considerable influence on the soil properties. Initially, plucking of blocks and subsequent abrasion produces a wide range of particle sizes and the distance over which the debris is subsequently transported governs the length of time particles are exposed to collisions and wear. The repeatability of the PSD plot is one of the defining characteristics of the soil (Hanrahan, 1977). As can be seen from Fig. **2.2.5**, the fines fraction is in the region of 35 - 40% of the deposit and the clay fraction is typically 15%. Hartford (1987) and Farrell et al. (1988) conducted scanning electron microscopy on dispersed (the process by which clay particles are removed) samples of Dublin boulder clay and showed that the clay fraction contains a large proportion of rock flour particles. This finding explains the soil's low plasticity and is the basis for the suggestion, although unproven, that the soil contains few clay minerals. Part of this

research was to examine the clay mineralogy using new methods of clay mineral identification and electron microscope investigations.

(d) Ice deposition has produced a very dense soil with a water content close to the optimum compactive effort (for the Proctor test); typical water contents, shown in Fig. **2.2.6**, are of the order of 10%. Note that the water content of the soil in the top metre, the deformation till, is substantially higher at about 20%.

The till is locally called boulder clay, despite the number and frequency of boulders being relatively low for a till. Boulder size and frequency in Scandinavian till was estimated by counting the boulders exposed in a cliff face (Foged et al., 1995). It was found that there was about 1 boulder of 2 - 2.5 m diameter, 10 boulders of 1.5 – 2 m diameter and 100 boulders of 1 - 1.5 m per 100,000 m^3 of soil. This distribution was close to that in the ground in subsequent excavations (Steenfelt, 2001), although it is uncertain if this distribution could be applied to Dublin conditions.

The most common fissures in lodgement till are relaxation joints parallel to the till surface (due to mechanical glacier unloading), shear planes (due to shear stresses under the moving glacier sole) and joints due to drying-out. Hanrahan (1977) produced a photograph that was given as evidence of fissuring (Lehane and Simpson, 2000) and suggested this was the cause of a tunnel collapse. Unfortunately, the location of the tunnel and properties of the till were not given by the authors. However, the fissured soil may have been the soil shown in Fig. **2.2.7**, which was photographed at Griffith Avenue, Marino or the fissures may have been induced by the tunnelling. That there is no evidence of fissuring being common to Dublin boulder clay[3] is supported by the observations of most workers in the soil (e.g. Farrell et al. (1988)).

Discontinuities do occur in the till in the form of sand lenses, which originate from englacial melting and flow (Boulton, 1972), possibly involving flow into gaps and cavities that form in the lodgement till as it is folded. A typical sand lens is shown in Fig. **2.2.8**. Tunnel roof failure in till has been found to be due to veins of sand running above the tunnel crown (Matheson

[3] The reason for this is the high resistance the soil has to swelling due to structural strength, which is shown in Chapter 6.

(1970), Bevan and Parkes (1978)[4] and Baker et al. (1998)). Typically, blocks of boulder clay fall away from the crown under the influence of gravity and the lack of cohesion of sand; it is expected that sand lenses would also act as discontinuities in slopes. Treacy (1995) and Eisenstein and Thomson (1978) reported that the sand lenses are saturated and under pressure and discharge large amounts of water into excavations before the flow stops, hence the lenses are not connected to recharge sources. It is noted that sand lenses probably alter long-term ground movements by acting as a conduit for ground water flow and hence affect mass permeability. In tunnelling, the greater pore space will also limit the effectiveness of compressed air (Bevan and Parkes, 1978).

Eisenstein and Morrison (1973) measured the stiffness of sand lenses with the pressuremeter and found these to be comparable with the surrounding overconsolidated till. Tests conducted during the course of the Dublin Port Tunnel investigation (Geoconsult-Arup, 1997) indicated values for the shear strength of the sand lenses to be in a range similar to the surrounding till (404 kNm^{-2} to 1033 kNm^{-2}, varying with cell pressure in the consolidated triaxial test). Hence, the sand lenses are comparable to the till in terms of stiffness and strength. DeJong (1970), who showed that the deformation of a sand unit underlying lodgement till was comparable to that of the till, supports this view.

Stiff laminated clay is found around the Dublin Port and Ringsend area of thickness 0 – 5 m, increasing significantly near Poolbeg to about 15 m (Naylor, 1965) and is known as the Port Clay. It is a stiff laminated clay, filling depressions in the underlying boulder clay. The origin of the Port Clay has been variously attributed to outwash and glaciomarine deposits, owing to the presence of shells and quarternary marine molluscs (Hoare, 1991). More recently, however, Eyles and McCabe (1991) made a convincing argument for the presence of glaciomarine sediments due to marine flooding. This flooding is caused by glacio-isostatic depression at the ice sheet margin; i.e. sea flooding of the isostatically-depressed land on glacier retreat. (During deglaciation, interaction between ice-margins and the isostatically recovered earth's crust results in high relative sea levels, as evidenced by the raised beaches along the east and south coasts of Ireland (Hoare, 1987)). McCabe (1996) gives a similar description, where 'discrete wedges' of glaciomarine material are a function of isostatic depression and high relative sea levels at ice

[4] Although not explicitly stated in the paper, it can be deduced that this tunnel was in Dublin.

margins. The Port Clay is firm in situ but, when tested in the laboratory, is found to be normally consolidated, indicating significant sample disturbance (Farrell and Wall, 1990).

Since the time of deposition of the Port Clay on glacier retreat, soft estuarine clay of Holocene origin has been deposited in Dublin harbour and bay. Furthermore, isolated pockets of soft alluvium can be found that are attributable to old streams.

The properties of Dublin boulder clay, the soil of interest to this study, are given in Tables **2.2.1(a)** and **2.2.1(b)**. These tables also represent a database of similar, very stiff, till that is found in Britain, Scandinavia and Canada, i.e. in the same latitudes (see the end of Table **2.2.1(b)** for references). A large amount of research work has been conducted on these tills, particularly the limestone based, Scandinavian tills, and this work therefore represents a valuable source of information. Hence, the tables are also given as a way of validating the use of these data, i.e. if it can be shown that the fundamental properties are similar to Dublin boulder clay, it is likely that the soil behaviour is similar. The stiffness characteristics of the tills are not collated because of recent developments in the measurement and understanding of soil stiffness, which has rendered much of the available data obsolete. Instead, the soil stiffness data are given special treatment in Section 2.5. It is evident from the tables that the Dublin soil is of a similar consistency, density and strength to many of the tills found at similar latitudes.

Table 2.2.1(a). Database of the index and state properties* of stiff tills

Paper Reference. Till	w_n: %	w_l: %	w_p: %	γ_b: kNm^{-3}	e_0	G_s	γ_d: kNm^{-3}
1a. Tallaght black	10.6	23	17	22.4	0.33	2.69	
1b. Tallaght brown	8.7	26	17	22.4	0.28	2.69	
1c. Merrion black	9.5	30	16	22.8	0.29		
1d. Merrion brown	8.6	26	14	23.5	0.24		
2a. Amager	13.4				0.36		
2b. Odense	10.1	19.2	10.5		0.27		
2c. Carlsberg II		19.9	11.1		0.33		
2d. Krathbjerg	12	17.9	10.8		0.32		
2e. Odense IV	12	20	9.8		0.32		
2f. Carsberg I	9	20.9	10.6		0.24		
3. Edmonton	15	30	16				20.8
4a. Glasgow	~ 10	0.1: I_l†					
4b. Redcar	~ 20	-0.5: I_l					
5. Edmonton	7-23	22-39	15-20	21			
6. Tallaght	8-11	19-31	5-14:I_p				
7a. Tallaght	12						
7b. Croke Park	12						
8. Dublin		21					
9. Storebaelt: Lower till	<11	16	5-7: I_p				
10. Edmonton	16	36	19				
11. Edmonton	15	20-40	10-20				
12. Edmonton	12	31	15		0.36		22
13a. Selset, Yorkshire	12			22			
13b. Salford, Lancs.	18			22.3			
13c. Taff Valley	9-17			18-21			
13d. Glasgow	13			21.5			
13e. Comes, Norfolk	5-13						
13f. Hartlepool lower till	10-16	27-40	15-				
13g. Braden Dam, Ayr	7-13	13-22	22:I_p	19.1-24.5		2.66-2.71	
13h. Unknown: weathered	17.8		1-8: I_p	20.3			
unweathered	15.5			22.6			
13i. Unknown	10.3						18.6

* w_n is natural water content, w_p is the water content at the plastic limit, w_l is the water content at the liquid limit, γ_b is the bulk unit weight, e_o is the in situ void ratio, G_s is specific gravity and γ_d is the dry unit weight.

† I_l is liquidity index and I_p is plasticity index where w_l and w_p are not given in the paper.

Table 2.2.1(b). Database of the strength properties* of stiff tills

Paper. Till	c_u: kNm^{-2}	ϕ': deg.	c': kNm^{-2}	q_b: MNm^{-2}	ε_f: %	c'_{ps} kNm^{-2}	ϕ'_{ps}: deg.
2a	113-130						
2b	200-530						
2c	194-250			0.9-2.6			
2d	183-200	30-34.5	23.5-42.5	1.18-2.57			
2e	270						
2f	700-750	31-34	28-72	5			
3	373-538†				13.1-15.4		
	381-682				6.7-12.3		
6		39	0			0	37
7a/b‡	450	35	0			0	35
8		42	0				
		34 ± 1¶	0				
9	>500						
10	275†						
11	140-245†						
13a		32	8.5				
13b		36	32				
13c		28-42	0-40				
13d		28-32	9.5-24				
13e		25-30	34-55				
13f	245-575						
13g	143-162	41.3	0-37				
h: weathered							
unweathered			58				
13i	140-245	25					
14.Storebaelt lower till	150-400						
15. Dublin		42	0			0	43.8

* c_u is the undrained shear strength, ϕ' is the effective friction angle, c' is the cohesion intercept, q_b is plate bearing capacity, ε_f is the strain at failure in undrained triaxial test and ps is plane-strain

† Confined Undrained (cell pressure 207 kNm^{-2})

‡ Assumed values ¶ Reconstituted soil

1. Farrell et al. (1995b); 2. Jacobsen (1970); 3. DeJong and Harris (1971); 4. Weltman and Healy (1978); 5. DeJong and Morgenstern (1973); 6. Farrell et al. (1988); 7. Farrell et al. (1995a); 8. O'Shea (1996); 9. Sloan (1994); 10. Matheson (1970); 11. Eisenstein and Thomson (1978); 12. Thomson and El-Nahhas (1980); 13. Numerous papers in 'The Engineering Behaviour of Glacial Materials (Proceedings of the Symposium held at the University of Birmingham, 21-23rd April, 1975, revised and reprinted), Geo Abstracts, Norwich, 1978, 129-137'; 14. inter alia Foged et al. (1995); 15. Treacy (1995).

2.2.6 Rock.

The rocks that have contributed to Dublin boulder clay, i.e. the Palaeozoic shales, mudstones and limestones, give rise to the typical black colour of the boulder clay. The rock underlying the till is generally intact limestone, although granite predominates in the south. An incised channel, running NE-SW is incised into the limestone rock, the discovery of which is attributed to Farrington (1924). This channel is believed to be in-filled with boulder clay (Farrell and Wall, 1990) and is, therefore, attributed to an ancient river valley.

Ice abrasion and plucking gives rise to an improved, intact, rockhead surface that may have been previously weathered over time (Boyer et al., 1985). This appears to be the case with the limestone under Dublin. Where the surface is not improved it will be evident in localised rubble zones and faults due to glaciotectonic activity. Extremely high water pressures can occur in the cracks in the rock, thus generated, by the weight of ice, which further increases the width of the faults. Experience of these faults in Toronto (Baker et al., 1998) suggests that these are inconsequential in terms of load bearing and settlements in the till above because of small throws and narrow fault planes.

The limestone in the Dublin area has not yielded any evidence of karstic features, possibly due to the shale/mudstone inclusions sufficiently lowering the pH. However, shale and mudstone intrusions can act as low-angle slip surfaces.

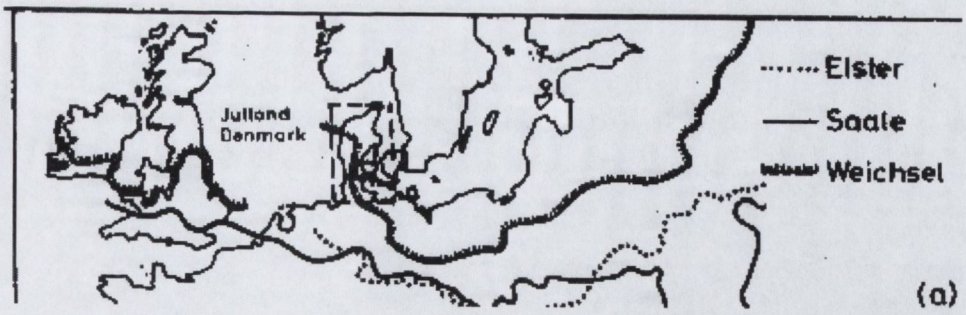

Fig. 2.2.1. The Europe-wide extent of the Last Glaciation, after Steenfelt (1997)

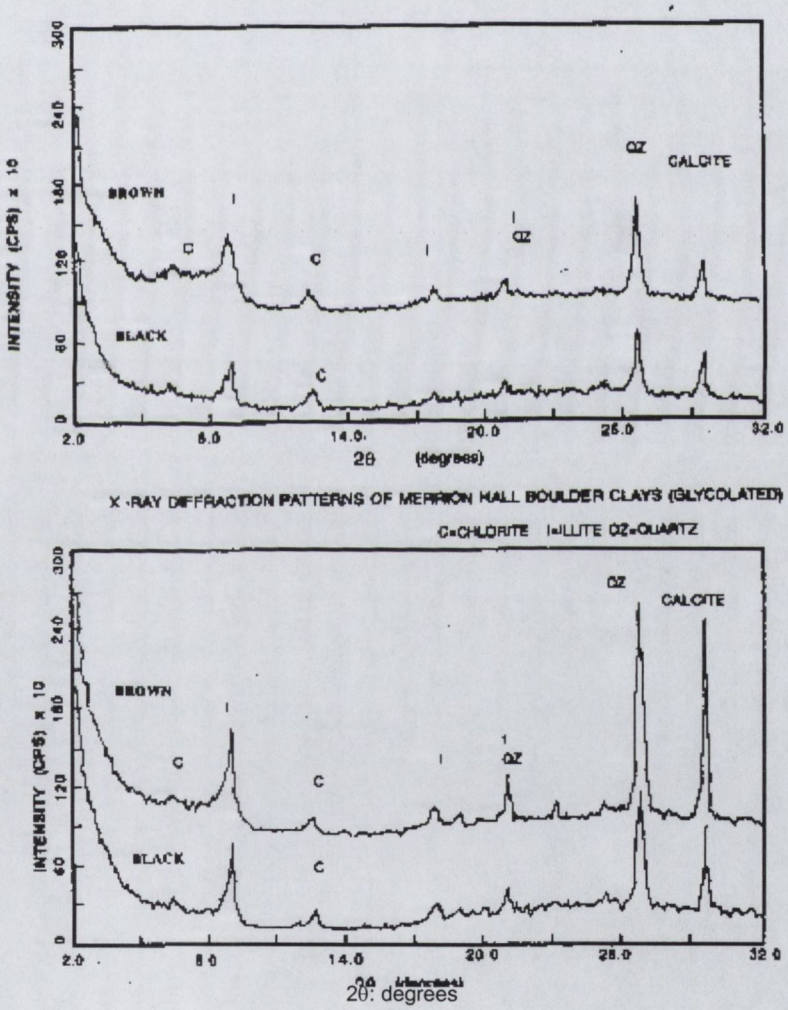

Fig. 2.2.2. X-ray diffraction trace for Dublin boulder clay, after Farrell et al. (1995b)

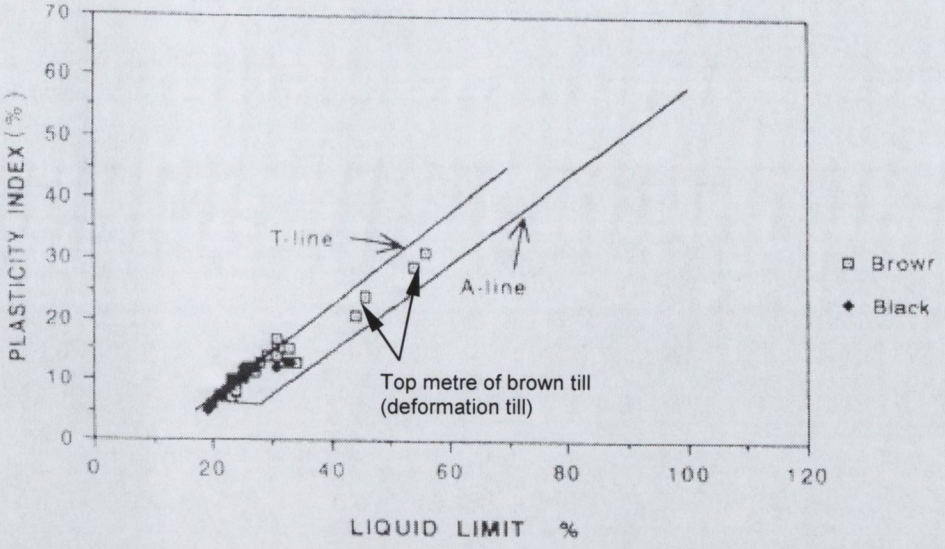

Fig. 2.2.3. Typical plasticity chart for Dublin boulder clay, after Farrell et al. (1995b)

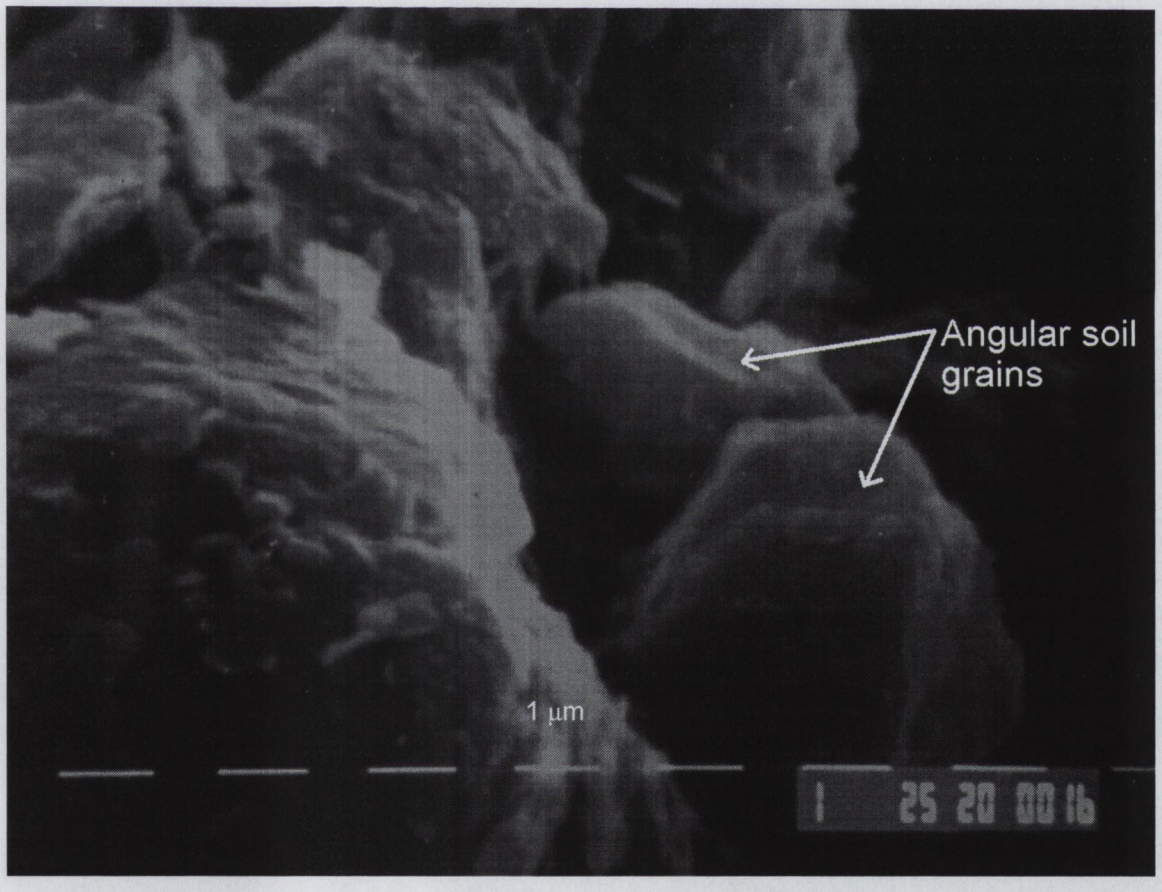

Fig. 2.2.4. Scanning electron micrograph showing the angularity of the soil grains, after Farrell et al. (1988)

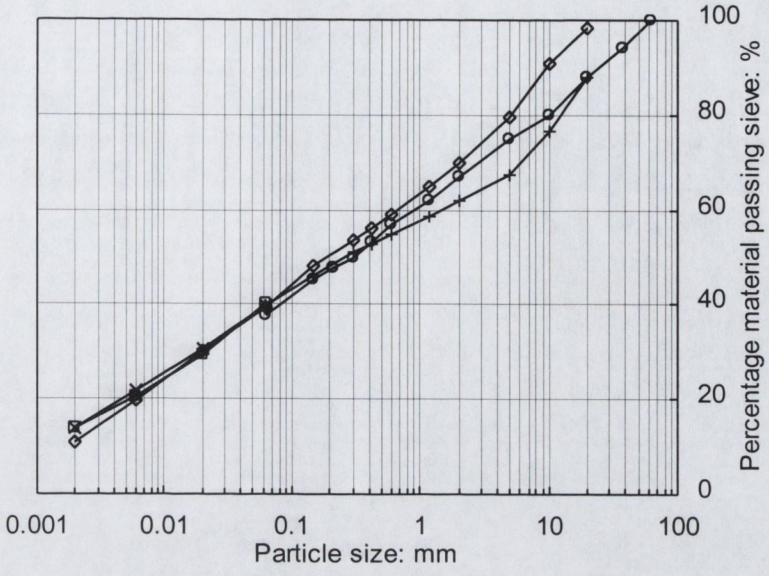

Fig. 2.2.5. Typical PSD plot for Dublin boulder clay

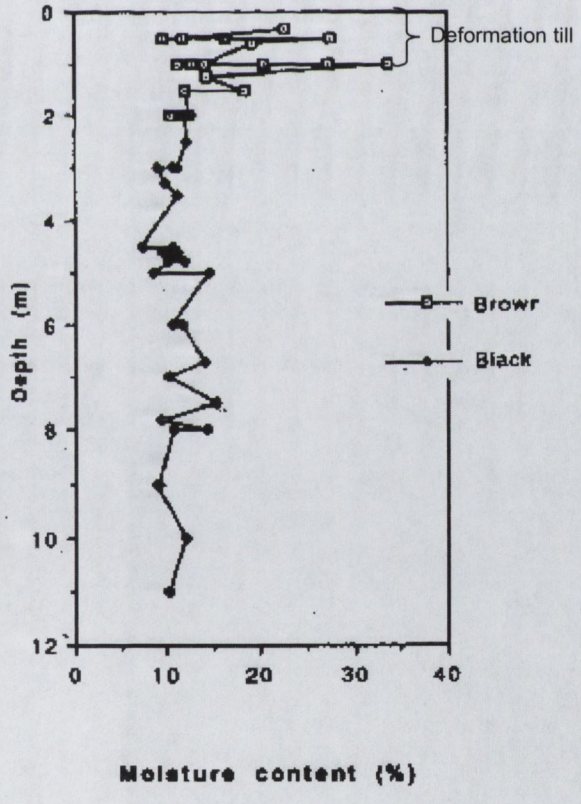

Fig. 2.2.6. Typical water contents of Dublin boulder clay, after Farrell et al. (1995b)

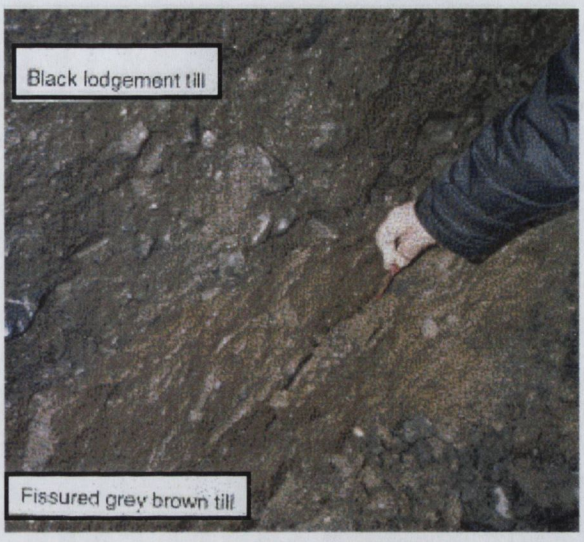

Fig. 2.2.7. Fissured soil underlying Dublin boulder clay at Griffith Ave., Marino

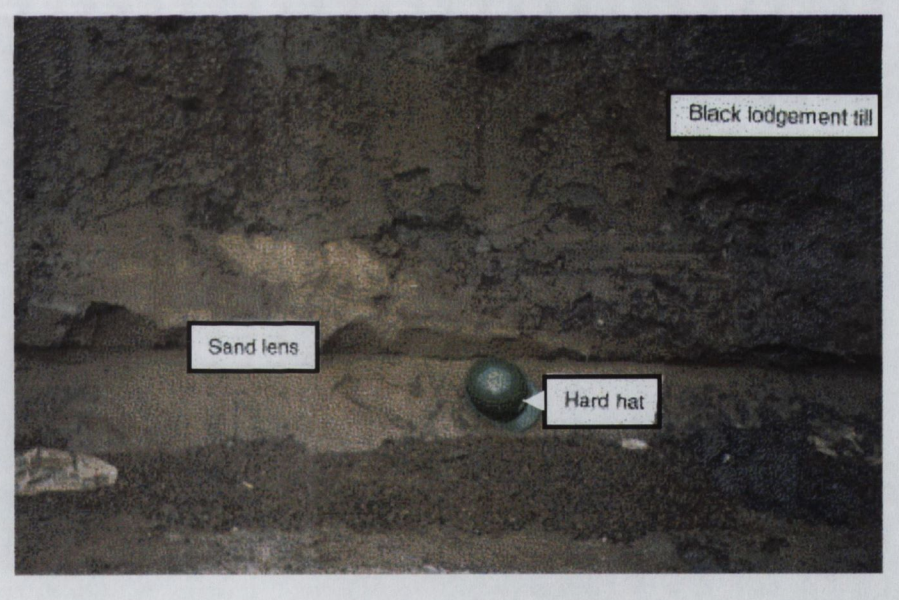

Fig. 2.2.8. Typical sand lens in Dublin boulder clay (Griffith Avenue, Marino)

2.3 Sampling.

2.3.1 Representative Sampling of Boulder Clay.

Representative sampling is the term given to the process that allows small soil samples tested in the laboratory to be representative of the soil mass. The presence of joints and fissures generally controls the representative sample size of soil, as shown in Fig. **2.3.1**. Fissures are of greatest consequence in relation to soil properties and anisotropy, particularly strength (Anderson and McKinlay, 1978). Fortunately, as discussed in Section 2.2.5, fissuring is not common to Dublin boulder clay. The lack of fissuring is particularly helpful in laboratory testing; which can be seen in Fig. **2.3.2**, where the adverse effects of fissuring on the, intensely fissured, London clay is evident.

The size of a sample is believed to have a relatively insignificant effect on laboratory measured strength; this is in contrast to the adverse effects of fissuring (see above) and of the sampling method (e.g. drive sampler versus cores; Faillace and Silver (1978)). Incompressible stones will tend to have greatest influence on soil compressibility characteristics; hence the till sample should contain a gravel fraction to be representative. (An increase in gravel content will increase strength and soil stiffness and vice versa.) Fookes et al. (1978) suggested that a sample of boulder clay is unrepresentative if above medium size gravel is absent. Furthermore, owing to the wide range of particle sizes (see Fig. **2.2.5**) and gravel and boulder inclusions, it is often necessary to be selective when taking samples for testing.

2.3.2 Soil Disturbance.

Sampling of soil disturbs a specimen through mechanical shearing and through relief of stresses. Sampling in Dublin boulder clay with the U100 drive-sampler requires the use of a thick wall (wall thickness greater than 85 mm), owing to the high stiffness of the ground and the presence of stones. The subsequent disturbance involves the pushing of gravel ahead of the cutting-shoe. If the soil sample is allowed to swell excessively, a decrease in density will accrue and the strength of the soil will be underestimated. Furthermore, there is evidence that the yield stress of the soil decreases with time if the soil is allowed to swell (Arman and McManis, 1976). Hence, sampling tubes should fit tightly around the soil to provide restraint, thus

preventing stress relaxation, and to preserve the soil's water content from the time of extraction to testing in the laboratory. The standard U100 drive sampler is a good method of sample preservation in these respects. It follows that the disturbance caused by driving the thick-walled shoe into the boulder clay may be outweighed by the positive effect of sample preservation. Therefore, good quality samples may be obtained with the standard drive sampler.

It would be expected that low plasticity Dublin boulder clay would be relatively insensitive to sampling remoulding by either the shear stress of the cutting shoe or rotary corer. Furthermore, the very high soil density should maintain the original soil macro-structure by holding large particles in their original place in the soil matrix. However, the high density also means that large shear stresses can develop (at small shear strains), which can cause excess pore water pressures to develop. Hence, the soil should be stored for some weeks before testing to allow equalisation of the excess water pressure (Chandler et al., 1992b). It is clear that no single sampling effect can be taken in isolation.

It is generally thought that soil samples chiselled from blocks improve upon cores. A comparison of the strength of block samples of Treacy (1995) with the cores of O'Shea (1996) does not support this view, however (these tests are shown in Fig. **2.6.2**). This is probably due to the effects of soil variability, which out-weigh the, relatively minor, effects of sampling disturbance, discussed in this section, in the case of Dublin boulder clay.

When sampled, soil takes the stress path shown in Fig. **2.3.3**. The deviator stress is reduced to zero and the stress in the sample is a mean stress. If the sample has been perfectly sampled, measurement of the soil suction will give the mean effective stress in the ground. However, Vaughan et al. (1993) and Chandler et al. (cited) showed that an open-tube drive sampler could increase the effective stress in samples of stiff to very stiff London clay.

The most important factor in soil sampling of boulder clay is obtaining a cylindrical specimen of sufficient length for testing in the laboratory that does not contain fractures induced by extraction or handling. If this is done, the disturbance effects discussed above can be mitigated in the consolidation stage of the soil test. To do this, the SHANSEP approach (Ladd and Foott, 1974) is often used. With reference to Fig. **2.3.4**, it can be seen that SHANSEP recommends reconsolidating to well beyond the yield stress, σ_{vy}', in order that the NCL (normal

consolidation line) be rejoined. However, in the case of very stiff lodgement till, the yield stress is very high and there is evidence (Hight et al., 1985) that σ_{vy}' must be greatly exceeded in order that the NCL be rejoined. Therefore, any attempt to apply the SHANSEP approach to very stiff till will result in a substantial increase in the soil density. Instead, this thesis investigated the reconsolidation of boulder clay by examining the stresses set-up in the sample as a result of a reconstructed stress-history, without exceeding σ_{vy}', which is the practice followed by the DGI and SGI for stiff clay tills (e.g. Jacobsen (1970), Foged et al. (1995) and Steenfelt (1997)).

Measurement of the yield stress, which is obtained from the primary loading curve in the oedometer, requires that very high quality sample be tested. It is evident from the discussion in this section that, prior to testing, three events can cause the soil sample to differ from the in situ soil: (a) soil sampling, (b) handling and (c) storage. Hence, throughout the laboratory test series conducted for this thesis, great care was taken to minimise the disturbance effects.

Standard soil sampling in Dublin boulder clay is conducted with driven tubes (U100) and rotary coring. The latter requires an air-mist/water drilling fluid/flush. From experience, however, these methods often lead to low total core recovery (TCR) (Weltman and Healy, 1978). In an attempt to overcome this problem, a new method of coring in stiff boulder clays was examined by Jonsson et al. (1995) and applied successfully to stiff boulder clay in the course of the Storebaelt bridge project (inter alia Foged et al. (1995)). Based on this, the method, called Geobor S, was adopted for this project.

2.3.3 Reconstituted Soil Testing.

Owing to the difficulty of obtaining undisturbed samples of boulder clay, there is an interest in the use of the reconstituted soil in soil testing. (The relevance of reconstituted testing to Dublin boulder clay is critically examined in this thesis.) Reconstituted clay is a clay mixed at a water content of 1-1·5 times the soil liquid limit; the soil is then preferably consolidated one-dimensionally (Burland, 1990). When tested, reconstituted soil gives the intrinsic properties of the intact soil, i.e. the properties inherent to the soil but independent of the natural state. For

example, overconsolidation and soil structure affect the compressibility characteristics of clay but these are not intrinsic properties.

It was of importance to the study to compare intact and reconstituted soil behaviour to aid the understanding of the behaviour of the intact till. However, to allow a true comparison of the intact and reconstituted soils, the particle sizes in the samples must be equal. This generally presents a problem in Dublin boulder clay due to the limit on maximum particle size in oedometer tests and the wide-range of particle sizes in the soil. In the past, this has led to the entire fraction greater than 2 mm being removed, which has caused significant differences in the saturation moisture content of the intact and reconstituted samples and therefore different void ratios (Faulkner, 1998).

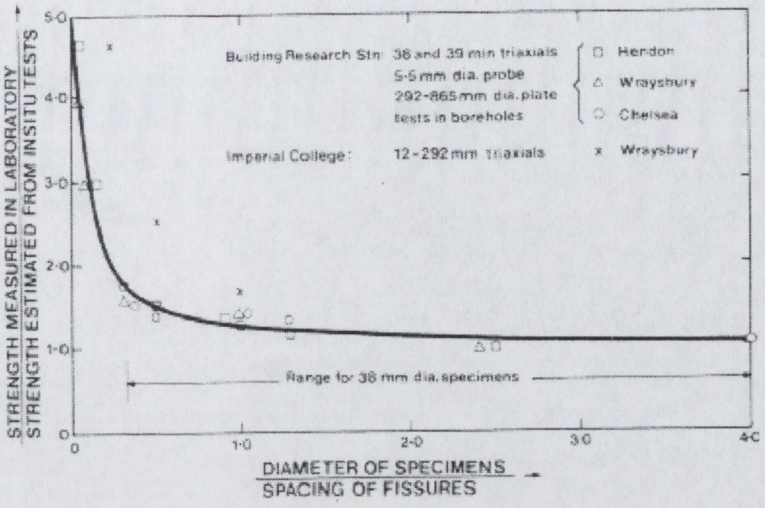

Fig. 2.3.1. Influence of the ratio of sample size to fissure spacing on the strength of London clay, after Simpson et al. (1979)

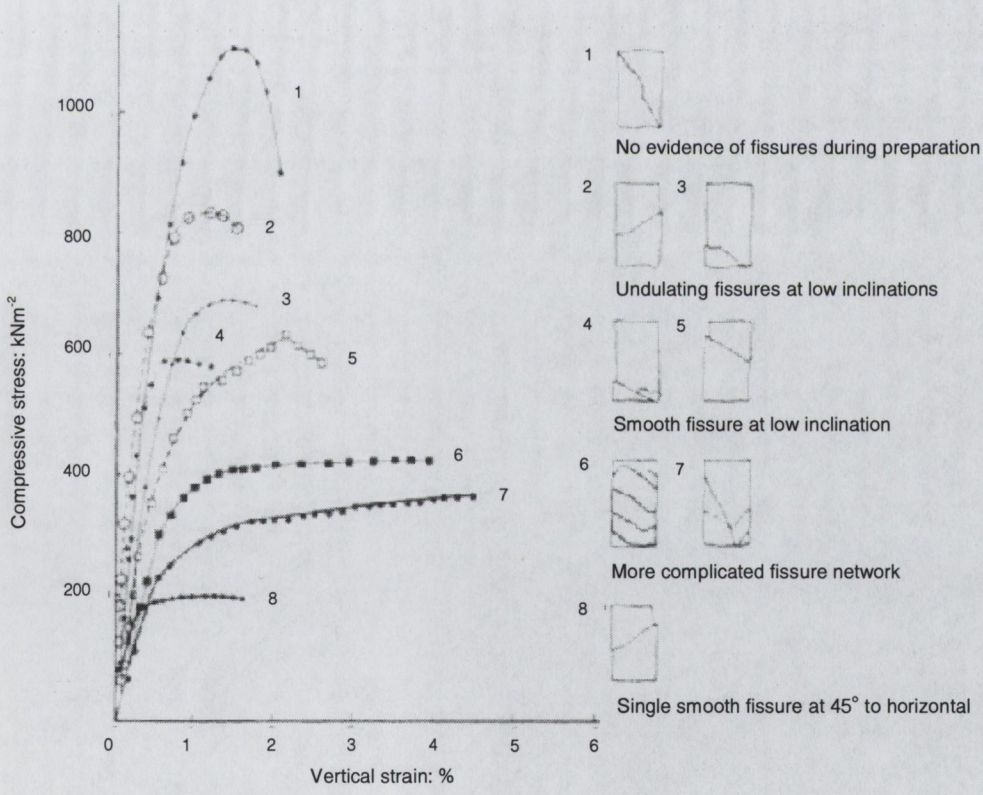

Fig. 2.3.2. The adverse effects of fissuring on the stress-strain characteristics of stiff clay, after Simpson et al. (1979)

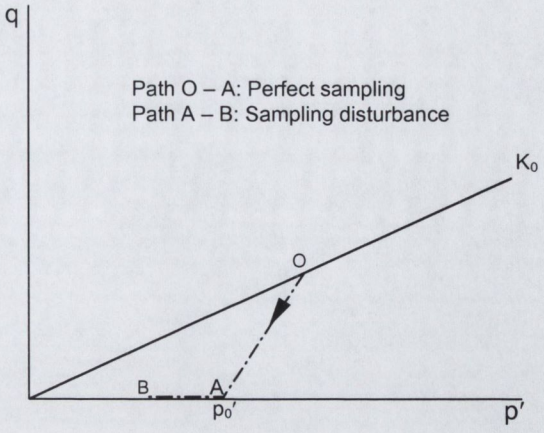

Fig. 2.3.3. Stress-path taken by soil when sampled, adapted from Hight et al. (1985)

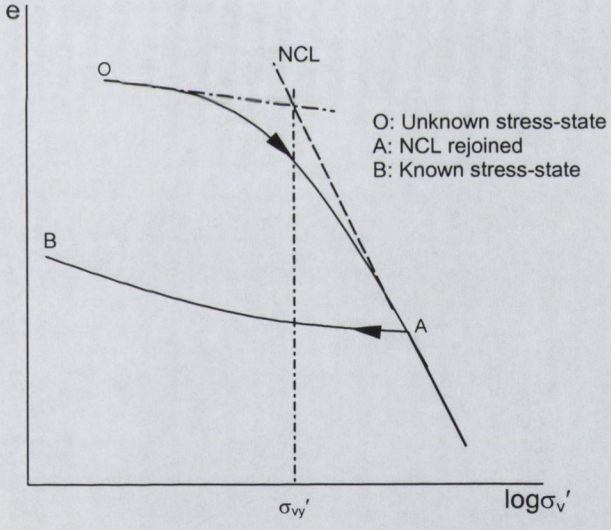

Fig. 2.3.4. SHANSEP method of removing sample disturbance effects, adapted from Ladd and Foott (1974)

2.4 Stress-History.

2.4.1 Soil Overconsolidation.

The importance of accurately measuring the stress-history of the till is adequately demonstrated by examining the controlling influence of the overconsolidation ratio, OCR or R_p (the latter for isotropic stress conditions), on very important properties of soils, namely stiffness, strength and the in situ stress-state.

Viggiani (1992) developed the following formula for the shear modulus of soil at very small strain, G_0, which shows a dependence of G_0 on R_p:

$$G_0/p_a = A(p'/p_a)^n(R_p)^m \qquad [2.4.1]$$

where p_a is a reference pressure, p' is the mean effective stress and A, n and m are measurable constants (Atkinson, 2000).

Wroth (1984) showed that the following theoretical formula for undrained shear strength is fundamental to critical state soil mechanics (CSSM):

$$c_u/\sigma_v' = (c_u/\sigma_v')_{nc}.(R_p)^{\Lambda} \qquad [2.4.2]$$

where c_u/σ_v' is the undrained shear strength ratio (CIU test) and Λ is the 'plastic volumetric strain ratio'.

Furthermore, Wroth demonstrated the importance of Equation [2.4.2] by showing its similarity with the empirical formula based on the SHANSEP (Ladd and Foott, 1974) approach (see Mayne (1988)):

$$c_u/\sigma_{v0}' = (c_u/\sigma_v')_{nc}.(OCR)^m \qquad [2.4.3]$$

where m is an empirical number that varies with OCR and corresponds to Λ.

Schmidt (1966) examined the data of Hendron (1963) and found the following relationship, which showed that K_0, the coefficient of earth pressure, is controlled by the soil OCR. Mayne and Kulhawy (1982) subsequently adopted the equation in a generalised form:

$$K_0 = K_0^{nc}.(OCR)^{\sin\phi_p'} \qquad [2.4.4]$$

where K_0^{nc} is the coefficient of earth pressure in the normally consolidated state and ϕ_p' is the peak effective angle of friction.

Furthermore, K_0 obtained from well-known elastic theory demonstrates the controlling influence of OCR on the in situ stress-state:

$$K_0 = K_0^{nc}.OCR - (OCR - 1).\nu'/(1 - \nu') \qquad [2.4.5]$$

where ν' is the Poisson's ratio.

The yield stress, σ_{vy}', is the vertical effective stress beyond which plastic straining becomes significant in one-dimensional compression (Burland, 1990), which is generally considered to be the past maximum stress that a soil has been subject to. The OCR of a soil is the ratio:

$$OCR = \sigma_{vy}'/\sigma_{v0}' \qquad [2.4.6]$$

where σ_{v0}' is the in situ vertical effective stress.

The yield stress is generally measured in the oedometer by applying increments of load well beyond (about ten times) its possible value and graphically determining the actual value by the Casagrande method. Other methods of interpretation are available (Tavenas et al. (1979), Butterfield (1979) and Janbu (1991)), which are examined in detail in this thesis.

Strain rate effects can have a significant effect on the measurement of σ_{vy}'. However, these effects are reduced by loading the soil for non-constant duration and with $dP/P \approx 1/3$ (Leroueil et al., 1983), where P is the current load and dP is the load increment, as opposed to the

standard, dP/P = 1, method. There is also evidence that the value of the yield stress decreases with time if the soil is allowed to swell (Arman and McManis, 1976).

Practical experience with estimating the yield stress of stiff boulder clay from standard oedometer tests suggested that it is very difficult (e.g. DeJong and Harris (1971)). However, some, small diameter, intact consolidation tests have been conducted on Dublin boulder clay (Lehane and Simpson, 2000). These tests, which were conducted in the standard apparatus and adjusted for apparatus compliance, are shown in Fig. **2.4.1**. The value of the yield stress estimated (by the Butterfield (1979) method) was very high, namely 1300 ± 300 kNm^{-2}. There is evidence from Fig. **2.4.1** that the consolidation curve was insufficiently defined, possibly owing to the high-pressure requirement and system compliance, for accurate measurement of σ_{vy}'. For this reason, a special, high-pressure, device was developed for this thesis. Boulton and Paul (1976) have suggested a theoretical value of 500 kNm^{-2} for the near-surface deformation till based on measurements of the apparent preconsolidation of soil by freezing. (Freezing of the soil will have occurred in post-glacial times – see Section 3.4).

2.4.2 Coefficient of Earth Pressure, K_0.

Donath (1891) defined the coefficient of earth pressure at rest, K_0, as the ratio of the horizontal to vertical earth pressure resulting in a soil from the application of vertical load under a condition of zero lateral strain. This condition is relevant to glacial consolidation. For soils in a normally consolidated state, the ratio is K_0^{nc}. The stress history of the soil, as reflected by the initial K_0 stresses, has a major influence on the response of a soil and a numerical model, owing to the stress-dependency of stiffness and other important parameters.

The direct measurement of K_0 is conducted in the field with the pressuremeter and in the laboratory with specially designed apparatuses (for example, Hendron (1963) and Brooker and Ireland (1965)). It is important that both these methods be compared and be compared, in turn, with empirical formulae that have been proposed and with the estimation of the swelling pressure (Bishop et al., 1965) or soil suction. The swelling pressure, p_k, of a soil, is the pressure at which the soil neither consolidates nor dilates and is a mean stress (as is the soil suction). Hence, to obtain K_0 the following formula is employed:

$$p_k = \sigma_v'(K_0 - A_s(K_0 - 1)) \qquad [2.4.7]$$

where A_s is the pore pressure parameter. Estimation of K_0 by suction stress is possible if the suction stress is representative of the in situ effective stress, as discussed in Section 2.3.2.

The main requirement for the measurement of K_0 in the laboratory is the condition of zero radial strain. According to Terzaghi (1934), K_0 tends to K_a, the lowerbound active limit, for a lateral strain in the order of 0·1%. Hendron (1963) and Brooker and Ireland (1965) obtained an accuracy of 0·002% in their corrective motion oedometer and Bishop (1958) obtained an accuracy of 0·008% in a modified triaxial cell with a mercury dial to measure radial strain. This thesis adapted the Bishop triaxial cell approach but with local strain transducers and computer control, mainly because it allowed subsequent shearing of the K_0 consolidated soil specimen.

An alternative to active measurement of K_0 is passive measurement in a pressure cell. However, this thesis developed an apparatus based on active control of the radial strain rather than the apparatus of Dyvik et al. (1985), for example. This was because, in passive measurement: (a) the energy stored on loading is released on unloading and is believed to overestimate K_0, (b) zero drift and (c) temperature sensitivity (Martin (2001) and Germaine (2002)).

Hight et al. (1985) found that the sample disturbance effects were removed only when an anisotropic stress-path with continuous stress changes is followed in the consolidation stage of triaxial tests. This K_0 consolidation procedure is in contrast to the simple, two-step, method (Kirkpatrick and Khan, 1984), which is not suitable to brittle (low plasticity) clays, as it can cause failure in the sample.

K_0 measurement and K_0 consolidation is not straightforward and a number of factors must be taken into account. In the triaxial apparatus, the fluid pressure applies a uniform surface stress and a significant pore pressure gradient (either vertically or radially) towards the drainage surfaces can lead to a significant departure from zero lateral yield. Appreciable pore pressure gradients are avoided in low permeability, fully saturated soils if the test is run at a steady, slow rate of loading, i.e. not step-wise, which would cause an undrained response (Bishop, 1958). Furthermore, radial strain should preferably be measured along the length of the sample.

However, in the triaxial method of K_0 consolidation, shear stresses along horizontal and vertical boundaries are minimised and are practically zero for zero lateral yield; this is in contrast to the pressure cell type of oedometer, where vertical shear stresses, developed on the ring wall, can be significant.

In the field, the pressuremeter can be used to measure the value of the total horizontal ground pressure. In the vicinity of σ_{h0}, the in situ horizontal effective stress, the soil behaves elastically and the pressure versus cavity strain curve is therefore linear. The procedure is discussed in detail in Section 4.7.1.

Mayne and Kulhawy (1982) demonstrated a power law dependence (Equation [2.4.4]) of K_0 on the OCR of the soil, based on the work of Schmidt (1966), who, in turn, based the power law on measurements of K_0 by Hendron (1963) in sands and Brooker and Ireland (1965) in clays. The results showed a linear relationship between the horizontal and vertical effective stresses on first load of normally consolidated soil. This constant slope value was found by Hendron (cited) to comply with the formula derived and simplified by Jaky (1944) for the lateral pressure of unconsolidated granular material in silos:

$$K_0^{nc} = 1 - \sin\phi' \qquad [2.4.9]$$

The value of ϕ' is often, but incorrectly, taken as the peak value rather than the constant volume value, ϕ_{cv}'. Several authors have derived theoretical equations for K_0^{nc} (see Schmidt (1966)) and recently Simpson (1992) derived an equation, which has validated Jaky's formula.

Fig. **2.4.2** shows a typical relation of the vertical effective stress to the horizontal effective stress of clay. On unload, the value of K_0, inferable from this plot, remains below 1 up to low vertical effective stresses, typical of those in the ground, at which point, the horizontal effective stress exceed the vertical effective stress. From Equation [2.4.4], it can be seen that the higher OCR is, the greater the potential value of K_0. In highly overconsolidated soils, the value of K_0 can approach the passive limit, at which point fissuring of the soil occurs, defined by the Rankine passive limit, K_p:

$$K_p = (1 + \sin\phi_p')/(1- \sin\phi_p') \qquad [2.4.10]$$

where ϕ_p' is the peak effective friction angle.

The coefficient of earth pressure of the Dublin boulder clay has not been measured but has been inferred from finite element back-analysis (Lehane and Simpson, 2000). This prediction involved applying a preconsolidation stress of 1300 kNm^{-2} to the surface of the soil modelled with the Brick (Simpson, 1992) FE code. In the code, K_0 tends to $(\sqrt{2} + \sin\phi')/(\sqrt{2} - \sin\phi')$ and ϕ' increases as the degree of overconsolidation increases. The results, shown in Fig. **2.4.3**, indicate potentially very high values of K_0 that are close to the passive value, K_p, near-surface. K_0 of stiff till has also been inferred from the deformation of tunnels in stiff till in Edmonton, Canada (Eisenstein and Thomson (1978) and Thomson and El-Nahhas (1980)). Edmonton till is a highly overconsolidated, low to medium plasticity, well-graded, sandy or silty clay. The properties of this till are such that it is suitable for comparison with Dublin boulder clay, as demonstrated in Tables **2.2.1(a)** and **2.2.1(b)**. Inferring K_0 from tunnel deformation is conducted by examining the inward horizontal and vertical deformations of the tunnel lining; if the horizontal deformation exceeds the vertical deformation then the value of K_0 is greater than 1. However, the results from Edmonton are inconclusive (K_0 was variously reported as being greater and less than 1), possibly because the value of K_0 is substantially reduced by the movement of the ground, as discussed before. There remains, therefore, a need for an assessment of the variation of K_0 in boulder clay with depth.

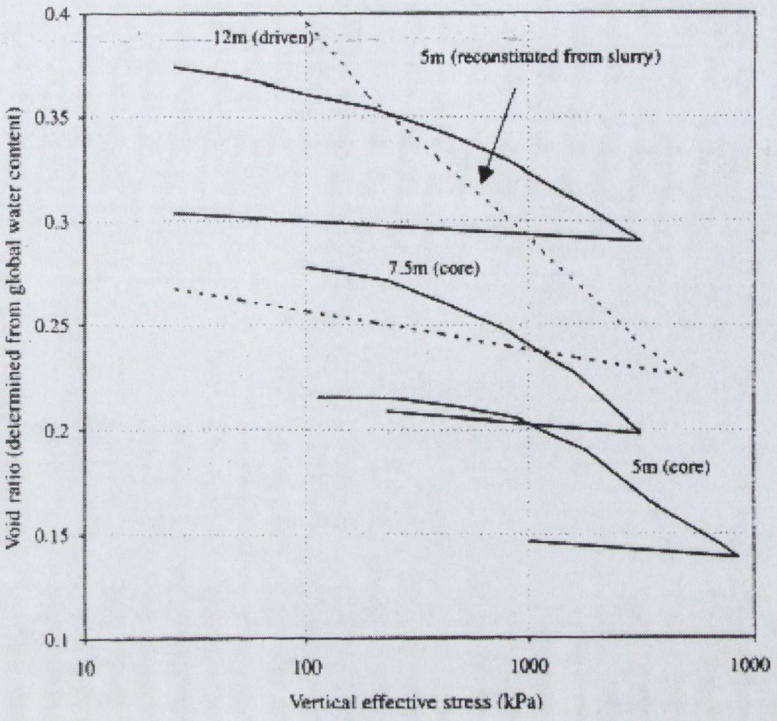

Fig. 2.4.1. Oedometer tests on Dublin black boulder clay, after Lehane and Simpson (2000)

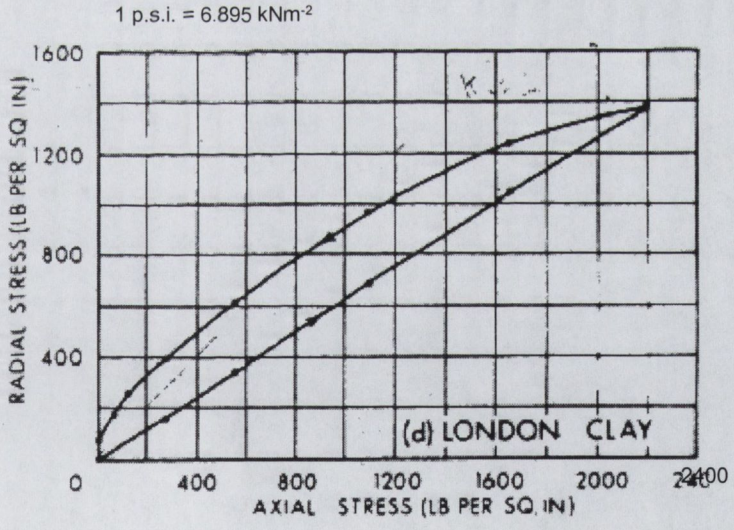

Fig. 2.4.2. Typical relationship between vertical and horizontal effective stresses in, initially normally consolidated, clay, after Brooker and Ireland (1965)

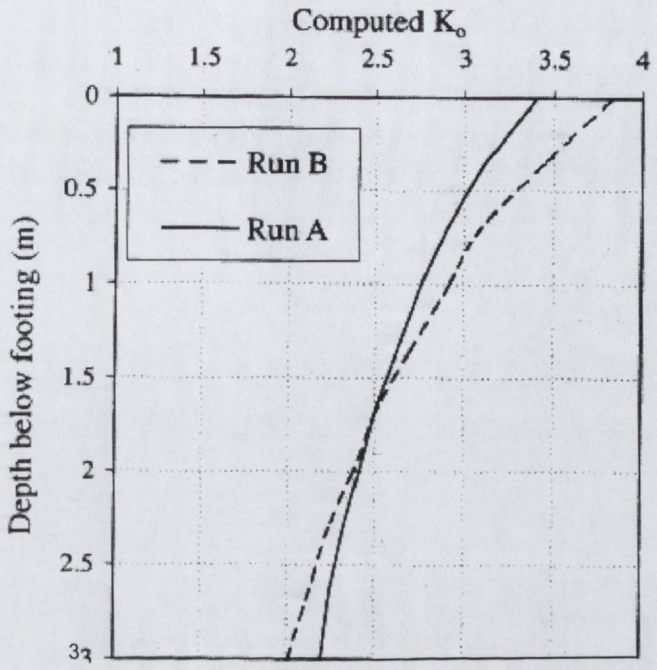

Fig. 2.4.3. 'Brick' estimates of K_0 of Dublin boulder clay, after Lehane and Simpson (2000)

2.5 Stiffness and Stress-Strain.

2.5.1 Introduction.

That the stress-strain behaviour of soil was linear and constant with depth in the ground was, for practical purposes, assumed to be commonplace practice for many years. It is now known that soil stiffness is highly non-linear, varying with strain level, confining stress level, stress-history, direction of loading and by definition, making the choice of a single stiffness modulus increasingly problematic. This section of the review aims to set-out the most relevant aspects of soil stiffness, the most relevant parameters and the most relevant methods of measurement.

2.5.2 Stress-Strain.

The laboratory stress-strain behaviour of isotropically consolidated, drained, triaxial compression tests (CID), on undisturbed Dublin black boulder clay (Treacy (1995) and O'Shea (1996)) are shown in Fig. **2.5.1**. (The pressures indicated beside the curves are the effective confining stresses.) These curves exhibit a distinct non-linearity and a dependence of the strength of the soil on the effective confining stress applied in the test. Three of the four curves are practically hyperbolic, which is consistent with the well-known work of Konder (1963), who identified a trend of hyperbolic stress-strain curves in CID tests on cohesive soils.

The applicability of such non-linear stress-strain behaviour measured in the laboratory to actual foundation loading is rarely examined, however. Fig. **2.5.2** shows an early appreciation of the effect by DeJong and Harris (1971) for footings founded on stiff lodgement till. In a similar way, Fig. **2.5.3** represents a re-examination of a foundation on Dublin boulder clay (Farrell et al., 1988). The non-linear curve-fit on the diagram is non-linear hyperbolic, which appears to improve upon the linear curve-fit (also shown) suggested originally. The variability of soil stiffness, apparent from these examples, is examined in detail in the following section.

2.5.3 Factors Affecting Soil Stiffness.

The variation of stiffness with stress-strain is firstly dependent on whether the stiffness is defined by a secant or tangent modulus, which is demonstrated in Fig. **2.5.4**. Furthermore, in contrast to the term 'soil modulus' etc, the use of the term shear, Young's or bulk modulus are unambiguous and are therefore preferable.

As discussed in Section 2.4.1, the influence of stress-history on stiffness can be seen in Equation [2.4.1], i.e. as the overconsolidation ratio increases, so too does the soil stiffness.

The variation of the stiffness of till with strain is evident in Fig. **2.5.5**. In these tests, reported by Atkinson (2000), reconstituted till was consolidated isotropically to various overconsolidation ratios, R_p. The plot shows the importance of overconsolidation to the magnitude of soil stiffness and to increased brittleness, which is evident from the greater reduction in stiffness with strain in the heavily OC soil relative to the lightly OC soil.

The influence of 'recent' stress-history on soil stiffness is demonstrated in Fig. **2.5.6**. This figure shows that if the direction of loading is reversed ($\theta = 180°$[1]), the soil becomes very stiff, in contrast to the case of no change in the direction of loading ($\theta = 0°$) and that for changes in direction between these extremes, the soil becomes progressively stiffer. At about 0·1% strain, the stiffness of the soil, regardless of recent stress history, converges. Simpson (1992) demonstrated that this behaviour is caused by reorientation of the soil particles. In the case of $\theta = 180°$, the soil particles have to fully reverse/realign; to do so the particles must overcome inter-particle forces before sliding relative to one another. The initial reorientation is elastic and very stiff; the elastic stiffness, which is the maximum shear stiffness of the soil, G_{max}, is a soil constant. Typical stress-path reversal cases are the unloading of soil in an excavation and the loading of a foundation placed in an excavation. As loading continues, the particles progressively realign and begin to slide, hence the soil becomes increasingly plastic/non-elastic, resulting in a highly non-linear stiffness variation with strain.

[1] For the precise definition of θ, see Fig. **2.5.10**.

This soil behaviour results in the characteristic stiffness-strain 'S' curve shown in Fig. **2.5.7**. (A feature of the S-shape curve is that a similar plot is obtained if shear stiffness is plotted against deviator stress.) The curve is initially defined by G_{max} up to a threshold strain (typically 0·001% - see Atkinson (2000)). G_{max} is generally measured in dynamic tests, e.g. bender element tests, and has been found by Viggiani (1992) to be given by Equation [2.4.1]. Once the threshold has been exceeded, the reduction in stiffness is pronounced.

The existence of a threshold for very small stress increments, below which the stiffness of the soil is well in excess of the stiffness for larger increments, has been known for some time (see Simpson et al. (1979)). It is often stated (inter alia Atkinson and Salfors (1991) and Atkinson (cited)) that the very small strain range is up to 0·001% of shear strain. This strain is called the threshold shear strain, ε_t, which separates elastic behaviour (i.e. all strains recoverable) from non-elastic behaviour (i.e. strains only partly recoverable). Theoretically (Hendron, 1963), ε_t should increase as the soil stiffness increases. In contrast, Atkinson (cited) has shown that the magnitude of ε_t decreases with decreasing plasticity, which is associated with an increase in stiffness. Matthews et al. (2000) demonstrated, however, that, overall, as the in situ stiffness of the ground increases, the limit of elastic behaviour increases, up to about 0·01% for weak rock. Fig. **2.5.8** shows small strain data adapted from a test conducted by O'Shea (1996) on Dublin boulder clay. The curve exhibits linearity up to about 0·006% axial strain and the threshold deviator stress associated with ε_t, of about 50 kNm^{-2}, is higher than the 10 kNm^{-2} generally quoted, owing to the very high stiffness. The value of the very small strain, drained Young's modulus of the test, E_0', is 820 MNm^{-2}. This value is very high, close, in fact, to E_0' of soft rock, which is in the range 960 – 1920 MNm^{-2} (derived in the same way by Izumi et al. (1998)). The relevance of elastic straining at axial strains of the order of 0·01% can be seen in Fig. **2.5.9**, which shows typical working strain ranges for various field structures. It may be expected, therefore, that very high stiffness is relevant to excavations in Dublin boulder clay.

Lehane and Simpson (2000) showed a dependence of the stiffness of Dublin boulder clay on the recent stress-history (i.e. the excursion of the stress-path from the previous direction of loading), on strain level and on stress level, as shown in Fig. **2.5.10**. It is evident from this graph that the boulder clay response to changes in direction of loading is not as obvious as the, ideal, reconstituted clay, case, shown previously in Fig. **2.5.6**. Nevertheless, there are some

indications of the phenomena, particularly the effects of strain level and stress-dependency on the soil stiffness. The nature of the stress-dependency of soil stiffness was shown by Janbu (1963) and has been widely used since to model soil stiffness (e.g. Duncan and Chang (1970) and Schanz and Vermeer (1998)). The relationship is in the form of a power law:

$$E_{50} = E_{50}^{ref}(\sigma_3'/p_{ref})^m \qquad [2.5.1]$$

where E_{50} is the secant Young's modulus at 50% strength in the triaxial drained compression test (CID), E_{50}^{ref} is the stiffness E_{50} at the reference pressure, p_{ref}, σ_3' is the effective confining pressure, p_{ref} is the reference pressure and m is a soil constant that reduces as the in situ soil stiffness increases and is typically 0·5 in stiff clays. Equation [2.5.1] has also been shown to be applicable to E_{oed}, the tangent stiffness measured in oedometer tests (Schanz and Vermeer, cited), which is defined in Fig. **2.5.11**, and to the stiffness measured on unload-reload in the CID test (Duncan and Chang, cited), which is defined in Fig. **2.5.12**. The stress-dependency stiffness equation of Janbu (cited) (Equation [2.5.1]) has, unfortunately, not been widely publicised (Schanz and Vermeer, cited) and its use is, therefore, not widespread. Instead, a Gibson soil has traditionally been adopted, where the soil stiffness is assumed to increase hydrostatically with depth. In the recent literature, G_{sec}, the secant shear modulus, is set proportional to $(p')^m$, where p′ is the mean effective stress and $m <= 1$ (e.g. Hird and Pierpoint (1998) and Lehane and Simpson (2000)). There is evidence that the exponent m varies with strain (Atkinson, 1993).

Lehane and Simpson (2000) measured the compression index, λ, of intact Dublin boulder clay as 0·03, indicating a high stiffness. More interesting than this, however, was the difference between the swelling index, κ, of the intact and reconstituted soils (0·004 and 0·008, respectively) compared to the difference in λ (0·03 and 0·04 for the intact and reconstituted soil, respectively). This is an indication of a fundamental, fabric based, difference between the intact and reconstituted soil in terms of swelling. Lehane and Simpson (cited) considered, however, that the difference in the values was due to the difference in the gravel content of the test samples, which would have caused differences in void ratio. This was investigated in this thesis by testing intact and reconstituted samples of the soil with identical particle sizes.

Stiffness anisotropy has been measured in highly overconsolidated clay, with stiffness in the horizontal greater than stiffness in the vertical (Ward et al., 1965). Recent research has shown that this is consistent throughout the strain range (Yimsiri and Soga, 2001). However, the research has been confined to sedimentary (London) clays; hence, the assumption of stiffness anisotropy does not necessarily translate to lodgement till, which is kneaded and then lodged in place. It would be expected that this process would result in isotropic stiffness characteristics, indirect evidence for which is given by the results of the unsupported excavation in Dublin till of Treacy (1995). In this earthwork, the ratio of vertical to horizontal ground movements was about 1, in contrast to excavations in other stiff clays (O'Rourke, 1981) (see Section 2.10.2.2). Hence, for a given strain/stress level, a single modulus should be applicable to the soil mass. This is discussed in more detail in later sections of this thesis.

The large majority of research on soil stiffness has been based on shearing in the triaxial test. Hence, the variation in stiffness due to boundary conditions has been relatively unstudied. Nevertheless, differences are known to arise between the one-dimensional stiffness of soil measured in the laboratory and the one-dimensional stiffness measured in the field and between soil stiffness measured in the oedometer and triaxial apparatuses.

A typical example of this is the very low stiffness measured from the primary loading curve of the oedometer, vis-à-vis other methods of measurement, evident from Fig. **2.5.13**. Jacobsen (1970), however, has shown the importance of the compliance of the oedometer apparatus for stiff boulder clay, indicating that the compliance of undisturbed samples of stiff boulder clay tested in standard oedometers can be as great as the true deformation of the soil under load.

On the familiar bi-linear, void ratio against the logarithm of vertical effective stress (e-logσ_v'), plot, the indices C_c, C_s and C_e are used to represent one-dimensional compression, swelling and recompression. When the oedometer test is plotted as σ_v' against axial strain, ε_a, Young's moduli are obtained, namely E_{oed}, the tangent oedometer stiffness, which was defined in Fig. **2.5.11** and E_{ur}, the elastic unload-reload modulus, respectively. An approximate linear relation was found between E_{ur} and σ_1' in boulder clay by Jacobsen (1970) and more recently by Kristensen et al. (1995) and Steenfelt (1997), as shown in Fig. **2.5.14**, where σ_1' is the vertical

effective stress at which reloading is commenced. A typical relationship for the 'Lower' (Danish) till unit, which is the closest till in character to Dublin boulder clay, is:

$E_{ur} = 50 + 3 \times \sigma_1' \text{ MNm}^{-2}$ (Kristensen et al., 1995). [2.5.2]

For typical in situ values of σ_1', say 100 kNm^{-2}, Equation [2.5.2] gives a one-dimensional soil modulus of 350 MNm^{-2}, which is substantially greater than the stiffness measured from the primary loading curve.

The value of m_v, the coefficient of volume compressibility[2], which is required to predict long-term settlements, is considered to be unreliable when obtained from laboratory tests on lodgement till. This is due to the discrepancies between the settlements predicted with m_v and those back-analysed from the field (the latter settlements being much lower) and also the practical difficulties of the test when applied to undisturbed boulder clay. It is considered that this is because the m_v values are being wrongly inferred from the laboratory tests, for the reasons identified in the previous paragraph. This was demonstrated by Farrell et al. (1988), who measured m_v values of 0·3 to 0·6 m^2/MN on loading and between 0·002 m^2/MN (initial) and 0·02 m^2/MN (final) on unload. Hence, Equation [2.5.2] suggests that the m_v value of the till should be taken from the unload curve of the standard test.

Owing to the perceived unreliability of laboratory m_v, it is, instead, generally correlated with SPT N in boulder clay:

$m_v = 1/(f_2.N)$, $440 < f_2 < 600 \text{ kNm}^{-2}$ (Weltman and Healy, 1978). [2.5.3]

This method does not seem rational, however, considering the even greater variability in the value of N in boulder clay. Butler (1975) found that the correlation:

$m_v = 1/100.c_u$ [2.5.4]

[2] Note that $m_v = 1/E_{oed}$ on the primary consolidation curve and $m_v = 1/E_{ur}$ on unload/reload.

gave a good estimate of the long-term settlements of heavy foundation loads on heavily overconsolidated clay, although this, like Equation [2.5.3], suffers due to the variability of c_u in boulder clay. It is evident that there is a need for an accurate assessment of m_v.

c_v, the coefficient of consolidation, is related to m_v by the equation:

$$c_v = k/(m_v.\gamma_w) \qquad [2.5.5]$$

where k is the soil permeability and γ_w is the unit weight of water.

Tables given by Mc Kinlay et al. (1978), of values of c_v and k of boulder clay, are replotted in Figs. **2.5.15** and **2.5.16**, respectively, as c_v and k against vertical effective stress, σ_v', to determine if there is any variation of these parameters with stress level. The tests of McKinlay et al. (cited) were conducted on representative samples of large diameter. Unfortunately, the gravel content of the three samples was not given, as variations in gravel content have an effect on the permeability and deformation characteristics. Nevertheless, there is an evident reduction of c_v and k with σ_v'. The nature of the variation of k with σ_v' is particularly interesting as it is linear on the semi-logarithmic plot shown, i.e. the relationship between k and σ_v' is exponential. Differences in the slope of the lines for a given test are evident and this may be due to differences in gravel content. The values of k, about 10^{-10} ms^{-1}, are typical of very low permeability clay. The average values of c_v are about 5 m^2/year, which are very low but are consistent with the field observations of Farrell et al. (1988).

2.5.4 Strain Measurement.

Fig. **2.5.17** shows the stiffness degradation curves of Dublin boulder clay in CID tests (Faulkner, 1998), measured externally and locally (the latter with the 'videoextensometer' method). Generally, the external strain measurements underestimate stiffness up to about 0·1%. In the past, routine laboratory testing, with external strain measurements, was unconcerned with this region, expecting that the relevant strain level (to ground conditions) was much higher. The discrepancy between triaxial laboratory tests with external measurement and field back-analysis became increasingly evident however. For example, as early as 1971, DeJong

and Harris found that the stiffness modulus from laboratory tests on clay till compared very unfavourably with the stiffness of the ground back-analysed from foundations, as can be seen in Fig. **2.5.18**. Since then, it has been recognised (e.g. Simpson et al. (1979) and Burland (1989)) that the typical strain level in the ground is the same, small strain, region that was neglected, hence the higher ground stiffness measured in reality. Evidence for small strains at working loads in stiff clay and boulder clay is shown in Fig. **2.5.19**. As can be seen from this figure, large strains are confined to near the area of loading, while most of the ground remains in the stiff, small strain region.

Measurement of the stiffness in the small strain region is complicated by the adverse affects of system compliance, including soil bedding and seating errors (Atkinson and Evans, 1985). This problem, and the acceptance of the importance of stiffness at small strains, has led to the development of local measurements in routine laboratory testing, including submersible strain transducers attached to the soil and, more recently, bender elements. The importance of this type of testing is evident from Figs. **2.5.5** and **2.5.6**, which show that the variation in stiffness due to changes in stress path direction and overconsolidation is relevant for practical purposes only to the small strain region.

2.5.5 Stiffness Moduli of Stiff Till.

2.5.5.1 Static Stiffness.

In typical cases of stiffness selection in till, a secant modulus is taken, e.g. E_{25} or, more usually, E_{50} (Weltman and Healy, 1978). Actual soil modulus values remain highly variable in till, however, depending on the strain level associated with the method of measurement. This is shown in Fig. **2.5.20**. Due to this variability, and because of the difficulties associated with laboratory testing, the SPT remains popular, the correlation $E' = 2000 \times N_{60}$ being typically applied to Dublin boulder clay conditions (Farrell, 1989). This correlation is consistent with the work of Stroud and Butler (1975) on the SPT, for a glacial soil with a plasticity index of about 10%. However, it is well known that SPT N is very variable in Dublin boulder clay, which can, in turn, lead to large variations in settlement predictions (Lehane and Simpson, 2000).

Plate bearing tests are believed to give a good estimate of the soil modulus for piles (Weltman and Healy, cited). Farrell et al. (1988) found that good agreement could be obtained between the value of E_u (the undrained Young's modulus) back-analysed from plate bearing tests and E_u back-analysed from a footing, both on Dublin boulder clay, namely about 100 MNm^{-2}.

Unlike the SPT and plate-bearing tests, the pressuremeter gives a direct measurement of soil stiffness. In boulder clays, pressuremeter testing is conducted in pre-formed boreholes. The value of the soil stiffness is obtained from the Gibson and Anderson method; with reference to the symbols defined in Fig. **2.5.21**, the value of the Young's modulus from the pressuremeter test is:

$$E = 2V_0(1 - \nu).(\Delta P/\Delta V) \qquad [2.5.6]$$

where V_0 is the datum volume at the start of the pseudo-elastic phase, ν is the soil Poisson's ratio and ΔP and ΔV are increments of pressure and volume, respectively.

Due to borehole disturbance effects, the modulus of deformation that is determined from the primary curve shown is frequently unrealistically low. In these cases, the soil stiffness is obtained from the unload-reload loops that are generally conducted during a test. The procedure is described in detail in Section 4.7.1. The pressuremeter method of stiffness determination was used by Eisenstein and Morrison (1973) to predict the settlements of foundations and heave of excavations in stiff till in Edmonton (reported in detail by DeJong and Morgenstern (1973) and discussed in Sections 2.10.2 and 2.10.3). Edmonton till is sandy, silty, well-graded boulder clay of low to intermediate plasticity, the properties of which are given in Tables **2.2.1 (a)** and **(b)**. The till deformation modulus, measured as 175 – 250 MNm^{-2} with the pressuremeter, was found to give very good predictions of base heave and foundation settlement.

2.5.5.2 Dynamic Stiffness.

The determination of G_{max} of very stiff soil using either bender elements or in situ seismic tests is not straightforward and, therefore, a major review of the measurement of stiffness by dynamic tests was undertaken.

Dynamic stiffness measurement has generally proved unpopular owing to the traditional discrepancies between the stiffness measurements and those measured in conventional laboratory tests. Furthermore, the interpretation of seismic tests is outside the range of common engineering experience. The importance of measuring G_{max} lies in its possible relevance to ground movements around excavations in very stiff clay and its increasing importance in advanced soil models (Simpson (1992), Atkinson (2000) and Lehane and Simpson (2000)). In Section 2.5.3, it was shown that soil stiffness depends on overconsolidation, strain level, recent stress history and how stiffness is defined. The Viggiani (1992) Equation [2.4.1], however, shows a dependence of G_{max} entirely on overconsolidation and stress level; i.e. the value of G_{max} is not affected by direction of loading or if a secant or tangent modulus defines the stiffness. Furthermore, the Viggiani (cited) equation is in the form of a power law, indicating a linear dependence of the logarithm of stiffness on the logarithm of the confining stress. The validity of this double-logarithmic relationship has been shown for a wide range of soils including stiff clays (e.g. Hird and Pierpoint (1998)).

As the pore water is unable to sustain shear stress, the shear modulus does not vary depending on drainage conditions. Under undrained axial loading the pore water does provide a substantial resistance to a load; therefore, the axial stiffness (Young's modulus) under undrained conditions is greater than the Young's modulus under drained conditions. As the deformations due to the shear (S) wave are elastic, the conversion from G_{max} to E_0, the very small strain Young's modulus, is easily done with elastic theory. Furthermore, the S-wave disturbance is very fast, causing an undrained (u) response. These features of the dynamic method result in the following set of formulae:

$$E_{0,u} = 2(1 + \nu_u)G_{max} \qquad [2.5.7]$$

$$E_0' = 2(1 + \nu')G_{max} \qquad [2.5.8]$$

$$E_0' = 2/3.(1 + \nu')E_{o,u} \qquad [2.5.9]$$

where ν' is the drained Poisson's ratio and ν_u, the undrained Poisson's ratio, is 0·5.

V_s, the velocity of an S-wave, is a function of the direction of wave propagation and the direction of wave vibration. G_{max} is, in the triaxial test apparatus, taken to mean $G_{max,vh}$, i.e. the shear modulus determined from a shear wave propagating vertically with a horizontal vibration. However, if the soil is cross-anisotropic, it will be stiffer in shearing in one particular plane (Atkinson, 2000). Stiffness in other orientations can be relatively easily obtained by orientating the soil sample in the required direction, although the measured modulus should be closest to the significant direction of loading (Atkinson, 2000), which is generally vertical. This simplification is necessary if the material is considered to be cross-anisotropic because there exist some five elastic parameters to describe cross-anisotropy, which require special measurements (Lings et al., 2000). If compression (P) waves are transmitted and the waves are constrained, in that there is no lateral deformation, the constrained modulus, M_{max}, is measured. If the P-waves are unconstrained, Young's modulus, E_0, is measured (Brignoli et al., 1996).

The laboratory method of measuring G_{max} is by the bender element (BE) method due to Shirley and Hampton (1977). A bender element consists of a piezo-ceramic plate of about 10 mm length that bends imperceptibly if there is a voltage change across it. A property of the bender element is that the reverse is true, i.e. if the element is made to vibrate, a voltage change occurs. This 'polarisation' is obtained by applying a high DC voltage between a pair of electrode faces (see Fig. **2.5.22**). Polarisation can be used to propagate an S-wave of known input voltage and measurable output voltage through a material. The speed of the wave, V_s, is therefore measurable. The S-wave barely disturbs the soil through which it is passing, with an estimated shear strain of less than 0·001%. The parameter obtained from V_s is, therefore, the elastic, very small strain shear stiffness, G_{max}. The wiring and direction of polarisation can be adjusted to give lateral (shear) or longitudinal (compressive) motion (Lings and Greening (2001) - see their Fig. 3).

The commonly followed BE procedure is to generate a square wave and to determine the time of first arrivals (inter alia Viggiani and Atkinson (1995)). Research has shown however (Sanchez-Salinero et al. (1986) and Mancuso et al. (1989)) that the time of first arrival is generally poorly defined, owing to the Near-Field Effect (NFE). The NFE is caused by very rapid waves that mask the first arrivals of the, slower, S-waves. Bodare and Massarsch (1984), for example, measured the first arrivals of impulse excitation waves that were about 50% faster than group velocities determined from steady-state vibrations. Mancuso et al. (1989) showed

that the NFE might mask the arrival of a shear wave when the distance between the source and the receiver is in the range ¼ to 4 wavelengths. In the field, this generally affects the first borehole receiver only. In bender element tests, however, there is a relatively small distance between transmitter and receiver (of about 2 to 3 wavelengths (Viggiani and Atkinson, 1995)) and, as such, the NFE occurs, as has been demonstrated by Brignoli et al. (1996). Sanches-Salinero et al. (1986) showed theoretically that there are three coupled components to the transverse motion, which comprise the near-field and far-field. This is because the motion of the elements are not pure motions (Brignoli et al., cited) and generally some compressive or shear motion occurs in turn. In BEs, the effect is amplified by the finite nature of the S-wave source and substantial P-wave energy is often developed.

A further problem common to seismic methods is dispersion, which is a reduction in amplitude of the high frequency components of waves due to propagation through a dissipative medium (Mancuso et al., 1989). In a non-dispersive medium, V_s is the same for all frequencies (Bodare and Massarsch, 1984). Dispersion occurs if the wave velocity varies significantly within a depth interval of one wavelength. As soils are dissipative/non-homogeneous mediums there is, as a result, two groups of wave propagation velocity: phase velocity and group velocity. Individual peaks of a wave travel at the speed of phase, V_p. Energy, however, generally propagates as a group, V_g.

The potential error in the measured stiffness is particularly affected by errors in the estimation of first arrivals produced by the NFE; hence the importance. Errors are magnified due to the square in the formula that is used to obtain G_{max} from the measurements of wave velocity:

$$G_{max} = \rho V_s^2 \qquad [2.5.10]$$

where V_s is the distance between the elements, L, divided by the propagation time, t, ($V_s = L/t$) and ρ is the soil density.

The absolute error in G_{max} is therefore:

$$G_{max} \pm \Delta G_{max} = (\rho \pm \Delta\rho)(V_s \pm \Delta V_s)^2 \qquad [2.5.11]$$

Neglecting terms higher than second order gives the potential fractional error in G_{max}:

$$\Delta G_{max} = \Delta\rho/\rho + (\Delta V_s/V_s)^2 \qquad [2.5.12]$$

where Δ is the error in the respective measure.

$\Delta\rho$ is low, as ρ is determined with accuracy. ΔL, the error in the measurement of the distance between the elements, could potentially cause a large error in G_{max}, owing to the square in the formula. However, Viggiani and Atkinson (1995) and others (Dyvik and Madshus (1985) and Brignoli et al. (1996)) have shown that the effective length, L_e, which a wave travels, is the distance between the ends of the elements. Any change in length of the sample in the course of the test should, therefore, be taken into account. As a result, the potential error in the measurement of G_{max} falls largely on the estimate of travel time.

Fig. **2.5.23** shows a typical square wave excitation signal and received trace. The first arrival due to a square wave could correspond to any of the points 0, 1 and 2. This is because of the Near-Field Effect. From Equation [2.5.12], the potential error due to the NFE is about 60% in G_{max}; hence the importance attached to this effect.

In an attempt to overcome the NFE, Atkinson and Viggiani (1995) have proposed complex numerical analyses. The authors used a sinusoidal pulse excitation, in preference to a square wave, and measured the propagation characteristics of the entire waveform by cross-correlation to give V_g. (A sine wave is mainly composed of one frequency and, therefore, the output wave is generally of a similar shape to the input wave.) Another method of analysis is based on a measure of the coherence of the waves: the range of frequencies that the waves are coherent over is determinable and, according to Bodare and Massarsch (1984), a group travel time can be obtained by linear regression, in this frequency range, of the stacked phase.

This thesis, however, applies recent, arbitrary wave generator, technology and the methods proposed by Jovicic et al. (1996). In the method, arbitrary input waves are generated such that numerical analysis is not required to remove the NFE. A substantial improvement in the quality of the received trace must be made, however; for example with cable shielding, such that no

external amplification or filtering is necessary. Jovicic et al. (cited) showed that the dimensionless factor, R_d, given by:

$$R_d = L_e/\lambda = L_e.f/V_s \qquad [2.5.13]$$

controls the shape of the received trace, where, λ and f are the wavelength and frequency of the wave, respectively and L_e and V_s are as before. With a low R_d value (of about 1), a downward deflection of the received trace is found, owing to the NFE (see point 0 on Fig. **2.5.23**). With a high R_d value (of about 8), there is no/nearly no downward deflection and hence no NFE.

It would appear, therefore, that the solution to the NFE problem is simply to apply a high frequency (and hence a high value of R_d). However, the frequency required by stiff soils is so high that overshooting of the transmitting element follows. There is, then, a limiting frequency that is a function of the relative impedance of the soil and the bender element. In effect, measurements in stiff soil necessitate low frequencies such that overshooting does not occur but the same low frequencies give rise to the Near-Field Effect. To overcome this, apparently intractable, problem of BE measurements in stiff soils, three methods have been proposed:

(a) Distort the input wave by reducing the amplitude of the rise until the near-field is cancelled on the oscilloscope trace (Jovicic et al., 1996).
(b) Adjust the frequency of the input wave to force oscillation of the receiver at one of it's natural frequencies, which creates resonance (Jovicic et al., cited).
(c) Take the first reversal of the trace that is generated by a square wave input (the part of the trace between the first deflection and first reversal representing the NFE) (Dyvik and Madshus, 1985).

It can be shown from the arguments that there is no bar to having a sample height to diameter ratio of 2, which then allows shearing of the sample on which the BE tests have been conducted during the consolidation stage.

The most common in situ 'seismic' test is seismic refraction, which consists of the measurement of the velocity of waves refracted from boundaries across which there is an increase in the wave

velocity. P and S waves are generated with sledgehammers hit against rigid blocks and geophones, spaced at around 2 m centres, measure the speed of travel. If the block is struck at the side, the method produces horizontally polarised S-waves down through the ground (Davis and Schultheiss (1982) and Matthews et al. (2000)), travelling with the velocity of shear waves, V_s. This is the same energy source as the bender element tests; hence the stiffness obtained by each of these methods were compared in this thesis.

The in situ tests measure stiffness at various depths within the till; therefore an estimate of the variation of the stiffness of the Dublin boulder clay layer with depth can be made. (Examination of borehole records in the vicinity of the seismic spreads allows the stiffness data to be assigned to specific depths within the till.) In this thesis, estimates of the confining stresses in the ground were made, which then allowed comparison with measurements of stiffness recorded at the various confining stresses applied in laboratory tests.

Poisson's ratio can be determined from dynamic tests by elasticity theory if the block is also struck with a downward blow, which produces compression, P-waves, which travel with the velocity, V_p:

$$\nu = ((V_p/V_s)^2/2 - 1)/((V_p/V_s)^2 - 1) \qquad [2.5.14]$$

The near-field component of the wave transmitted by the bender element moves with the velocity of P-waves (compression waves) in an unsaturated soil (Davis and Scultheiss (1982) and Brignoli et al. (1996)). However, in saturated soil, the near-field component moves faster than the velocity of P-waves, V_p. It follows from Equation [2.5.14], that Poisson's ratio, ν, will be underestimated in the BE tests. Furthermore, as dynamic methods cause very rapid elastic shearing of the soil, the measured Poisson's ratio would be expected to be the undrained ratio, ν_u.

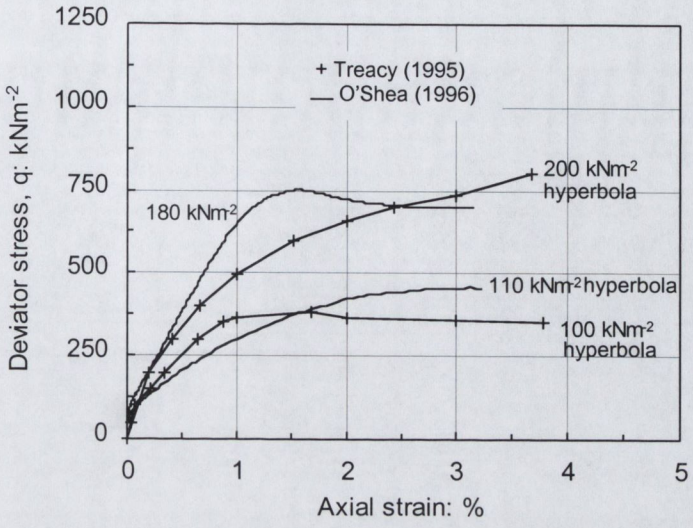

Fig. 2.5.1. Stress-strain behaviour of Dublin boulder clay in CID tests

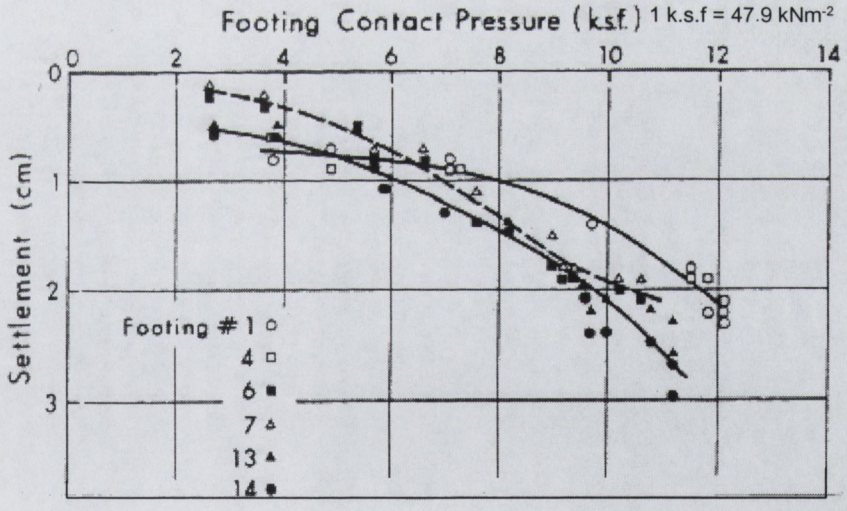

Fig. 2.5.2. Non-linearity of the response of foundations in glacial till, after DeJong and Harris (1971)

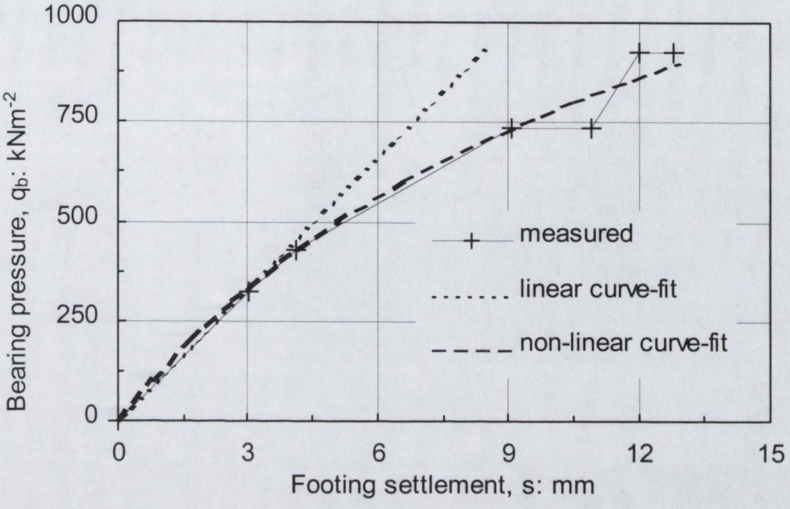

Fig. 2.5.3. Non-linearity of the response of a foundation in Dublin boulder clay

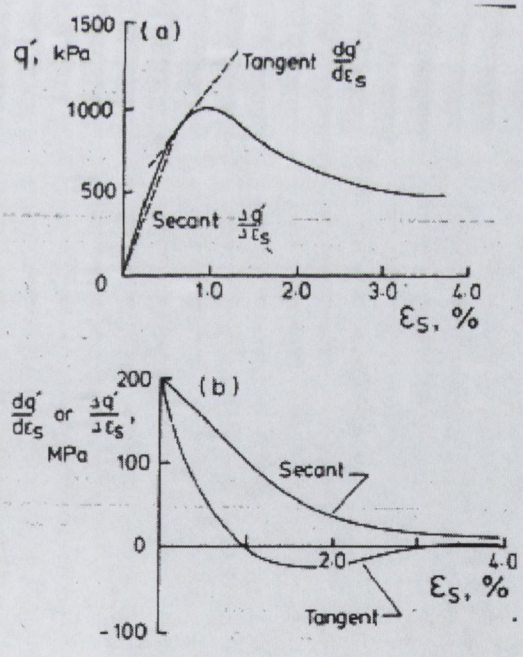

Fig. 2.5.4. Variation of stiffness due to definition, after Atkinson and Salfors (1991)

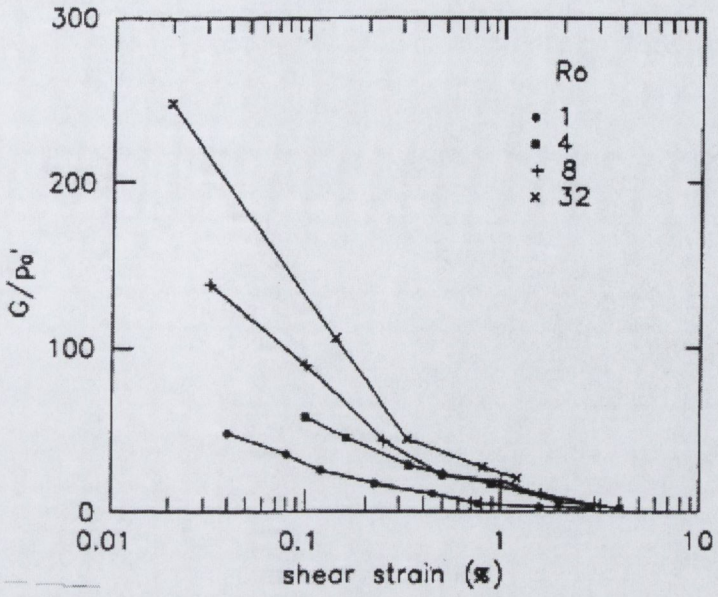

Fig. 2.5.5. Dependence of the stiffness of reconstituted boulder clay on overconsolidation, after Atkinson (1993)

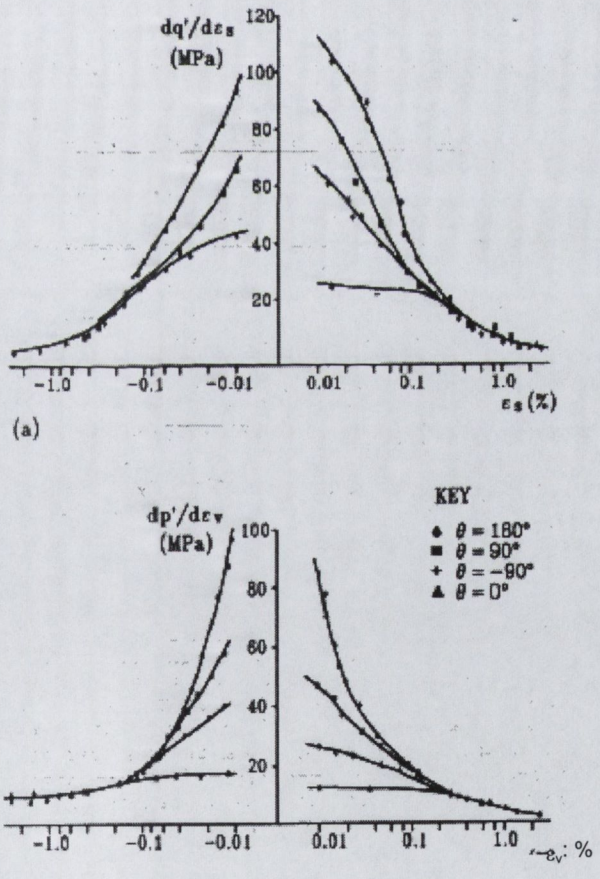

Fig. 2.5.6. Effect of 'recent' stress-history on the soil stiffness of reconstituted stiff clay, after Atkinson and Salfors (1991)

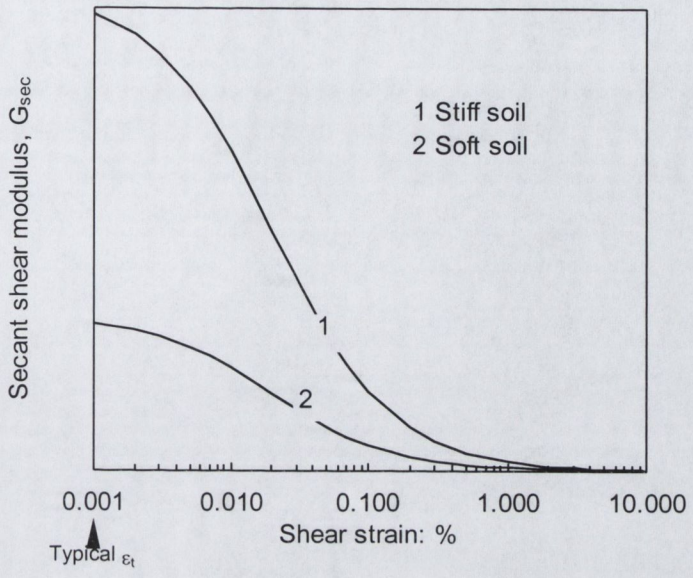

Fig. 2.5.7. Classical 'S'-shape curve

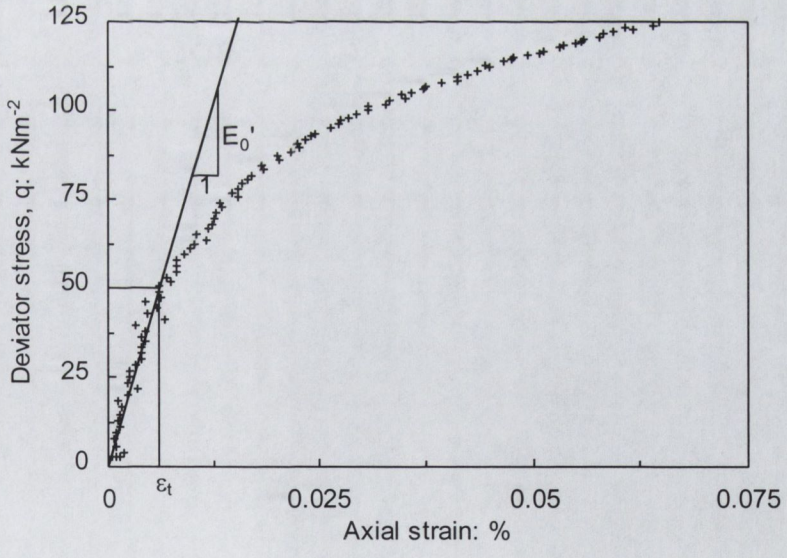

Fig. 2.5.8. Very small strain stiffness and the elastic threshold of Dublin boulder clay, adapted from a test by O'Shea (1996)

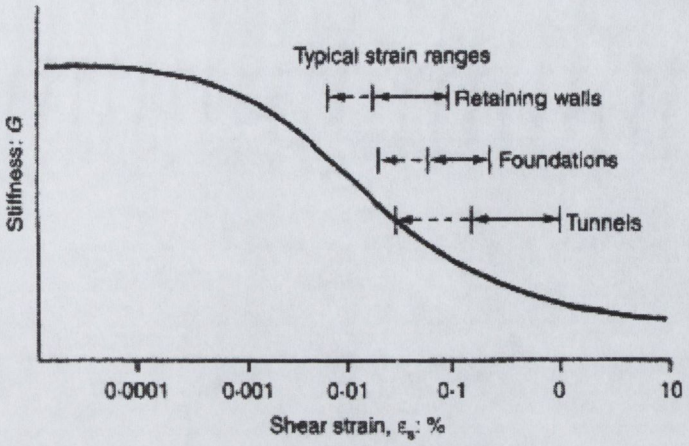

Fig. 2.5.9. Typical strains associated with foundations and excavations, after Atkinson (2000)

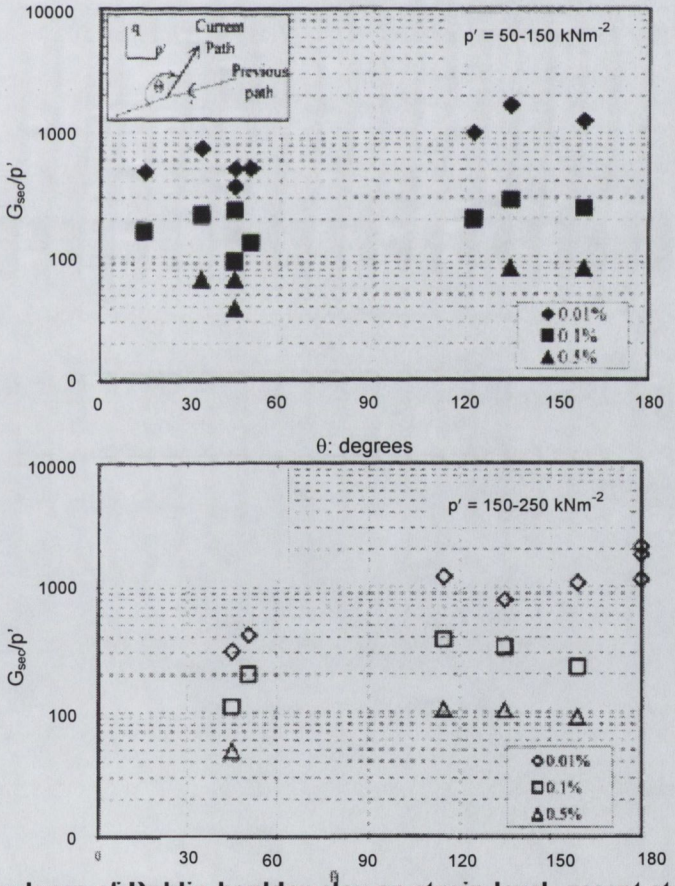

Fig. 2.5.10. Dependence of Dublin boulder clay on strain level, recent stress-history and stress-level, after Lehane and Simpson (2000)

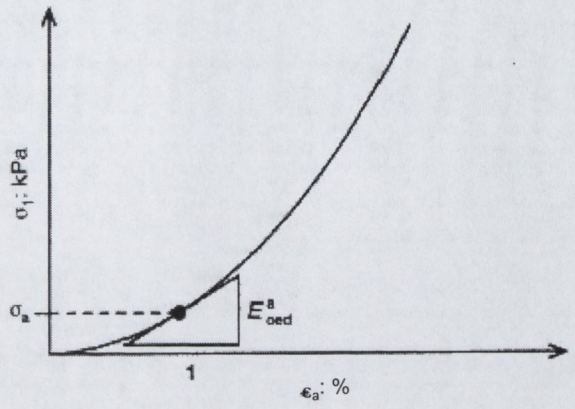

Fig. 2.5.11. Definition of E_{oed}, after Schanz and Vermeer (1998)

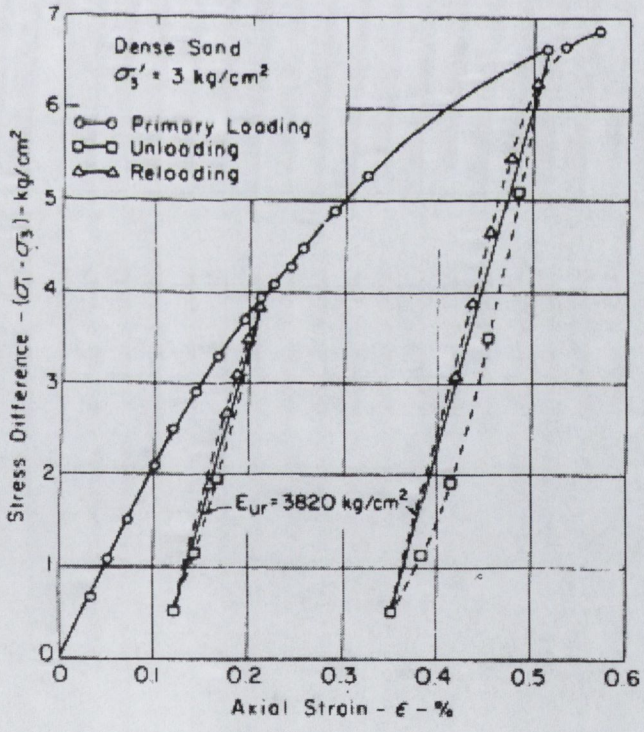

Fig. 2.5.12. Definition of E_{ur}, after Duncan and Chang (1970)

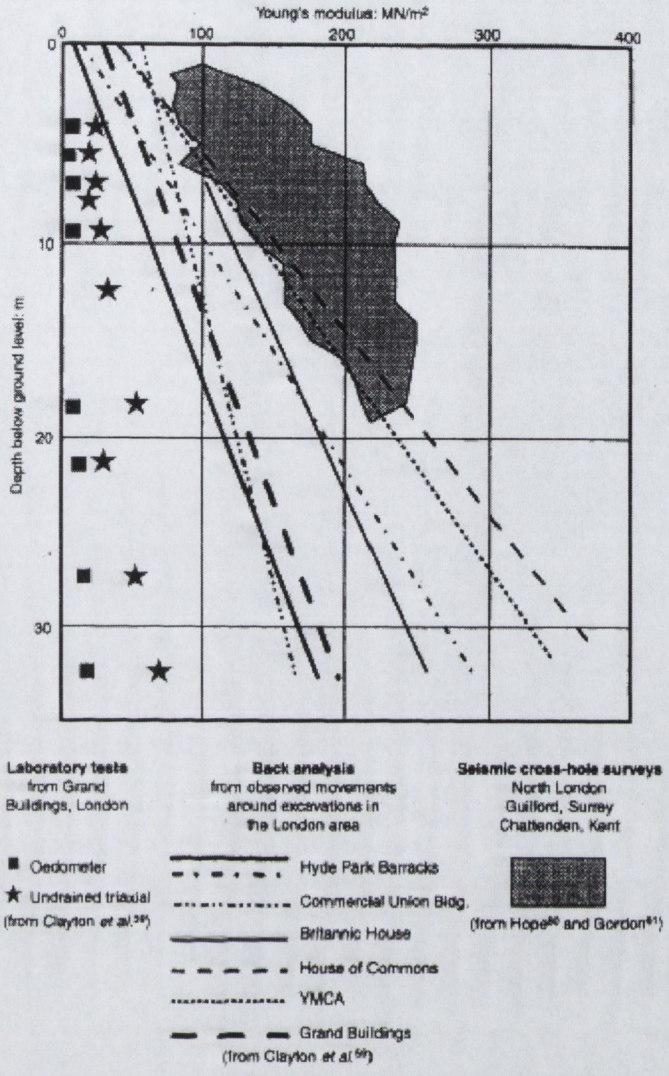

Fig. 2.5.13. Comparison of stiffness measured in standard oedometer test with other methods of measurement in stiff clay, after Matthews et al. (2000)

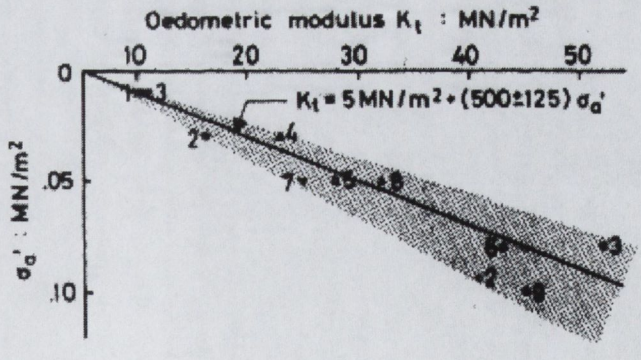

Fig. 2.5.14. Approximate linear relationship between E_{ur} (K_t) and σ_1' (σ_a') measured in the oedometer on stiff till, after Steenfelt (1997)

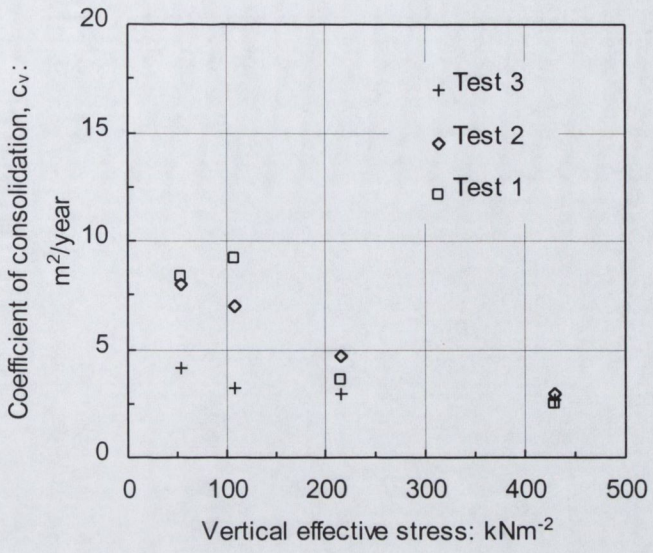

Fig. 2.5.15. Coefficient of consolidation of boulder clay against vertical effective stress, adapted from McKinlay et al. (1978)

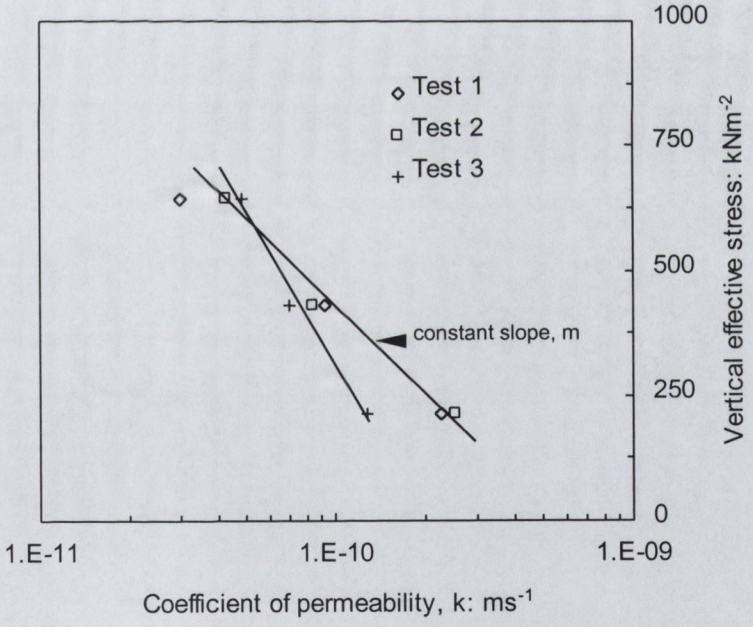

Fig. 2.5.16. Permeability of boulder clay against vertical effective stress, adapted from McKinlay et al. (1978)

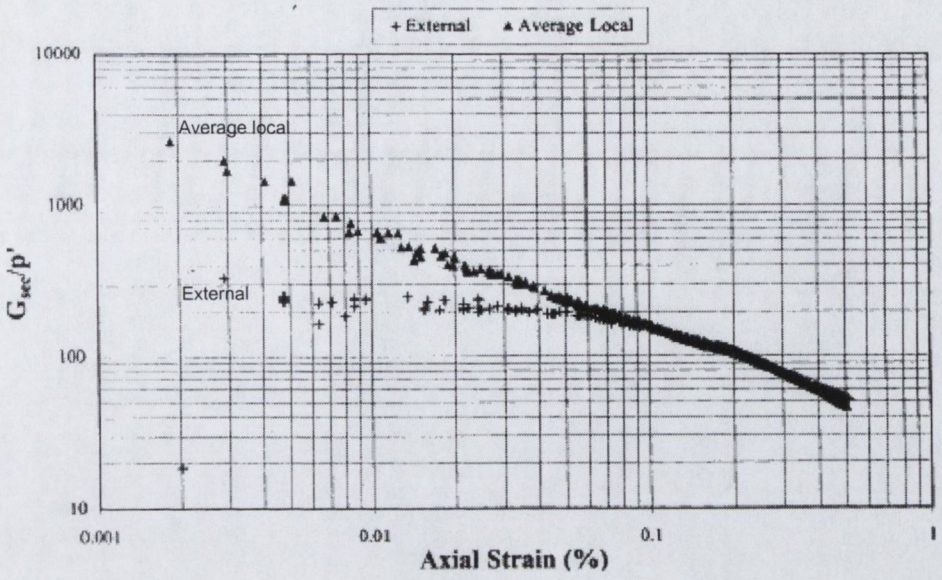

Fig. 2.5.17. Stiffness degradation of reconstituted Dublin boulder clay with strain measured locally and externally, after Faulkner (1998)

Method	Applicable stress range (k.s.f.)	Moduli of deformation,* $\mu = 0.4$ (p.s.i.)
CN Tower settlement data	3.5–11.3	71 300
Avord Arms settlement data	0–20	40 590
Consolidation tests	3.5–14.4	2996
Confined, undrained triaxial tests	4.3†	1480
Consolidated, undrained triaxial tests	10.8 and 20.2†	14 000

1 k.s.f. = 47.9 kNm^{-2}
1 p.s.i. = 6.895 kNm^{-2}

*Laboratory moduli are highest values from tests.
†Cell pressure

Fig. 2.5.18. Early indication of the discrepancy between standard laboratory test stiffness and stiffness back-analysed from the field, after DeJong and Harris (1971)

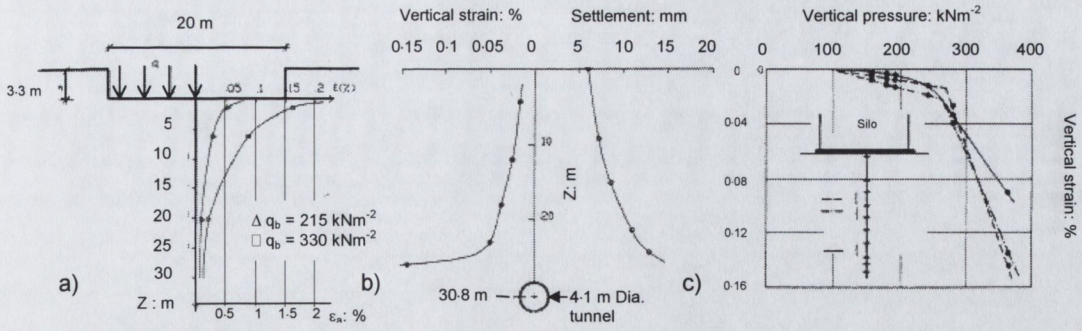

Fig. 2.5.19. Evidence of small strains at working loads in stiff clay and boulder clay, after Burghignoli et al. (1991): (a) axial strain beneath a foundation on boulder clay, (b) axial strain associated with a tunnel in stiff clay, (c) axial strain beneath a silo on soft rock

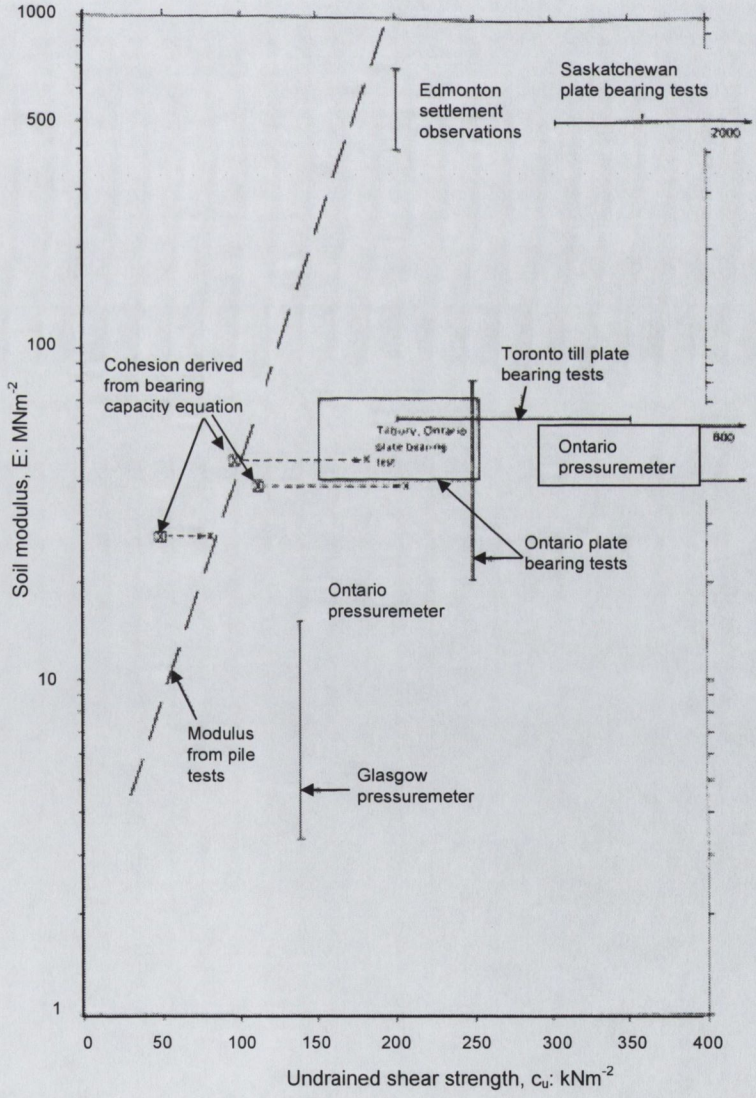

Fig. 2.5.20. Stiffness modulus obtained from various methods of measurement

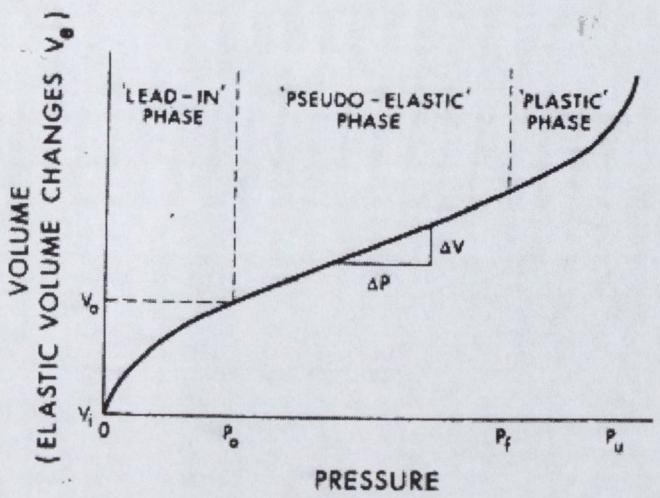

Fig. 2.5.21. Typical volume change-compression curve in the pressuremeter test

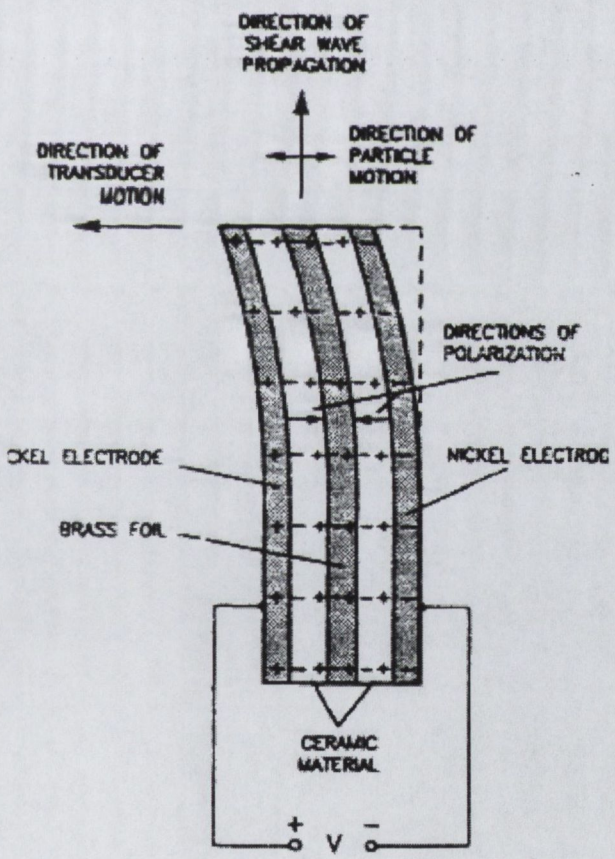

Fig. 2.5.22. Bender element detail, after Brignoli et al. (1996)

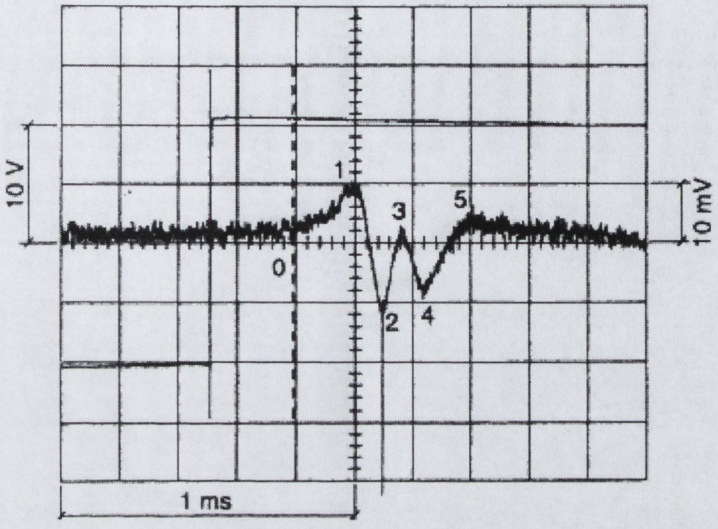

Fig. 2.5.23. Typical response of a bender element to a square wave input, after Viggiani and Atkinson (1995)

2.6 Strength.

2.6.1 Introduction.

The peak stress ratio in CIU tests corresponds to the point at which the undrained stress-path intersects the failure surface. The friction angle measured at this point is the peak effective friction angle, ϕ_p', of the soil. The stress-path then continues along the failure line to very large strain before the soil ruptures; this is because the soil continues to dilate and the excess pore water pressures that developed up to peak stress ratio slowly dissipate. In so doing, the soil approaches critical state. Hence, if the soil has moved sufficiently far along the failure envelope before failing, the friction angle at failure will approximate the constant volume effective friction angle, ϕ_{cv}'. In drained tests, the soil simply fails when the stress-path intersects the failure envelope because there is no dissipation of excess pore water pressure. ϕ_p' is therefore reached at a much lower strain than ϕ_{cv}'. The reader is referred to Fig. **2.6.1** for an explanation of the types of friction angles measured in triaxial CD and CU tests.

The variability in ϕ' is due to the dilatancy of the soil, which varies according to the strain. This gives rise to the problem of selection of the most appropriate friction angle, depending on the strain level. Therefore, one of the commonly measured friction angles, ϕ_p' or ϕ_{cv}', must be selected (assuming $\phi_{cv}' = \phi_r'$, the residual angle of friction, which is true for low plasticity soils). For ϕ_{cv}' to be relevant, very large strains need exist in the ground, and hence this friction angle/strain is limited in relevance to actual conditions; for example, pile driving and landslides (Skempton, 1964) in some clays.

It is expected that a difference in peak friction angles would be measured in triaxial tests corresponding to the method of measurement. In drained tests, as the soil dilates, there is an increase in volume and hence the soil has to do extra work against the cell pressure compared to the undrained test (Head, 1998). The measured friction angles will also be affected by the different strain rates used in the drained and undrained tests (Atkinson, 2000).

The undrained shear strength, c_u, is also non-constant, varying with boundary conditions (e.g. triaxial compression versus triaxial extension and direct shear versus simple shear) (Kulhawy,

1993). However, the CIU test has been suggested as the control test for c_u (Wroth, 1984) and it is this test that is referred to in this thesis.

Sample swelling, which reduces dilatant capacity and hence the distance the sample moves along the failure line before rupturing, has been suggested as a cause of variability in ϕ' measured in undrained tests (Burland, 1990). Hence, only those tests that finally rupture at very large strain should be selected. By doing this, those samples that rupture at relatively low strains, which is a sign of excessive sample swelling, are removed. This is the equivalent of applying the Hvorslev procedure, suggested by Burland (cited), which also takes account of the increase in void ratio due to swelling, by normalising with respect to the reference void ratio.

2.6.2 Effective Strength of Dublin Boulder Clay.

The CID triaxial tests, on large diameter samples of undisturbed Dublin boulder clay, of O'Shea (1996) and Treacy (1995) are shown in Fig. **2.6.2**. The linear regression line shown is $\phi' = 42°$ and $c' = 0$ kNm^{-2}. Despite the increased value of ϕ' that may arise from CID tests (explained in Section 2.6.1 above), 42° is considerably higher than the 33-35° commonly assumed for boulder clay (Weltman and Healy, 1978). An analysis of the strength of similar tills, given in Table **2.2.1(b)**, may prove useful at this point. These data show values of ϕ' over a wide range (25° - 42°). However, a closer examination reveals that the higher values are generally obtained for low c' and vice versa. It may be concluded that the low values and variation in ϕ' is a result of the (Mohr-Coulomb circle) method of analysis, owing to the skew that can occur if one of the three samples is non-uniform, which is a common occurrence in boulder clay.

Treacy (cited) also measured ϕ_p' in a 300 mm by 300 mm plan direct shear test apparatus. An angle of 43·8° was recorded on a block sample of the black lodgement till, suggesting a much higher ϕ' than is commonly accepted. However, Wroth (1984) has shown that there is a difference between plane strain and triaxial angles due to the limited degree of freedom in the plane strain test. The result of this is the following approximate relation between the plane strain effective angle, ϕ_{ps}', and the triaxial effective angle, ϕ_{tri}':

$8\phi_{ps}' \approx 9\phi_{tri}'$ [2.6.1]

Hence, 43·8° becomes 38·9°, which is closer to that commonly measured in triaxial tests on stiff till. The measurement of ϕ_p' and ϕ_{cv}' is pursued further in this thesis.

2.6.3 Undrained Shear Strength.

Fig. **2.6.3** shows the variation in undrained shear strength of boulder clay with moisture content. Farrell et al. (1988) showed a similar variation for Dublin boulder clay. These plots are typified by a high degree of variability and a large reduction of c_u for small increases in moisture content. For a given water content, the wide range of values results mainly from the natural variability of boulder clay samples and sample disturbance. It would be expected, therefore, that the upperbound strengths are representative of the ground condition, particularly as fissuring is generally not found in situ, which means that small samples do not overestimate the soil mass strength. (Fissuring is found in the Dublin Port area as a localised, fissured boulder clay, layer (see photograph of Fig. **2.2.7**).)

At the low water contents typical of Dublin boulder clay, of about 10%, there is clear scope, from Fig. **2.6.3**, for c_u of over 500 kNm^{-2}, increasing as the confining stress level increases. These very high values of c_u result from heavy overconsolidation, as can be seen from Equation [2.4.2] (Ladd and Foott (1974) and Wroth (1984)).

Due to the difficulties of the laboratory testing of boulder clay, there remains considerable interest in the correlation of SPT N with c_u. There are a number of problems associated with this, however: firstly, the difficulty of correlating the test confining stress (CIU) with the depth in the ground (SPT N) and secondly, the great deal of scatter that results from comparing two highly variable parameters. Hence, a large number of data is required to make a comparison. This thesis examines, at the end of Section 5.4.3, the correlation by comparing a large number of both sets of data.

2.6.4 Soil Structural Strength.

The stiffness and strength of a soil is due to a combination of geological compression and diagenesis, which is the term used to describe post-depositional changes to natural clays (Chandler, 2000). The 'structural strength' of an intact soil is the term used to describe the combination of fabric and bonding (Burland, 1990) that allows a natural clay to develop a structure stronger than the corresponding reconstituted, 'intrinsic', soil. The fabric of the soil describes the particle arrangement and the bonding refers to, non-frictional, inter-particle bonds; i.e. the characteristics of a structured soil are a combination of intrinsic and structural properties. Hence, the void ratio of a structured soil will not decrease with stress at the relatively high rate of the reconstituted soil.

There are a number of indicators of structural strength, abundant evidence for which is given by Kavvadas (1998) for hard soils/weak rocks. (These soils represent the transition from soil to rock; i.e. soils that possess some properties common to soils and some properties that are more rock-like.) Burland (1990) suggested the following as being indicative of high structural strength:

(a) For the same void ratio, the intact soil will carry a greater effective overburden pressure.

(b) A very high pressure is required for the intact consolidation curve to reach the ICL. The ICL is the intrinsic compression line of Burland (1990), to which all reconstituted clays tend when compressed one-dimensionally. The ICL equation is:

$$e = I_v.C_c^* + e_{100}^* \qquad [2.6.2]$$

where e is the voids ratio, I_v is the void index, C_c^* is the intrinsic (1-d) compression index, in the effective stress range: σ_v' from 100 to 1000 kNm^{-2}, and e_{100}^* is the void ratio of the intrinsic soil at an applied effective stress of 100 kNm^{-2}. I_v tends to:

$$I_v = 2{\cdot}6 - 1{\cdot}475x + 0{\cdot}075x^2 + 0{\cdot}0055x^3 \text{ (Chandler, 2000)} \qquad [2.6.3]$$

where $x = \log\sigma_v'$

Clarke et al. (1998) showed that the ICL was in reasonable agreement with the compression of reconstituted lodgement till.

Burland (cited) gives the following empirical correlation for C_c^*:

$$C_c^* \approx 0{\cdot}256 w_l G_s - 0{\cdot}04 \qquad [2.6.4]$$

where w_l is the soil liquid limit (about 25% for Dublin boulder clay) and G_s is the specific gravity (2·67 for Dublin boulder clay). Hence C_c^* of Dublin boulder clay would be expected to be about 0·131.

(c) If $C_e = C_s$ (these are defined in Section 2.5.3), then the soil has not destructured. This is particularly indicative of high structural strength if the (maximum) pressure applied in the test is very high.

(d) The swell sensitivity, which is the ratio:

$$\text{swell sensitivity} = C_s^*/C_s \qquad [2.6.5]$$

is strongly related to the inter-particle bonding in the soil. The higher the swell sensitivity, the greater the influence of inter-particle bonding. Gault clay, for example, has a swell sensitivity of about 4, i.e. the intact soil is four times less expansive than the reconstituted soil (Burland, 1990) and highly bonded Pappadai clay has a value of about 2·5 (Cotechhia and Chandler, 1998).

Structural strength is particularly important in low plasticity soil such as Dublin boulder clay. Low plasticity soils would be expected to behave somewhat like soft rock at yield, i.e. soft rocks fail suddenly, which is known as brittle behaviour. However, if the soil possesses a structural strength, the brittleness will be reduced. Furthermore, in excavations, structural

strength will have the effect of soil bonding and, hence, the apparent strength and rigidity of the soil will be higher than that due purely to inter-particle friction.

Structural strength may provide some answers to the (to date, unknown) cause of the stability of 90° excavations in Dublin boulder clay (see Section 2.10.2) and the very small deformations associated with these earthworks. Hence, there is a need for an evaluation of the structural strength of Dublin boulder clay, which this thesis investigates.

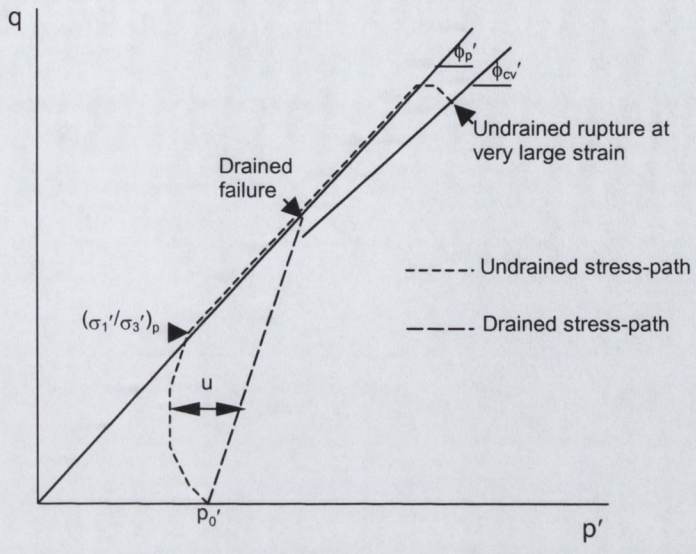

Fig. 2.6.1. Stress-paths and peak/failure conditions in undrained and drained triaxial tests

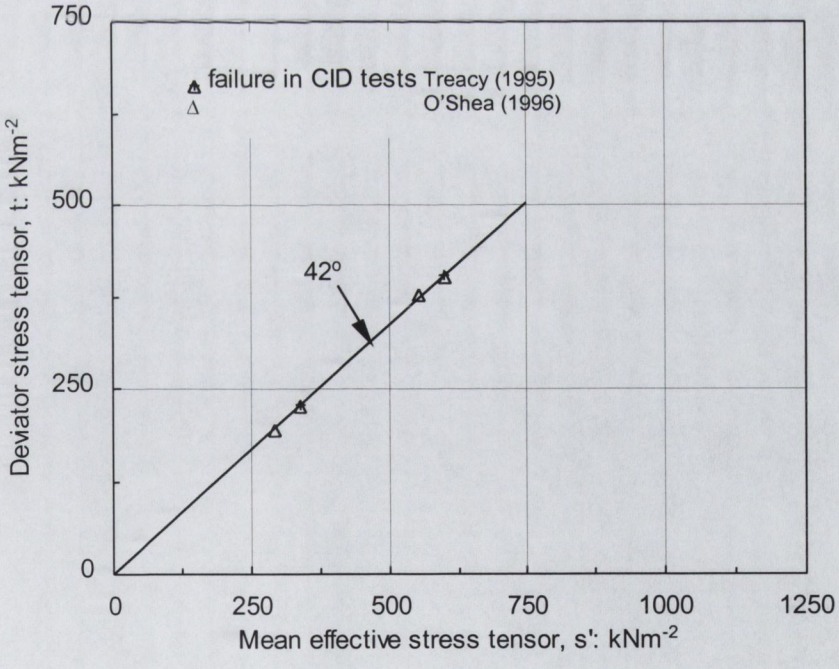

Fig. 2.6.2. Effective angle of friction in CID tests on Dublin black boulder clay

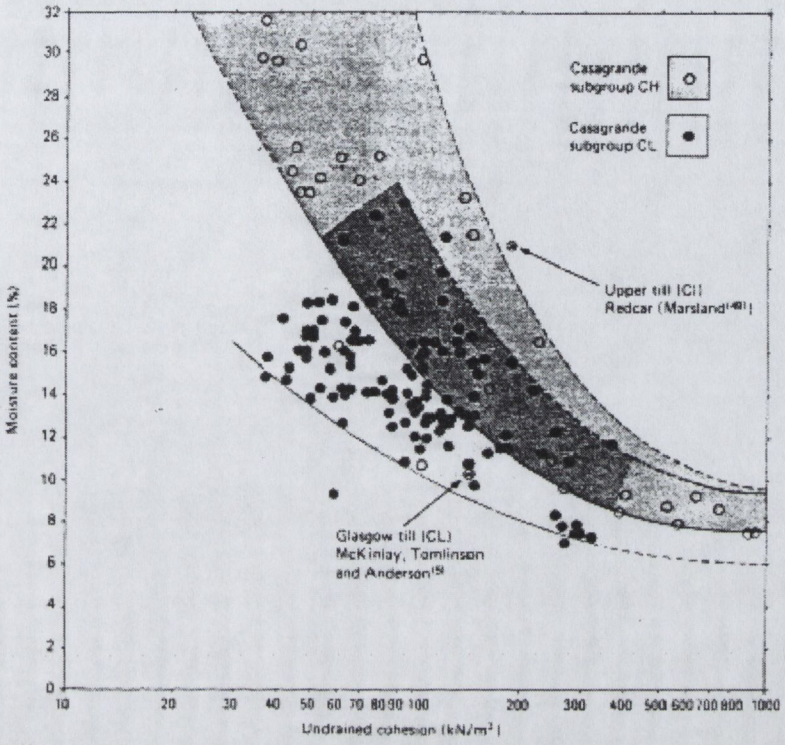

Fig. 2.6.3. Variation in c_u of boulder clay with moisture content, after Weltman and Healy (1978)

2.7 Dilatancy.

Dilatancy is a function of soil density, stress level, inter-particle friction, strain level and strain rate and is strongly associated with the development of shear bands (Atkinson, 2000). Fig. **2.7.1** shows the mobilisation of boulder clay dilatancy, adapted from the CID test data, on undisturbed Dublin black boulder clay, of O'Shea (1996). The figure shows that immediate dilatancy (negative volumetric strain) occurred on shearing, suggesting that a shear-plane formed almost immediately, i.e. non-elastic straining occurred from the start of shearing. This behaviour is contrary to the dilation behaviour common to all dense soils, which is illustrated on a plot of volumetric strain, ε_v, against shear strain, ε_s, in Fig. **2.7.2**, which also defines the peak angle of soil dilation, ψ. Dilatancy behaviour consists of compression, followed by dilation and ending at constant volume shearing. This behaviour is fundamental and, therefore, the variance in the results is serious and warrants further study. One possible reason for this variance is the isotropic consolidation stage, which is known to give different, subsequent, stress-strain characteristics to soils that are anisotropically consolidated (inter alia Ladd and Foott (1974) and Hight et al. (1985)).

Owing to the continuous variation in dilatancy, estimating this behaviour requires a dilatancy model (called a flow rule). An important feature of the rules is that they provide a link between peak states (ϕ_p' and ψ) and the mobilised state (ϕ_m' and ψ_m).

The peak angle of dilation, ψ, must be expressed in terms of the plastic components of strain (Houlsby, 1991), as follows:

$$\sin\psi = -(\delta\varepsilon_1 + \delta\varepsilon_2 + \delta\varepsilon_3)/(\delta\varepsilon_1 - \delta\varepsilon_3) \qquad [2.7.1]$$

$$\sin\psi = -\delta\varepsilon_v/\delta\varepsilon_s \qquad [2.7.2]$$

where ε_1, ε_2 and ε_3 are plastic major principal, intermediate and minor principal strains, respectively and ε_v and ε_s are the plastic volumetric and shear strains, respectively. However, elastic strains are small and total strains may be assumed to be very close to plastic strains. The negative sign is required because soil dilation is an expansive strain.

The simplest flow rule is the saw-tooth model, which consists of two saw-toothed blocks sliding with friction, relative to each other (see Fig. **2.7.3**). This model predicts that:

$$\phi_p' = \phi_{cv}' + \psi \qquad [2.7.3]$$

Taylor (1942) took the dilatancy theory further by formulating a frictional relationship in terms of energy dissipation. When work is done on a soil element, the total work done (WD) is the sum of the work done by the normal stress, σ_n', in resisting the soil dilation and by the frictional resistance. By the conservation of energy:

$$WD = \sigma_n'\delta\varepsilon_v + \tau\delta\varepsilon_s \qquad [2.7.4]$$

The resulting rule is similar in form to the saw-tooth model:

$$\tan\phi_p' = \tan\phi_{cv}' + \tan\psi \qquad [2.7.5]$$

Cam-clay applies Taylor's analogy, except it takes the Cambridge stress invariants q and p', giving:

$$WD = p'\delta\varepsilon_v + q\delta\varepsilon_s \qquad [2.7.6]$$

The following rule results, which is similar in form to Taylor in that M represents ϕ' at critical state and $\delta\varepsilon_v/\delta\varepsilon_s$ represents ψ:

$$M = q/p' + \delta\varepsilon_v/\delta\varepsilon_s \qquad [2.7.7]$$

Rowe (1962), however, took a different approach:

(a) Expressions were obtained for the stress and strain ratios for a regular assembly of spheres, under triaxial conditions (i.e. σ_1' and σ_3').

(b) Analogies were drawn with irregular assemblies.

(c) Sliding was assumed on a saw-toothed shear-plane (see Fig. **2.7.4**).

α (see Fig. **2.7.4**) may be eliminated to give the expression:

$$\sigma_1'/\sigma_3' = (\tan(\phi_\mu + \beta)/\tan\beta).(-\delta\varepsilon_3/\delta\varepsilon_a) \qquad [2.7.8]$$

where $\beta = \pi/4 + \phi_\mu/2$ and ϕ_μ is the angle of friction for grain-to-grain contact, which gives:

$$\sigma_1'/\sigma_3' = (\tan^2(\pi/4 + \phi_\mu/2)).(-\delta\varepsilon_3/\delta\varepsilon_a) \qquad [2.7.9]$$

By comparing the form of Equation [2.7.9] with the previous flow rules, ϕ_μ can be seen to appear as ϕ_{cv}.

A problem with all the flow rules is that they are formulated in plane strain (ps) and, because the angle of friction in plane strain is higher than it is under triaxial conditions (see Equation [2.6.1]), the rules are not applicable to the more general case. Bolton (1986) took a purely empirical approach to this problem, assuming $\phi_{cv}^{ps} = \phi_{cv}^{tri}$, and found an expression ($\phi_p' = \phi_{cv}' + 0{\cdot}8\psi$) that is very close to Rowe's rule, as shown in Fig. **2.7.5**. This is supported by Schanz and Vermeer (1996), who showed that, by letting $\varepsilon_2 = 0$ in Equation [2.7.1], the triaxial and plane strain dilation angles coincide, which was also supported by experimental evidence. It has been taken as validation of Rowe's rule that it corresponds well with the purely experimental rule of Bolton (cited).

Rowe's (1962) rule predicts that, when sheared, the soil will compress and then dilate. Schanz and Vermeer (cited) showed how Rowe's stress-dilatancy theory can then be expressed as follows:

$$\sin\psi_{m/p} = (\sin\phi_{m/p}' - \sin\phi_{cv}')/(1 - \sin\phi_{m/p}'.\sin\phi_{cv}') \qquad [2.7.10]$$

where:

$$\sin\phi_m' = (\sigma_1' - \sigma_3')(\sigma_1' + \sigma_3' - 2c'\cot\phi_p') \qquad [2.7.11]$$

Rowe's stress-dilatancy theory represents the most realistic theory proposed to date. Therefore, this theory was compared with the test data of O'Shea (1996) (see Fig. **2.7.6**) with a value of ϕ_{cv}' derived in a later section of this thesis. Unfortunately, there is a discrepancy between the prediction and the test results at the start of shearing; this is because Rowe's theory predicts negative dilatancy (compression) followed by a gradual change to dilatancy, whereas the CID tests dilated immediately. Note, however, that one of the tests tends to the prediction after a deviator stress of about 200 kNm^{-2} and that both tests tend to Rowe's prediction at failure.

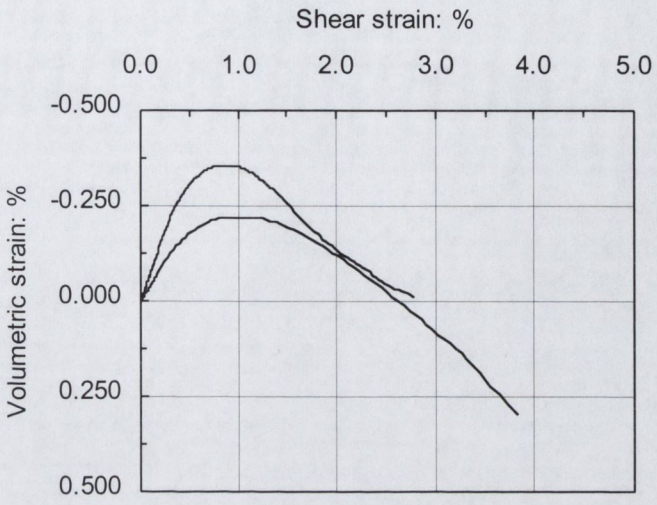

Fig. 2.7.1. Mobilisation of the angle of dilation in CID triaxial tests in Dublin boulder clay, adapted from tests conducted by O'Shea (1996)

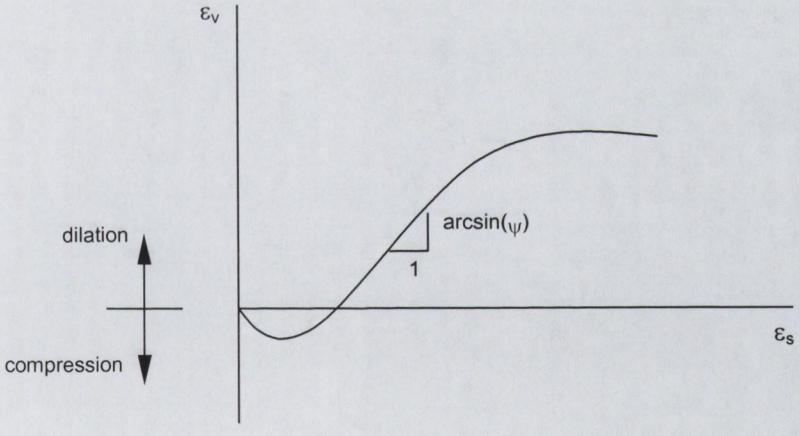

Fig. 2.7.2. Dilatancy behaviour of dense soil in triaxial shearing

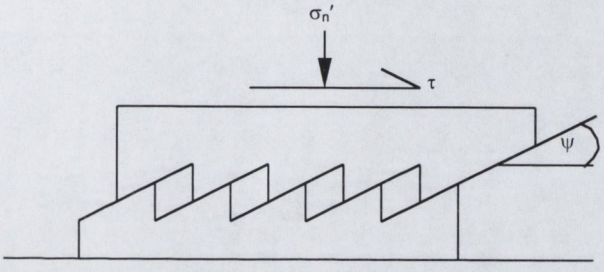

Fig. 2.7.3. Saw-tooth model of soil dilation

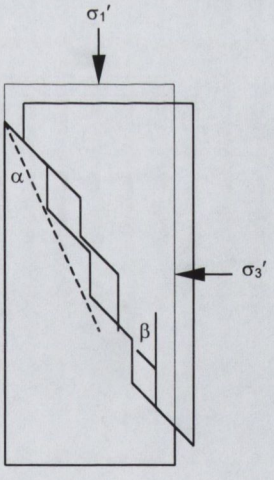

Fig. 2.7.4. Rowe's model of soil dilation, after Houlsby (1991)

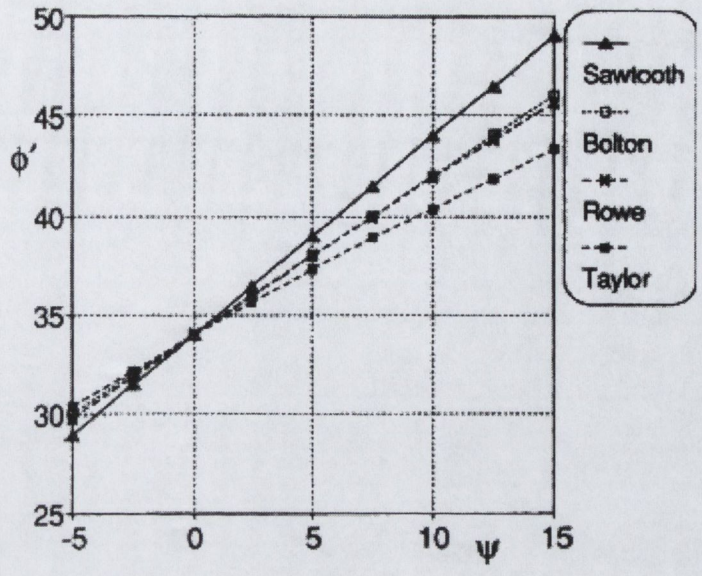

Fig. 2.7.5. Comparison of flow rules (for a nominal value of ϕ_{cv}'), after Houlsby (1991)

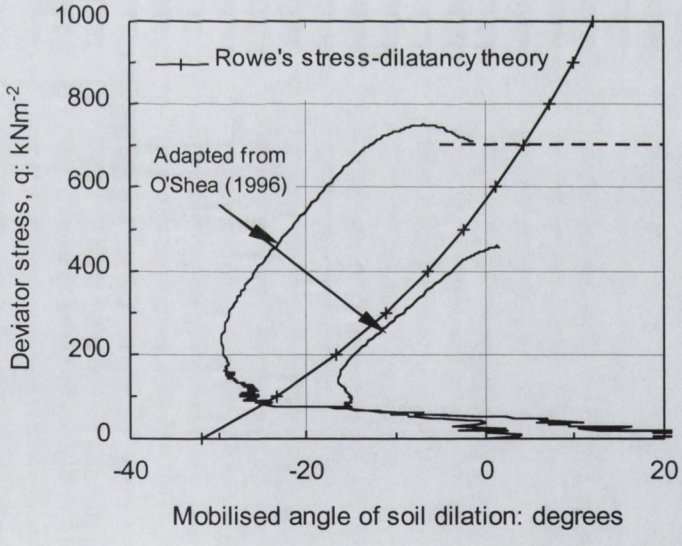

Fig. 2.7.6. Comparison of Rowe's stress-dilatancy theory with CID test data adapted from tests conducted by O'Shea (1996) (see Fig. 2.7.1)

2 8 Suction.

Total suction, ψ_t, is the term given to the sum of matric ($u_a - u_w$) and osmotic[1], ψ_0, suction:

$$\psi_t = (u_a - u_w) + \psi_0 \qquad [2.8.1]$$

These two components largely make up total suction, as can be seen in the soil-water characteristic curve in Fig. **2.8.1**. However, soil suction is the term generally used to describe the difference between the pore air pressure (u_a) and the pore water pressure (u_w), i.e. the matric suction, as it is this component that is of greatest significance to unsaturated soil mechanics:

$$\text{suction} = u_a - u_w \qquad [2.8.2]$$

In soil, suction occurs due to capillary attraction. A curved meniscus is formed, as in a capillary tube, giving rise to a tensile force on the soil particles that the meniscus is attached to. Water tension occurs when soils are excavated or sampled and in unsaturated soil above the water table. If a capillary tube is placed upright in standing water, the water will rise and a meniscus will form at the air-water interface. The relevance to soil is that a direct analogy may be drawn with the three-phase arrangement; this is explained in Fig. **2.8.2**. From the balance of the forces, illustrated in that figure, with gravity, it can be shown that:

$$u_a - u_w = \gamma_w.h \qquad [2.8.3]$$

where γ_w is the unit weight of water.

Jacobsen (1970) measured matric suction, in near-surface Danish till that is very similar to the upper metres of the Dublin boulder clay (see Tables **2.2.1(a)** and **(b)**: reference 2), in long-term tests with the tensiometer. The findings showed that a drop in suction (due to increased rainfall) of about 20 kNm^{-2} corresponded to a 2 m increase in the height of the water table level, which

[1] Osmotic suction is related to the salt concentration in the pore water; this affects the relative humidity of the pore air and, therefore, the soil suction (see Ridley and Wray, 1993).

is consistent with Equation [2.8.3]. Jacobsen's (cited) tests are shown in Fig. **2.8.3**. This level of suction is surprising in that it is very low and was, therefore, investigated (in Section 5.5).

Soil suction in situ is important as it adds to the shear strength, τ_f, and the stiffness of soil:

$$\tau_f = [\sigma_v' + (u_a - u_w)]\tan\phi' + c' \qquad [2.8.4]$$

$$E = E^{ref}((\sigma_3' + (u_a - u_w))/p_{ref})^m \qquad [2.8.5]$$

where u_a is the atmospheric pressure, u_w is the water pressure, E_{ref} is the reference stiffness, p_{ref} is an arbitrary pressure and m is a power that controls the level of stress dependency of stiffness.

Mancuso et al. (1998), for example, showed that the Young's modulus of a typical stiff soil increases approximately linearly with suction, throughout the strain range.

Ridley and Wray (1995) gave a very comprehensive review of suction measurement. In that paper it is explained that two levels of soil suction can be measured, namely the matric and total suction. To measure matric suction solely the measuring device must make contact with the pore water. To measure total suction, however, no contact is made with the pore water. Table **2.8.1** gives typical methods of measurement.

Table 2.8.1. Methods of measurement of suction, adapted from Ridley and Wray (1995)

Method	Type of Suction	Suction Stress Level	Time Required
Tensiometer	Matric	Low	Minutes
Axis translation	Matric	High	Minutes
In-contact filter paper	Matric	Low and high	7 days
Out-of-contact paper	Total	High	7 to 14 days
Ridley and Burland (1993) tensiometer	Matric	Low and high	Minutes

The standard tensiometer is beset with cavitation and air-lock problems and has failed to measure suction in Dublin boulder clay in the past (Gleeson, 2000). However, the filter paper method has been recently adopted as the standard method of measurement of soil suction by the ASTM (1992) and was used to calibrate the Ridley and Burland (1993) device. Furthermore, the filter paper method has been adopted in recent studies (Chandler et al. (1992a) and Chandler et al. (1992b)). For these reasons, the filter paper method was chosen to measure soil suction in this thesis, based on the BRE procedure of Crilly and Chandler (1993)[2] (see Section 4.5.2).

[2] The author was unable, however, to obtain reasonable results with the method (see Sections 4.5.2, 5.5.1 and A.3).

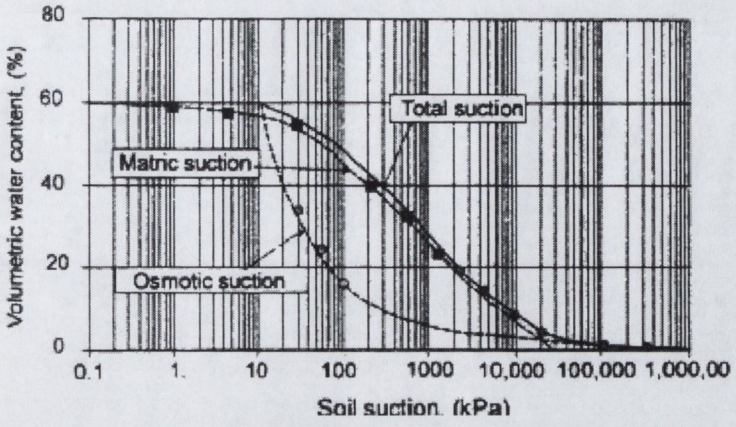

Fig. 2.8.1. Soil-water characteristic curve, after Fredlund et al. (2001)

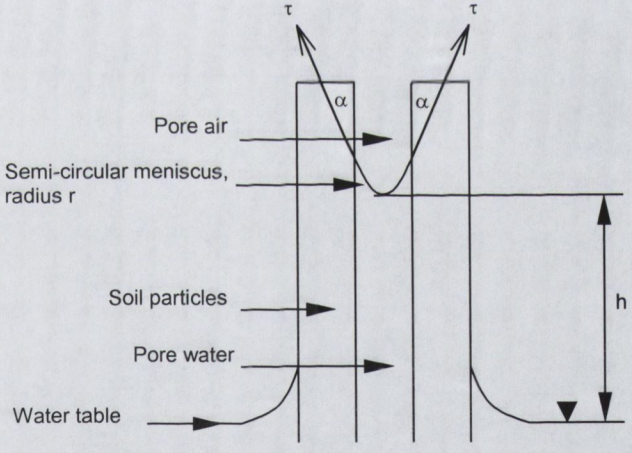

Fig. 2.8.2. Capillary rise model of soil suction

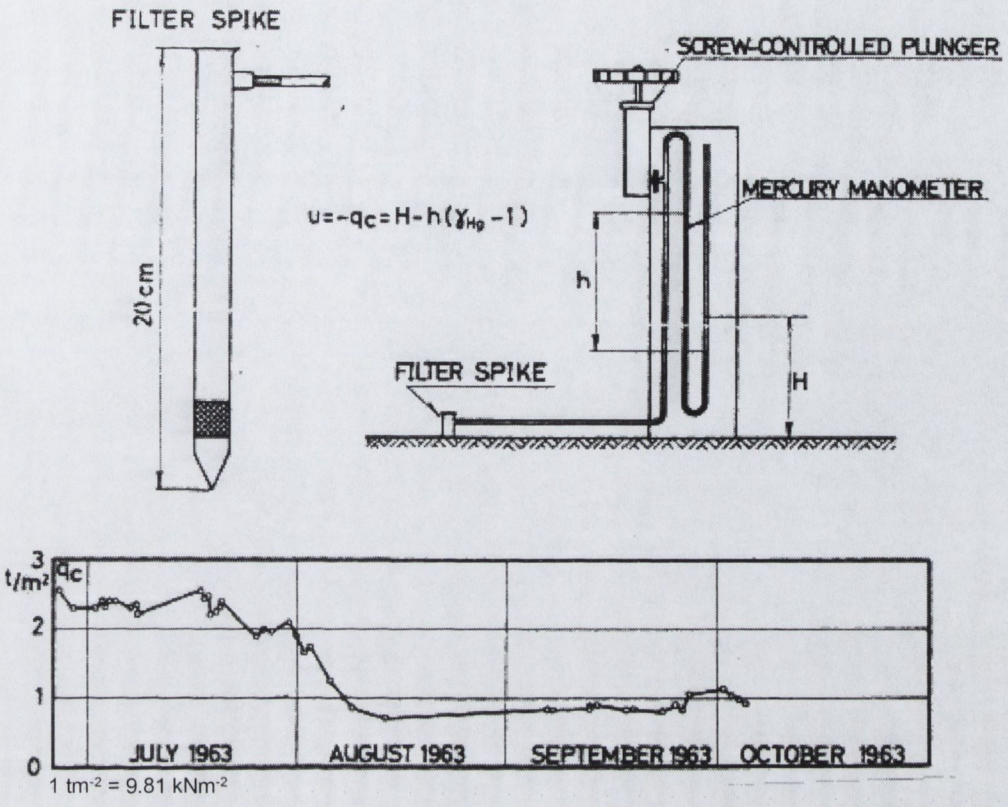

Fig. 2.8.3. Soil suction in stiff till, after Jacobsen (1970)

2.9 Soil Modelling.

2.9.1 Soil Models.

2.9.1.1 Elasticity.

A set of constitutive equations describing decisive aspects of the behaviour of soil is a soil model. The earliest and most widely used model is linear-elasticity. The equation for the settlement of a footing, for example, is given by:

$$\Delta = qB(1-\nu'^2)I_p/E_s \qquad [2.9.1]$$

where Δ is the vertical settlement, B is the width of the footing, ν' is Poisson's ratio, I_p is the influence/shape factor (when the footing is non-square) and E_s is the effective secant Young's modulus. This equation can be applied to both the drained and undrained cases, depending on the choice of parameters. To introduce the non-linearity of the soil response, E_s is often taken as an apparent stiffness, which reduces as the load increases (e.g. DeJong and Harris (1971) and Bernardi (1998)). However, such an approach requires specific data on the stiffness variation, which somewhat defeats the purpose of modelling the soil in such a simple way. Instead, the non-linearity of the soil response is often modelled with an elastic-perfectly plastic soil model, i.e. linear elasticity combined with the ideal theory of plasticity.

2.9.1.2 Elastic-Perfect Plasticity.

Elastic-perfectly plastic soil models differ from elastic models by introducing a yield function into the equations to evaluate plastic straining. If the yield function is of the Mohr-Coulomb type, these models are often described in those terms. The basic principle of elastic-perfectly plastic models is the separation of elastic and plastic strain and the determination of stresses using Hooke's law:

$$\delta\sigma' = D^e.\delta\varepsilon_e = D^e(\delta\varepsilon - \delta\varepsilon_p) \qquad [2.9.2]$$

where δ represents infinitesimal increments or rates, σ' is stress, D^e is the elastic stiffness matrix, ε is total strain, ε_e is elastic strain and ε_p is plastic strain.

According to classical plasticity theory, plastic strain rates are proportional to the derivative of the yield function, f, with respect to the stresses; hence, plastic strain rates are vectors perpendicular to the yield surface, which is known as associated plasticity. However, associated plasticity leads to an overprediction of dilatancy when coupled with Mohr-Coulomb type yield functions (because, by definition, $\phi' = \psi$: see Equation [2.9.6] below) and hence a plastic-potential function, g, is introduced for non-associativity. The plastic strain rate term, $\delta\varepsilon_p$, is given by the following:

$$\delta\varepsilon_p = \lambda.\partial g/\partial\sigma' \qquad [2.9.3]$$

where λ is a plastic multiplier. In the following equations of plasticity theory, elastic behaviour is given by $\lambda = 0$ and plastic behaviour by $\lambda > 0$:

$$f < 0 \Rightarrow \lambda = 0: \partial f^T/\partial\sigma'.D^e.\delta\varepsilon <= 0 \qquad [2.9.4]$$

$$f = 0 \Rightarrow \lambda > 0: \partial f^T/\partial\sigma'.D^e.\delta\varepsilon > 0 \qquad [2.9.5]$$

For the major and minor principal effective stresses (σ_1' and σ_3', respectively), the yield function and plastic potential functions are:

$$f_2 = \tfrac{1}{2}\left|\sigma_1' - \sigma_3'\right| - \tfrac{1}{2}(\sigma_1' + \sigma_3')\sin\phi' - c'.\cos\phi' <= 0 \qquad [2.9.6]$$

$$g_2 = \tfrac{1}{2}\left|\sigma_1' - \sigma_3'\right| - \tfrac{1}{2}(\sigma_1' + \sigma_3')\sin\psi \qquad [2.9.7]$$

For the case, $c' > 0$ (in Equation [2.9.6]), there are yield functions to limit or prevent tensile stress, σ_t, which is a negative integer. This yield function can be expressed as follows:

$$f = \sigma' - \sigma_t \geq 0 \qquad [2.9.8]$$

The yield function, f, is fully described by the strength parameters, ϕ' and c′, and the plastic potential function by the angle of dilation, ψ, the latter being used to model volumetric strain in dense soils. Fig. **2.9.1** shows the total yield contour, which is a cone in principal stress space. The stress-strain behaviour of an element described by the Mohr-Coulomb soil model is shown in Fig. **2.9.2**. The stiffness within the elastic section is the Young's modulus, E′. A value of Poisson's ratio must also be selected. The initial effective stresses in the ground are generated with the unit weight of the soil, the position of the water table and K_0.

2.9.1.3 Hyperbolic (Konder, 1963).

A well-known practical model of non-linear soil behaviour was formulated by Konder (1963), who found that CD triaxial tests on cohesive soils tend to describe a rectangular hyperbola with respect to two axes: deviator stress (q) and axial strain (ε_a), bounded by two asymptotes. From the hyperbolic curve, shown in Fig. **2.9.3**:

$$q - \beta = 0 \qquad [2.9.9]$$

$$\varepsilon_a + \alpha = 0 \qquad [2.9.10]$$

where α is the distance between the vertical asymptote and the y-axis and β is the distance between the horizontal asymptote and the x-axis.

Multiplying two mutually perpendicular lines gives the equation of the hyperbola:

$$q = \beta\varepsilon_a/(\alpha + \varepsilon_a) \qquad [2.9.11]$$

Differentiating q with respect to ε_a gives the tangent to the curve:

$$dq/d\varepsilon_a = \beta\varepsilon_a.\ln(\alpha+\varepsilon_a) + \beta/(\alpha+\varepsilon_a) \qquad [2.9.12]$$

Evaluating the derivative at $\varepsilon_a = 0$ gives the initial tangent to the hyperbola, which is the initial modulus:

$$dq/d\varepsilon_a = \beta/\alpha = \tan\theta \qquad [2.9.13]$$

Evaluating the derivative at q/2 gives the secant modulus at 50% strength:

$$dq/d\varepsilon_a = \tan\theta/2 \qquad [2.9.14]$$

Evaluating the derivative at $\varepsilon_a \rightarrow \infty$ gives:

$$\beta = q_a \qquad [2.9.15]$$

One difficulty with this model can be recognised in Equations [2.9.13] and [2.9.14], which imply that the initial soil stiffness is twice the stiffness of the soil at 50% strength, E_{50}. It is now known that initial stiffness of soil is far higher than $2E_{50}$, as discussed in Section 2.5.3. Hence, it would not be expected that this model would model the important very small strain stiffness.

2.9.1.4 Duncan and Chang (1970).

Duncan and Chang (1970) adopted the non-linear hyperbolic model of Konder (cited) and included the stress dependency of soil stiffness on confining stress and, importantly, the increase in stiffness when a soil is unloaded. On initial (primary) drained triaxial shearing, the axial strain was given by

$$\varepsilon_a = (1/2E_{50})(q/(1-q/q_a)) - q/E_{ur}, \text{ for } q < q_f \qquad [2.9.16]$$

where q is the deviator stress, q_a is the asymptotic value of the deviator stress at failure, $q_f = R_f q_a$ and E_{ur} is the unload-reload Young's modulus (see Fig. **2.5.12**).

E_{50} is the secant effective Young's modulus at 50% strength in the triaxial, isotropically consolidated drained compression test (CID) and R_f is a ratio that ensures failure at finite levels of strain. R_f is back-analysed from CID measurements of q_f and failure strain, using Equation [2.9.16]. E_{50} and R_f are determined directly from tests that give hyperbolic stress-strain curves.

Duncan and Chang (cited) adopted the fundamental stress dependent stiffness equation of Janbu (1963):

$$E_{50} = E_{50}^{ref}((c'.\cot\phi' + \sigma_3')/(c'.\cot\phi' + p_{ref}))^m \qquad [2.9.17]$$

where m is the power index that controls the amount of stress dependency of stiffness, E_{50}^{ref} is the reference E_{50} at p_{ref}, the reference pressure, and the remaining parameters are as usually defined. The same equation was adopted for E_{ur}, i.e. the elastic unload-reload stiffness defined previously in Fig. **2.5.12**, which is typically 4-5 times greater than E_{50} in stiff soils. Thus with this, double-stiffness, model it was possible to introduce the variability in stiffness of soil depending on stress-level and direction of loading.

2.9.1.5 Modified Cam-Clay.

Cam-clay is, like Duncan and Chang (cited), a double-stiffness model. In modified Cam-clay a logarithmic relation is assumed between specific volume, v, and mean effective stress in NC isotropic compression and isotropic unloading-reloading, as shown in Fig. **2.9.4**. The primary loading parameter is λ, the isotropic compression index, and the unload-reload parameter is κ, the isotropic swelling index:

$$v = \lambda.\ln(p'/p_0') \qquad [2.9.18a]$$

$$v = \kappa.\ln(p'/p_0') \qquad [2.9.18b]$$

The yield function, f, that separates elastic from non-elastic states is called the state boundary surface (SBS) and is described by an ellipse, which was obtained empirically from reconstituted soil testing:

$$f = q^2/M^2 + p'(p' - p_{pc}') \qquad [2.9.19]$$

where $M = q/p'$ at peak state is the critical state line (CSL) (the Cam-clay failure surface) and p_{pc}' is the mean preconsolidation stress. M also governs the height of the ellipse (in the q direction) and p_{pc}' governs the width of the ellipse (in the direction of the p′ axis). The total

yield contour is shown in Fig. **2.9.5**. The Cam-clay flow rule follows the work hypothesis of Taylor (1948) (see Section 2.7).

2.9.1.6 Kinematic Models.

A soil model based on the recently developed knowledge of stress-strain/stiffness behaviour is shown in Fig. **2.9.6**. For the increase in soil stiffness due to a change in stress-path direction to be included, the elastic yield surface must be kinematic, in that it is dragged around stress or strain space by the state point. Once the boundary surface is reached, non-elastic straining develops. A well-known model of this complexity is the 'Brick' model developed by Simpson (1992) and recently updated by Lehane and Simpson (2000).

Simpson (1992), in the Rankine lecture, formulated the Brick concept to model the dependence of stiffness on the previous stress-path direction. The model integrates Cam-clay and hence covers elasticity and plasticity with multiple kinematic yield surfaces expressed in strain space. Simpson drew an analogy with a man walking around in strain space, pulling a set of bricks on strings of various lengths. The man represents the current strain-state of a soil element and the bricks represent the current, plastic strains in proportions of the soil in the element. When the man moves without moving the bricks, strain is elastic. When all the bricks are moving by the same amount as the man, strain is entirely plastic.

As strain increases, it is assumed that an increasing proportion of the soil is plastic (the strings are of increasing length, which gives rise to a step-wise approximation). This gives an approximate S-shape, 'back-bone' curve of normalised tangent stiffness versus strain. Stiffness is assumed to vary in direct proportion to p′. The model is depicted in Fig. **2.9.7**. Volumetric plastic strain follows Cam-clay's flow rule. Subsequently, Lehane and Simpson (2000) introduced a 3-d modification for axisymmetric work.

Kavvadas and Amorosi (1998) developed the Cam-clay model (which is based on reconstituted clay) for 'structured soils'. The model features the behaviour typical of hard soils, such as high intact stiffness and strength and reduction of stiffness and strength due to destructuring. To do this, the Cam-clay yield surface (based on preconsolidation stress) is modified with a 'bond strength envelope', which is associated with the onset of significant destructuring and is distinct from the

onset of plastic yielding. The model includes a kinematic yield surface. The authors showed that the behaviour of hard Vallerica clay was well predicted, particularly the very brittle stress-strain response.

2.9.2 Examination of Soil Model Predictions in Boulder Clay.

Lehane & Simpson (2000) analysed the vertically loaded footing of Farrell et al. (1988) using an axisymmetric version of Simpson's (1992) 'Brick' model. A mean stress range and stress path suitable to this particular case was used to obtain the 'string' parameters. The results are shown in Fig. **2.9.8**. Initially ('run A'), the stiffness of the soil, based on laboratory tests, was underpredicted. When G_t/p' (tangent shear modulus normalised with respect to the mean effective stress) was increased by 33%, the results were improved ('run B'). A linear footing response was predicted, which was due to the increasing stress level in the ground, due to loading, compensating for the reduction in soil stiffness with increasing strain. It is considered, however, that the potential of the model is realised only when changes in the direction of loading takes place (and new S-curves are predicted). No such changes in the direction of the stress-paths will have occurred in the case of the shallow footing and, hence, the potential of the model was not demonstrated by this simple test.

Long (1997) published an observational method case history, concerning the prediction of the deformation of a, 5·5 m deep, basement retaining wall in Dublin boulder clay. A cantilevered retaining wall was constructed in Dublin boulder clay, overlying dense glacial gravels, overlying rock. Secant stiffness, the in situ stress-state and values for drained strength were based on those values commonly assumed for the soil, namely $E = 100$ MNm^{-2} (after Farrell et al. (1995)), $\phi' = 35°$ and $c' = 0$ kNm^{-2} (assumed). The model used in the calculations, a combination of conventional, free earth, design methods and the computer program, FREW (which models the soil as an elastic-plastic solid), predicted a maximum 6 mm of inward wall deflection. Subsequently, the inward wall deflection was monitored with standard surveying but no movements were recorded, suggesting that the wall deflection was less than 1 to 2 mm.

It is evident from these examples that workers are overpredicting ground movements in Dublin boulder clay by the FE method. This suggests that the stiffness of Dublin boulder clay is greater than is currently appreciated. Other workers in heavily overconsolidated clays have also

identified this problem. In particular, Rampello et al. (1998) identified that common numerical analyses are overpredicting surface ground movements at distance from excavations. Furthermore, the analysis of Hird and Pierpoint (1998), shown in Fig. **2.9.9**, is interesting in that their 'second analysis', which includes the stress-dependency of stiffness as being directly proportional to $(p')^{2/3}$, is a disimprovement on the case where no stress-dependency was assumed. This is possibly because, near surface, the stress level becomes very low if suction stress is not taken account of (see Equation [2.8.5]).

Eisenstein and Medeiros (1983) measured and predicted the deflections of a propped retaining wall, constructed through 15 m of glacial soil in Edmonton, and the surface ground movements associated with the excavation. (The excavation is discussed in detail in Section 2.10.2.) By taking account of the approximate variation in stress-paths in the ground around the excavation, the authors showed that better agreement between the measurements and predictions could be obtained than by assuming the conventional, triaxial passive compression, stress-path, which resulted in an overestimation of ground movements. For example, by assuming plane-strain conditions and deriving stiffness moduli from a plane-strain apparatus, very good agreement could be obtained, as shown in Fig. **2.9.10**. This example demonstrates the necessity of taking into account the effect of stress-paths and direction of loading on soil stiffness in routine analysis.

Kristensen et al. (1995) based deformation predictions of a bridge pier founded on stiff boulder clay on a double-stiffness type model of boulder clay stiffness behaviour. The authors used the parameters E_{ur} and E_{oed} measured in one-dimensional compression (as described in Section 2.5.3) and Equation [2.5.2]. For stresses below the yield/preconsolidation stress of the soil, E_{ur} was used and, for stresses beyond the yield stress, the soil stiffness was taken as E_{oed}, i.e. from the normal consolidation line. Creep/secondary consolidation settlement was also included. With this model, the authors predicted the settlement of a bridge pier founded on very stiff boulder clay and obtained very good agreement between the measured and predicted settlement, as shown in Fig. **2.9.11**.

Atkinson (2000) proposed an expression for a non-linear stress-strain prediction of shallow footings. The expression includes many of the essential elements of soil behaviour: very small strain

behaviour, failure strain, bearing stress and drained or undrained behaviour (depending on how the parameters are derived).

The expression given by Atkinson was:

$$E_t/E_0 = (1-(\varepsilon_f/\varepsilon_a)^r)/(1-(\varepsilon_f/\varepsilon_0)^r) \qquad [2.9.20]$$

where E_t is the tangent (Young's) modulus, E_0 is the very small strain stiffness, ε_f is the failure strain, ε_a is the axial strain, ε_0 is the threshold strain and r is a constant.

Equation [2.9.20] can be easily integrated by letting $E_t = dq/d\varepsilon_a$ to give the following stress-strain equation:

$$q = E_0(\varepsilon_a - \varepsilon_f^r\varepsilon^{1-r})/(1 - \varepsilon_f/\varepsilon_0)^r \qquad [2.9.21]$$

The method is compared with measured footing settlement (see Fig. **2.5.3**) in Fig. **2.9.12**. The parameters were derived from the CD test data of Treacy (1995), Faulkner (1998) and O'Shea (1996): $E_0' = 820$ MNm^{-2}, $\varepsilon_0 = 0{\cdot}006\%$; $\varepsilon_f \approx 3\%$ and r was taken as 0·3, which is mid-range of values quoted by Atkinson. It is evident that the initial stiffness of the soil is well predicted but the shape of the curve (which is obviously a function of the form of the equation) is a poor fit; in fact, the non-linear curve fit in Fig. **2.5.3** is a far better fit. This latter curve is a hyperbolic equation of the form:

$$\Delta = (1/2E_{50})(q/(1-q/q_a))*D \qquad [2.9.22]$$

where Δ is the foundation settlement, $E_{50} = 100$ MNm^{-2}, which was derived from the CID tests of Treacy (cited) and O'Shea (cited) (which were hyperbolic in stress-strain terms – see Section 2.5.2), q_a is the asymptotic maximum deviator stress ($q_a = R_f.q_f$, $q_f = 1500$ kNm^{-2} and $R_f = 0{\cdot}8$) and D is the thickness of the soil layer, taken as 15 m. A possible reason for this agreement is that the predominant stress-path in the ground beneath a footing is loading in shear (triaxial passive compression) (see Lehane & Simpson (2000)), which is the stress-path Konder (1963) based the hyperbola on.

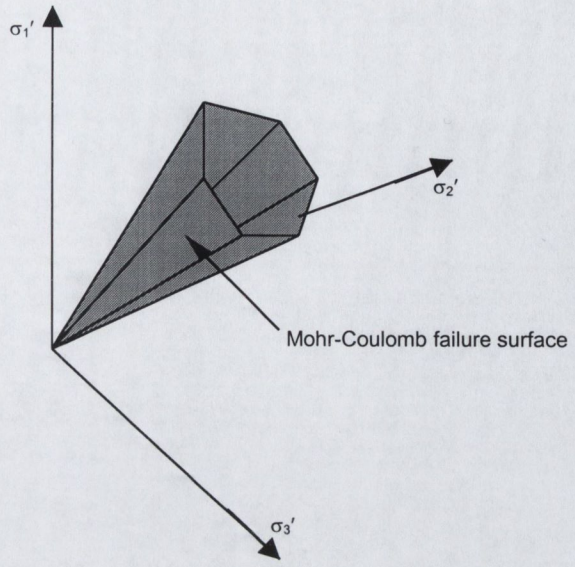

Fig. 2.9.1. Mohr-Coulomb total yield contour in principal stress space

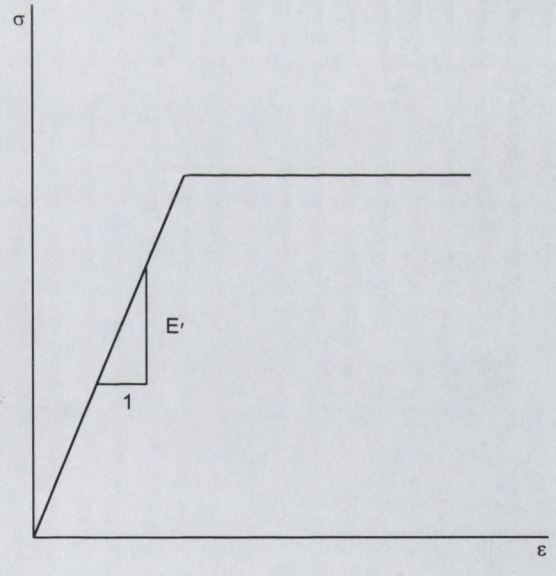

Fig. 2.9.2. Elastic-perfectly plastic representation of soil stress-strain behaviour

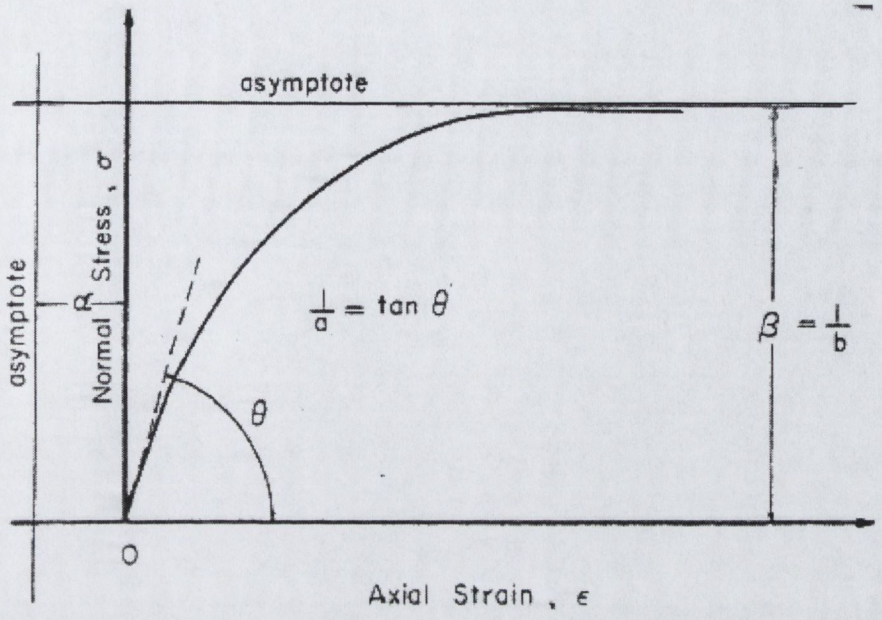

Fig. 2.9.3. Geometry of the rectangular hyperbola, after Konder (1963)

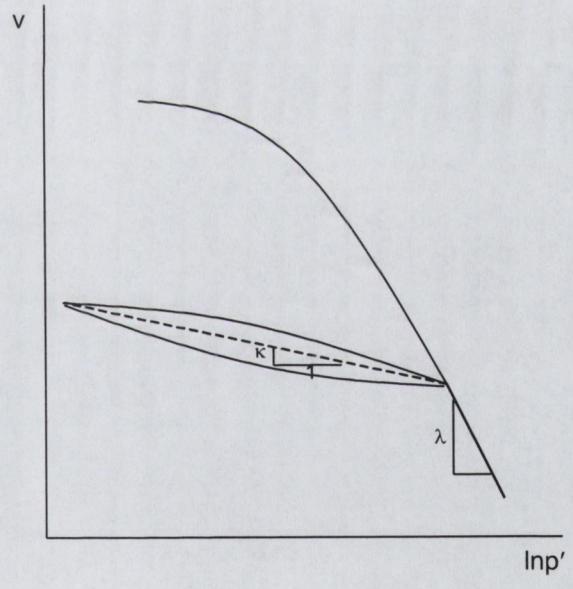

Fig. 2.9.4. v-logp′ relations in Cam-clay

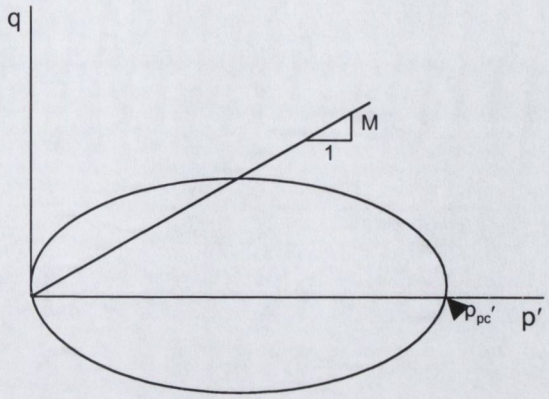

Fig. 2.9.5. Cam-clay yield contour in q-p′ space

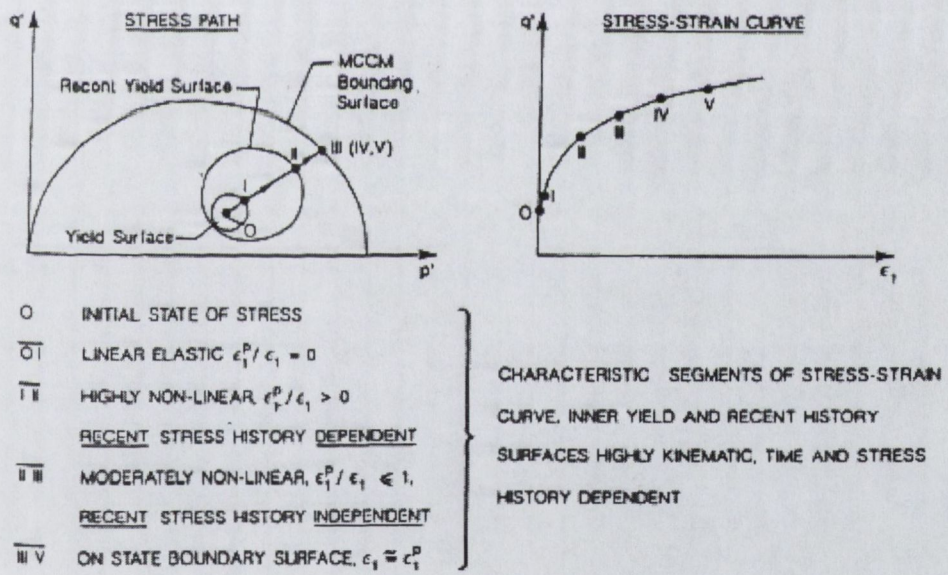

Fig. 2.9.6. Very advanced soil model, after Robertson and Ferreira (1993)

(a) Some paths travelled by man and bricks. (b) BRICK representation of stiffness reduction with strain.

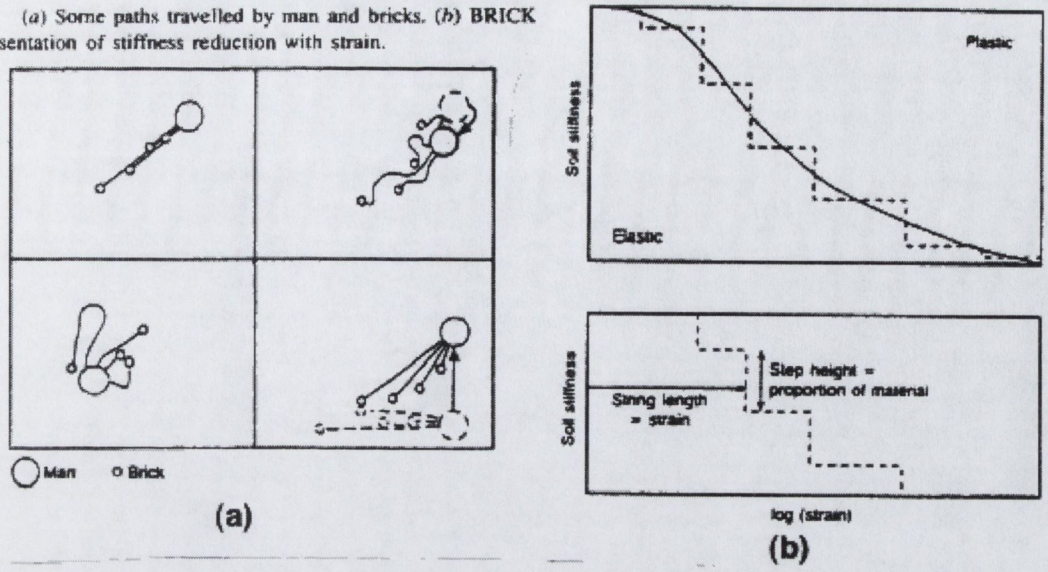

Fig. 2.9.7. Graphical depiction of the 'Brick' soil model, after Simpson (1992)

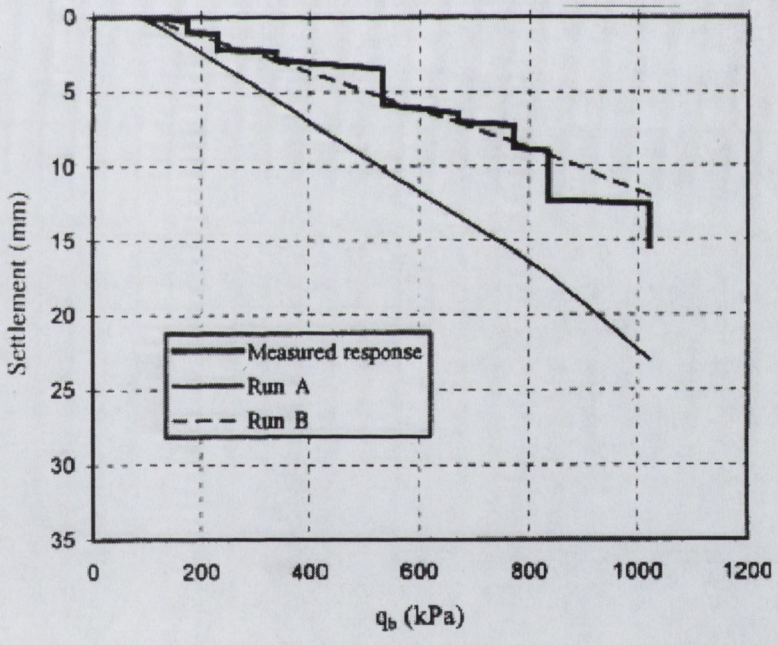

Fig. 2.9.8. Brick prediction of the settlement of a footing, after Lehane and Simpson (2000)

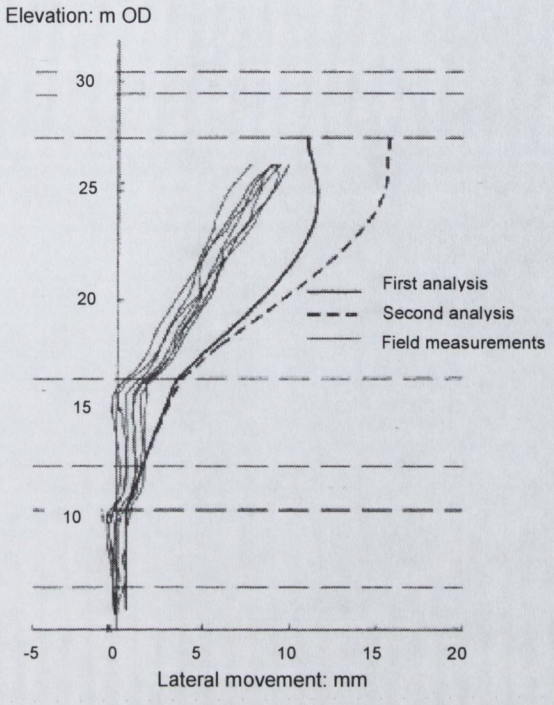

Fig. 2.9.9. FE prediction of ground movements in heavily OC clay, after Hird and Pierpoint (1998)

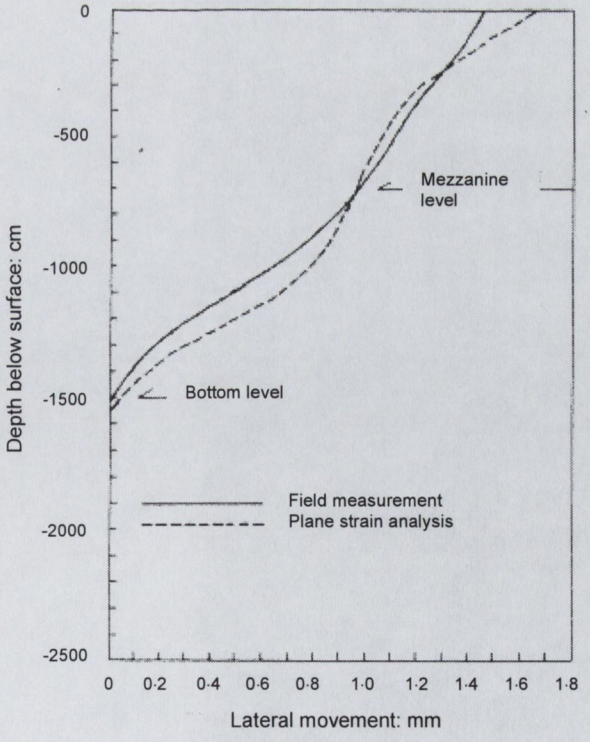

Fig. 2.9.10. Prediction of the deflection of a retaining wall in boulder clay, after Eisenstein and Medeiros (1983)

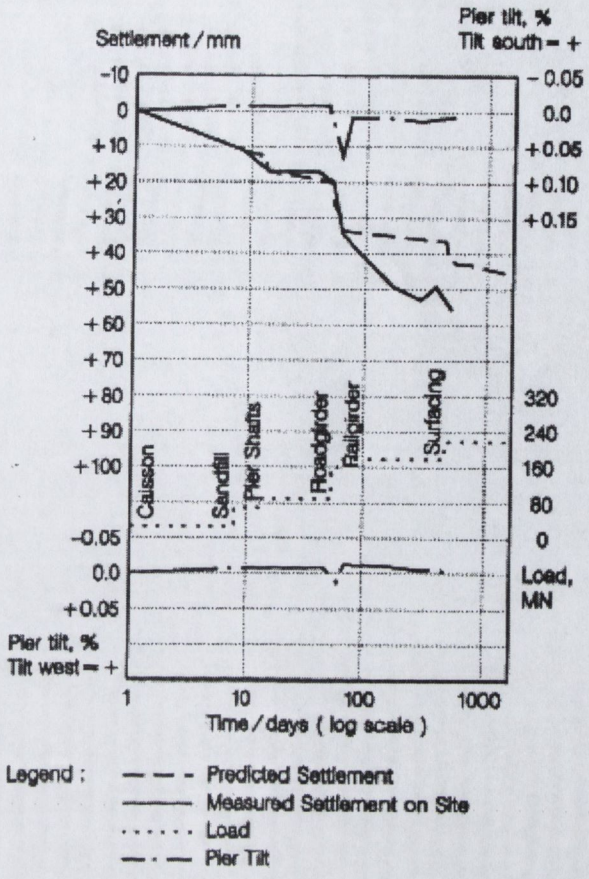

Fig. 2.9.11. Foundation settlement prediction in stiff till, after Kristensen et al. (1995)

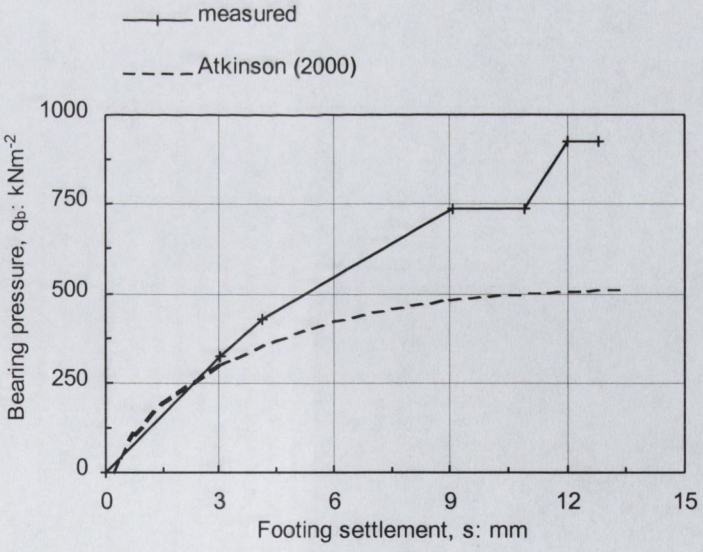

Fig. 2.9.12. Non-linear prediction of footing settlement with the Atkinson (2000) method

2.10 Conventional Methods.

2.10.1 Introduction.

Conventional methods of predicting and controlling ground movements in Dublin boulder clay are based on experience and the observational method. Published case histories remain, however, unfortunately rare. This review therefore gathers together experience of foundations and excavations in stiff boulder clay in general, with the intention of obtaining data for predictions and for general use in cases where construction experience is lacking in Dublin boulder clay (e.g. tall building loads and very deep excavations).

2.10.2 Excavations.

2.10.2.1 Stability.

A review of slope failures in Edmonton by Thomson and Yacyshyn (1977) found that on no occasion were, classical, translational failures seated in the stiff till. Failures that do occur in vertical cuts in till are, instead, generally found to be in bulging and slumping and not in a translational manner[1]. Minor slips in till slopes involve sloughing of the top soil and the till surface (Hartford, 1987). However, the discontinuous effect of sand lenses (see Section 2.2.5) on till mass slope stability may be significant.

Natural till slopes, which can be thought of as cut slopes of considerable age, are known to be very stable even when very steep, although, in engineering terms, the factor of safety is about 1 (Hartford, 1987). For example, that author reported on a slope failure in the Dargle Valley, which occurred after minor slope alteration. (Hartford suggested that the alterations caused cracks to develop to depth, allowing water ingress and a loss of strength – see Section 2.6.3.)

Fookes et al. (1978) reported that 70° angles were common in natural till slopes. Very steep slopes of this order can be seen in Dublin, for example, in the Killiney Bay and Howth

[1] A recent deep-seated, translational slip did occur in the Killiney Bay till exposure but was due to berm failure at the base of the till and possibly slope modification.

exposures (Kilkenny, 1990). Hartford (cited) reported that there was an apparent dichotomy between a stable, unsupported vertical cut and a superficially unstable 30°-35° cut, at the same site, in Dublin boulder clay. The cause of this was believed to be the reduction in strength when water is added to the till. A photograph (Fig. **2.10.1**) of a typical excavation in Dublin boulder clay supports Hartford's observations. The brown boulder clay/deformation till has been cut at a 45° angle and the black boulder clay is standing vertically. These angles are well in excess of the friction angles of the soil and, in the case of the black boulder clay, theoretically impossible in the absence of very substantial soil suction/cementation. Although soil cementation is not considered to contribute to the strength of the Dublin till, this may be an artefact of the laboratory test interpretation method (see Section 2.6.2). The exact reasons why such excavations are very stable therefore remain unknown and have been pursued in this thesis.

2.10.2.2 Ground Movements.

Excavations in stiff clay have been back-analysed in which it has been shown that the stiffness is close to the secant stiffness at small strain ($\approx 0{\cdot}1\%$) measured in laboratory tests (e.g. Simpson (1992)) and plate-bearing tests (e.g. Simpson et al. (1979)). Fig. **2.10.2** shows a plate-bearing test in stiff clay with the ratio $E_u/c_u = 1000$ (where E_u is the apparent, initial ground stiffness, i.e. $E_u = E_0$), which was subsequently back-analysed from excavations. It is evident, from the ratio $E_u/c_u = 1000$, that if excavations in stiff clay generally operate at small strain, for which there is increasing evidence (e.g. Jardine et al. (1986) and Simpson (1992), as demonstrated in Fig. **2.10.3**), the initial ground stiffness, E_u, is potentially very high in very stiff boulder clay, for which c_u is typically very high (of the order 500 kNm^{-2} to 750 kNm^{-2}), giving potential undrained stiffnesses of about 750 MNm^{-2}. When drainage takes place, however, the field evidence suggests that lower stiffnesses, such as those measured in the standard oedometer test (e.g. $m_v = 1/100.c_u$ in heavily overconsolidated clays (Butler (1975)), represent the long-term settlements beneath foundations well. If the initial ground stiffness is about 750 MNm^{-2} ($\approx 1000c_u$) and E′ (the apparent long-term ground stiffness) $= 1/m_v = 100c_u \approx 75$ MNm^{-2}, then the ground stiffness associated with excavations is approximately an order of magnitude greater than the apparent long-term ground stiffness of foundations. These calculations demonstrate the highly non-linear stiffness of stiff clay and the need for advanced methods of analysis that automatically take account of this non-linearity.

DeJong and Morgenstern (1973) measured the heave of a very deep (40 m) excavation involving stiff till (SPT N_{avg} = 80) in Edmonton, overlying a sand and gravel layer (of similar stiffness (SPT N = 80-100)), overlying dense interbedded mudstones and sandstones with coal seams. From the SPT data, the stiffness of the till was about equal to that of the bedrock (N = 75-100). The heave data, from points at the base of the excavation (which was in till) and points below the till, showed however that the bulk (˜81%) of the heave occurred in the bedrock formation and not the till. Furthermore, the ground movements outside the excavation were considerably less than those inside; hence, ground movement predictions based on the heave of the floor of the excavation would lead to an overestimate of the movements of the surrounding soil. (The magnitude and distribution of these latter ground movements, which are the sum of the wall cantilever movement and surface consolidation, are of great importance to excavations in urban areas, as they can cause damaging differential settlement to adjacent buildings.)

These, very deep, basements have traditionally been rare in Dublin boulder clay. This situation is likely to change, however, in which case an appreciation of ground and retaining wall movements associated with excavations, of 10 m depth or more, in boulder clay will be of interest. Eisenstein and Medeiros (1983) measured and predicted the deflections of a propped retaining wall constructed through 15 m of glacial soil in Edmonton and the surface ground movements associated with the excavation. At the maximum depth of excavation (15·2 m), near the base of the till layer, the inward wall movement was a maximum of about 10 mm. The development of wall deflection with depth of excavation is shown in the figures of Fig. **2.10.4**. (Note that the top 450 mm of ground is fill and firm to stiff lacustrine clay and the rest boulder clay.) The surface (1·5 m deep measurement points) settlement at distance perpendicular to the excavation is shown in Fig. **2.10.5**. Interestingly, the soil-concrete adhesion was very high and such that the smallest surface settlement occurred closest to the wall.

It is evident from this example that settlements are influenced by soil-structure interaction. For this reason, Treacy (1995) measured surface ground movements behind a (4·5 m) unsupported, vertical cut through brown and black Dublin boulder clay. Vertical soil movements were measured with a precise level and horizontal movements with taut wire strain gauges. The instantaneous and 14 day vertical and horizontal ground movements are shown in Figs. **2.10.6(a)** and **(b)**, respectively.

The results show that the immediate vertical movement, at a distance of 0·5 m from the face, was less than 1 mm and that this increased to about 2·5 mm after 14 days. The maximum initial horizontal movement was about 1·5 mm, increasing to about 4·5 mm after 14 days. These movements were limited to within about 2 m of the excavation face and were less than 0·5 mm beyond 2 m.

Hence, the ground adjacent to the excavation was very stiff, which is in accordance with DeJong and Morgenstern's (cited) measurements. Figs. **2.10.6(a)** and **2.10.6(b)** also show that there was no appreciable, immediate, differential settlement. After 14 days of swelling, however, there was differential settlement due to substantially increased settlement within about 2 m of the excavation. In urban areas, excavation related building damage is due to differential settlement of the adjacent soil; hence, the magnitude of angular distortion caused by the ground movements recorded by Treacy (cited), although low, may be more significant as the depth of excavation increases.

No two excavations are the same, differing in depth and support structure. Hence, for design purposes, it is useful to plot the excavation deformations as the ratio of deformation over excavation depth, as explained by O'Rourke (1981)[2]. Therefore, the vertical settlement profile shown in Fig. **2.10.6(a)** has been replotted in Fig. **2.10.7**, by normalising the distance back from the face, D, with the depth of the excavation, H, and dividing the maximum recorded settlements by H. Comparisons could then be drawn with other recorded ground movements in very stiff to hard till. The upper bounds shown are those suggested by O'Rourke (cited) and are due to the 'cantilever effect' in very stiff to hard clays. The ground movements by Treacy (cited) lie within the range occupied by supported excavations in very stiff clays and tills, indicating a very high level of stiffness. It would seem logical, therefore, that the relevant stiffness is the very small strain stiffness.

O'Rourke (cited) measured a ratio of vertical to horizontal ground movements, δ_v/δ_h, of 2·5, based on measurements around excavations in very stiff clay. From the immediate measurements in Dublin boulder clay, $\delta_v/\delta_h \approx 1$, which indicates that the stiffness in the horizontal and vertical directions is about the same. This is consistent with the mode of deposition (see Section 5.7.1.2).

---

2 The method is originally attributed to Prof. R.B. Peck.

2.10.3 Footings.

DeJong and Harris (1971) measured the response of Edmonton till to footing pressure. The till overlies a dense sand and gravel layer over very dense interbedded mudstones and sandstones. However, as the footings were founded high in the till layer (see Fig. **2.10.8**), the stress influence on the underlying layers was negligible. Typical load and settlement is shown in the figures of Fig. **2.10.9**. The maximum settlement recorded was 30 mm under a bearing pressure of about 575 kNm^{-2} and the maximum differential settlement was 11 mm over 11·3 m (angular distortion of about 1/1000), which was well within allowable limits. The majority of the settlement (about 87%) occurred rapidly (in the construction phase), which, from those author's experience, is a feature of foundation settlement in overconsolidated clays.

Normal practice for the design of footings in Dublin boulder clay is to assume an allowable bearing capacity, q_a, of about 400 kNm^{-2} (excluding self-weight), which is within the range for very stiff boulder clays quoted by BS 8004 (300 - 600 kNm^{-2}). This value of q_a is considered to be very conservative. In the footing test of Farrell et al. (1988), for example, the settlement measured under a bearing pressure of 400 kNm^{-2} was about 4 mm. The settlement under a bearing pressure of 575 kNm^{-2}, of about 6 mm, was also considerably less than that recorded in the Edmonton till (see previous paragraph) under the same pressure.

A maximum bearing pressure of about 1000 kNm^{-2} was applied to the foundation on Dublin boulder clay, which gave a long-term settlement of about 13 mm, without evidence of the ultimate capacity, q_u, being reached. An indication of the value of q_u of stiff till comes from Thomson (1981), who reported on a type of shallow, spread footing in Edmonton, the ultimate capacity, q_u, of which was about 1300 kNm^{-2}, defined as excessive or plunging settlement.

It was found that the load-deflection curve of the Dublin footing trial could be approximated by linear elasticity (Equation [2.9.1]), with the following parameters: width of footing, B, 1·5 m, $\nu' =$ 0·2 (0·5 undrained) and an influence factor (for the circular footing), I_p, of 0·85. The back-analysed value of the effective secant Young's modulus, E_s', thus obtained, was 85 MNm^{-2} and the undrained ground modulus, E_u, was 100 MNm^{-2}. (DeJong and Harris (cited) found that about 80% or more of foundation settlement is immediate in stiff till, which is in keeping with Farrell et al. (cited)).

Equation [2.9.1] was also used by DeJong and Harris (cited) in their back-analysis. The back-analysed modulus is shown, in Fig. **2.10.10**, for various stages of the construction of a tower. There is evidence here for the stiffness non-linearity of the till, i.e. as the load increases, the overall stiffness of the ground decreases. It is interesting to note that the very high values of the apparent ground modulus, in the region of 700 MNm^{-2}, are far higher than was accepted at the time of writing. From what is now known of soil stiffness behaviour (e.g. very high stiffness on stress-path reversal), these moduli are less surprising. Another point regarding Fig. **2.10.10** is that the stiffness degradation is less in actual ground conditions than would be expected from the results of laboratory triaxial tests (e.g. Fig. **2.5.6**). This is because the increased stress level in the ground imparted by the building is partly compensating (see Equation [2.5.1]) for the reduction in stiffness caused by increased strain. In laboratory triaxial tests, the load applied is a pure deviator load and, therefore, the reduction in stiffness (see Fig. **2.5.5**) is more pronounced than that in the field. This factor must be taken into account when interpreting laboratory data for the field condition.

2.10.4 Piles.

2.10.4.1 Pile Design Methods.

The cone penetration test (CPT), which is a widely used method of pile design, based on sleeve friction and end resistance, has been found to be unreliable when applied to Dublin boulder clay, owing to the presence of inert intrusions, such as large cobbles and boulders. For example, data analysed by Faulkner (1998), suggests an erroneous (CPT) classification of Dublin boulder clay as a very stiff sand and negative pore water pressure in a CPTu test. This inapplicability of the CPT method, when applied to Dublin boulder clay, demonstrates the importance of accurate predictions of pile behaviour; for example, traditional methods based on predictions of the ultimate load of a single pile and the application of partial factors to these predictions.

The most common of such methods, applied to Dublin boulder clay, are the total stress and effective stress methods. Following this, typically 10% of the piles are load tested to 1·5 times working load to ensure that the design is adequate.

The total and effective stress methods are respectively:

$$\tau_t = \pi r^2.N_c.c_u + \pi dl.\alpha.c_u \qquad [2.10.1]$$

$$\tau_t = \pi r^2.N_q.\sigma_v' + K_0.\sigma_v'.\tan\delta \qquad [2.10.2]$$

where τ_t is the total pile resistance (in units of force), r is the pile radius at the base, d is the pile diameter, l is the length of the pile, c_u is the undrained shear strength of the soil (as an average over the length of the pile and as a single value at the base), α is a partial factor, N_b and N_q are dimensionless base bearing factors, σ_v' is the vertical effective stress in the ground, K_0 is the coefficient of earth pressure and δ is the pile-soil interface friction angle.

α is an average shaft friction parameter that is assumed equal to 0·4-0·45 for bored piles in high strength boulder clay (Weltman and Healy (1978), Thomson (1981) and O'Riordan (1982)). The total stress bearing capacity factor, N_c, is generally taken as 9 in stiff boulder clay (Weltman and Healy (cited) and Thomson (cited)). The estimation of δ and K_0 is not straightforward, however, as is the case with the value of N_q (Weltman and Healy, cited). The uncertainty in δ and K_0 has led to the overwhelming popularity of the 'α' method (Looby, 1996), which is also possibly more fundamental to the fine grained till, as it is based on total stresses.

The recent Eurocode 7 method of pile design (see Orr and Farrell, 1999) is based on the total stress and effective stress methods. The method relies on partial factors and an estimate of the level of certainty; e.g. uncertainty in ground conditions at a site (see Lawler and Farrell (2003) for details).

Another method of pile design, not based on the effective stress and total stress methods, is that proposed by Chin (1972). Chin (cited) proposed that the load deflection behaviour of a pile is describable by a hyperbola. By measuring the pile head load against deflection up to loads below ultimate, the (working) pile test data, if it describes a hyperbola, can be extrapolated to determine probable failure loads. Chin's well-known method has been found to work particularly well in friction piles or end bearing piles but not when there is a sharing of the load (Fleming, 1992).

The methods described above are found to give adequate designs. However, the methods are also considered to give conservative designs, when applied to Dublin boulder clay, owing to conservatism in the selection of the relevant soil parameters. Frequently the design is based on limiting values of shaft friction, which have been interpreted from field tests carried out in other types of soils. These limiting values are not necessarily applicable to fine grained lodgement tills, such as those found in Dublin, which have high undrained shear strength and relatively high angles of shearing resistance. For example, O'Riordan's, 1982, α value of 0·4, widely applied to Dublin till, was back-analysed from London clay, which, although classified as a stiff clay (like Dublin till), is intensely fissured, sedimentary and of high plasticity.

These approaches can thus lead to uneconomical designs; hence, it is believed that the application of accurate numerical models to routine pile analysis could contribute to pile design in Dublin boulder clay. Such models have the potential of accurately estimating pile settlement and, more importantly, the differential settlement of combined foundations.

2.10.4.2 Pile Capacity and Settlement in Boulder Clay.

Thomson (1981) examined three cast-in-place concrete piles in the Edmonton till (the piles discussed here are those presented by Thomson (cited) without enlarged bases, which is not common practice in Dublin boulder clay). The capacity of the piles, defined as excessive or plunging settlement, was found to be 2350 kN (610 mm ϕ, 14·3 m length), 3900 kN (760 mm ϕ, 18·3 m length) and 4000 kN (760 mm ϕ, 20·1 m length). The capacity of the piles were equated in terms of soil strength, estimated using Equation [2.10.1] with $\alpha = 0{\cdot}45$ and $N_c = 9$; the calculations showed that the value thus obtained was about equal to the unconfined compressive strength of the soil (306 kNm^{-2}), when tested in the laboratory.

Farrell et al. (1995a) reported on the settlement of a large number of working, pre-cast concrete pile tests in Dublin boulder clay. The pile load-settlement ('t-s') data are shown in Fig. **2.10.11**. Up to working loads, the settlement of the piles was essentially linear, although the secant modulus was somewhat higher ($E_u = 150$ MNm^{-2}) than the footing test (see Section 2.10.3), which was considered to be due to the difference in strain levels in the ground, or, moreover, due to differences in the degree of soil shearing and, thus, dilatancy (Houlsby, 1991). Weltman and Healy

(1978) gave the following expression based on the apparent secant modulus, E_s, for a situation involving a large number of piles of various types in boulder clay:

$$\log E_s = c_u/70 + 3{\cdot}23,\ c_u < 250\ kNm^{-2} \qquad [2.10.3]$$

The pile base modulus, E_b, is generally taken to be higher than E_s, not exceeding 3-5 times. In Continuous Flight Auger (CFA) piles, which are the subject of an FE modelling study in this thesis, the loose soil at the base of the pile is removed in the concrete placement stage, resulting in a high value of E_b, which is typically taken as E_{25} (Fleming, 1995).

DeJong and Harris (1971) recorded the settlements for end bearing pile groups, bearing on Edmonton till, the results of which are shown in the figures of Fig. **2.10.12**. The maximum settlement of the groups was about 32 mm, under heavy loads in the region of 400 – 3200 kips (1780 – 14235 kN). It is evident from the figures that the majority of the settlement occurs very rapidly. The largest group of piles (10 No.) settled least, despite carrying typically twice the load of the smaller groups (3 – 4 No.), because the average load per pile for the larger pile groups was less than that for the smaller pile groups.



Fig. 2.10.1. Typical excavation practice and slope angles in Dublin boulder clay (Griffith Avenue)

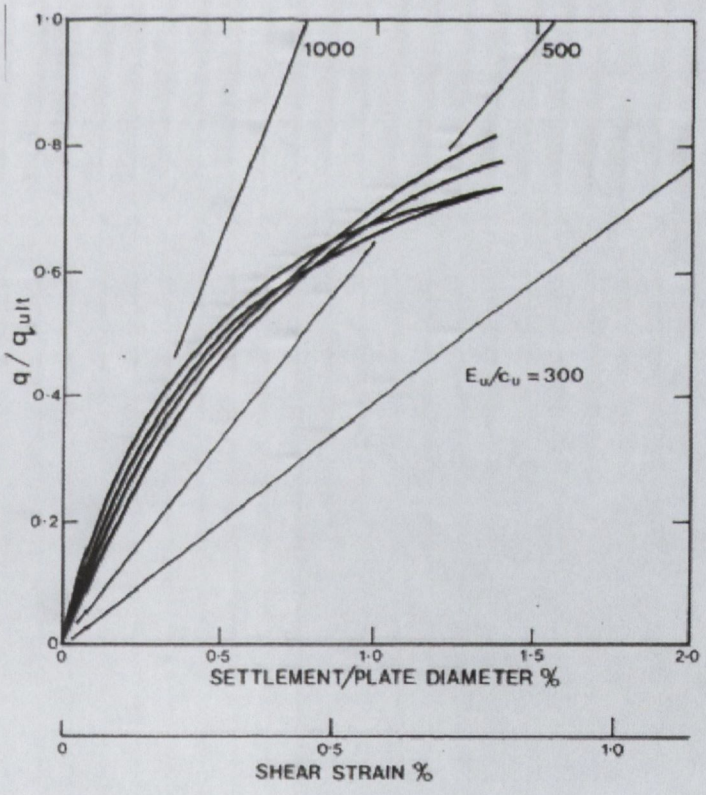

Fig. 2.10.2. Stiffness in plate bearing tests on very stiff clay; $E_u/c_u = 1000$ represents the stiffness of excavations, after Simpson et al. (1979)

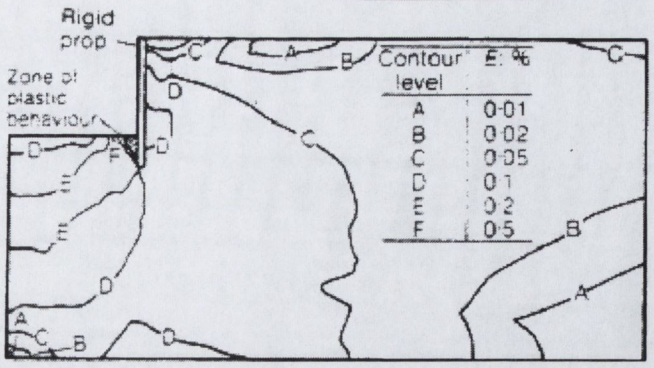

Fig. 2.10.3. Evidence of small strains in excavations in stiff clay, after Jardine et al. (1986)

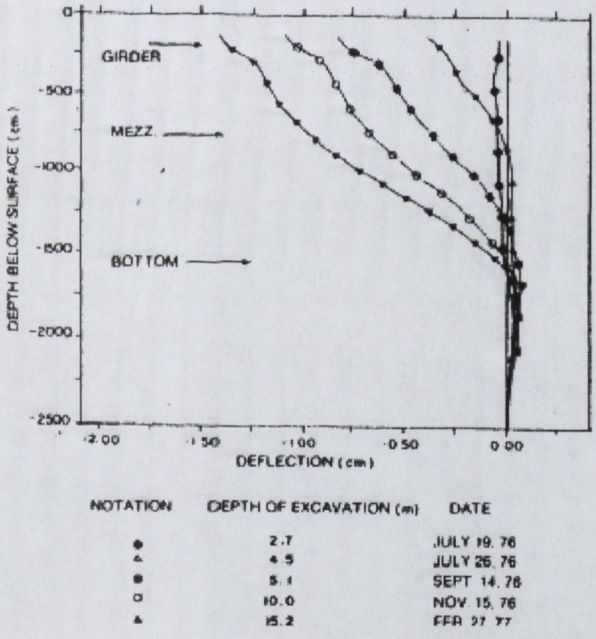

Fig. 2.10.4. The development of inward wall deflection with increasing depth of excavation in boulder clay, after Eisenstein and Medeiros (1983)

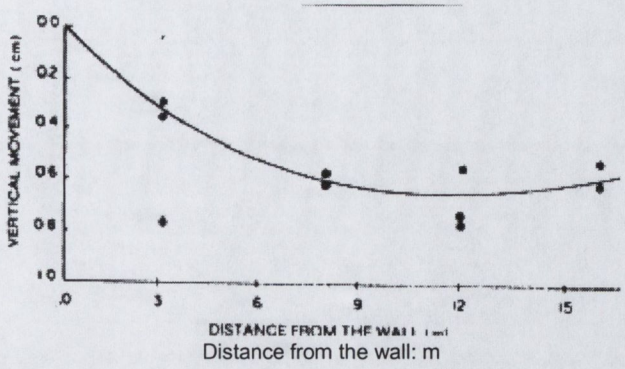

Fig. 2.10.5. Surface settlement of boulder clay at distance perpendicular to a supported excavation, after Eisenstein and Medeiros (1983)

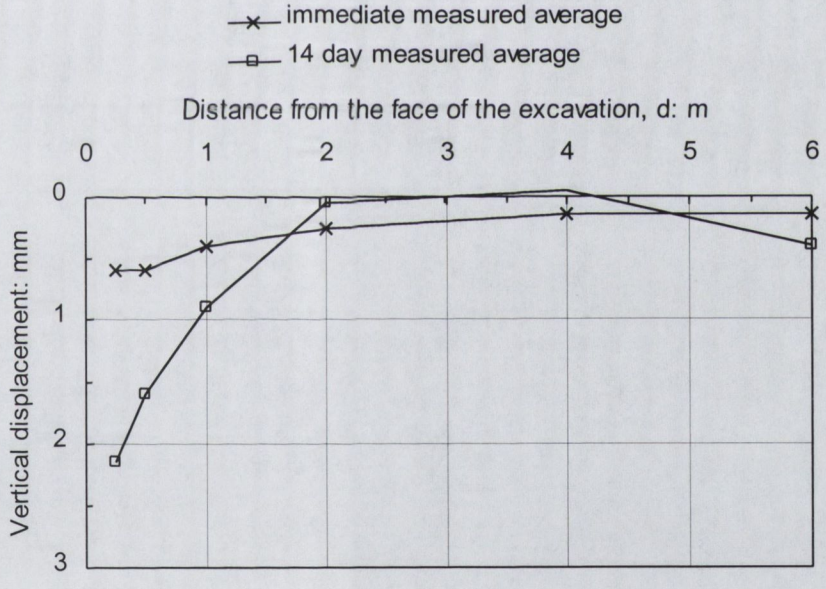

Fig. 2.10.6(a). Vertical surface settlement in Dublin boulder clay, adapted from Treacy (1995)

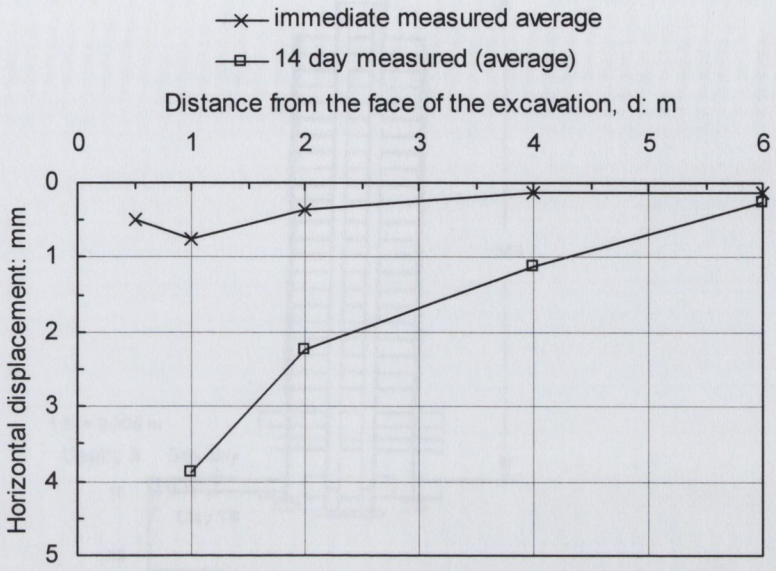

Fig. 2.10.6(b). Horizontal surface settlement in Dublin boulder clay, adapted from Treacy (1995)

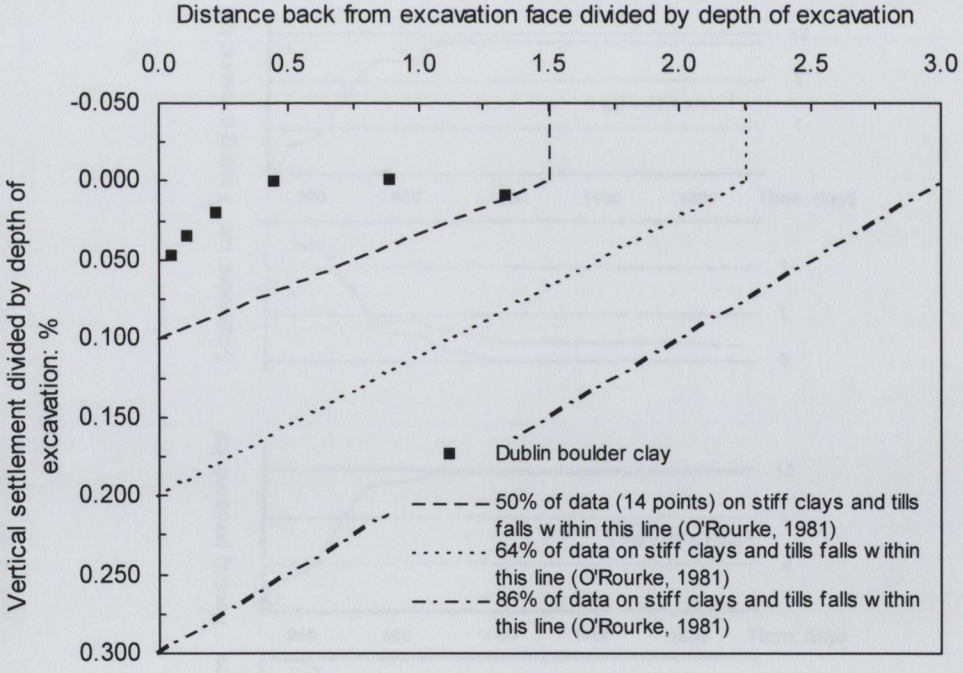

Fig. 2.10.7. Fig. 2.10.6(a) replotted with a normalising procedure and compared to data on stiff clays and till given by O'Rourke (1981)

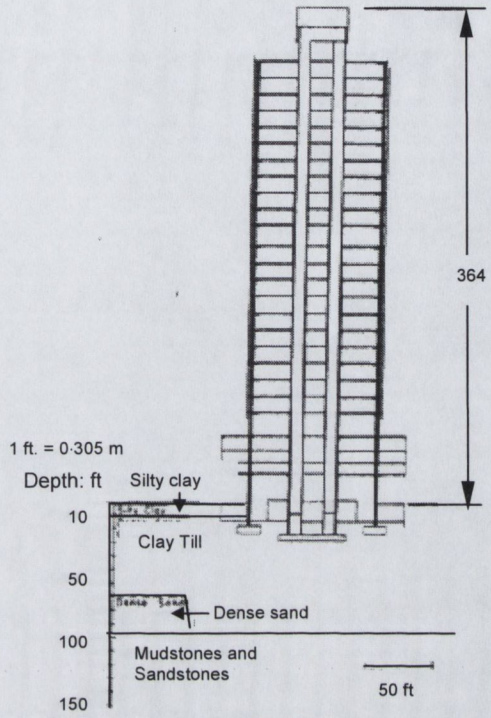

Fig. 2.10.8. Foundation details (CN tower), after DeJong and Harris (1971)

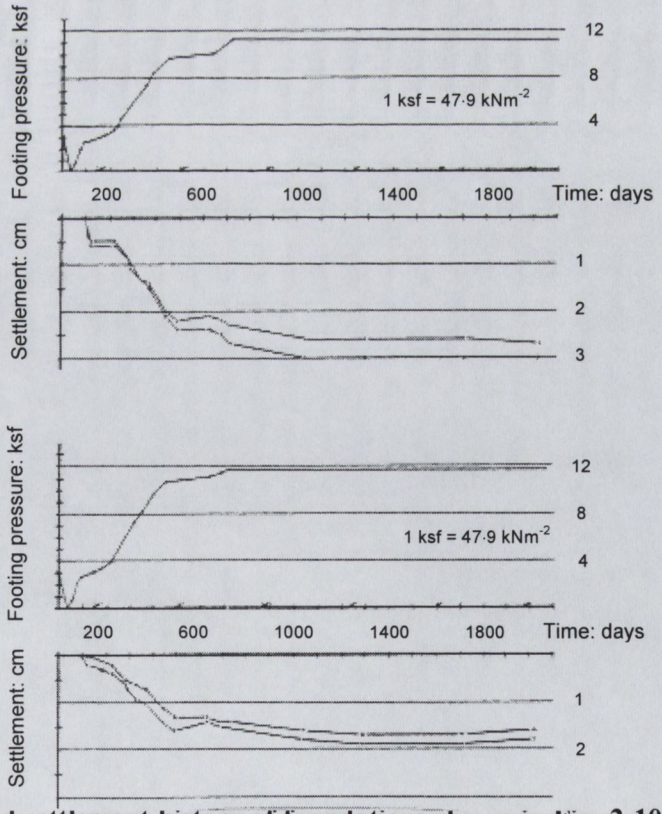

Fig. 2.10.9. Load and settlement history of foundations shown in Fig. 2.10.8, after DeJong and Harris (1971)

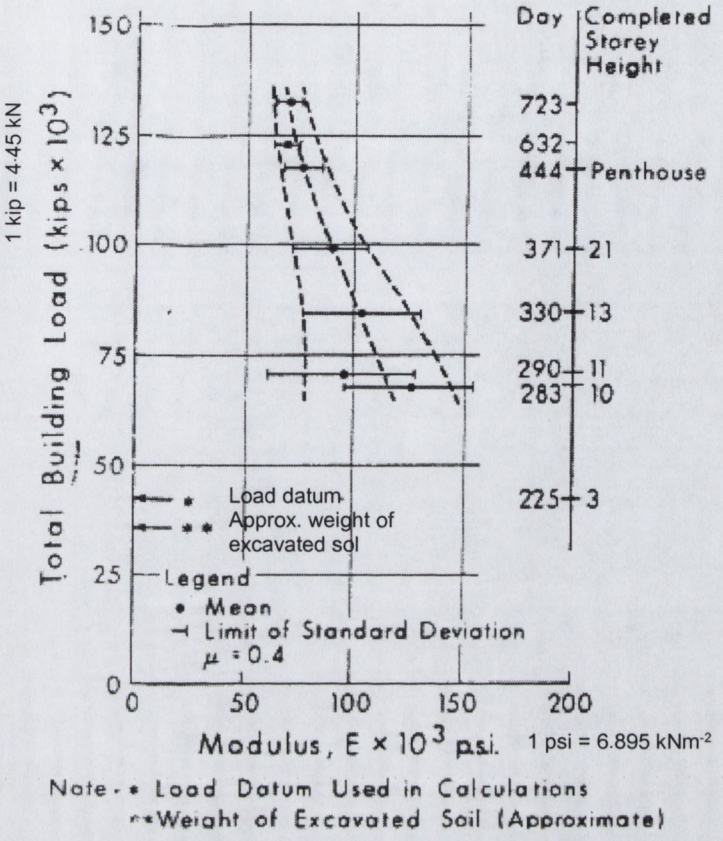

Fig. 2.10.10. Non-linear stiffness of foundations in Edmonton till, after DeJong and Harris (1971)

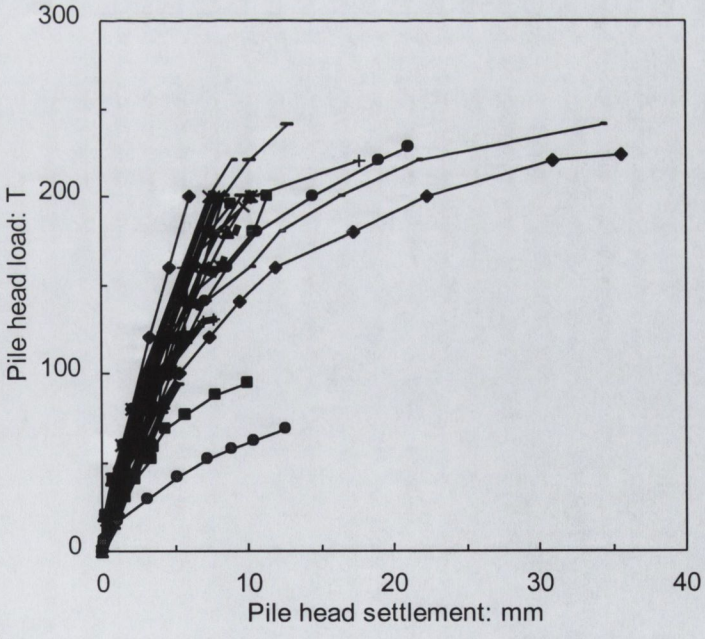

Fig. 2.10.11. Driven pile tests in Dublin boulder clay, adapted from Farrell et al. (1995a)

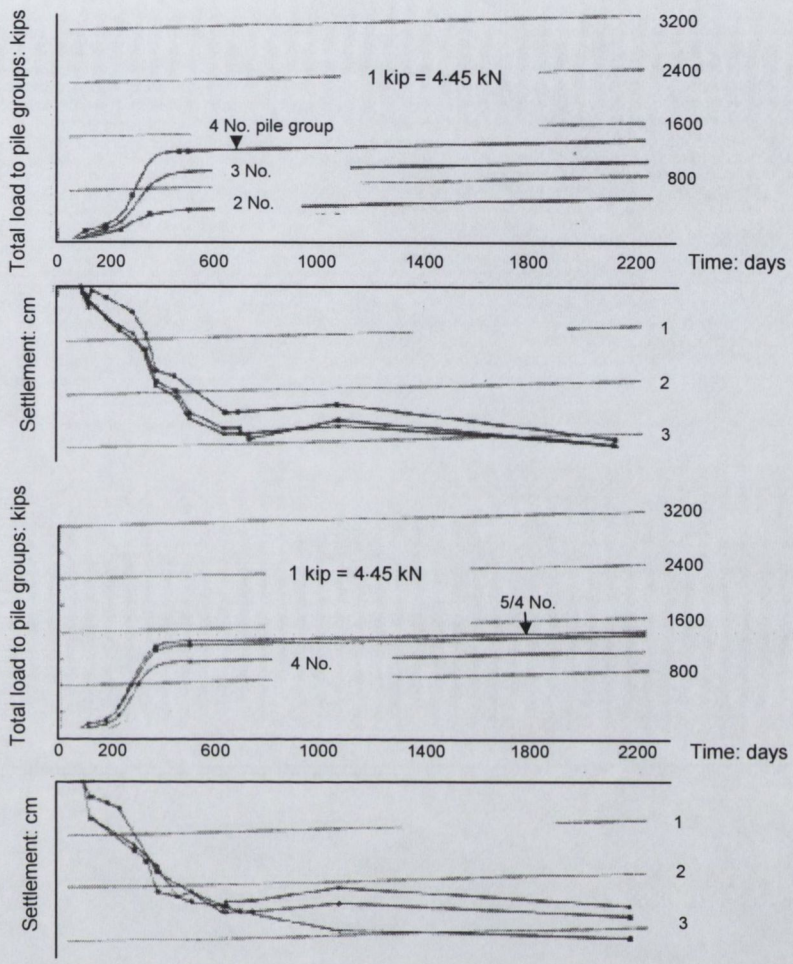

Fig. 2.10.12. Settlement of pile groups in stiff till, after DeJong and Harris (1971)

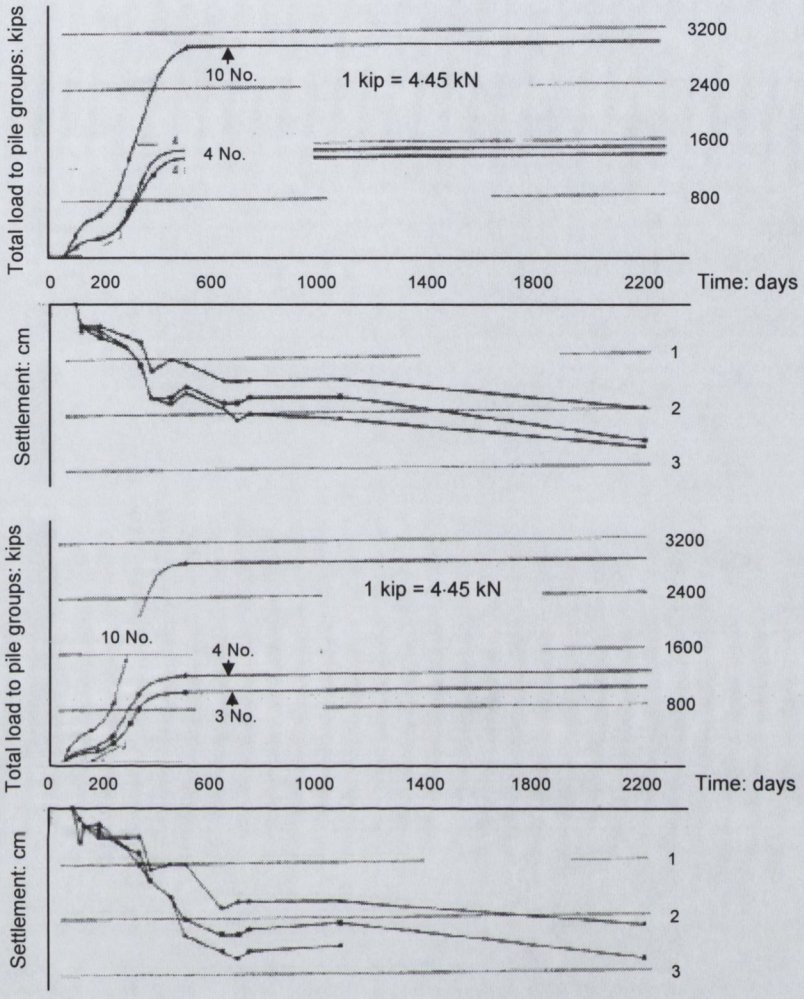

Fig. 2.10.12 cont'd…. Settlement of pile groups in stiff till, after DeJong and Harris (1971)

CHAPTER 3

GLACIAL HISTORY - RELATED GEOLOGY AND TILL PROPERTIES

CHAPTER 3

GLACIAL HISTORY - RELATED GEOLOGY AND TILL PROPERTIES

3.1 Glacial Advance - Climate System Research and the Timing of Glacial Events.

Site investigation evidence studied by the author over a very wide range of the land area defined in Section 2.2 (inter alia BMA (1995), Fairhurst Garland and Partners (1978), Farrell and Wall (1990), Farrell et al. (1995b), Farrell et al. (1998), Geoconsult-Arup (1997), IGSL (1992), LRT (1997), Thomas Garland and Partners (1996), TJ O'Connor and Associates (1997)), suggests that a single till sheet is widespread in Dublin. This finding is inconsistent with the theories of up to five separate glacial events, with long inter-glacial periods, that are believed to have affected Dublin (see Section 2.2.3). If the latter were the case, it would be expected that boreholes would indicate a multiple till stratigraphy with interstitial layer sequence, as is found in Edmonton, Canada, for example (inter alia May and Thomson (1978)). The interstitial layer within the Edmonton till is due to inter-glacial deposition. Furthermore, variations in lithology would be expected from glaciers of different provenance. However, Farrell et al. (1995b) undertook lithological comparison of till from a wide area; the clast lithologies and till mineralogy of which were remarkably similar. Warren (1991b) suggested that analysis of the resistant and durable chert and sandstone contents relative to the limestone content are a measure of the diamicton age. Hence, the analysis of Farrell et al. (cited) indicates that the till is of generally the same age and phenoclastic origin throughout.

The most straightforward explanation for this is that the stratigraphic sequence in Dublin represents a simple glacier advance and retreat with ice oscillations but without long inter-glacial periods. The mechanism may involve re-working of material from earlier glacial cycles by later oscillations. This extended glaciation would also allow the temperate glaciers, which covered Dublin during this time, to deposit the thick till sheet found today[1].

---

[1] Although temperate based glaciers are believed to have covered Dublin (see Section 2.2.4), these glaciers are associated with till sheets of a few metres thickness (Boulton et al., 1974). This can be reconciled if the glacier was of extended duration.

McCabe (1996) details the recent ideological shift from the low frequency, Heinrich, events (examined in the literature review) of about 10000 years period to millennial scale, climate driven, synchronous ice advances/oscillations of ice sheets of different ice centres. These occur on a circum North Atlantic ice sheet scale as opposed to a local British Isles scale, as previously thought. At least five oscillations are known of in the area studied in the interval between the Late Devensian maximum (to the south) and the Loch Lomond limit (to the north) in the interval 21k - 10·5k BP (McCabe, cited). These oscillations may be comparable to the glaciations that have been considered to date to be unconnected events; hence the single till sheet found in Dublin.

Irish ice flow patterns, commonly given in ice flow diagrams, support the possibility of joint ice-streams, as shown in Fig. **3.1.1**. These joint ice-streams are a consequence of climate driven ice oscillation. For example, synchronous ice movement around the time of the glacial maximum would have caused mutual deflections and hence formed the joint ice-streams of Irish Sea and Midlandian ice that sent a lobe of ice down the flat east coastline towards Wexford (Mitchell, 1986).

In summary, the site investigation evidence suggests a single, thick till sheet throughout Dublin, which can be explained in terms of climate driven ice oscillation. The theory is backed-up by available evidence for the direction the ice was moving in and on clast lithologies.

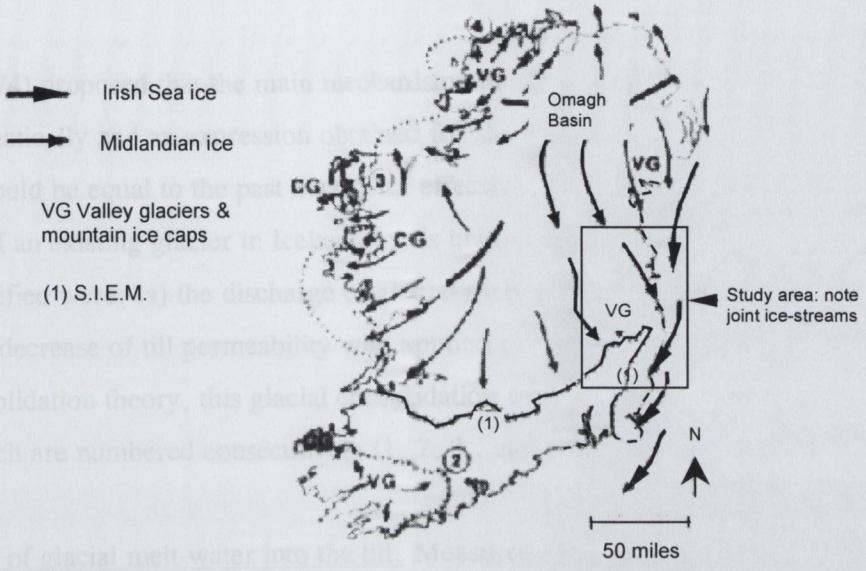

Fig. 3.1.1. Ice flow patterns over Ireland

3.2 Glacial Consolidation.

3.2.1 The Glacial Consolidation Equation.

Boulton et al. (1974) proposed that the main mechanisms of glacial consolidation could be expressed mathematically and an expression obtained for the effective stress in the till[1]. This effective stress would be equal to the past maximum effective stress applied to the soil. Based on observations of an existing glacier in Iceland that is uncovering lodgement till, the main mechanisms identified were: (a) the discharge of glacial melt-water into the till, (b) the pressure of ice and (c) the decrease of till permeability with applied pressure. As with Terzaghi's one-dimensional consolidation theory, this glacial consolidation theory makes a number of assumptions, which are numbered consecutively (1, 2, 3...etc) in the following derivation.

(a) The discharge of glacial melt-water into the till. Measurements of the piezometric level within the till under the Icelandic ice sheet indicated a down-glacier gradient, which was explainable by (1) steady-state discharge through the till out towards the glacier margin. It is assumed that (2) the specific discharge, Q_x, due to an excess pore water pressure (p_w) (to avoid ambiguity, some alternative symbols are used in this section) gradient, dp_w/dx, through the soil can be given by Darcy's law. (3) One-dimensional flow is assumed, giving:

$$Q_x = \frac{-kt}{\gamma_w}\frac{dp_w}{dx} \qquad [3.2.1]$$

where the x-direction is down-glacier, k is the material permeability, t is the layer thickness and γ_w is the unit weight of water. (4) For steady-state conditions, Q_x must equal the rate of water production at the base of a melting glacier. Water, W, is produced at the ice-bed interface[2] by a combination of pressure melting (W_1) and the earth's geothermal heat (W_2). The water thus produced can flow through sub-glacial channels, a very thin water layer at the ice-bed interface and within permeable sub-glacial material. (5) It is considered, however, that the last

---

[1] The solution originally proposed by Boulton et al. (1974) does not balance and hence it was considered worthwhile, given the importance of stress-history to this research, that the correct solution be derived.

[2] The ice-bed interface is a very thin layer; thus W is the volume of water produced per m^2/s.

mechanism dominates (Boulton et al., cited). The sliding velocity of Icelandic glaciers has been found to increase down-glacier (Boulton and Paul, 1976); as sliding is facilitated by pressure melting (see Section 2.2.4), it follows that W increases down-glacier, giving:

$$Q_x = Wx \qquad [3.2.2]$$

$$Q_x/LW = x/L \qquad [3.2.3]$$

where L is half the glacier width (i.e. L is measured from the glacier pole to the glacier margin), which assumes (6) a horizontal glacier base.

(b) The total pressure of ice. (7) The surface profile of the ice-sheet may be approximated by an ellipse. The thickness of ice, H, is therefore the semi-minor axis and half the width, L, the semi-major axis:

$$(h/H)^2 + (x/L)^2 = 1 \qquad [3.2.4]$$

where h is the height of the glacier at any point, x, distant from the pole.

[3.2.4] can be rewritten as:

$$(p/p_0)^2 + (x/L)^2 = 1 \qquad [3.2.5]$$

where p_0 is the maximum pressure of ice and p is the applied stress at x.

Combining [3.2.1] and [3.2.5] gives:

$$Q_x = \frac{-kt}{\gamma_w} \cdot \frac{d\left(\frac{p_w}{p_0}\right)}{d\left(\frac{x}{L}\right)} \cdot \frac{p_0}{L} \qquad [3.2.6]$$

(c) Decrease in till permeability with applied pressure. Boulton et al. (cited) conducted one-dimensional consolidation tests (hence, (8) one-dimensional consolidation is assumed) on samples of the Icelandic till and found an exponential relation between permeability and the vertical effective stress, $p-p_w$. (9) Assuming permeability is the same in the horizontal and vertical directions, this experimental result gives:

$$k = k_i . e^{m(p-p_w)} \qquad [3.2.7]$$

where m^3 is a material constant (a negative integer in units of pressure) and k_i is the permeability of the soil at zero vertical effective stress. The exponential relationship between permeability and vertical effective stress was verified in this thesis (see Fig. **A.1.5**).

Combining the three mechanisms, represented by Equations [3.2.3], [3.2.6] and [3.2.7], gives the following differential equation:

$$\frac{d\left(\frac{p_w}{p_0}\right)}{d\left(\frac{x}{L}\right)} = -\frac{LWx\gamma_w}{p_0 T_r e^{m(p-p_w)}} \qquad [3.2.8]$$

where T_r (= kt) is the soil transmissivity.

Rearranging [3.2.8] in two steps gives:

$$\left(\frac{p_0 T_r}{L^2}\right) e^{mp_w} d\left(\frac{p_w}{p_0}\right) = -W\gamma_w \left(\frac{x}{L}\right) e^{mp} d\left(\frac{x}{L}\right) \qquad [3.2.9]$$

$$\left(\frac{p_0 T_r}{L^2}\right) e^{mp_0\left(\frac{p_w}{p_0}\right)} d\left(\frac{p_w}{p_0}\right) = -W\gamma_w \left(\frac{x}{L}\right) e^{mp_0\sqrt{1-\left(\frac{x}{L}\right)^2}} d\left(\frac{x}{L}\right), \text{ by [3.2.5]} \qquad [3.2.10]$$

It is possible to separate out [3.2.10] in the following way:

$$I_1 = \frac{p_0 T_r}{L^2} \frac{e^{mp_w}}{mp_0} + A \qquad [3.2.11]$$

$$I_2 = -W\gamma_w \left(\frac{x}{L}\right) e^{mp_0\sqrt{1-\left(\frac{x}{L}\right)^2}} d\left(\frac{x}{L}\right) \qquad [3.2.12]$$

Equation [3.2.12] is best integrated by substitution:

$$u = 1-(x/L)^2 \qquad [3.2.13]$$

$$du = -2(x/L)d(x/L) \qquad [3.2.14]$$

$$I_2 = \left(\frac{W\gamma_w}{2}\right) e^{mp_0\sqrt{u}} du \qquad [3.2.15]$$

Equation [3.2.15] turns out to be a very complex derivative. However, a similar integrand, which is very complex and best shown by back-analysis of the anti-derivative, was found in World of Mathematics (2000). Inputting that integrand gives:

$$I_2 = \left(\frac{W\gamma_w}{2}\right) 2e^{mp_0\sqrt{u}} \left(\frac{1}{(mp_0)^2} + \frac{\sqrt{u}}{mp_0}\right) + A' \qquad [3.2.16]$$

Re-substituting [3.2.13] into [3.2.16] gives:

$$I_2 = W\gamma_w e^{mp_0\sqrt{1-\left(\frac{x}{L}\right)^2}} \left(\frac{1}{(mp_0)^2} + \frac{\sqrt{1-\left(\frac{x}{L}\right)^2}}{mp_0}\right) + A' \qquad [3.2.17]$$

The solution is obtained by re-combining [3.2.11] and [3.2.17] as follows:

---

[3] Rearranging [3.2.7] gives $p-p_w = (1/m).\ln(k/k_i)$. Hence, the formulation implies that $m \neq 0$.

$$\frac{p_0 T_r}{L^2}\frac{e^{mp_w}}{mp_0} = W\gamma_w e^{mp_0\sqrt{1-\left(\frac{x}{L}\right)^2}}\left(\frac{1}{(mp_0)^2}+\frac{\sqrt{1-\left(\frac{x}{L}\right)^2}}{mp_0}\right)+B \qquad [3.2.18]$$

Rearranging [3.2.18] in two steps gives the solution:

$$e^{-m(p-p_w)} = \frac{L^2 W\gamma_w}{T_r p_0}\left(\frac{1}{mp_0}+\sqrt{1-\left(\frac{x}{L}\right)^2}\right)+C \text{ , by [3.2.5]} \qquad [3.2.19]$$

$$p - p_w = -\frac{1}{m}\ln\left|\frac{L^2 W\gamma_w}{T_r p_0}\left(\frac{1}{mp_0}+\sqrt{1-\left(\frac{x}{L}\right)^2}\right)\right| \qquad [3.2.20]$$

3.2.2 The Importance of the Glacial Consolidation Equation.

When approximate parameters are inputted into this equation[4], the predicted value of σ_{vy}' ($p - p_w \approx 4500$ kNm^{-2}) is found to be about three times greater than laboratory estimates for the Dublin till (1500 kNm^{-2} - see Sections 2.4.1 and 5.3.1.1). This quantitative inaccuracy may be due to fundamental differences between glacial and laboratory consolidation (see Section 3.1), the fact that the yield stress is not simply the past maximum pressure (see Section 5.3.1), or, moreover, to a number of the assumptions made in the derivation. However, closer examination reveals that the major assumptions are reasonable. Assumptions (8) and (9), for example, are considered accurate as glacial consolidation is one-dimensional and because the permeabilities in both the horizontal and vertical directions are the same[5]. Related to the latter, the assumption (3) that flow is one-dimensional is also considered reasonable in this regard. As such, it is concluded that Equation [3.2.20] is of qualitative, if not quantitative, value.

---

[4] m = -0·004 (see Equation [5.3.8]), L = 258 km (distance from Ailsa Craig (Irish Sea) ice source to Dublin), W = $W_1 + W_2$ = 2·8×10^{-10} m^3/m^2/s (for basal velocity 17 m/year (Boulton and Paul, 1976)) + 1·67×10^{-10} m^3/m^2/s (see Weertman (1957 and 1964) for derivations), γ_w = 10 kNm^{-3}, T_r = kt = 10^{-11} ms^{-1} (see Section 5.3.4.2) × 15 m, p_0 = 9 kNm^{-3} (unit weight of ice) × 950 m (approximate thickness of ice at glacial maximum over Dublin based on depth of glacier on Wicklow Mts. (610 m - see Section 2.2.3) and assumption (7)) and x = 258 km - 16 km (the latter is distance from Dublin to northern slopes of the Wicklow Mts.).

[5] This is because lodgement tills, unlike sedimentary clays, are unlayered

In this respect, the solution, which balances, shows that, of the major glacial variables (total ice-sheet pressure (p_0), melt-water (W), till transmissivity (T_r), the glacier dimensions (x and L) and the constant m), only m lies outside the Naperian logarithm. Hence, the material parameter m, which controls the rate of reduction of material permeability as vertical effective stress increases (see Equation [3.2.7]), largely influences the value of σ_{vy}'. The value of m was found, in the consolidation tests conducted for this thesis (see Figs. **A.1.5** and **2.5.16**), to decrease as the gravel content of the sample increased. This implies, from Equation [3.2.20], that a well graded, stony till will theoretically possess a higher preconsolidation pressure, and thus a higher stiffness, strength and in situ K_0 (see Equations [2.4.1], [2.4.2] and [2.4.3], respectively), than a lodgement till with a higher fines fraction.

This theory can be tested with the results of the high-pressure consolidation tests conducted for this thesis; the data, shown in Table **5.3.1**, confirm that the very gravelly sample possessed a higher OCR than the less gravelly sample.

This positive result is not limited to the laboratory, however. The author, on expeditions to deep excavations in the Marino area of Dublin (Whitehall Dublin Port Tunnel (DPT) access shaft and Griffith Ave.), observed (Fig. **2.2.7**) that *very stiff* (grey black) *gravelly* boulder clay overlaid *firm to stiff* (grey brown/brown grey) boulder clay with significantly *less gravel*. Moreover, examination of very detailed DPT site investigation reports (Geoconsult-Arup, 1997) reveals that the firm to stiff boulder clay overlies *soft to firm* brown *silt*[6].

Nor is the result limited to Ireland: a similar stratigraphic sequence is also found in Northern Britain (Clarke, 2002) and Canada. The latter is evident when an examination is made of the extensive geological reports that have been conducted there, including those of Boyer et al. (1985) in Montreal, Baker et al. (1998) in Toronto and May and Thomson (1978) in Edmonton. Boyer et al. (cited), for example, show very clearly (their Fig. 15) that the coarse grained Montreal till possesses a higher stiffness than fine grained Montreal till from the same stratigraphic sequence. The remaining authors also report similar stiffness variations. Such

[6] From experience of lodgement tills in northern England and from observations of lodgement in present day glaciers in Iceland, Clarke (2002) proposed that fingers of pre-glacial material could be broken off *en masse* by moving ice and deposited, *en masse*. Subsequent deposition of lodgement till could result in the confusing changes in stratigraphy observed by this author.

sequences can be reconciled if, as the evidence suggests it is, the theory of glacial consolidation proposed in Section 3.2.1 is qualitatively accurate.

3.3 Glacial Retreat - Shearing and Remoulding.

Boulton et al. (1974) described newly deposited Icelandic lodgement till as a two-layer material: an upper zone of high void ratio and a lower zone of relatively low void ratio. The upper zone had been remoulded by subglacial shearing, which occurs when the basal shear stress exceeds the shear strength of the soil. (As the Icelandic glacier is temperate (see Section 2.2.4), there is very little englacial material, therefore the upper till could not represent melt-out.) The remoulded till has since been termed deformation till (Boulton, 1996) to indicate that the lodgement till has been remoulded in situ without transport away from where the till was deposited. This is to distinguish it from lodgement till, which can be composed of material from anywhere the glacier has passed over. The remoulding process results in a lower strength soil of relatively low gravel content due to shearing and particle crushing.

Basal shear stresses (τ_b) are understood to be within a narrow range because of the proportionality with total basal slip velocity (Weertman, 1964). Basal velocities have been measured in the range 5 m/year to 150 m/year, suggesting a limited theoretical range for τ_b of about 0·8 bar to 4·5 bar (these latter values were derived from equations developed by Weertman (1957 and cited)). A typical value of τ_b of 150 kNm^{-2} has been suggested (Boulton and Paul, 1976). The shear strength of the till is given by:

$$\tau = \sigma_v' \tan\phi' + c' \qquad [3.3.1]$$

Hence, for a ϕ' of about 40° and $c' = 0$ kNm^{-2} (see Section 5.4.3), shear failure can only occur for a vertical effective stress in the till of less than about 175 kNm^{-2}. The combination of basal shear stress, τ_b, and this low effective stress can occur at ice sheet margins, i.e. the effective stresses imposed by the glacier are especially low as the ice retreats over newly deposited lodgement till. This theory would explain why deformation till is widespread (evidence for which can be found in Dublin (this thesis), Iceland (Boulton and Paul (1976) and Boulton et al. (1974)) and Canada (inter alia DeJong and Morgenstern (1973) and Boyer et al. (1985))).

The remoulding of the till will have created a constant volume condition. Hence, the deformation till will have properties similar to the constant volume properties of the lodgement till beneath. The depth of the deformation zone depends on a combination of the vertical stress in the ground and the basal shear stress. Boulton et al. (cited) found the zone was about 0·5 m thick. Measurements taken by this author, in an excavation and in a soil core in Dublin, suggest a thickness of about 1·5 m, which is in keeping with the measurements of Boulton and Paul (cited) (1 - 1·5 m thickness) and with measurements of the thickness of the layer in Edmonton (about 1 m) (inter alia Boyer et al. (cited) and DeJong and Morgenstern (cited)).

3.4 Post-Glaciation – Apparent Preconsolidation and the Formation of the Brown Boulder Clay.

On inspection, it is found that the deformation till is firm to stiff, which is inconsistent with glacial remoulding. However, such stiffness and strength can develop due to post-glacial apparent overconsolidation. Possible post-glacial mechanisms are desiccation, fluctuations in the water table and freeze-thaw. Freeze-thaw, for example, can create substantial suction in excess of 500 kNm^{-2} in advance of the freeze front (Boulton and Paul, 1976). As the high void ratio of the deformation till has resulted in a high water content, the zone is more susceptible to such freezing. In Canada there is much experience of the yearly freezing of till; Boyer et al. (1985) suggest that the freeze-front attenuates to about 2 m, coinciding with the extent of the deformation till. Evidence of post-glacial apparent overconsolidation is given in Section 5.7.1.

The freshly exposed Icelandic deformation till (Boulton et al., 1974) was of the same colour as the lodgement till. Hence, the difference in colour between the upper metres of the Dublin boulder clay and the remainder of the till found here (and elsewhere) must be post-glacial in origin. The coloration has been explained as being due to the subaerial oxidation of the ferrous-rich clay minerals present in the soil (Farrell et al., 1995b).

The brown colour is, therefore, due to soil rusting. For rusting to occur, there must be: (a) a reducing agent (e.g. Fe in the ferric minerals), (b) water, (c) an acidic substance (CO_2 in the air) and (d) oxygen and inorganic salts (e.g. NaCl). Furthermore, the consistent and relatively high subterranean temperature increases the rate of the reaction. In a fully saturated soil (below the water table), the oxygen component is missing, hence the till will not rust. Above the water

table, however, the soil is unsaturated and will rust. This corresponds with observations that the base of the brown till approximately corresponds with the water table. Furthermore, it would be expected that the water table will tend to perch on the lower permeability lodgement till; hence, the base of the deformation till will correspond with the mean water table.

Seasonal fluctuations in the water table, however, will cause a transition zone between the brown and black soil. In this zone the soil will be mottled brown/black as opposed to the vivid brown of the deformation till. This corresponds with observations of mottled grey/brown till in a transition zone between brown and black till (this author and Farrell et al. (cited)). From simple field tests, conducted by the author with a geologist's adze, and more complex laboratory and seismic tests (see Sections 4.1 and 5.7.2), the brown lodgement till (beneath the deformation till) has been found to be of similar stiffness to the black till.

Air-filled voids can support active root growth down to 1·5 m to 2 m depth, which can thus produce exudates that extract minerals from the soil that may alter the soil mineralogy (Gleeson, 2000). Root growth could be assisted by the higher void ratio of this deformation zone and could contribute to breaking down the soil, thereby forming clay minerals. Electron microscope images and quantitative X-Ray diffraction of the deformation till, on samples 0·25 m below the top of the till level (BTL), indicate a relatively high clay mineral content, which explains the high plasticity of the deformation till, as shown in Fig. **2.2.3** (see Section 5.6).

3.5 Implementation of Dublin Geology in FE Analysis.

Knowledge of likely ground conditions and potential problems that may be encountered requires an understanding of the geological history of a site. (It also requires a knowledge of the recent history, although this problem is obviously site specific.) This chapter presented an analysis of the geological history of Dublin, centred round the last ice age, aimed at producing a simplified yet accurate engineering geology for use in numerical modelling and site investigations. Excavations in Dublin boulder clay typically[7] show evidence of three distinct tills overlying intact, black limestone bedrock, which together make up the Dublin boulder clay, as shown in Fig. **3.5.1**. The soils identified in the photograph are:

[7] Note that exceptions were discussed in Sections 2.2.5, 2.2.6 and 3.2.2.

(a) A firm to stiff, reddish brown clay, from 0 m to 1·5 m BTL.

(b) Stiff to very stiff mottled brown clay, from 1·5 m BTL to the water table.

(c) Very stiff black clay, from the water table to rock head.

Soils (b) and (c) are lodgement tills, in the sense that they are composed of material from anywhere the glacier has passed over. Consequently, the brown and black lodgement tills are of similar stiffness and strength. The difference is that the brown lodgement till lies above the water table and is therefore not saturated and, thereby, the soil is subject to oxidation.

Soil (a) is a deformation till (Boulton, 1996), in the sense that it has been sheared by the base of the moving glacier but not transported, similar to a large shear box. The extent of this shearing has been identified as being limited to about 1·5 m BTL. The remoulding means that the strength of the deformation till is similar to that of the lodgement till at constant volume and has relatively less large intrusions, owing to particle crushing. This is reflected in a soil with a water content of two to three times that of the lodgement till and a relatively high void ratio. The latter has aided biological weathering by plants rooted in the overlying top soil, which has resulted in a soil of relatively high clay mineral content (Table **A.4.2(b)**); hence, the deformation till has a high plasticity. The relatively high void ratio of the deformation till has also resulted in a permeability higher than that of the lodgement till beneath.

Fig. **3.5.2(a)** shows a simple stratigraphic model for Dublin boulder clay based on the discussions outlined in this section and discussed in detail in preceding sections. However, this model may be simplified further because the extent of the brown till is often limited to about 2 m BTL; *ergo*, the thickness of the brown lodgement till is often negligible. Furthermore, Table **4.1.1**, Fig. **2.2.3** and Fig. **A.5.5** show that the brown lodgement till has about the same engineering properties as the black lodgement till. Therefore, it is generally acceptable, particularly if the water table is high, to simplify the stratigraphic model to the one shown in Fig. **3.5.2(b)**.

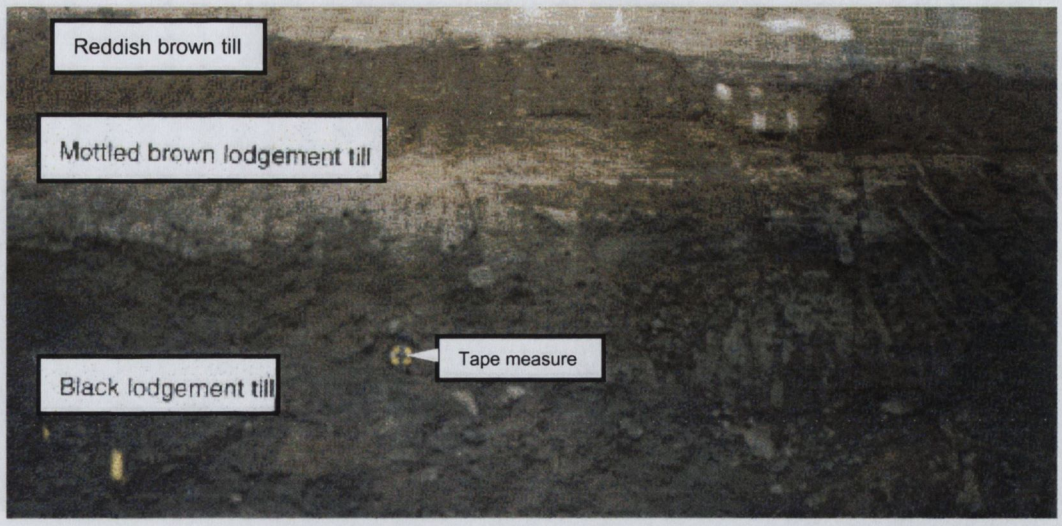

Fig. 3.5.1. Dublin boulder clay stratigraphy

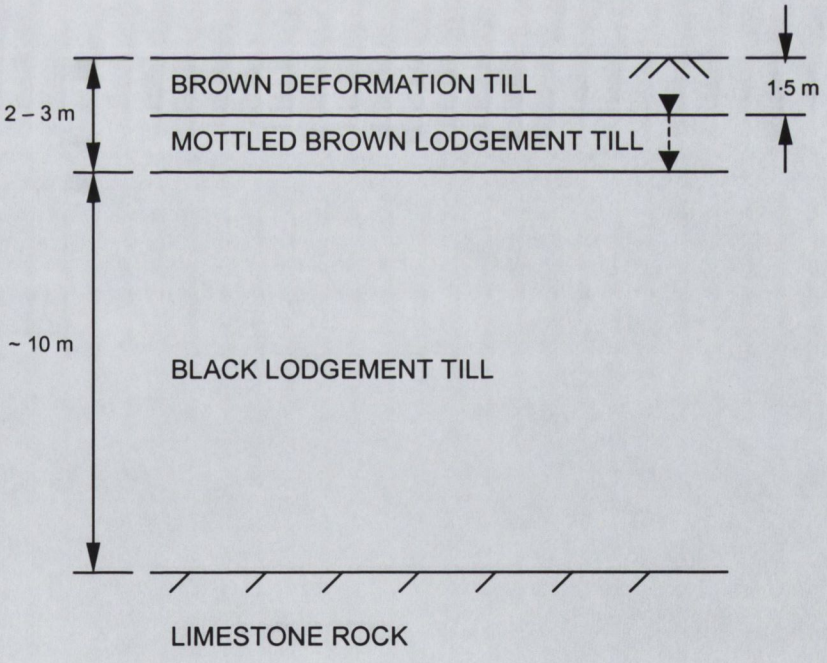

Fig. 3.5.2(a). Typical stratigraphic sequence in Dublin boulder clay

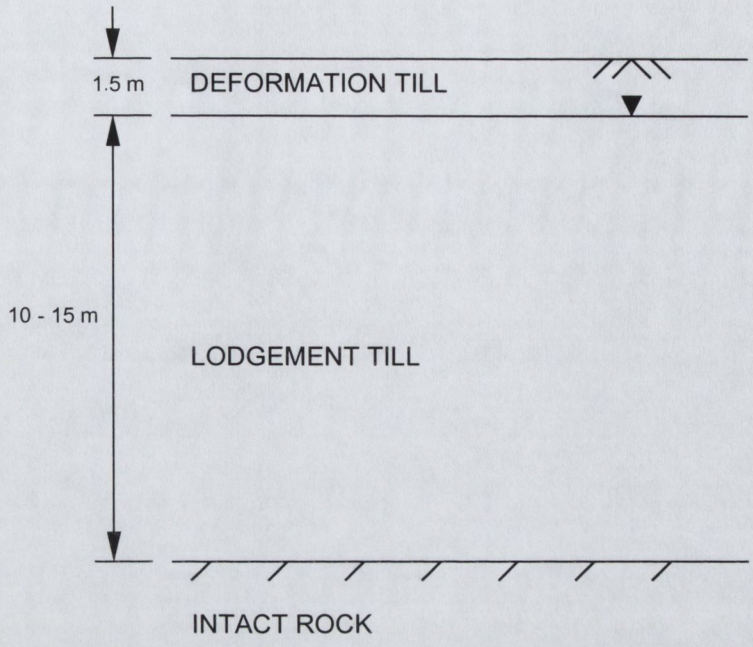

Fig. 3.5.2(b). Simplified stratigraphic sequence for use in FE analysis

CHAPTER 4

FIELD AND LABORATORY WORK - MATERIALS AND METHODS

CHAPTER 4

FIELD AND LABORATORY WORK - MATERIALS AND METHODS

4.1 Description of Soils Tested.

The lodgement tills tested were from various areas around Dublin. The particle size distributions, index properties and index property variation compare favourably with those given by Farrell et al. (1995b). The data shown are typical of the various sites at the depths and locations of interest, e.g. at the depths of tested soil samples or, in the case of the pile tests, over the length of the piles. Test data borrowed from commercial site investigations are indicated with an asterix. Natural water contents, Atterberg limits and PSD of the soils tested are given in Figs. **4.1.1**, **4.1.2** and **4.1.3**, respectively. The methods of testing followed BS 1377: Part 2 (1990). The liquid limit tests were carried out with the fall cone apparatus and sedimentation analysis was conducted by either the pipette or hydrometer methods.

A large amount of consistency data arose from the Dublin Port Tunnel site investigation (Geoconsult-Arup, 1997). Natural water content, unit-weight and plasticity index variation with depth, obtained from these reports and from Farrell et al. (cited), are summarised for the three tills, as determined from the accompanying borehole logs, namely the brown deformation till, brown lodgement till and black lodgement till, in Table **4.1.1**. Standard deviation is given where enough data existed to justify the statistical analysis.

Table 4.1.1. Mean consistency indices and standard deviation (SD) about the mean*

	Unit weight, γ: kNm^{-3}	Water content, w_n: %	Plasticity index, I_p: %
Deformation till	N/A	20 – 30	20 – 30
Brown lodgement till	N/A	11·5	10·75
Black lodgement till	22·56 (SD 0·68)	9·8 (SD 1·73)	9·2 (SD 1·9)

* Note the similarity in the properties of the brown and black lodgement tills, suggesting that these can be taken as the same for engineering purposes.

(a) Saint James's St.;

Very stiff grey black well graded silty sandy gravelly CLAY with cobbles. From 2 m to 13 m BGL (water table (WT) at 2 - 3 m BGL). Classification: clay of low plasticity (from Casagrande chart). Index properties in area of interest: w_n = 10 - 20%, w_l = 29 - 33%, w_p = 15 - 21%. Density: γ = 23·9 kNm^{-3}.

(b) Ballinteer Rd., Dundrum;

Very stiff grey brown to grey black well graded silty sandy gravelly CLAY with occasional limestone and granite cobbles. From 7 m to 11 m BGL (WT 1·95 m BGL). Classification: clay of low to intermediate plasticity (from Casagrande chart). Index properties in area of interest: w_n = 13%, w_l = 35%, w_p = 16%, Activity = 1·3. Density: γ = 23 kNm^{-3}, γ_d = 22 kNm^{-3}, γ_s = 24 kNm^{-3} (γ_s is saturated unit weight).

(c) U.C.D., Dublin 4 (Grid reference: O 1825 3045);

Stiff to very stiff grey brown brown in spots well graded silty sandy gravelly CLAY with limestone cobbles and boulders. Sample taken at 1·75 m BTL (4·55 m BGL) (above WT). Classification: clay of low plasticity (from inspection). Index properties in area of interest: w_n = 8·2%, w_l = 25%, w_p = 15%.

(d) U.C.D., Dublin 4 (Grid reference: O 1825 3045);

Firm rusty brown silty sandy gravelly CLAY with limestone cobbles. Sample taken at 0·25 m BTL (2·95 m BGL) (above WT). Classification: clay of intermediate plasticity (from inspection). Index properties in area of interest: w_n = 11·5 %; w_l = 32·03 %, w_p = 20·18 %; Activity = 0·9.

(e) Dublin Port tunnel access shaft: Whitehall (Grid reference: O 1609 3804);

Very stiff grey black well graded silty sandy gravelly CLAY to Very stiff brown grey silty sandy CLAY with gravel). From 13·3 m and 14 m BGL (WT 5 - 7 m BGL). Classification: clay of low plasticity (from Casagrande chart). Index properties in area of interest: w_n = 11·7%, w_l = 27·6%, w_p = 13·8%, Activity = 1·1. Density: G_s = 2·67, γ = 22·6 kNm^{-3}, γ_d = 20·6 kNm^{-3}, γ_s = 26·2 kNm^{-3}.

(f) Marino: Griffith Avenue (Grid reference: O 1750 3715);

Very stiff grey black well graded silty sandy gravelly CLAY with cobbles. From 3 m to 7 m BGL (below WT). Classification: clay of low plasticity (from Casagrande chart). Index properties in area of interest: w_n (assumed) = 11%, w_l = 25·2%, w_p = 14·9%, Activity = 0·74.

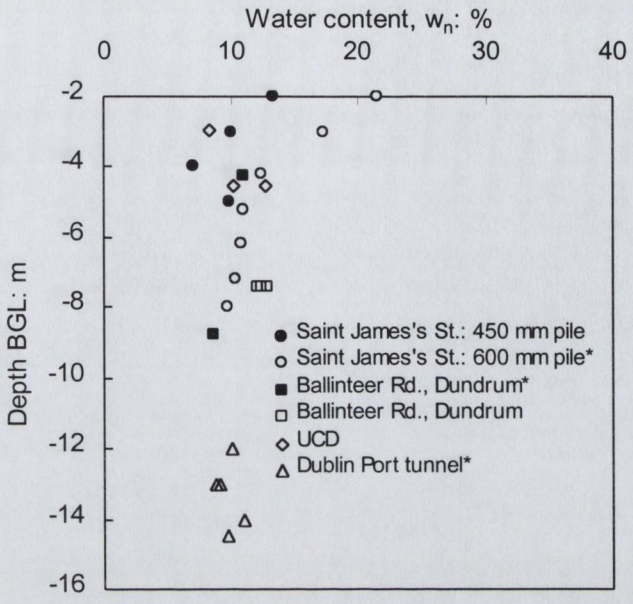

Fig. 4.1.1. Natural water contents of soils tested

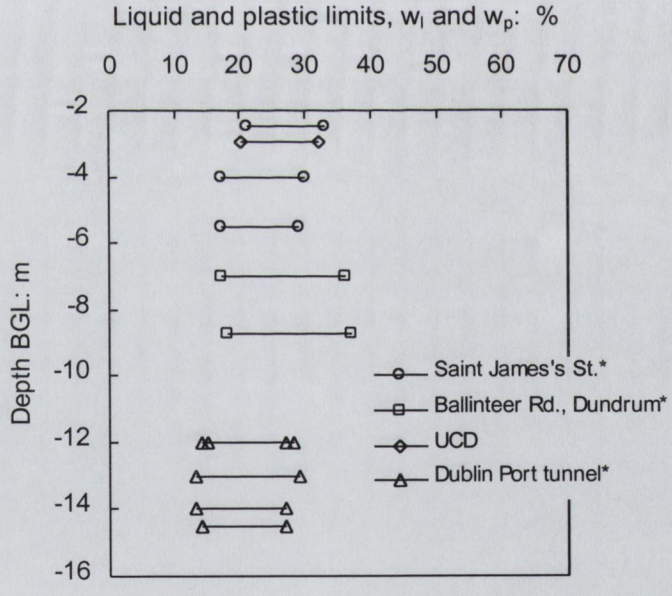

Fig. 4.1.2. Atterberg limits of soils tested

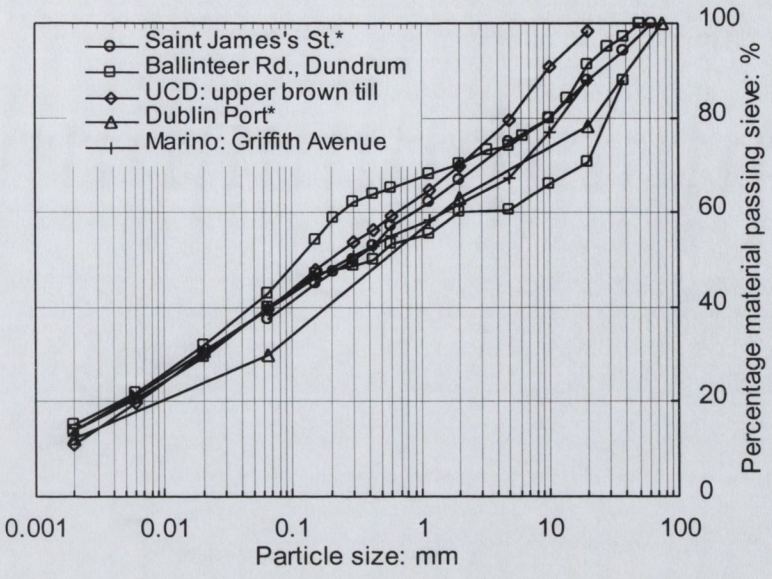

Fig. 4.1.3. Particle size distributions of soils tested

4.2 Sampling Method: Geobor S.

Soil sampling by the Geobor S method was conducted by Davies Drilling Ltd. under the supervision of the author. Geobor S essentially consists of a diamond drill bit, which cores the soil, a wire line and a drilling fluid/flushing agent (see Fig. **C.6**). Polymer gel was used as a drilling fluid because of the damaging effect of water on clay tills. The innermost tube was a core liner. Drilling was conducted at a high rotational speed and relatively low weight on bit (WOB) to avoid gravel and boulders being pushed in front of the bit. This approach was slow (1 No. core run took over 1 day) but secured good recovery. Fluid pressure, rotation speed and WOB were selected from operator experience in these soils.

The drill bit was a 102 mm ID Geogem Geocube. This core bit was surface set and was equipped with face discharge, meaning that the flushing agent was never in direct contact with the soil. The bit comprises 10 sets of 5 tungsten carbide cubes in the drill face and a diamond matrix on the outside circumference of each set. Hence, the wear rate for the 11 m core run was small (less than 1 mm). The drilling rig was a 16 T truck (as shown in Fig. **C.6**).

The top 1 m of soil was drilled with a 203·2 mm casing and blown with water flush to create a seal for drill fluid recirculation. This was followed by a run of 450 mm to remove cobbles that were not blown-off. Drilling was progressed at about 100 Bar (10000 kNm^{-2}) drill fluid pressure and 800 RPM, which remained about constant throughout, except where gravel and boulders were encountered, at which point the RPM was increased. The WOB was observed to be relatively constant. The seal was broken soon after the commencement of the second run, immediately reinstated, and drilling resumed.

On each occasion a core run (1·5 m length rods plus 100 mm of core in the catcher) was ended the liner was carefully pulled from the 2nd barrel and generally with two or three pairs of hands (to reduce bending), moved to a flat work surface consisting of one or two core boxes placed on level ground. This handling procedure was carried over to the laboratory. The ends of the core tube were immediately sealed, the liner cut and carefully placed in boxes. Any gaps between the liner and the wall of the boxes was jammed to stop the core moving around in the

boxes in transit to the laboratory. After the rods were pulled, the water table was allowed to settle and the level recorded.

As the inner core liner was oversized by approximately 2·5 mm and, as there is evidence to suggest that the soil yield stress measured in the oedometer decreases if the soil is not restrained radially before testing (Arman and McManis, 1976), it was considered necessary to restrain the sample. A 1 m length of liner with black boulder clay was moved to a workbench saw, the saw adjusted for liner wall thickness, and cut longitudinally. Thick, 101·6 mm (about the diameter of the core) Wavin pipe was then halved longitudinally with the saw. The Wavin pipe was lined carefully with cling film to prevent drying-out. The remaining half of the cut Wavin pipe was then placed on the covered core and Jubilee clips attached along the length of the pipe at 100 mm spacing. The tightness was considered sufficient to resist the swelling pressure of the soil.

4.3 One-Dimensional Consolidation.

4.3.1 Introduction.

A standard oedometer test on undisturbed boulder clay is adversely affected by the effects of sampling disturbance, obtaining a representative undisturbed soil slice, sample compliance to the apparatus, side-wall friction, compliance of the apparatus itself and radial strains in the oedometer ring causing excursions from the (K_0) condition of zero lateral strain. Most of these have been addressed in the literature review.

The zero radial strain requirement in oedometer tests is examined in Fig. **4.3.1**, which shows the radial strains in rings of increasing thickness subjected to uniform internal pressures, of the order applied in the tests described in this thesis. (The continuous line represents the internal pressure due to the maximum load applied in the tests.) These curves, calculated from elastic, thick-walled cylinder theory, indicate that the fully active state (lateral strain of 0·1% - see Section 2.4.2) is approached in the standard oedometer ring at maximum load. The new apparatus, described in detail in the following section, is not affected in this way however.

4.3.2 Design and Operation of New Oedometer.

4.3.2.1 Components.

A new, robust, oedometer was designed by the author to test Dublin boulder clay at the very high pressures required of an estimate of the yield stress, σ_{vy}' (which should be about ten times the estimated value of σ_{vy}'). The design drawings and photographs of the apparatus are shown in Appendix C, Figs. **C.1** and **C.2**. (N.B. Some of the dimensions shown arise from the fixed dimensions of the loading frame.) The apparatus was essentially built around the Geobor S, 102 mm diameter soil cores. The stainless steel construction consists of the following components:

(a) A very thick ring bolted to the cell base and designed to limit radial strains, as demonstrated in Fig. **4.3.1**. The bolts ensure the ring moves with the base.

(b) An internal ring diameter machined to the exact dimensions of the soil core to minimise sample adaptation.

(c) A heavy duty base that acts as a lower pressure head, a mount for the LVDTs, a drain and as a stable (three-footed) pedestal.

(d) Two diametrically opposite LVDTs mounted on the cell base, thereby reading the deflection of the top cap and any eccentricity. Thus, the measured deflections are those between the base and top cap only. The LVDTs are high resolution, 600 mV/mm (± 2 mV drift).

(e) The ring acts as guidance for the top cap but the amount of guidance is minimised to limit piston friction.

(f) Filter discs. Head (1998) gave the requirements for porous discs:

(i) The disc should be the same diameter as the soil specimen.

(ii) The disc should be rigid; hence, a 3 mm thick steel disc was employed.

(iii) Breaking of the disc during testing should be avoided. (From experience, breakage of sintered stone discs is a regular problem in undisturbed boulder clay tests; hence, stainless steel was used.)

(iv) Water permeability characteristics must be substantially greater than those of the soil specimen (to ensure a free drainage surface). The sintered disc chosen had 5 micron voids (GKN Sika-R5), corresponding to a uniform, fine silt-size material of permeability about 10^{-7} ms^{-1}. This permeability is about three orders of magnitude greater than that of Dublin boulder clay, while at the same time minimising the possibility of clogging by very fine soil particles. One disc, giving a drainage path, H, equal to the sample height, was bolted to the cell base with a counter-sunk screw to minimise compliance.

(g) The apparatus is incorporated in a Wykeham-Farrance, 10 T stepless-loading machine. This apparatus is capable of sustaining a controlled load. Load is transferred uniformly to the piston by way of a top cap and ball recessed into the piston.

4.3.2.2 Calibration.

Proving rings were used to recalibrate the loads applied by the Wykeham-Farrance machine. The apparatus compliance was found in the following way:

(a) Gypsum was cast to the ends of a 101·6 mm circular steel section.

(b) The consolidation piece was placed between the lower pressure head and loading head and left to set for 3 days under the pressure of the loading frame (47 kNm^{-2}). This procedure ensures that very smooth surfaces are formed with no high points, which would concentrate pressure and give misleadingly high apparatus deflections. (Note that the ring was not included in the calibration, to avoid sidewall friction with the gypsum.)

(c) The load was applied and included an unload-reload loop (which formed part of the testing programme), followed by unloading.

The calibration thus conducted is considered to be repeatable because of the procedure followed and because there are no free parts in the apparatus. The deflection of the apparatus was found to be 0·06 mm under a pressure of about 13,000 kNm^{-2}, which is only significant (to the void ratio measured in the tests) at the fourth place of decimal. This is considered one decimal place greater than the experimental accuracy; hence, in effect, there is zero apparatus compliance.

4.3.2.3 Soil Bedding Effects.

To minimise bedding effects, Jacobsen (1970) cast gypsum against the soil and against the pressure heads except for a small area in the middle-third of the lower pressure head, where a small filter-disc was placed. However, the drainage paths were compromised as a result. A different approach to bedding effects was taken in this study, as follows. The soil cylinder was carefully sawn with a dry, diamond-bladed, angle grinder converted to a drop saw by means of a specially constructed frame (see Appendix, Fig. **C.3**). It was essential that the diamond blade sliced cleanly through the gravel sized stones in the soil; this was found to be possible in Dublin boulder clay (with a blade of high teeth-per-inch) because the stones were held rigidly in-place by the very stiff clay matrix. The sawing was conducted dry to avoid adding to the moisture content of the soil (hence the specially built frame because, it was found, all industrial drop saws require water-cooling). As it was imperative that the faces of the soil slice were parallel, a stable frame and workbench was constructed that could accommodate a 102 mm soil cylinder held in a half-pipe; this half-pipe was necessary to avoid damage to the soil cylinder.

4.3.2.4 Procedures Followed in Oedometer Tests.

A slice was cut with the drop saw described above, without damaging the circumference by holding the soil cylinder in-place in a half-pipe. When the first cut was made, the required sample thickness was measured and a second cut made. It can be demonstrated that a substantial reduction in sidewall friction accrues if the diameter to sample thickness ratio is of the order of 4 or higher. Hence, for a 102 mm specimen, the sample thickness should be about 25 mm.

The undisturbed soil samples were carefully pushed into the cell by placing a cylindrical piece of metal of the same diameter on the soil and allowing the weight of the loading frame to push the sample in. This procedure worked very well and a very tight radial fit was observed. The LVDTs were adjusted in place by checking the output voltages until these were suitable for the gauge travel required. The bars that the LVDTs were attached to were bolted down and the LVDTs secured rigidly in place by two nuts on either side of the LVDT housing bar-clamp.

4.3.2.5 Reconstituted Test.

It was of importance to the study to compare the behaviour of intact and reconstituted till. However, to allow comparison of the soil stiffness, the particle sizes had to be equal in the intact and reconstituted soil, as discussed in the literature review.

One of the oedometer specimens (Test E) proved a suitable specimen for comparison by merit of containing relatively few large particles and because the large particles that were present were sliced by the diamond saw. After testing, the sample was examined for particle size and the particle size distribution recreated in the reconstituted test specimen. The stress-history was then recreated by loading the slurry to the yield stress measured in the undisturbed test.

The preparation of the sample involved the following. Boulder clay was air-dried and the sub-425 micron fraction well ground-down by pestle and mortar to the constitutive particles of the material. As the initial height of the soil had to be greater than that of the undisturbed soil (to allow for the greater compression of the soft soil), the particle sizes were added to the mix according to the mass dry density and particle size distribution of the equivalent undisturbed soil sample. The soil was thoroughly mixed dry in an industrial mixer and then thoroughly

mixed with water, with a palette knife, at a water content about 3% less than the liquid limit (of the fraction passing the 425 μm sieve). (It was necessary not to mix the till close to the liquid limit as it is found to become sticky, hindering the placement of the soil in the cell.) All the soil was placed in the cell and lightly compacted down in layers to remove air pockets. The height of the sample in the cell was then measured with a depth gauge.

Generally, there are five types of water in standard laboratory tests: distilled, deaired, tap, saline and ground water (pumped from site). The effect of the type of water is sometimes seen in sedimentation: if the fine particles flocculate very quickly, this can be due to the effect of the water on the inter-particle forces. In these cases, site ground water often solves the problem. No such difficulties were encountered by the author during pipette tests with distilled water; hence distilled was used throughout, i.e.: for Atterberg limits, sedimentation and reconstitution.

4.3.2.6 Testing.

The soil samples, thus prepared, were loaded step-wise. Strain rate effects were mitigated by loading the soil for non-constant duration and with $dP/P = ¼$, where P is the current load and dP is the load increment. This is believed to be effective in mitigating strain rate effects and hence improving the reliability of yield stress determinations in the oedometer (see Section 2.4.1). The first load step, which was applied immediately, was large enough to resist any swelling due to the submerging of the cell. Loads were left on for a minimum of about 24 hours, which was enough time to determine secondary consolidation characteristics. Some longer times were included to investigate very long-term, 'creep' behaviour.

The tests that involved unload-reload were conducted as follows:

(a) The soil was loaded near to, but without exceeding, the value of σ_{vy}', approximated in the first test. The value chosen was about 80% of σ_{vy}'.

(b) The soil was then unloaded to typical in situ vertical effective stresses, followed by reloading. The lower values of σ_v' required that the machine was switched off and the load applied manually with calibrated weights.

(c) Finally, the soil was loaded to maximum pressure to determine σ_{vy}', followed by unloading to the approximate minimum in situ vertical effective stress (i.e. $\sigma_v' = 47$ kNm^{-2} which was, incidentally, the stress applied by the dead-weight of the frame)

To remove the soil the bolts holding down the ring were loosened and the ring removed with the soil in the ring. The soil was then pushed out using a 101·6 mm diameter circular section.

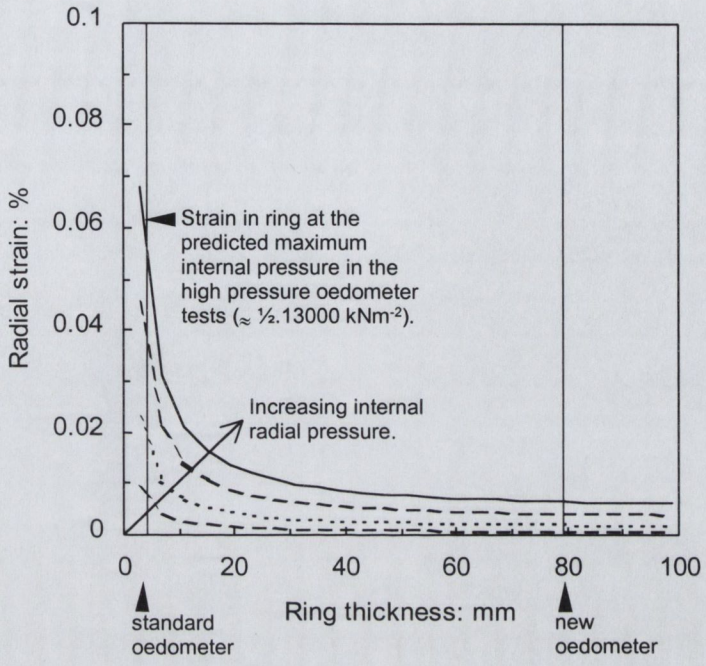

Fig. 4.3.1. Radial strains in stainless steel rings subjected to internal pressure

4.4 Triaxial Testing.

4.4.1 Introduction.

The objective of the triaxial testing was to obtain stress-strain, stiffness and strength data that were representative of the in situ soil behaviour. To do this, the in situ stress-state was first re-established in the consolidation stage of the tests, based on the data obtained from the oedometer tests; isotropic and anisotropic consolidation was carried out. Each test was optimised to produce the maximum amount of information, which was accomplished utilising the large amount of apparatus described in this section. The test series was also optimised to complement previous testing. As the number of tests conducted was limited, major variables, such as strain rates and effective confining stresses, were kept constant, to allow comparisons to be drawn between the tests[1]. Finally, reconstituted soil testing was included to aid in the interpretation of the intact soil tests. (The reader is referred to the triaxial results section, Section A.2, for details of each test.)

4.4.2 Apparatus.

The following is a summary of the hardware and software integrated into the tests. All equipment is designed for 100 mm diameter soil samples. The transducers were calibrated within a few months, at least, of testing. The cell, pressure controllers and water submersible transducers work to a recommended maximum pressure of 2 MNm^{-2}. A flow diagram of the test set-up is shown in Fig. **4.4.1**. Photographs of the apparatus and instrumentation are given in Appendix C, Fig. **C.4**.

The basic apparatus included: (a) A Wykeham-Farrance Tritest 50 triaxial loading machine. This machine can be either software or manually controlled; the load is applied at a constant rate of strain. (b) GDS cell pressure and back pressure controllers. These controllers can be either software or manually controlled. The back pressure controllers accurately measure volume change in a drained test.

---

[1] The effective confining stress chosen was based on *a priori* estimates of the in situ stress-state.

The specialist bender element test equipment included: (a) A Wykeham-Farrance triaxial cell with bender elements fitted to the top and base pedestals suitable for 100 mm diameter samples. (b) A Thurlby Thandar TGA 1240 function generator. (c) Thurlby Thandar Wave Generator software. (d) A Pico ADC-212 high-resolution oscilloscope. (e) PicoScope software. (f) Shielded output cables.

Specialist K_0 consolidation equipment involved: (a) GDSLab software. (b) A GDS radial strain transducer device. (c) A 20 kN submersible load cell.

Finally, the isotropic consolidation and shearing equipment consisted of: (a) GDSTAS triaxial test software. (b) GDS local axial LVDT strain transducers. (c) An external displacement LVDT transducer.

4.4.3 Bender Element Testing.

4.4.3.1 Apparatus Description.

The receiver bender element is generally wired in series, as series wiring gives a high voltage output for a given distortion, the output voltage being the sum of the potentials available to the electrodes of each ceramic element. The transmitter is, conversely, better wired in parallel, which gives a large distortion for a given input voltage, the available voltage being applied to both plates without the need for amplification between the function generator and element (Brignoli et al., 1996). The triaxial cell pedestal and top cap were designed to hold the bender elements and associated wiring. An improvement to the common system was made by Wykeham-Farrance, whereby the elements can be removed easily (in the event of breakage or for use in another apparatus). The ceramics are waterproofed and insulated, as are the cables, which are coaxial.

Typically, the function generator signal, which is an analog excitation, is amplified, sent to the base/top pedestal element, transmitted through the soil, the receiver signal amplified, converted to a digital signal by an ADC, averaging of the signals conducted and the trace displayed on a high resolution, digital storage oscilloscope (Brignoli et al., cited). However, amplification and averaging may hide some important details, depending on the excitation waveform, in which

case shielding and axis magnification (possible with a PC-based oscilloscope) is preferable. Besides these considerations, due consideration must be given to analog signal filtering (generally Bessel or elliptical 10 MHz/16 MHz), scan rates and anti-aliasing routines, digital signal filtering, the type, form, amplitude and frequency of the excitation signal (see Section 2.5.5.2) and the visual and numerical interpretation of the received signal. Again, filtering and maximum frequency (which are related to scan-rate and high-frequency noise) need to be optimised such that no important details are smoothed-out of the received trace. The oscilloscope needs to be of very high resolution, owing to the very low wave propagation times and small magnitude of deformations/voltage involved.

The PC based oscilloscope was chosen to aid acquisition and signal interpretation. The PC was a high-speed Pentium 3 processor of 750 MHz processor speed. The traces thus obtained were converted to spreadsheet cells (1000 cells per trace) to allow extensive analysis. The oscilloscope ADC (Pico, 2001) is characterised by: (a) a resolution of 12 bits, (b) an accuracy of +/-1%, (c) overload protection of +/-100 V, (d) a sampling rate of 1·5 MS/s, (e) an analog bandwidth of 1·5 MHz and (f) a buffer size of 32K.

The system is programmable with a stopping trigger, which is programmed for some suitable time after a wave generation event to allow examination of the trace. On-screen rulers allow very fast determination of the travel time. A pulse train can be programmed, such that more than one method of velocity measurement may be employed (and, therefore, accuracy increased) at the same moment in time. By exporting the computer data to a spreadsheet, it was found that the resolution of the received trace was increased over the screen trace and hence an improved measurement was made. This was found to be important at high consolidation stresses, where the strength of the received signal can be greatly reduced.

The excitation signal wave used in BE tests is commonly 20 V peak-to-peak. The function generator, a Thurlby Thandar TGA 1240 arbitrary wave generator, allows, in addition to the standard waveforms, user defined waves. This was necessary to allow the advanced analyses applied in the test series (see Table **4.4.1**, below, and Section 2.5.5.2). Channel B (bender element receiver) cables were well shielded, such that averaging of signals was minimised and, furthermore, the base of the cell (receiver end) was earthed to an electrical conduit.

4.4.3.2 Set-Up of Soil Sample.

For the intact soil tests, an area of boulder clay on the soil cylinder face was removed to the depth of the protruding element and filled with remoulded boulder clay, with the coarse fraction removed. This allowed the bender elements to protrude into the soil and ensured that the elements were surrounded with soil. The subsequent isotropic and K_0 consolidation to very high effective stresses consolidated the remoulded soil to a stiffness similar to that of the surrounding soil, prior to shearing.

Stone filter discs were cored with a diamond cutter to allow the bender elements to protrude into the sample. Different configurations of filter thickness/element protrusion were examined. It was found that the longer the length of element in the soil cylinder, the better the traces. However, this must be balanced with the possibility of breaking in the shearing stage. (It is noted that it is one of the advantages of the bender elements that the soil can be sheared to deflections beyond the range of high resolution LVDTs.) The following configurations were attempted (with 10 mm length elements):

(a) Two 3·5 mm thick (sintered stone) filters, giving strong traces but some distortion of the lower element at about 7% axial strain (15 mm vertical deflection).
(b) One 3·5 mm filter at the base with filter paper at the top platen, giving traces at very low effective stress (5, 50, 150 kNm^{-2}).
(c) Two 6·5 mm thick filters gave virtually no traces.
(d) One 6·5 mm filter at the base with a 3·5 filter at the top platen, which improved traces over attempt (c).

The configuration chosen was configuration (a). Note that the effective length, L_e (see Section 2.5.5.2), is different in each of the above configurations.

4.4.3.3 Calibration.

The large number of electronic system components may introduce delay to the BE measurements (Brignoli et al., 1996). To investigate this delay, the transducer pair were placed

in direct contact. (The top platen was held in retort and the platens/elements brought into contact.) The polarity of the received trace was noted and the top platen marked with respect to the base platen, in order that any ambiguity in test interpretation was avoided. The time delay was then noted. The calibration trace thus obtained, given in Fig. **4.4.2**, shows that there is no lag time evident and, hence, no zero-offset (probably the result of using a PC with a very fast processor and large available memory and a high-end ADC (see Section 4.4.3.1).

4.4.3.4 Testing Method.

The oscilloscope was programmed with a trigger to stop data acquisition and hold the trace on the scope screen. A negative time delay was applied in the case of standard waveforms. The 'save on trigger' option was selected. The TGA1240 was then programmed with a manual trigger, sending a single pulse of the standard or arbitrary waveform selected when the manual trigger button on the fascia was pressed. Signals were sent top down, from the top cap to the cell base (although there is no difference found when the signals are sent top down or bottom up (Lings and Greening, 2001)).

A BE test was run on homogeneous clay, which was found to give an ideal response. Hence, tests were run on this clay to fine-tune the testing process. The findings, which were subsequently applied to the tests on the glacial till, were:

(a) Distortion of the received trace due to overshoot does not always mask arrivals.
(b) Amplification of the received trace decreases as the input frequency increases and as the effective stress in the sample increases. However, magnification of the received trace, captured at a set scanning-rate, is easily done without loss of resolution.
(c) Averaging of the traces does not appear to mask details for the arbitrary (distorted sine and burst/resonance) tests. Hence, averaging of the traces should be conducted if details, particularly the Near-Field Effect (NFE), are not hidden.
(d) The natural frequency of vibration of the receiver was found to be (multiples of) 2·5 kHz. A signal frequency of 2·5 kHz was possible in conjunction with the resonance test.

(e) All the methods (square at first reversal, high frequency sine and low frequency arbitrary sine pulse), obtained using the expressions given in Table **4.4.1**, gave values of G_{max} that were very close to each other. However, at very high effective stress (e.g. 1275 kNm^{-2}), the resonance test was superior.

(f) The maximum accuracy that could be obtained was about 5 microseconds. This approximately corresponds to a G_{max} accuracy within 7 MNm^{-2} of the real value, which is an accuracy to within about 1·5%, when the soil is isotropically consolidated to an average mean effective stress.

(g) The advantages/disadvantages of the various waveforms may be summarised as follows:

(i) Square: infinite frequency and 0-20 V rise gives a strong trace/S-wave first arrival at first reversal.

(ii) 10 kHz standard sine: no near-field/received trace is weak, even at low effective stresses.

(iii) 2 kHz arbitrary sine: no near-field and received trace should be stronger than 10 kHz wave/averaging not recommended (though, in reality, averaging has little effect) and no received trace at very high effective stress.

(iv) Resonance test (2·5/5 kHz): very good all-round, particularly at very high effective stresses.

Typical traces for the tests on the homogeneous clay are shown in Appendix C, Figs. **C.5**: (a) square wave - note first arrival, (b) sine wave – near-field, (c) arb sine – no near-field, (d) resonance – near-field negated. Note that the instability in waves (a) to (c) was due to an inappropriate time-scale. This was corrected, as shown in trace (d).

In summary, the result of the preliminary testing was that the waveforms shown in the following table (Table **4.4.1**) were routinely used.

Table 4.4.1. Waveforms generated routinely in the BE tests

Waveform	Amplitude (V)	Frequency (kHz)	Expression*
Square pulse	0/+20	Spectrum	A.pulse[d,r,h,f,c]
Sine pulse	-10/+10	5-10	A.sin[nωt+ϕ]
Distorted sine (arbitrary pulse)	-10/+10	5	A.sin[nωt+ϕ]+N
Sine burst	-10/+10	5	A.sin[nωt+ϕ], n>1
Composite	-10/+10	5 (resonance part)	A.sin[nωt+ϕ] add A.pulse[d,r,h,f,c]

* where A is amplitude, d is delay, r is rise, h is high time, f is fall, c is cycles, ω is 2πf, n is an integer, t is time, f is frequency, ϕ is phase-shift and N is A offset. The composite wave was used for tests where a quick succession of waves was required, e.g. at the start of shearing. Note that all waveforms incorporate static delay and end times, set with the oscilloscope, to aid in the interpretation of the last three waveforms.

4.4.4 K_o Consolidation Method.

In the oedometer, the steel ring (see Fig. **4.3.1**) prevents significant radial strains. A K_o stress-history reconstruction (K_oR test) in the triaxial apparatus, designed to re-establish the in situ stress-state in the consolidation stage prior to shearing, however, requires special computer control to prevent radial strains in the sample. The K_oR tests thus conducted by the author for this thesis were carried out based on the literature review of K_o consolidation (Section 2.4.2).

The K_o consolidation was conducted following the recommendations of Bishop (1958) for the test requirements for determining K_o in the triaxial apparatus. By carrying out the consolidation in a cell fitted with bender elements, the stiffness variation was determined at different consolidation stresses. Furthermore, the soil could be subsequently sheared to determine the stress-strain characteristics.

Several methods of triaxial K_o consolidation were attempted. However, problems were found with the strain belt controlled K_o tests (of the Brooker and Ireland (1965) type). Experimentally, it was found that the best control method was one based on volume change. In this case, a radial strain belt acts as a check that the radial strain is zero. (It is noted that this test controls the diameter of the entire specimen, as opposed to the area in the region of the mid-mounted

strain-belt, in the case of the strain-belt-controlled tests.) The K_0 consolidation (loading) procedure followed by the computer program is as follows:

> (a) An effective cell pressure is applied at a very slow rate of stress such that excess pore water pressure does not develop. (b) The volume change (dV) of the soil is measured on the back pressure line. (c) The increase in cell pressure has the effect of reducing the diameter of the soil. To counteract this, the height of the sample is reduced (dH) such that the sample diameter (D) does not change, according to the following formula:

$$dH = H_0 - (V_0 + dV)/A_0 \qquad [4.4.1]$$

> where H_0, V_0 and A_0 are the original height, volume and area of the sample, respectively. The unloading procedure is the reverse of this procedure.

As with standard isotropic consolidation, K_0 consolidation includes a back pressure, which remains constant during the test. (The back pressure is best brought up in the saturation stage.) Owing to the very high consolidation stresses involved in the tests, it is advantageous to balance the fluid level in the pressure controllers at the start of a test[2]. Furthermore, due to the experimental procedure, one must be present to unload and stop the test at the required stress levels. The axial displacement causes an axial load, measured with a submersible load cell, which is in addition to the axial effective stress due to the cell pressure. (It is noted that this, triaxial test, approach limits the stresses that may cause fissuring in the sample, owing to the large differences in the major and minor principal effective stresses that can develop.) The large cell pressures form the majority of the effective axial stress on the sample and this has to be accounted for in reaching the required pressures. For accuracy, a submersible load cell is used, which removes the effects of piston friction.

---

[2] This is done so that the test does not have to be interrupted to empty/fill the pressure controllers, which allow consolidation/swelling of the sample as the pressure is increased/decreased.

4.4.5 General Triaxial Testing.

4.4.5.1 Definitions and Calculations.

Sign convention: compression of soil is positive.

$$\varepsilon_v = \Delta V/V_0 \quad [4.4.2]$$

$$\varepsilon_a = \varepsilon_v - 2\varepsilon_r \quad [4.4.3]$$

$$\varepsilon_s = 2/3(\varepsilon_a - \varepsilon_r) \quad [4.4.4]$$

where ε_v is volumetric strain, ε_a is axial strain, ε_r is radial strain, ε_s is shear strain and ΔV is measured volume change.

$$\sigma_1' = P/A_c + \sigma_c - \sigma_b \quad [4.4.5]$$

where σ_1' is the major principal effective stress, P is axial load, σ_c is the cell pressure, σ_b is the back pressure and A_c is the corrected area, given as:

$$A_c = (V_1 + \Delta V)/(H_1 + \Delta H) \quad [4.4.6]$$

where V_1 and H_1 are the current volume and height, respectively.

$$\sigma_3' = \sigma_c - u_b \quad [4.4.7]$$

$$q = \sigma_1' - \sigma_3' \quad [4.4.8]$$

$$p' = 1/3(\sigma_1' + 2\sigma_3') \quad [4.4.10]$$

where σ_3' is the minor principal effective stress, u_b is the back pressure, q is deviator stress and p' is the mean effective stress.

$$G_{sec} = 1/3(\Delta q/\Delta\varepsilon_s) \quad [4.4.11]$$

$$E_{sec} = \Delta q/\Delta\varepsilon_a \quad [4.4.12]$$

$$K_{sec} = \Delta p'/\Delta\varepsilon_v \quad [4.4.13]$$

where G_{sec} is the secant shear modulus, E_{sec} is the secant Young's modulus, K_{sec} is the secant bulk modulus. (The 1/3 term in Equation [4.4.11] is required owing to the (Cambridge) definition of shear strain.)

$$\nu' = -\Delta\varepsilon_v/\Delta\varepsilon_a \qquad [4.4.14]$$

where ν' is the effective Poisson's ratio.

$$\psi = \text{arcsine}(-2/3(\Delta\varepsilon_v/\Delta\varepsilon_s)) \qquad [4.4.15]$$

where ψ is the angle of soil dilation. (The factor 2/3 is required owing to the Cambridge definition and the minus sign is required to give a positive angle.)

Fig. **4.4.3** shows the stresses in triaxial K_0 consolidation. To avoid ambiguity, the deviator stress in this case is defined as:

$$q = \sigma_v' - \sigma_c' \qquad [4.4.16]$$

4.4.5.2 Triaxial Test Procedure.

The typical procedure followed in the triaxial tests was as follows. (Any variations in the procedure are referred to in the triaxial results section, Section A.2.)

(a) Set-up soil on bender elements. If soil is too stiff to deform easily around the elements, make two holes and fill with remoulded boulder clay. Any small holes in the surface of the sample should be filled with remoulded soil. Clean out/de-air drain leads and fit saturated porous stones.. (The filter disc at the top is for the benefit of the bender elements.) Fit side-drains. Fit membrane. Fit radial strain belt. (It was found

that hanging the radial strain belt LVDT-side-down prevents top-heaviness and tilting of the belt.) Fit local axial strain transducers[3,4].

(b) Checks. Pressure controller fluid. Calibrations and zero-offset of: load cell, pore pressure transducer, external axial transducer, local axial transducers and radial strain transducers.

(c) **Table 4.4.2. Table of typical triaxial test procedure**

Type of test	Cell pressure (kNm^{-2})	Back pressure (kNm^{-2})	Control	Time (days)	Bender Elements
Undisturbed	0	0	None	-	3 waveforms*
B-test	~ 200	Undrained (U/D)	Manual	Until pore water pr. equalisn.	None
Saturation B-test†	305 350	300 U/D	Computer Manual	1-2	3 waveforms
Isotropic consolidation	50 kNm^{-2} or 250 kNm^{-2} increments	U/D (300)	Manual Manual - d/a‡	1+	3 waveforms
K_0 - load Check σ_c' K_0 - unload	1500 Max. ~2000 Stop when cell pressure less back pressure is 250 kNm^{-2}	(300) (300) (300)	Computer - hold pressure	2+ 2+	Resonance Every 250 kNm^{-2} or every 2 hrs. 3 waveforms
C.D.	(E.g. 550)	(300)	Manual - d/a (dock manually very carefully) Rates¶ 0·001%/min	4+	

* Arbitrary sine, square and resonance
† Repeat if necessary ‡ d/a: data acquisition
¶ The data acquisition scan rate is set so as to obtain data in the small strain region.

[3] For test SS1, which was very stoney and had a large amount of local instrumentation, it was not considered possible to pin all the instrumentation to the sample, particularly without damage. Therefore, the instruments were stuck to the soil membrane with super glue.
[4] The LVDTs were adjusted in-place to mid travel.

4.4.5.3 Corrections Applied.

The corrections applied at all stages of the consolidation, swelling, bender element, K_0 and shearing stages were: (a) volume change in isotropic and K_0 consolidation and swelling stage, (b) area correction and (c) change in effective length, L_e. The membrane, effective contact area and side (filter) drain corrections given in the literature (see Head (1998)), were not applied owing to the negligible effect of these on the deviator stress (at the very low strains in Dublin boulder clay), the very low failure axial strain that was typical in the tests (about 3%) and because of the combination of slip-plane and barrelling failure modes that were observed in the CD shear tests. (The corrections in the literature are negligible for barrelling and the corrections for slip-planes are determined only for pure slip-plane surfaces).

4.4.5.4 Reconstituted Sample Preparation for Triaxial Testing.

Undisturbed soil was air-dried and passed through the 425 μm sieve. The soil mass was then divided into roughly three equal parts (by mass), to aid preparation. The soil was weighed and the fraction less than 425 μm was ground thoroughly by mortar and pestle. The dry soil (including the fraction retained on the 425 μm sieve) was mixed in an industrial mixer. The total soil mass was used (including some stones retained on the 20 mm sieve). It was possible to include the entire particle size range in the disturbed soil sample, owing to the large size of the test sample (a height of 200 mm and a diameter of 101·6 mm), which aided in reducing the consolidation times of the sample and in improving the relevance of the test. The mass of water added was 25·2 % (the measured liquid limit, w_l) of the mass passing the 425 μm sieve (giving an overall mass of a few percent less than w_l, assuming a saturated water content of the mass retained on the 425 μm sieve of less than 3%. The soil was then mixed again. A thick-walled, U100 (450 mm length), tube was prepared with two porous caps and wet, 90 mm ϕ, filter paper. (The top porous cap is also a loading cap and is free to move in the tube.) The soil was added to the U100 in layers (there were about a dozen layers, each layer lightly compacted-down to remove air voids) and the tube placed in a water bath with geotextile at its base. The soil was loaded by means of a graduated concrete cylinder (3·5 kg mass) and weights in 10 kg increments up to a vertical effective stress of 150 kNm^{-2} (to stiffen the soil to allow handling). The water level was maintained above the top of the soil during this time.

4.4.5.5 LVDTs.

The soil was instrumented with mid-mounted (GDS) radial strain and axial strain transducers. The radial strain device is shown in the photographs (Fig. **C.4**) in Appendix C. The radial strain device essentially consists of a submersible LVDT attached to a thin metal belt that is, in turn, attached to the soil by pinned or glued mounts. The transducer, hinge and mounts are all equidistant. The transducer slug moves freely in the transducer housing by means of a free-movement mechanism. The calibrated, submersible LVDT details are as follows: (a) Transducer full-scale = 10 V. (b) Sensitivity $\approx$ 0·0005 mm/mV. (c) Slug range = 10 mm.

There are 2 No. axial strain gauges. The gauges (see photograph Fig. **C.4**) essentially consist of a LVDT and two mounts. The system is attached to the membrane with a fixed gauge length, L_0, (L_0 = 65 mm) by the aid of two removable bars, which aid in pinning the transducers to the soil. The specifications of the LVDTs are as for the transducer used in the radial strain belt (but with slightly different sensitivities). The transducers were mid-mounted and adjusted to give about full travel. The full travel allows a local axial strain of about 15% and the test was carefully monitored to ensure this was not exceeded. These LVDTs, when set up as shown in the photographs, were found to be stable.

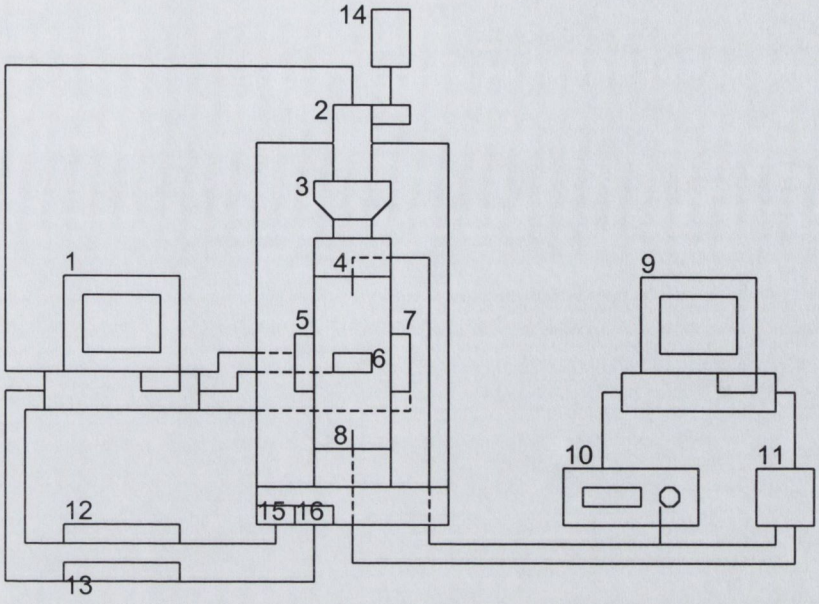

1 Stress-path computer control and data acquisition
2 Computer controlled/manual CRS machine
3 Submersible load cell
4 Transmitter BE
5 Local axial LVDT
6 Local radial LVDT
7 Local axial LVDT
8 Receiver BE
9 PC oscilloscope and wave equation editor
10 Function generator
11 ADC
12 Computer controlled/manual cell pressure controller
13 Computer controlled/manual back pressure controller and drainage line
14 External axial LVDT
15 Cell pressure transducer
16 Back pressure transducer

Fig. 4.4.1. Flow diagram of triaxial test set-up

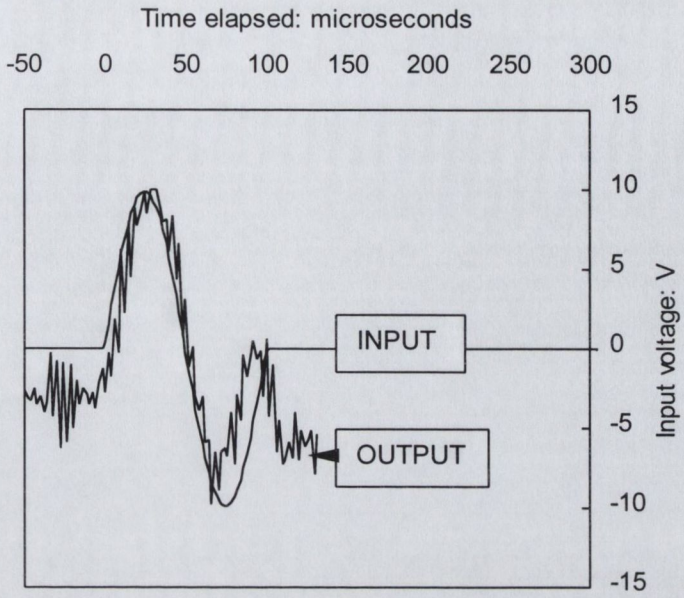

Fig. 4.4.2. Calibration of bender elements

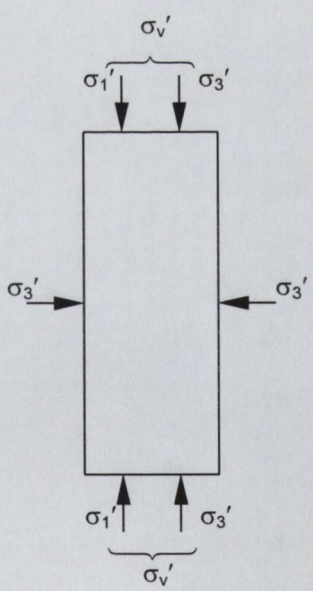

Fig. 4.4.3. Stresses in triaxial K_0 consolidation

4.5 Soil Suction.

4.5.1 Introduction.

The background to soil suction and soil suction measurement was given in the literature review (Section 2.8). This section details the filter paper method of measurement used for the measurement of soil suction.

4.5.2 Filter Paper Method.

The BRE procedure (Crilly and Chandler, 1993) for soil suction was adopted. This procedure involves details of soil preparation and storage (of both soil cylinders and block samples) and filter paper calibration. The soil was placed in a temperature controlled environment, with a min-max thermometer to measure any variations from the suggested value of 20°C. The precise weighing procedure adopted was as follows:

(a) Light polythene bags were cut open at both ends, large enough to be folded around papers.
(b) The polythene was folded to an area less than the area of the balance plate to prevent updrafts. The balance used was accurate to four places of decimals.
(c) Zip-locks© were used to close the polythene bag and to act as a handle. Each bag and zip-lock were numbered.
(d) Tweezers and surgical gloves were used.

The above implements aided in preventing the wet papers being exposed to the atmosphere for more than 5-10 seconds, which is the most critical part of the procedure. Some soil contamination of the papers was unavoidable.

The moisture contents of the filter papers, thus obtained, were converted to the equivalent suction values, p_k, using the calibration for the Whatman No. 42 paper given by Crilly and Chandler (cited).

4.6 Mineralogical and Microscopic Soil Studies.

4.6.1 Introduction.

Recent advances in X-Ray Diffraction (XRD) and Scanning Electron Micrography (SEM) have meant that it now possible to quantify clay minerals (in a quantitative X-Ray Diffraction, QXRD, test) and examine large soil samples in the undisturbed state.

The soil samples used in the tests were obtained as follows:

(a) The outer layer of soil was removed from an excavation face by hand before the soil samples were taken (to avoid the risk of any contamination) and preserved.
(b) The soil was tested in the SEM within a few days of sampling. Rigorous avoidance of contamination of the samples meant that only small amounts of soil were fit-for-purpose (see point (a)).
(c) The samples were split for SEM and QXRD analysis to allow comparison.

4.6.2 X-Ray Diffraction.

An X-ray beam falling on an atom is either absorbed or causes scattering of radiation of the same frequency as the primary beam. Ideal (unmodified) scattering is describable by the classical Bragg's law. This law is easily derived and explains why the cleavage faces of crystals appear to reflect X-rays at a certain angle, θ:

$$n\lambda = 2d\sin\theta \qquad [4.6.1]$$

where n is an integer, λ is the X-ray wavelength, and d is the distance between atomic layers in a crystal. By examining the outgoing angle and peak breadth, a mineral can be identified. Perfect crystals give single line diffraction peaks (on the graph of intensity against 2θ). However, strains, defects, finite size effects, and instrument resolution conspire to broaden the peaks. A typical powder sample (of the clay fraction) consists of a very large number of crystals (of less than 10^{-3} cm side). However, as a natural, 3-d, crystal must be arranged at the

correct orientation with respect to the incoming beam, a truly random orientation is required. This orientation is not conducted in typical XRD analysis. However, the quantitative XRD tests were treated to produce a truly random specimen, as follows.

Hillier (2002)[1] developed a spray-drier (that gives a completely random clay particle orientation) and computer modelling techniques for the purpose of clay mineral quantification. Hillier (cited) performed tests on three soil samples in this way[2]. In the method, the samples are prepared in an orientated preparation and the relative percentage of clay minerals in the clay fraction determined, which can then be compared with the bulk mineral content. It is considered that the relative percentage of clay minerals test is the more accurate for soils with a large number of individual minerals.

4.6.3 Scanning Electron Microscopy.

4.6.3.1 Introduction.

In clay samples, the inter-particle configuration is a function of the inter-particle forces, which are, in turn, a function of the amount of pore water and the polarity and dialetric constant of the water. Therefore, drying or absorption of water will disturb the inter-particle configuration. Furthermore, if calcite is present in the water, this will be deposited in the pore space to form precipitates when the water evaporates (Smart and Tovey, 1981). Hence, there is a requirement to examining the soil in the natural state.

4.6.3.2 Apparatus.

SEM involves the thermionic emission of an electron beam (cathode ray), the acceleration of the electrons emitted from the irradiated area, the conversion and amplification (with a photmultiplier) of the emitted electrons to an electrical signal and a scanning raster and screen. The reader is referred to Smart and Tovey (cited) for further details. The SEM used in these

---

[1] The reader is referred to Hillier (2000) for details of the test method, which involves computer simulation of the XRD patterns of clay minerals.
[2] The results will form part of an upcoming edition of the 'Clay in Construction' series of the Engineering Division of the Geological Society.

studies was the Hitachi S-3500N. A variable pressure (VP) mode allows the microscopy of wet, non-conductive and insulating materials (such as soil) in their natural state without conventional sample preparation and coating; thus, the micrographs will not possess anomalous features due to traditional sample preparation. A Peltier stage, i.e. electrical cooling of the metal stub, minimises water loss. The stub and chamber are large, accommodating relatively big, irregular samples. Standard gold plated tests can also be accommodated.

4.6.3.3 Test Method.

The mode of operation (reflective-emissive), sample size, surface preparation, coating, beam voltage, working distance and final aperture, magnification and tilt angle were selected based on the type and condition of the material and the information required. Initially the accelerating voltage was set at 10 kV but this was increased to 20 kV to improve the resolution. The partial vacuum was in the range 20 - 50 kNm^{-2} in the VP mode. This, relatively large, vacuum, coupled with the higher accelerating voltage, improved the resolution of the images considerably over the initial, 10 kV, attempts. (Note that the vacuum was difficult to obtain owing to some loose debris from the sample.) The soil was scored and then fractured in tension and the upper fracture surface (the surface that was to be examined) blown with nitrogen. No smearing of the test surface was evident from the micrographs as a result. The sample was then mounted on the stub. These samples were large (about 30 mm^3) and the entire area of the test surface was covered during the examinations. Towards the end of each test, the sample showed signs of cracking, caused by the frozen water beneath the image surface evaporating owing to electron bombardment.

4.7 In Situ Soil Testing: Pressuremeter and Seismic Tests.

4.7.1 Pressuremeter Tests.

4.7.1.1 Apparatus.

Pressuremeter tests were conducted and analysed for site investigations connected with the Dublin Port Tunnel project (Geoconsult-Arup, 1997). The pressuremeter used was a six-armed, High Pressure Dilatometer (HPD). Menard (1965) originally devised the pressuremeter primarily to measure the deformation modulus at depth in a borehole. The apparatus consists of a guard cell that protects an inner measuring cell, expanding radially but not axially. The guard cell produces a (near) plane strain condition in the region of the (smaller) measuring cell by increasing the axial extent of the radial stress field. All non-uniform and non-cylindrical induced stresses occur outside of the measuring cell. The condition is, therefore, an axisymmetric, thick-walled cylinder problem in linear elasticity.

4.7.1.2 Test Procedure.

A large number of individual HPD tests were conducted in several boreholes at various depths (about two dozen tests). The borehole records and p-ε_v diagrams were subsequently examined by the author and those tests that demonstrated the following classical behaviour were analysed.

The test procedure involves increasing the pressure in predetermined increments and noting the volume expansion at each increment. In unfissured clays, the response is undrained. Three distinct phases should be produced when volume change, ε_v, is plotted against pressure, p (the reader is referred to Fig. **2.5.21** for this):

> (a) A lead-in phase, which represents the restoration of the in situ horizontal total stress, σ_{h0}[1]. In the case of prebored tests, this is generally not considered a measure of the lateral earth pressure, owing to considerations of borehole drilling disturbance and softening, in most clays (Clarke, 1997). However, owing to the insensitive and very

[1] Note that σ_{h0} is referred to as p_0 on Fig. **2.5.21**.

stiff nature of the boulder clay, coupled with careful preparation of the borehole wall with rotary coring and a suitable iterative procedure to obtain a new datum, it is considered that some of the tests were accurate in this respect. Furthermore, the six-armed apparatus used for the tests will have reduced the compliance of the HPD to the borehole and aided in obtaining an average result. The value of K_0 thus obtained could then be checked against known limits, such as K_a and K_p.

(b) A pseudo-elastic phase, in which the ratio of pressure increments to elastic volume change increments is determined, is utilised in the determination of the deformation modulus.

(c) Finally, there is the plastic phase, which provides a basis for the measurement of undrained shear strength.

4.7.1.3 Test Interpretation Methods.

The inspection method involves determining the cavity reference pressure, p_0, indicating that the previous in situ stress-state is restored. However, this method is applicable only to good self-boring pressuremeter tests. For prebored tests, the Marsland and Randolph (1977) analysis is generally used, as follows:

(a) In the vicinity of σ_{h0}, the soil behaves elastically and the pressure versus cavity strain curve is therefore linear.

(b) When the undrained shear strength, c_u, is reached the soil will yield (at a pressure, p_f) and the curve will then be non-linear. The soil must, therefore, have an undrained response for this analysis to work; for example, the clay cannot be jointed or fissured. Hence, it is applicable to Dublin boulder clay (see Section 2.2.5).

In effect, the analysis involves assuming an ideal stress-strain behaviour (thus only very good tests can be analysed) and examining certain parts of the curve.

4.7.1.4 Determination of In Situ Stresses.

The Marsland and Randolph (cited) analysis, described in the previous section, gives:

$$\sigma_{h0} = p_f - c_u \qquad [4.7.1]$$

However, actual clays often yield prior to reaching c_u (at large strains). Hence, c_u can be replaced with the shear stress, τ_f, corresponding to apparent yielding.

σ_{h0} is solved by iteration by initially guessing σ_{h0}, to generate an origin for the graph, and a corresponding estimate of τ_f made (see Fig. **A.5.1**). These estimates are then compared with p_f. A more informed estimate can then be made of σ_{h0} and so on.

4.7.1.5 Stiffness.

The soil horizontal shear modulus, G_h, can be obtained from the stress-strain curves. Generally, the shear modulus is obtained from unload-reload loops, which gives G^h_{ur}. (G_{ur} is defined in the same way as E_{ur} (see literature review, Fig. **2.5.12**)). The stiffness obtained from an unload-reload loop, in the case of the pressuremeter is, however, a function of the stress and strain levels over which the loop was conducted.

4.7.1.6 Strength.

The value of c_u is determined from the latter part of the pressuremeter curve, where the soil is behaving essentially perfectly-plastically.

4.7.2 Seismic Tests.

A large amount of seismic test data was made available to the author through the Dublin Port Tunnel project (Geoconsult-Arup, 1997) and through a research project at Scholarstown (BMA, 1995). The tests consisted of seismic refraction (see Section 2.5.5.2). P and S waves were generated with sledgehammers and geophone spacing was in the region of 2 m. This is the same

energy source as the bender element tests; hence, the stiffness obtained by each method could be compared.

The seismic refraction tests measured stiffness[2] at various depths within the till, hence an estimate of the variation of the stiffness of the Dublin boulder clay layer with depth could be made by drawing a comparison with the borehole records in the vicinity of the seismic spreads (see Section A.5.2 for the results of this analysis).

[2] The research tests of BMA (cited) were processed as follows:

(a) First arrivals were identified and travel time plotted.
(b) Seismic velocity was thus obtained from each seismic spread and the thickness of each velocity unit interpreted using the Intercept-Time method. Other methods of interpretation used were the Plus-Minus method and the Generalised Reciprocal method.

CHAPTER 5

FIELD AND LABORATORY WORK - DISCUSSION

CHAPTER 5

FIELD AND LABORATORY WORK - DISCUSSION

5.1 Introduction.

If the potential of the FE method is to be realised, it is of uppermost importance that the observed behaviour of the soil be correctly incorporated. The purpose of the tests, described in the previous chapter, was to examine, in a very detailed way, the behaviour of the boulder clay, to measure the required soil model parameters and to provide essential data for validation and verification of the soil models. This chapter is also concerned with obtaining an appreciation of the reliability of the use of laboratory values and laboratory behaviour in predicting the actual in situ ground behaviour under loading. The discussion draws on the literature review and the test results, of Chapter 2 and Appendix A, respectively.

5.2 Sampling.

A new method of soil sampling, called Geobor S (Jonsson et al., 1995), was employed especially for this study, and various methods developed by the author, to ensure that samples of boulder clay, as undisturbed as possible, were obtained for the research tests described herein. The main findings arising from the application of Geobor S, specifically developed for coring in stiff boulder clay, were as follows:

(a) In contrast to standard rotary coring (with air-mist or water flush), and the difficulties associated with U100 sampling, the Geobor S method provided near total core recovery (TCR).
(b) Gravel was sliced clean through and the surface of the soil cylinder was smooth as a result. The clasts were not disturbed from the soil matrix.
(c) The top metre of soil could not be recovered.

It may be concluded that the Geobor S method, coupled with good handling and storage procedures, was a success, which is in keeping with the findings of Steenfelt (2001), when applied to Scandanavian lodgement till (Storebaelt link).

5.3 One-Dimensional Consolidation.

5.3.1 Yield Stress, σ_{vy}'.

5.3.1.1 Methods of Determination and Laboratory Estimate.

Fig. **A.1.1** shows the initially surprising result that the e-logσ_v' curve is not bi-linear. σ_{vy}' cannot, therefore, be determined by the classical Casagrande method. Several other methods of the determination of σ_{vy}' have been proposed, however. These are:

(a) Tavenas et al. (1979) suggested a graph of strain energy against effective stress. In the oedometer, the strain energy is $\frac{1}{2}\sigma_v'\varepsilon_a$ (in units of kNm/m^3). In practice, however, it was found by the author that the σ_v' component controlled the curve, owing to the combination of low strains/high stresses in tests on stiff boulder clay; *ergo*, the method led to an overprediction of σ_{vy}'. This is demonstrated in Fig. **A.1.3(a)**, which shows that unreasonable[1] σ_{vy}' values, in the region of 3000 kNm^{-2}, are obtained.

(b) Butterfield (1979) stated that "the natural volumetric strains and stresses are linearly related," is a fundamental soil behaviour, i.e. a double logarithmic plot of ε_v against σ_v' is bi-linear. This method was successfully applied by Lehane and Simpson (2000) to oedometer tests in Dublin boulder clay. However, the author found that the method did not improve upon the bi-linear Casagrande method, as is shown in Fig. **A.1.3(b)**.

(c) Janbu (1991) plotted $1/m_v$ against σ_v' and found that the soil stiffness variation is an indicator of yield. Fig. **A.1.3(c)** shows Tests O and E plotted on $1/m_v$ versus logσ_v' axes. As can be seen, the curves are bi-linear but do not exhibit the destructuring, i.e. loss in stiffness as the yield point is approached, as suggested by Janbu (cited). This is because of the structural strength of the soil, which is demonstrated in Sections 5.3.3 and 5.6. σ_{vy}' was, therefore, measured as shown in the graph of Fig. **A.1.3(c)**.

---

[1] These values compare very unfavourably with previous estimates, namely 1300 kNm^{-2} (see Section 2.4.1).

Table **5.3.1** gives the measured values of σ_{vy}' for the tests and the overconsolidation ratios, OCR, of the soils. The mean[2] value is about 1500 kNm^{-2}.

Table 5.3.1. Measured σ_{vy}' and OCR

	σ_{vy}': kNm^{-2}	OCR
Test O – gravelly lodgement till	1700	11·4
Test E – relatively low gravel lodgement till	1350	5·6

5.3.1.2 Semi-Empirical Prediction of Yield Stress.

Owing to the difficulties in obtaining an estimate of σ_{vy}', it was considered worthwhile to make an independent prediction of the yield stress for comparison with the measured value. Fig. **5.3.1** is a plot of the isotropic overconsolidation ratio, R_p, against effective cell pressure, p_0', in CIU tests. R_p was calculated from c_u/p_0', the undrained shear strength ratio, using the following formula from critical state soil mechanics[3] (CSSM) (Wroth, 1984):

$$c_u/p_0' = (M/2)(R_p/r)^{\Lambda} \qquad [5.3.1]$$

Rearranging gives:

$$R_p = r\left(\frac{2}{M}\frac{c_u}{p_0'}\right)^{\frac{1}{\Lambda}} \qquad [5.3.2]$$

where the spacing ratio between the critical state line (CSL) and the normal consolidation line (NCL), r, is 1·6 for Dublin black boulder clay (Lehane and Simpson, 2000)[4]. M is the slope of the

[2] A mean value is justified because Test O was of high gravel content and Test E was of low gravel content. It is considered that this produces an upper and lower bound yield stress, respectively, as shown in the glacial consolidation section of Chapter 3 (Section 3.2.2).

[3] It is noted that the SHANSEP formula (Ladd and Foott, 1974) could have been used instead of CSSM. However, the isotropic effective confining stresses of the CIU tests would have to be converted into their equivalent vertical effective stress because SHANSEP is in terms of OCR and σ_v' and not R_p and p'.

[4] This value is lower than the value of 2 commonly assumed and is the result of the CSL being pushed closer, than is usual for clay, to the NCL, owing to a high rate of dilatancy as failure is approached.

Cam-Clay failure line ($M \approx 1{\cdot}29$ with $\phi' = 32°$, derived in Section 5.4.3). c_u/p_0' is the undrained shear strength ratio, where c_u is taken as half the failure, deviator stress in the CIU triaxial test[5]. Λ is the 'plastic volumetric strain ratio', which is a factor that takes account of sample disturbance[6]; a value of $\Lambda = 0{\cdot}8$ was taken, which is reasonable for isotropically consolidated, overconsolidated clays (Mayne, 1988). The continuous line through the resulting data, shown in Fig. **5.3.1**, is:

$$R_p = p_{pc}'/p_0' \qquad [5.3.3]$$

where p_{pc}' is the mean preconsolidation stress, which is found from:

$$p_{pc}' = \sigma_{vy}'(1 + 2K_0^{nc})/3 \qquad [5.3.4]$$

where $\sigma_{vy}' = 1500\ kNm^{-2}$ (measured in the oedometer) and $K_0^{nc} = 1 - \sin\phi_{cv}'$ (Jaky (1944) and K_0 test measurement on reconstituted soil[7]). The curve thus found (directly from the laboratory data) is in reasonable agreement with the R_p data derived indirectly from CIU tests and CSSM. It may be concluded that:

(a) The laboratory measurements of σ_{vy}' (and K_0^{nc}) are reasonable.

(b) The yield stress is linked with the soil strength; i.e. σ_{vy}' is not simply the past maximum pressure.

(c) The soil is reasonably well described by CSSM, which is in keeping with the findings of Lehane and Simpson (cited).

5.3.2 Soil Stiffness in One-Dimensional Compression.

An approximate linear relation was found between E_{ur} and σ_1' by Jacobsen (1970) and, more recently, by Steenfelt (1997) (see Section 2.5.3), where E_{ur} is the stiffness measured on unload-reload in the oedometer and σ_1' is the vertical effective stress at which reloading is commenced. However, when the stiffness is determined from the reload curves in Fig. **A.1.7**, the points plot along a linear line (of slope m) on a double-logarithmic plot of stiffness against σ_1', as can be

[5] Which is theoretically true for $\phi_u = 0$ analysis and a degree of saturation of 1.

[6] Reducing Λ has the effect of increasing R_p, particularly for low effective confining stresses.

seen in Fig. **A.1.2**. Hence, for Dublin boulder clay, the following power law equation for oedometric, pseudo-elastic, stiffness is appropriate:

$$E_{ur} = E_{ur}^{ref}(\sigma_1'/p_{ref})^m \qquad [5.3.5]$$

The value E_{ur}^{ref}, shown in Fig. **A.1.2,** is considerably higher than the value E_{oed}^{ref}, the latter being determined from the primary loading curve (see Fig. **2.5.11**)[8].

Once the yield stress has been exceeded, the primary curve is rejoined, which can be seen on the e-logσ_v' plot (Fig. **5.3.2**) with the unload-reload curves included. Hence, the primary loading curve represents plastic, post-yield strains. It follows that the oedometer tangent modulus, E_{oed}, which is determined from the primary loading curve, is more suitable to characterise post-yield, non-elastic straining. This is because, without a stress-history reconstruction, there is a very small boundary surface, separating elastic from non-elastic behaviour. (These boundary surfaces are explained in Section 5.4.1.) Therefore, on primary loading, the soil behaviour is almost entirely non-elastic, which is associated with relatively large strains. It appears that for this till, which possesses a high in situ deviator stress (see Fig. **5.4.9**), the stress relief on sampling is to the extent that, when subsequently tested, the stress-state of the soil sample, without stress-history reconstruction, is unrepresentative. (Note that this view is supported by Fig. **5.3.2**, which shows that, although inapplicable to primary loading, the Casagrande method is applicable to reload.)

Typical values of m_v, the coefficient of volume compressibility, are shown in Fig. **5.3.3**. Although the value of m_v, evident from this plot, is highly variable, the value of m_v on reload is a constant up to the yield stress, in the case of the intact soil. Furthermore, the value of m_v on reload was found, in a similar way to E_{ur}, to increase as σ_1' increased. For this part of the curve, which is considered to be representative of the in situ stiffness for the reasons discussed previously (in this section and Section 2.5.3), a typical value of m_v is 0·008 m^2MN^{-1}.

---

[7] See triaxial Test T1.

[8] On the familiar bi-linear, e-logσ_v', plot (Fig. **5.3.2**), the indices C_c, C_s and C_e represent one-dimensional compression, swelling and recompression. The equivalent of the parameters, C_c and C_s/C_e, when the oedometer test is plotted on σ_1' against ε_a axes are E_{oed}, the tangent oedometer stiffness and E_{ur}, the elastic unload-reload modulus, respectively (see Section 2.5.3).

The average values of C_c (= 0·078) and C_s (= 0·01), measured in the oedometer tests on intact soil, compare favourably with those of Lehane and Simpson (2000), as do the reconstituted indices. It is noted that the reconstituted indices are typically two to three times higher than the equivalent intact indices. Good agreement was also found between C_c* (based on w_l) (see Equation [2.6.4]) and C_c of the reconstituted soil, which is consistent with the findings of Clarke et al. (1998), who conducted tests on reconstituted lodgement till from Northern England. The results also show that the swelling index of the intact soil is about equal to the recompression index, suggesting that the unload-reload curve is elastic.

5.3.3 Soil Structural Strength.

5.3.3.1 Soil Structural Strength Measurements.

There are a number of indicators of the structural strength of Dublin boulder clay. For example, C_e and C_s of the intact soil are about equal (see Table **A.1.1**); hence, the soil did not destructure even under a pressure of 13 MNm^{-2}, indicating a substantial structural strength[9]. Secondly, the swell sensitivity ratio, C_s*/C_s (see Equation [2.6.5]), which was determined from unload from the maximum pressure (see Fig. **5.3.4**[10]), was measured as about 3; i.e. the intact soil resisted swelling three times more than the reconstituted soil. (The reconstituted soil was prepared with the same particle sizes as the intact soil and a very high stress was applied; consequently, the soil was swelled from about the same void ratio as the intact soil.) The value of 3 is comparable with, highly bonded, Gault and Pappadai clays[11], which possess swell sensitivities of about 4 and 2·5, respectively.

---

[9] Note that this structural strength suggests that the intact soil will not have been adversely affected by the unload-reload cycles applied in the test, particularly as care was taken not to exceed the yield stress prior to unloading.

[10] The reconstituted till is reasonably close to the ICL of Burland (1990)/Chandler (2000) (Equation [2.6.3]), but deviates at high effective stress; i.e. the reconstituted till ICL is linear at high stress, as opposed to the curved ICL of sedimentary clays. This result is very similar to the test results of Clarke et al. (1998) on reconstituted lodgement till (their Fig. 13). Furthermore, it is noted that the intact consolidation curve does not cross the ICL, as might be expected for a structured soil. This is because, as explained by Kavvadas (1998), the very low in situ void ratio corresponds to a very high pressure on the ICL.

[11] Note that this is a pre-yield value for the Pappadai clay: post-yield values are about unity, suggesting substantial destructurisation, not evidenced in the boulder clay.

This is a particularly good indicator of structural strength gained entirely through inter-particle bonding (Burland, 1990). In the absence of substantial clay mineral aggregation, the reconstituted soil differs from the intact soil only in respect of the structural component, which was also identified in mineralogical and microscopic studies (see Section 5.6).

From the graph of $1/m_v$ versus $\log\sigma_v'$ (Fig. **5.3.3**), it can be seen that, on reload around the value of σ_{vy}', the intact soil is very much stiffer than the reconstituted soil. The reconstituted soil loses stiffness as the past maximum pressure is reached, whereas the intact soil does not lose any stiffness. This behaviour is entirely attributable to the structural strength of the intact soil. By increasing the pressure beyond σ_{vy}', the resistance of the reconstituted soil can be seen to gradually approach that of the intact soil, but only as the soil becomes very stiff. Hence, it may be concluded that the intact and reconstituted soils are fundamentally different materials.

5.3.3.2 The Origin of Structural Strength.

It is uncertain at first as to where the structural strength of the black lodgement till is originating, vis-à-vis the reconstituted soil. The activity ratio and the soil mineral and microscopic studies all indicate a soil of low clay mineral content and, hence, limited clay mineral aggregation/cohesion. However, besides suction (which exists in the reconstituted soil as well), inter-particle bonding can originate from diagenesis[12] and possibly electrical bonds (Jacobsen (1970) and Kavvadas (1998)). The latter is, however, not considered significant to Dublin boulder clay, owing to a low overall cation exchange capacity (CEC), as is demonstrated in Section 5.6.4. Hence, emphasis is placed on the possibility of cementation, indicative, evidence for which was obtained from the results of the oedometer tests discussed in the previous sub-section, but also from actual evidence obtained from scanning electron microscope images of unsaturated till in Section 5.6.3.2.

[12] This may be particularly true in this boulder clay, which has a wide range of constitutive minerals (see Section 5.6.4), the effects of which on the soil behaviour are largely unknown.

5.3.3.3 Importance of Structural Strength.

The effect of the structural strength is to reduce the brittleness of the soil. This is particularly important in low plasticity soil such as Dublin boulder clay, which would be expected to be very brittle. The effect is evident in triaxial compression tests, where the reconstituted soil is far more brittle than the intact soil (see Section 5.4.7), failing at a much lower strain. The yield point of the intact till is not as distinct as it is for clays and rocks with true inter-particle bonding, however. Hence, estimating the yield stress of the soil is difficult, as has been shown in Section 5.3.1.1.

5.3.4 Primary and Secondary Consolidation and Consolidation Characteristics.

5.3.4.1 Analysis of Consolidation Data.

Fig. **A.1.6** shows some consolidation curves that were recorded during the course of the oedometer tests. These curves show a parabolic section (primary consolidation) followed by a linear section (secondary consolidation), as explained by Janbu (1991). From an analysis of these, and many similar consolidation curves, the following has been concluded:

(a) The point, t_0, which represents the transition from primary to secondary consolidation, is a function of the applied effective stress, increasing as the applied effective stress increases. This is in keeping with the work of Janbu (cited).
(b) The secondary curve is about linear and constant over a long time.
(c) The slope of the secondary consolidation stage is zero for NC reconstituted soil, as can be seen in Fig. **A.1.9**, suggesting that preconsolidation and/or soil structure control secondary settlement of the till.

5.3.4.2 The Coefficient of Consolidation, c_v.

Consolidation curves, such as those shown in Fig. **A.1.6**, were transformed to the well-known root-time and log-time curves to graphically determine the value of t in the one-dimensional consolidation formula:

$$c_v = T_v d^2/t \qquad [5.3.6]$$

where T_v is the time factor and d is the drainage path length.

Owing to possible uncertainty in determining t, three different methods were applied by the author to the consolidation curves: root-time (t_{90}), log-time (t_{50}) and inflexion-time (t_i). The last method was proposed by Cour (1971) and is based on the semi-log plot. The settlements associated with a stress increment were calculated at the end of primary consolidation, t_{100}, this from the semi-log time-settlement plot. Fig. **A.1.4** shows a graph of c_v against σ_v' for all the oedometer tests in the range shown. Published data on boulder clay is also shown for comparison (Mc Kinlay et al., 1978). (It is noted that the majority of the data falls below 25 m^2yr^{-1} and that there is no data in the range 25 m^2yr^{-1} to 70 m^2yr^{-1}. This is evidence that c_v measurements over 25 m^2yr^{-1} are in error.) c_v appears to decrease with increasing σ_v', although this is the case only at uncommonly high stress levels. Therefore, an average c_v of about 5 m^2yr^{-1} is suggested. This low c_v value is consistent with field observations (Farrell et al., 1988).

Inputting this value of c_v into Equation [2.5.5], with the value of m_v of 0·008 m^2MN^{-1}, interpreted in Section 5.3.2, gives a permeability of $1{\cdot}27\times10^{-11}$ ms^{-1}.

5.3.4.3 Coefficient of Permeability, k.

Fig. **A.1.5** shows permeabilities[13] calculated with Equations [2.5.5] and [5.3.6]. The points are plotted for $c_v < 25$ m^2yr^{-1} (see Section 5.3.4.2 for the reasons for this). The resulting data lie close to straight lines, with each test lying on a separate line[14]. This result is consistent with the data published by McKinlay et al. (1978), as shown in Fig. **2.5.16**.

---

[13] The horizontal permeability of the till is considered to be the same as that of the vertical permeability because lodgement till, unlike sedimentary clays, is not laid down in layers.

[14] The permeability of the reconstituted soil decreases with increasing stress up to a point, after which the permeability remains essentially constant at about 5×10^{-12}. This may be due to plugging of the pore space in the intact soil, owing to diagenesis (see Sections 5.3.3.2, 5.6.3 and 5.6.4 for a discussion of diagenesis), thereby reducing the potential for low permeability in the reconstituted till vis-à-vis the intact till.

The form of the graph Fig. **A.1.5** produces a straight line if the curve is exponential. Furthermore, the difference in the slope of the lines is probably caused by the variable gravel contents of the soil specimens; i.e. higher permeabilities are measured when the gravel content was high and vice versa. The equations of the lines shown are:

$$k = 5\times10^{-10}\exp[-0{\cdot}0008\sigma_v'] \qquad [5.3.7]$$

$$k = 5\times10^{-10}\exp[-0{\cdot}004\sigma_v'] \qquad [5.3.8]$$

At typical in situ effective stress levels ($\sigma_v' = 100$ kNm^{-2}), however, the permeability is about the same in all of the tests; thus, significant variations in permeability of samples of varying gravel content only occur over a much wider stress range, as is demonstrated in Fig. **A.1.5**. Hence, the permeability of the soil in situ would be expected to be about constant, regardless of variation in gravel content. This is a surprising result but does correspond with experience in the field.

A comparison with boulder clays of similar void ratios in Denmark, on which permeability tests were conducted (Jacobsen, 1970), suggested that a boulder clay of the void ratio of the deformation till has a permeability of about an order of magnitude greater than a boulder clay of the void ratio of the lodgement till.

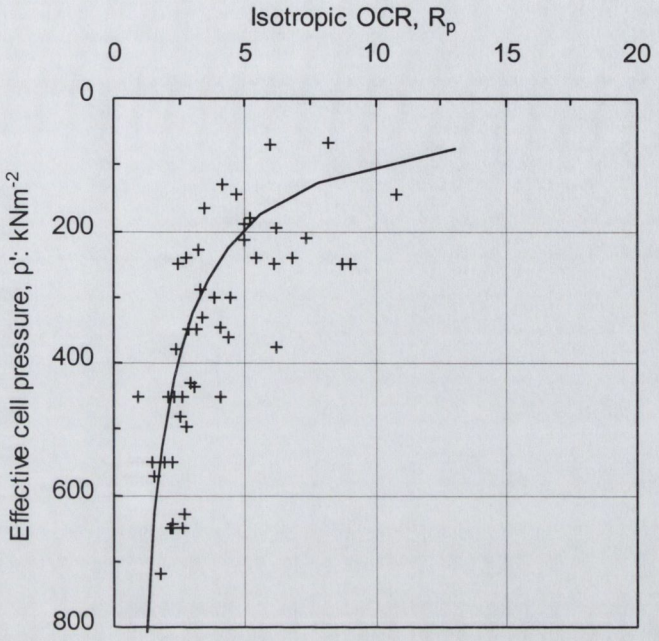

Fig. 5.3.1. Isotropic overconsolidation ratio prediction

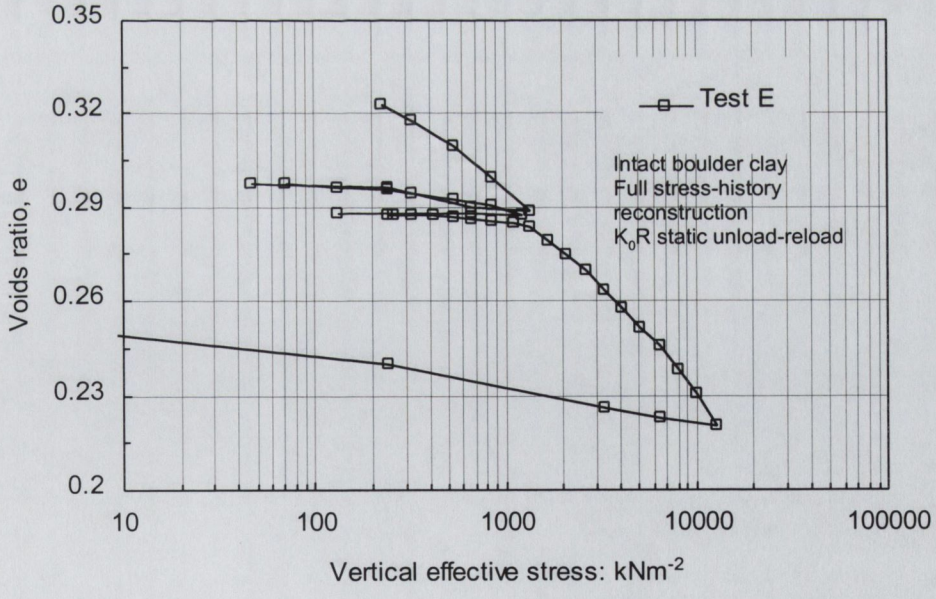

Fig. 5.3.2. Consolidation curve including unload-reload loops

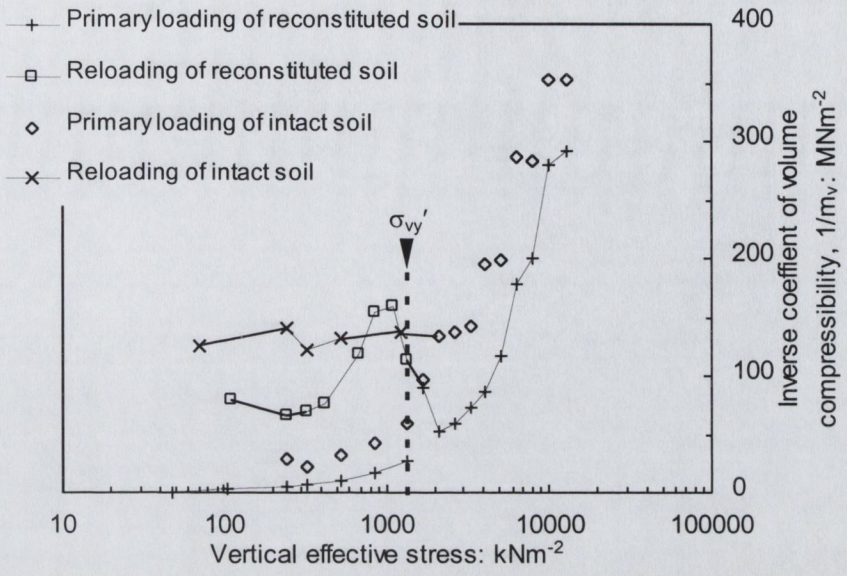

Fig. 5.3.3. Comparison of the behaviour of reconstituted and intact till

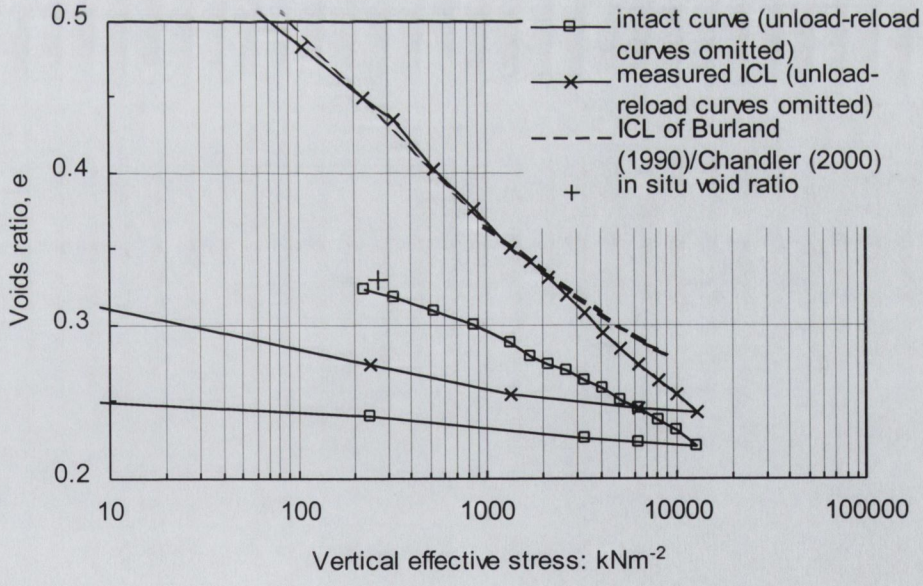

Fig. 5.3.4. Comparison of intact and reconstituted oedometer tests

5.4 Triaxial Tests.

5.4.1 General Behaviour.

In the literature, soil behaviour in the triaxial test is demonstrated in terms of various boundary surfaces and stress-strain behaviour. The factors that control and shape the boundary surfaces have been demonstrated and the soil behaviour within the boundary surfaces has been qualified, e.g. elastic, non-linear elastic and plastic. Another stream of research has developed where the actual behaviour of the soil has been examined independently of the state boundaries. For example, Atkinson (2000) examined the threshold effect and the development of shear bands and Simpson (1992) demonstrated the fundamental effect of particle realignment on soil stiffness. This section examines how these different approaches relate to each other, i.e. how the actual behaviour of Dublin boulder clay relates to the state boundaries.

Fig. **5.4.1** shows the overall measured behaviour of intact Dublin boulder clay in consolidated drained (CD) triaxial tests. The tests identified on the figure have been described elsewhere (the reader is referred to Figs. **2.5.1** and **2.7.1** for Tests 1 and 2 identified on Fig. **5.4.1**). The graphs show a comparison of the stress-strain behaviour of the soil (on q-ε_s axes), the dilatancy behaviour (on ε_v-ε_s axes) and the stress-paths (on q-p′ axes). Fig. **5.4.2** is a diagrammatical depiction of Fig. **5.4.1**, intended to clarify the various stiffnesses, states and boundary surfaces involved. The following discussion represents a concise description of the sequence of stages, evident in these plots, in the behaviour of Dublin boulder clay.

Path O-A. At very small strain levels up to the threshold strain, ε_t, the soil response is linear, elastic and very stiff with a stiffness very similar to that derived from the bender element tests, E_0'. The threshold strain is exactly equal to the point at which the slope of the ε_v-ε_s curve changes, as shown in the magnified graph in Fig. **5.4.1**, which represents a realistic test; i.e. a test with a full K_0 stress-history reconstruction (K_0R) and, therefore, realistic stress-strain characteristics[1]. This finding is surprising because the soil is observed to resist a change in

[1] Loading of the soil near to the value of the yield stress, followed by unloading, induces in the soil sample an anisotropic stress-state close to that in situ and reconstructs the boundary surfaces that separate elastic from non-elastic behaviour. As will be shown, these, CK_0RD,...

volume up to the threshold strain (at A); hence, the slope of the compression phase is not negative from the start of shearing (negative dilatancy represents compression) and only becomes negative once the threshold strain has been exceeded. The extent of the initial elastic region is about constant; i.e. ε_t = 0·006% - 0·01% of shear strain (see Figs. **2.5.8** and **5.4.7**)[2]. This value of the threshold strain is relatively high compared to other soils, i.e. higher than 0·001%. The corresponding, very high, initial stiffness (G_{max} in the order of 750 MNm^{-2} – see Fig. **5.4.4**) results from a high degree of particle interlock and resistance to movement as the particles adjust and realign to the direction of loading. This very high degree of particle interlock is partly attributable to the structural strength/diagenesis of the intact lodgement till (see Sections 5.3.3 and 5.6.4). (ε_t is discussed further in Section 5.4.2.2.)

Path A-C. The stress-strain behaviour in this region is highly non-linear and stiff. The region is delineated by the threshold strain and the exact point, C, at which the soil starts to dilate at the maximum rate of soil dilation (, which is represented by constant slope on the ε_v-ε_s curve). This part of the curve corresponds to the small strain region (i.e. from ε_t to 0·1-0·2% shear strain). In this region, the stiffness has reduced from E_0' (at point A) to E_s' (at point C), the latter being the secant stiffness at small strain, and soil dilatancy has changed from compression to the maximum rate of soil dilation, with a shear band developing at point B, representing the onset of soil dilatancy; i.e. at $\psi_m = 0°$ on the ε_v-ε_s plot.

In the region A-C, the soil particles are realigning, the degree of interlocking is decreasing and the particles are beginning to slide relative to each other; i.e. the soil mass is becoming increasingly non-elastic. The region is recent stress-history dependent, which is evident when the stress-strain and ε_v-ε_s curves are compared with the value of the isotropic preconsolidation pressure, p_{pc}', (or the one-dimensional preconsolidation stress, σ_{vy}'), as follows. p_{pc}' (σ_{vy}') is applied in the tests prior to shearing; the tests with higher values of p_{pc}' are found to resist yield more than tests with lower p_{pc}' values. For example, Test 3 (σ_{vy}' = 1400 kNm^{-2}) represents a full K_0 stress-history reconstruction (CK_0RD test). In this test, the yield surface, evident from the q-ε_s plot in Fig. **5.4.1**, is very high, with a correspondingly large zone of compression on

---

...tests subsequently exhibit compression-dilation behaviour, whereas the CID and CIRD tests, unrealistically, dilate almost from the start of shearing (see Section 2.7).

[2] This experimental result is consistent with the Viggiani (1992) equation for G_{max} (Equation [2.4.1]); this formula is discussed in Section 2.5.5.2.

the ε_v-ε_s plot. It follows that the overall stiffness of the till is, in actuality, dominated by E_s'. E_s' would, therefore, be very useful to characterise and approximate the pseudo-elastic stiffness of the soil. The following table (Table **5.4.1**) shows that the reference value of E_s', $E_s^{ref\prime}$ (see Equation [2.5.1]) is about constant for the tests (the value of m taken in the calculation of E^{ref} was 0·5, which was measured from the data shown in Fig. **5.4.6** – see end of Section 5.4.2.1).

Table 5.4.1. Small strain secant modulus, E_s', values in tests

	E_s' (MNm^{-2})	E_{sref}' (MNm^{-2})
BE1	386·3	244·3
T2S3 (O'Shea, 1996)	324·3	241·7
T3S3 (O'Shea, 1996)	245·3	233·9
SS1	361·6	228·7
BE4	207·3	131·1
		Mean = 216 MNm^{-2}

Path C-D. From point C onwards, the soil begins to dilate at the maximum rate; i.e. the shear band is fully developed and the soil particles are sliding on a shear-plane at the peak angle of soil dilation, ψ. In the tests without stress-history reconstruction, this region predominates the soil response[3]. The stress-strain curve in this region is hyperbolic and is defined by the stiffness E_{50} (see Equation [2.5.1]). Unlike O-A and A-C, path C-D is recent stress-history independent.

Path D-E-D. This path represents an unload-reload hysteresis loop. The paths D-E and E-D are a mirror image, as can be seen for example in Fig. **A.2.3**. The loop is begun in the region of plastic straining; hence, the strain is evidently only partly recoverable (i.e. the soil is behaving elasto-plastically). The beginning of the paths D-E or E-D represent a stress-path reversal and, therefore, the soil particles must realign. Hence, the stiffness is initially very high, with values in the region of E_0'. The stiffness then proceeds to reduce from E_0' to its lowest value, which is equal to E_s' (see Table **5.4.1** and Fig. **5.4.6**). This stiffness is also called E_{ur}, hence $E_{ur} = E_s'$. The stiffness in the region D-E-D does not reduce below E_s' due to strain hardening. As has been demonstrated in Section 5.3.2, the same stiffness (E_{ur}) is measured in the oedometer test on unload-reload from the preconsolidation pressure, which shows that the boundary surfaces, A and C, are kinematic and independent of the type of loading. Hence, the same boundary

[3] Although isotropically consolidated drained (CID) tests do not represent the true stress-strain behaviour, these tests remain useful, as the important non-elastic soil behaviour can be characterised.

surfaces can be used for different types of loading. Furthermore, E_{ur} is not affected by the strain level at which unloading commences or the consolidation procedure, as the same E_{ur}^{ref} was measured in the CIRD and CK$_0$RD tests and in the oedometer.

Recent research (Faulkner (1998) and Lehane and Simpson (2000)) has shown a dependence of the stiffness of Dublin boulder clay to changes in the direction of loading. As E_{ur} is measured at the point at which primary loading is resumed (see Fig. **2.5.12**), the definition of stress path direction (Fig. **2.5.10**) dictates that E_{ur} should be equivalent to a zero degree stress-path reversal (i.e. $\theta = 0°$). Faulkner (1998) showed that the stiffness of Dublin boulder clay at $\theta = 165°$ (which is close to the maximum stiffness, E_0) is about four times higher than the stiffness at $\theta = 45°$ (which is the lowest θ value given by Faulkner (cited)). The measured ratio between E_{ur}^{ref} and E_0^{ref} (i.e. G_{max}) found in the tests conducted for this thesis (see Fig. **5.4.6**) was:

$$E_0^{ref} \approx 5E_{ur}^{ref} \qquad [5.4.1]$$

Thus, the dependence of Dublin boulder clay on changes in stress-path direction is further demonstrated, as is the reliability of the stiffness measurements.

Path D-F. Once the primary stress-path is rejoined, the soil resumes path C-D, up to the failure surface, at which point the soil strains perfectly-plastically (zero slope on the stress-strain curve), which is associated with large strains. In the reconstituted test (Test T1), the conditions were such that dilatancy cut-off occurred; i.e. the soil was straining at constant volume (no particle interlock) and some strain softening occurred, as shown in Figs. **A.2.16** and **A.2.17**.

Table 5.4.2. Summary of soil behaviour measured in the triaxial tests

Path	Stress-strain	Dilatancy behaviour	Stiffness	Strain
O-A	Linear	No volume change	E_0' (G_{max})	0 - ε_t
A-B-C	Highly non-linear	Changes from onset of compression to onset of dilatancy to maximum rate of soil dilation	Reduces from E_0' to E_s'	ε_t to small strain
C-D	Hyperbolic	Maximum rate	Defined by E_{50}	Small to large
D-E-D	Elasto-plastic	See Fig. **5.4.2**	As for O-C	As for O-C
D-F	Hyperbolic	Maximum rate	As for C-D	Large
F onwards	Perfectly-plastic and strain softening	Maximum rate to constant volume	Low	Very large

5.4.2 Soil Stiffness.

5.4.2.1 Stiffness Parameters.

The bender element (BE) tests were carried out based on the methods developed by Jovicic et al. (1996) on samples at different confining pressures under isotropic and K_0 consolidation and swelling (see Sections 2.5.5.2 and 4.4.3). Fig. **5.4.3** shows the results of the BE tests in detail. G_{max} measured in the BE test immediately prior to the CK_0RD test shearing stage (i.e. the BE tests were conducted at the test confining stress) is superimposed on Fig. **5.4.4**. As can be seen from this figure, there is good correspondence with an S-shape, which is a characteristic of these semi-logarithmic plots (Simpson, 1992). This effect is also shown in Fig. **A.2.5**, for Test BE1. The stiffness interpreted from these tests represents the (elastic) stiffness of the soil at very small strains, i.e. below the threshold strain, ε_t. Importantly, because the tests were conducted on intact soil, these bender element tests include any (additive) effects of soil structure on the stiffness of the soil.

The received signals of the sine wave and square wave excitations were found to be of low amplitude, particularly at high confining stresses. However, the resonance test proved to be an effective method of mitigating the low amplitude. Note that the data shown in Fig. **5.4.3** lie approximately on straight lines (as do the static stiffness data), showing that the stress dependency of stiffness is given by the following power law:

$$E_0' = E_0^{ref'}(\sigma_3'/p_{ref})^m \qquad [5.4.2]$$

Fig. **5.4.3** also shows that there is a difference in dynamic stiffness when measured in isotropic and anisotropic (K_0) consolidation. However, as has been shown in the previous section, K_0 consolidation is the more fundamental; hence, G_{max} values of the lodgement till were interpreted from this test. Test BE1 gave G_{max} = 75 MNm^{-2} (E_0' = 180 MNm^{-2} in Fig. **5.4.5**) at σ_c' = 5 kNm^{-2}, which was consistent with the extrapolation of the best-fit line for the stiffness measurements at higher effective stress. Hence, the power law is applicable over a wide range of effective stress. It is noted, however, that it was generally not possible to obtain strong BE traces under very low effective consolidation stresses. Furthermore, it was found that averaging

of the received trace is necessary in this very stiff, intact boulder clay, although this is not considered to have adversely affected the measurements, as demonstrated in Section 4.4.3.4.

The reliability of the BE test data is demonstrated by the favourable comparison of the measurements with in situ seismic tests[4] and with the static stiffness, E_0' (derived directly from the stress-strain curve), as shown in Fig. **5.4.6**. The data is also found to correspond well with semi-empirical estimates of G_{max}[5], in the following way:

$$\frac{G_0}{p_a} = A\left(\frac{p'}{p_a}\right)^n (R_p)^m \qquad [5.4.3]$$

where A, n and m are measurable constants. Atkinson (2000) showed experimentally that these constants vary with plasticity. From Atkinson's figures, at a plasticity index of 10%, $A \approx 2300$, $n \approx 0{\cdot}65$ and $m \approx 0{\cdot}2$. p_a is atmospheric pressure and R_p is given by Equation [5.3.3]. Equation [5.4.3] is plotted on Fig. **5.4.5**, in terms of E_0' (with $\nu' = 0{\cdot}2$), which shows that there is good agreement between the measured data and the semi-empirical stiffness formula. (Note that an even better fit is obtained with $n = 0{\cdot}7$ instead of 0·65.) It can be concluded that:

(a) Equation [5.4.3], with Atkinson's (cited) constants, gives a good estimate of the stiffness of Dublin boulder clay measured by dynamic methods. This means that the in situ stiffness of a soil is largely a function of the in situ effective mean stress, soil plasticity and apparent overconsolidation.

(b) An effective Poisson's ratio of 0·2 is a suitable factor for conversion of the in situ shear modulus to the in situ effective Young's modulus.

Fig. **5.4.6** shows that the stiffness data at very small (E_0), small (E_{ur}) and large strains (E_{50}) all lie on straight lines on the double logarithmic plot of stiffness against confining stress, indicating that the stress dependency of stiffness is uniquely given by a power law. At very small and small strains, the slope is constant at about 0·5, whereas, at larger strain (E_{50}), the

---

[4] See Section 5.7.2, on the discussion of the in situ seismic tests.

[5] Note that a similar formula, in terms of Young's modulus and OCR can be obtained by combining Equations [5.4.2] and [2.4.4].

slope appears to increase to about 0·6. This is evidence of strain level effects and is in keeping with the analysis of Faulkner (1998).

5.4.2.2 The Threshold Effect[6].

It is often stated (inter alia Atkinson and Salfors (1991) and Atkinson (2000)) that the very small strain range is up to 0·001% of shear strain. This strain is called the threshold shear strain, ε_t, which separates elastic behaviour from elasto-plastic behaviour. Fig. **5.4.7** shows small strain data taken from various test types. The graph shows that the soil exhibits a threshold strain well in excess of 0·001% axial strain[7], which, according to Kavvadas (1998), is evidence for substantial structural strength. The threshold deviator stress, q_t, is also higher than the 10 kNm^{-2} generally quoted. The threshold point has been found, in Section 5.4.1, to be the point at which significant volumetric strain occurs in a sample and corresponds to the point of onset of non-linearity on the stress-strain curve.

The relevance of elastic straining at axial strains of 0·006% to 0·01% (see Fig. **5.4.7**) can be seen in Fig. **2.5.9**, which shows typical working strain ranges for various field structures. Thus, elastic behaviour, and therefore G_{max}, is relevant to excavations in Dublin boulder clay. However, the threshold deviator stress is low in respect of the stresses applied by foundations; hence, E_0' would not be expected to be relevant to footings, for example. Instead, Figs. **2.5.9** and **2.5.19(a)** show that the small strain region predominates in this foundation case and, therefore, it would be expected that E_s' (which is equivalent to E_{ur}) would be relevant (see Section 5.4.1).

5.4.2.3 Local versus External Strain Measurement.

Fig. **A.2.5** shows the stiffness strain curves of Test BE1 (CIRD test – see Section A.2.1 for details), measured externally and inferred locally[8]. As can be seen, the external measurements

---

[6] This effect is also discussed in Section 5.4.1, in relation to Path A-C.
[7] As a result, the threshold deviator stress associated with ε_t is also higher than the 10 kNm^{-2} generally quoted.
[8] Local axial strain was inferred from local radial strain readings and measured volume change using Equation [4.4.3].

underestimate stiffness up to about 0·1% (in keeping with the findings of Faulkner (1998)). This is in contrast to Test BE4 (CK_0RD test – see Section A.2.2), which had an axial load applied before shearing, thereby eliminating bedding and seating errors. Fig. **A.2.12** shows that the external and inferred local strain measurements are, unlike the CID tests (Fig. **2.5.17**), comparable, as a result. This was confirmed by Test SS1 (CK_0RD test – see Section A.2.4), in which, in addition to local radial strain measurements, local axial strain measurements were taken (see Fig. **A.2.19** and Fig. **C.4**). Therefore, CK_0RD tests do not, for practical purposes, require local axial strain measurement or local radial strain measurements, as the radial strains can be inferred from the external axial measurements and the volume change of the specimen.

5.4.3 Effective Strength Parameters.

The effective stress strength tests discussed in the literature review (Section 2.6.2) are supplemented here with the results of a large number of CIU tests conducted by Geoconsult-Arup (1997) and are shown in Fig. **A.2.6**. The mean effective peak friction angle found by linear regression on the CIU test data was 36·4° (coefficient of correlation, $R^2 = 0{\cdot}984$). The CD tests with isotropic consolidation gave $\phi_p' = 41{\cdot}7°$ ($R^2 = 0{\cdot}999$) and the CD tests with anisotropic consolidation (three tests) gave a mean ϕ_p' of 36·8°. The higher friction angle measured in the isotropic drained tests corresponds with the method of measurement, as discussed in the literature review, and the relatively low brittleness of these samples (see Section 5.4.1 above).

It is considered that the lodgement till does not possess a true c′ component due to a lack of true cohesion (see Sections 5.5 and 5.6). Furthermore, the variability of soil samples, and the very high failure stress levels, will tend to mask the c′ value. It is noted that c′ is often reported in Mohr's circle analysis, in conjunction with a low friction angle. However, this is because of variability in the three samples (generally tested) and because the tests are also subject to systematic errors, which results in a skewed failure envelope (see Section 2.6.2). It is also noted that, in Fig. **A.2.6**, there is no strong evidence for the curved failure envelope expected of a high OCR soil. It was thus concluded that c′ was about equal to zero, giving a ϕ_p' of 40°, interpreted from Fig. **A.2.6** and the Treacy (1995) shear box test (see Section 2.6.2).

Not all of the CIU tests ruptured at a near constant volume condition. This is possibly because of sample swelling, which reduces dilatant capacity and hence the distance the sample moves along the failure line (see Section 2.6.1). Hence, in the analysis of ϕ_{cv}', only those tests that finally ruptured at very large strain (the mean axial strain measured for the tests that approximated constant volume conditions at rupture was 17·5% with a standard deviation of 3·5%) were selected. This is the equivalent of applying the Hvorslev procedure, suggested by Burland (1990), which takes account of the increase in void ratio, e, due to swelling, by a normalising procedure with respect to reference e. Linear regression on the data that tended to constant volume, in Fig. **A.2.6**, gives ϕ_{cv}' of 31·5° (R^2 = 0·982). This value of ϕ_{cv}' compares favourably with the effective friction angle measured at large strain in Test BE1 (32·6°).

In reality, ϕ' varies according to the dilatancy of the soil and, therefore, the strain level. However, it is important for routine practice to select an average strength suitable to the strain in the ground. Therefore, one of the commonly measured friction angles: ϕ_p' or ϕ_{cv}', must be selected (as $\phi_{cv}' = \phi_r'$, the residual angle of friction). For ϕ_{cv}' to be relevant, very large strains need exist in the ground. This friction angle/strain is relevant only to pile driving and landslides (Skempton, 1975). Conversely, the axial strain at which peak strength was mobilised in the CIU tests had a mean of 2·2% (SD = 0·7%), which is more relevant to typical problems.

SPT N_{60} data are compared with c_u from the CIU tests described above ($c_u = q_f/2$, where q_f is the deviator stress at rupture) in Fig. **5.4.8**. The effective cell pressure in the CIU tests were converted into equivalent approximate depth by assuming typical stratigraphy and soil unit weights and a K_0 variation with depth (K_0 is derived in the next section). The figure shows that N_{60} must be multiplied by about 6 to obtain a reasonable correlation with the c_u values.

5.4.4 $\underline{K_0}$.

Fig. **5.4.9** shows a comparison, of field tests (with the pressuremeter - see Section 5.7.1.1) and laboratory measurements, of K_0 against OCR with the Schmidt (1966) power law and with elastic theory. (The power law has been given in Equation [2.4.4] and the elastic prediction, of

K_0, in Equation [2.4.5].) These equations compare well[9] with the pressuremeter measurements and with the laboratory K_0 test, when $K_0 = \sigma_3'/\sigma_1'$. (Note that the reconstituted test underestimates K_0, possibly due to the lack of structural strength.) The value of K_0^{nc}, used in these equations, was found to correspond very well with $K_0^{nc} = 1 - \sin\phi_{cv}'$, in keeping with Jaky (1944) (see Section 2.4.2), when measured from the virgin K_0 consolidation of reconstituted till (Test T1 – see Fig. **A.2.15**), when $K_0^{nc} = \sigma_c'/\sigma_v'$ (see Fig. **4.4.3**).

Note that, in Fig. **5.4.9**, the data lie within the passive failure limit, K_p (see Equation [2.4.10]); this is consistent with the observation that the Dublin black boulder clay is generally not fissured (see Section 2.2.5).

5.4.5 Angle of Soil Dilation.

The measured values of ψ, the peak dilation angle, were 2° to 3°, but the mobilised dilation angle, ψ_m, was observed to vary considerably. The value of ψ is considered to be low due to the very low strain rate necessary in the drained test (Atkinson, 2000). Therefore, as the soils were tested under a limited range of, very low, strain rates, it is not considered accurate to give a single value of dilation angle based on the tests conducted here. Furthermore, soil dilatancy is also a function of soil density, stress level, inter-particle friction and strain level (see Section 2.7). Hence, it is necessary that a dilatancy model be used as an approximation. Flow rules were examined in Section 2.7, in which it was found that Rowe's (1962) stress-dilatancy theory represents the state-of-the-art.

Fig. **5.4.10** shows that, unlike the CID tests, there is reasonable agreement between the stress-dilatancy characteristics of the CK_0RD tests and the stress-dilatancy theory predicted by Rowe's theory[10]. Note that the CIRD test (BE1), in common with previous isotropically consolidated samples, is a poor fit to the predicted curve because there is a high rate of dilatancy from the start of shearing. O'Shea's (1996) CID tests also show a high variability. Note, however, that Rowe's theory overestimates the compression of the till (negative dilatancy) but that the peak state is well predicted (i.e. all the tests shown in Fig. **5.4.10** tend to a common angle of dilation

[9] Although good correspondence was obtained, it is considered that the actual ground conditions are too variable to warrant the increased accuracy of the power law.

at failure, given by Rowe's rule). Hence, it is reasonable to use this theory to predict a typical value of ψ, using the values of ϕ_p' and ϕ_{cv}' interpreted in the strength tests, giving $\psi \approx 10°$.

5.4.6 Poisson's ratio.

The value of ν_u (the undrained Poisson's ratio), which was obtained from in situ seismic tests (the results of which are discussed in Section 5.7.2) and Equation [2.5.14], was about 0·5 (see Table **A.5.1**). This value, which is the undrained value, is as expected from seismic tests and is due to the very rapid distortion of the soil caused by the seismic waves. (The BE measurement of ν_u was lower, also as expected, owing to the relatively fast propagation of the near-field compared to P-waves – see end of Section 2.5.5.2.) The value of ν' derived by Farrell et al. (1988), namely 0·2, was shown (in Section 5.4.2.1) to be an appropriate factor for converting G_{max} to E_0'. Hence, this value of ν', thus validated, was assumed throughout the relevant analyses discussed in this thesis.

5.4.7 Behaviour of Reconstituted Soil.

The reconstituted test (Test T1) was found to possess about the same shear strength as the intact soil. However, the failure strain was far lower (see Fig. **5.4.11**). This is considered to be due to the lower structural strength of the reconstituted material, compared to the intact material. The structural strength of the intact soil, which is distinct from shear strength and was discussed in detail in Section 2.6.4, contributes to resisting yield and, therefore, the intact soil is less brittle than the reconstituted soil; i.e. the intact soil does not fail as suddenly as the reconstituted soil. Comparing the stress-strain behaviour of Tests T1 and BE4 in Fig. **5.4.11** shows this behaviour. This essential difference between the intact and reconstituted tests is evidence that the gradual yield of the intact till is due to progressive destructurisation.

The reconstituted till was found to compress more than the intact till on shearing, as can be demonstrated by a comparison of Figs. **A.2.13** and **A.2.17**. Furthermore, the reconstituted soil tended to constant volume (i.e. 'dilatancy cut-off'), as shown in Figs. **A.2.16** and **A.2.17**.

---

[10] The constant in the equations, ϕ_{cv}', was taken as 32°, from the strength tests at constant volume shearing.

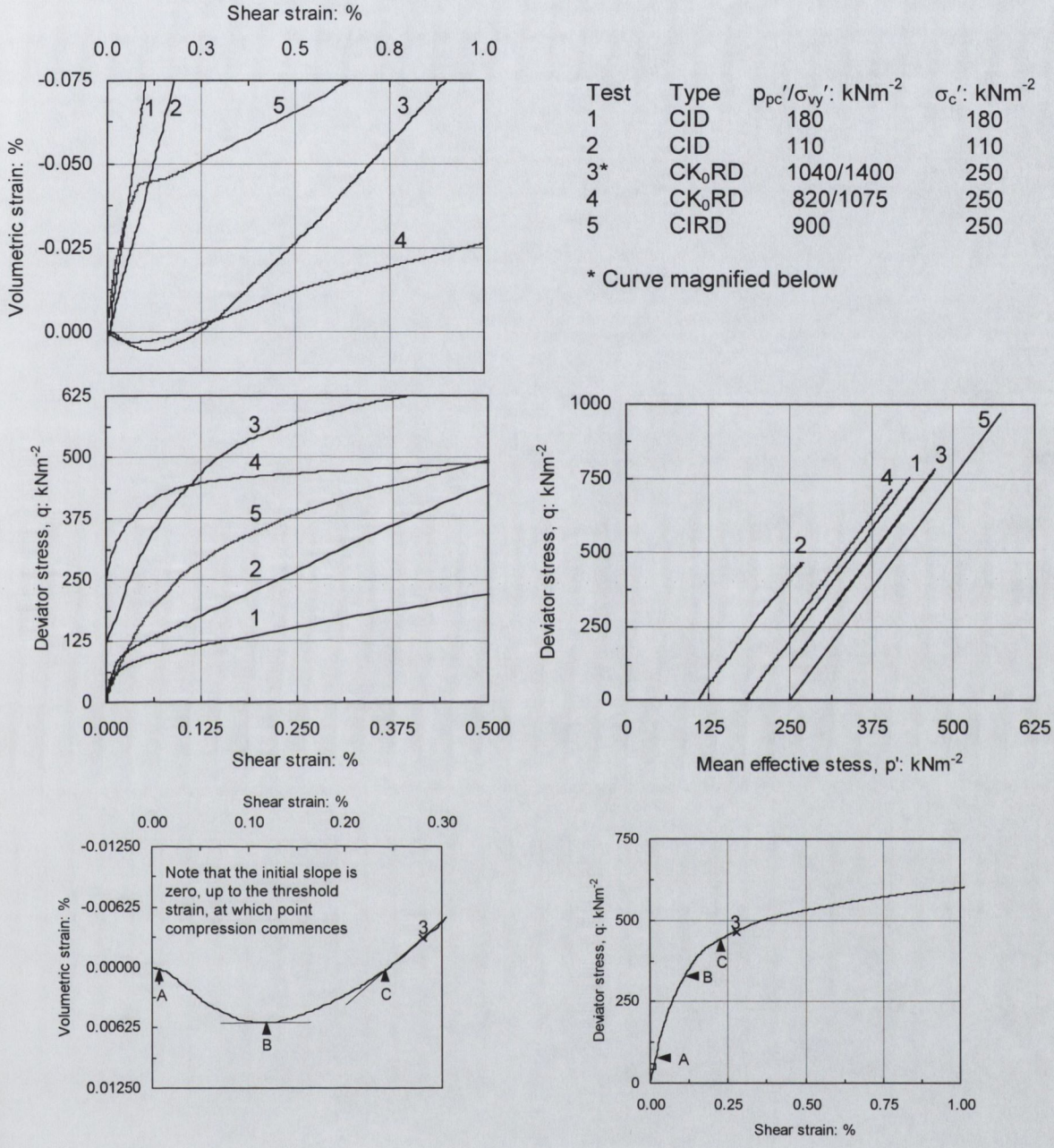

Fig. 5.4.1. Overall behaviour of Dublin boulder clay in the CD triaxial test

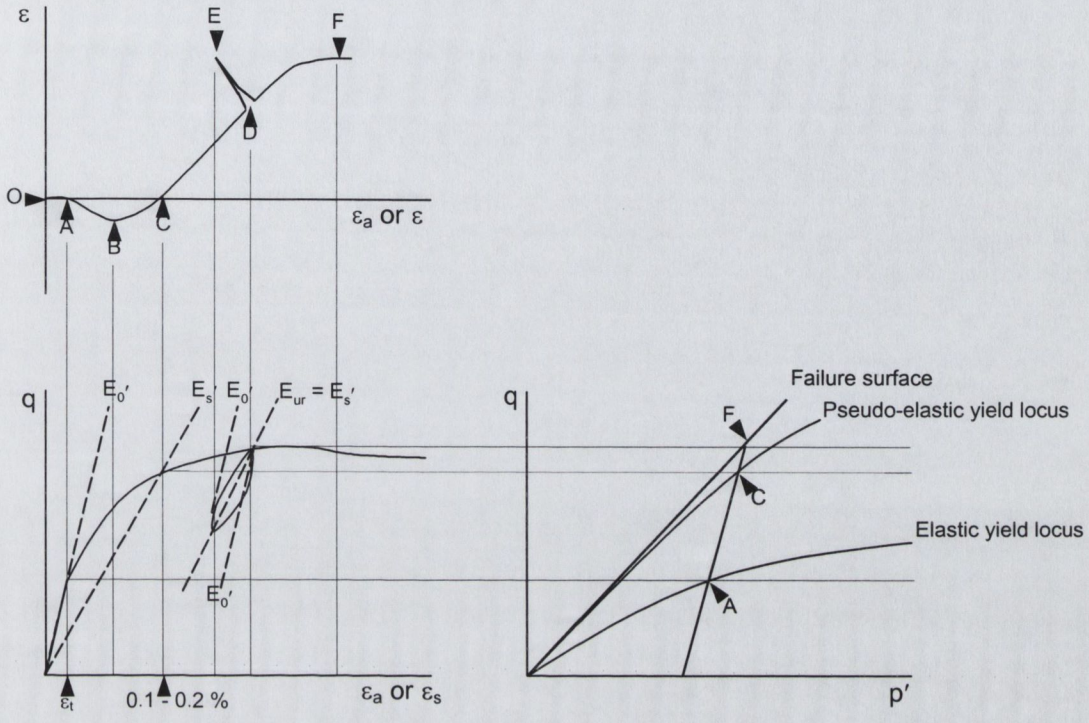

Fig. 5.4.2. Depiction of overall behaviour of Dublin boulder clay shown in Fig. 5.4.1

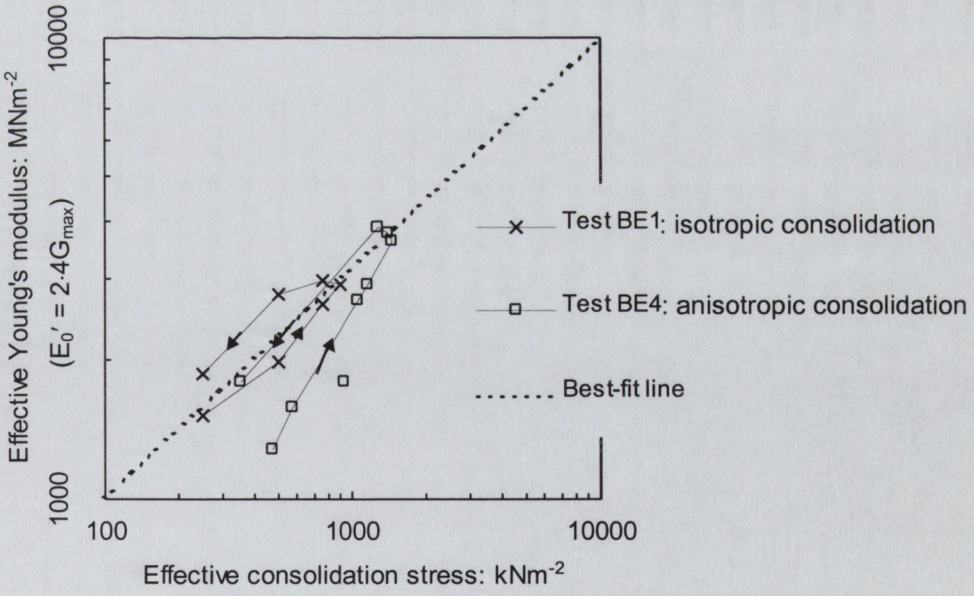

Fig. 5.4.3. Detail of the bender element tests of Tests BE1 and BE4

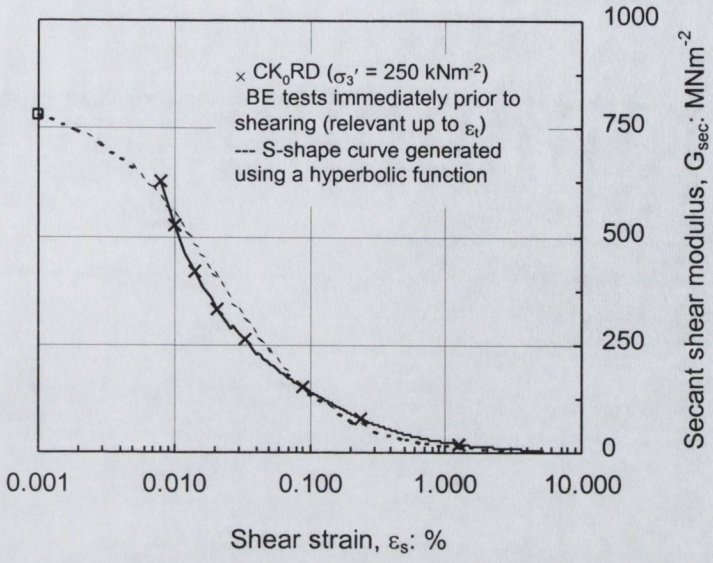

Fig. 5.4.4. Shear modulus versus logarithm shear strain curves: CK_0RD test

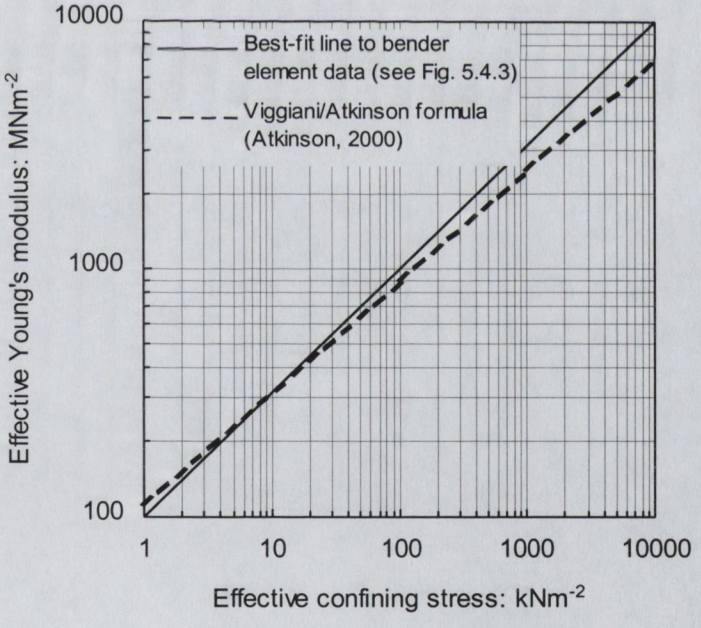

Fig. 5.4.5. Very small strain stiffness tests: comparison with theoretical value

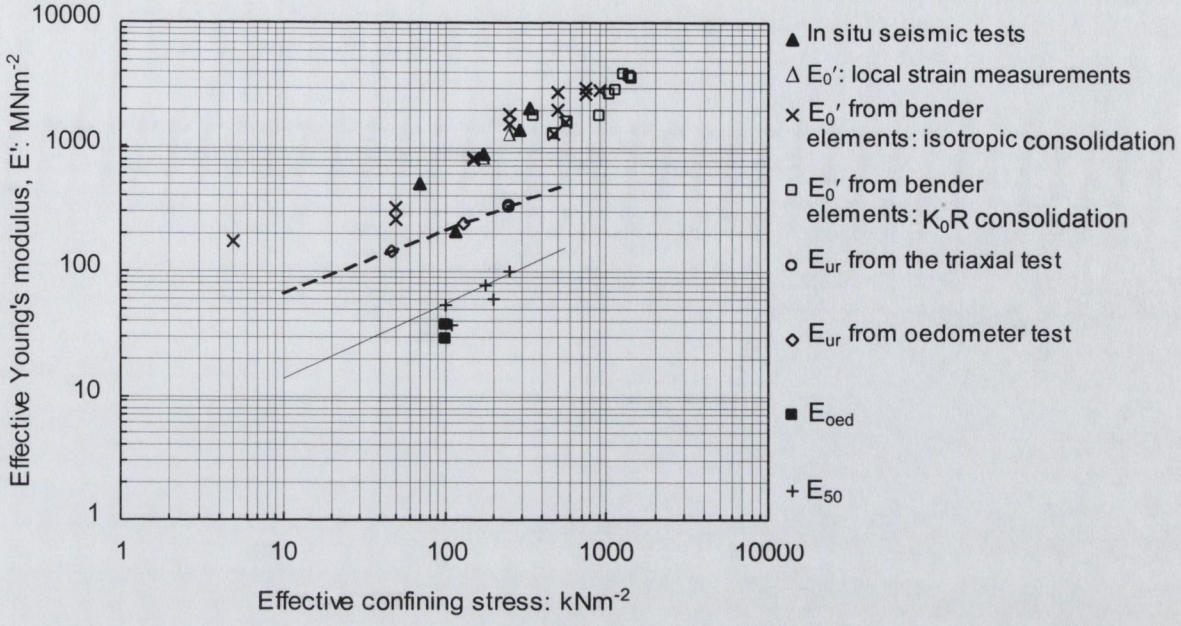

Fig. 5.4.6. Plot of stiffnesses measured in all laboratory tests

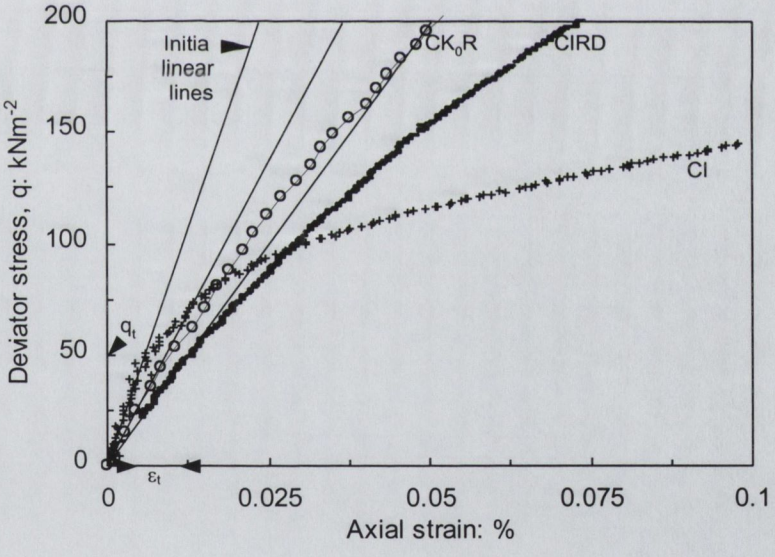

Fig. 5.4.7. Deviator stress against axial small strain of various test types in the region of small strain showing high threshold to initial yield

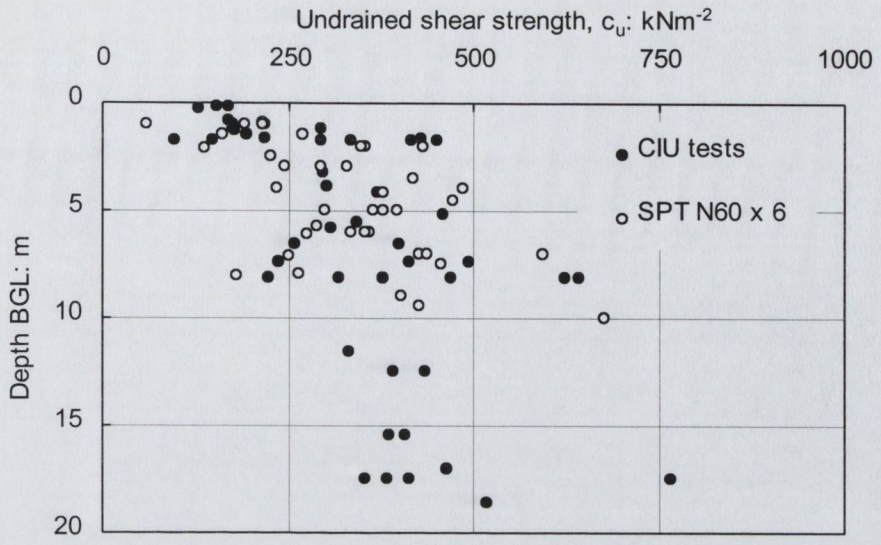

Fig. 5.4.8. Comparison of N_{60} and c_u measured in CIU tests

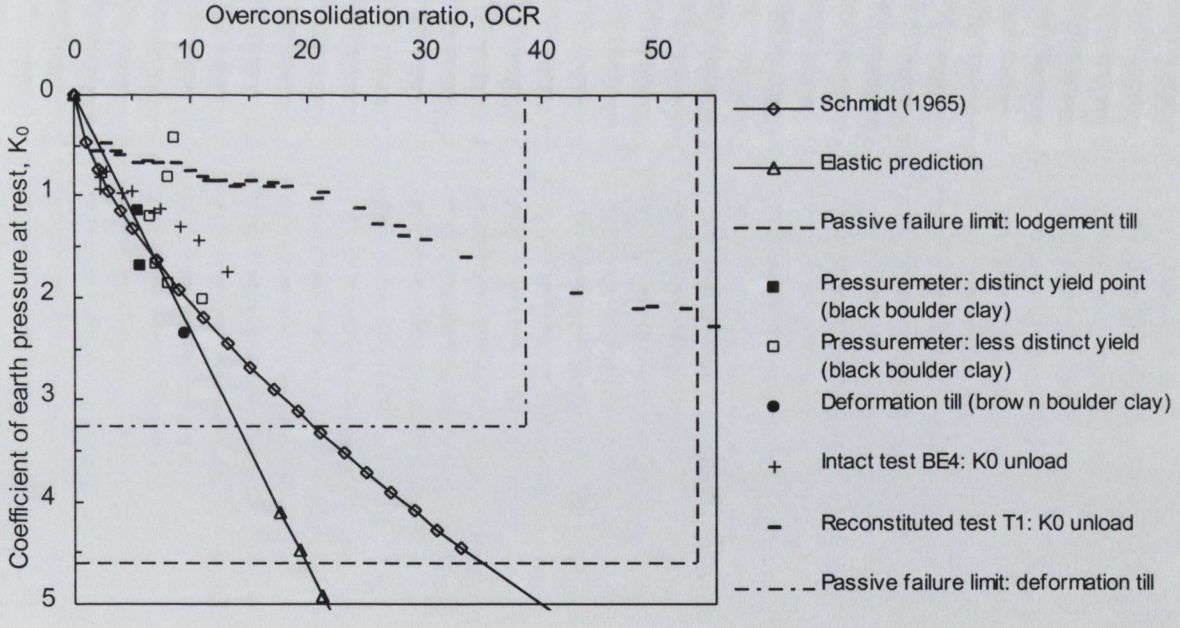

Fig. 5.4.9. Comparison of K_0 measurements in the laboratory and field with predictions

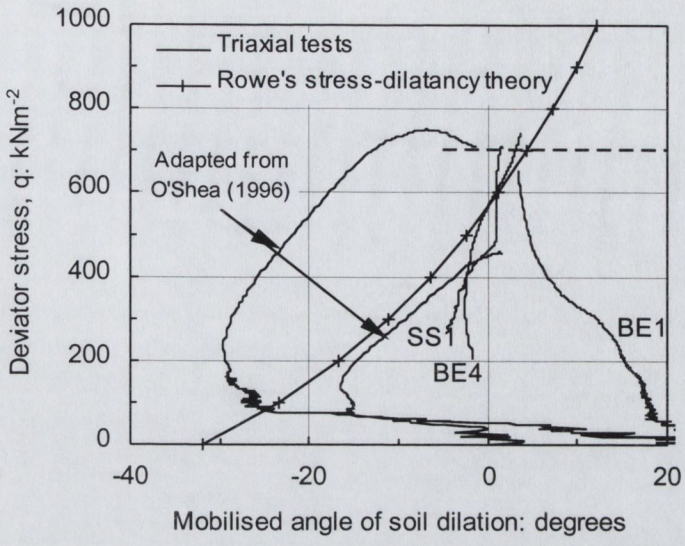

Fig. 5.4.10. Comparison of Rowe's stress-dilatancy theory with measured data

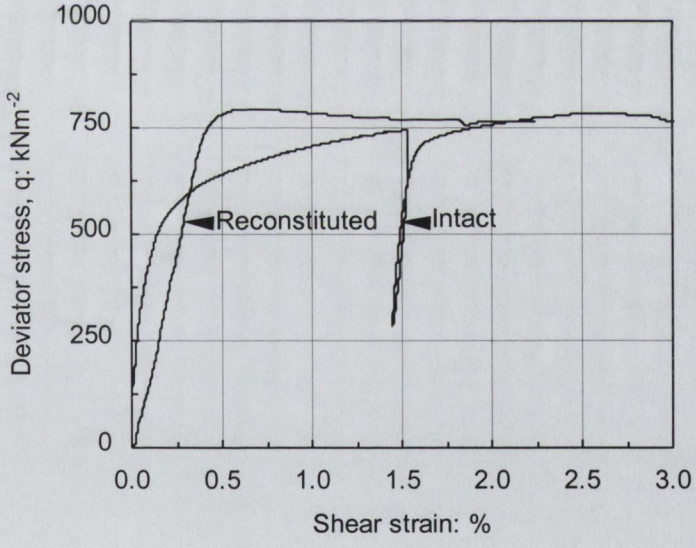

Fig. 5.4.11. Comparison of the stress-strain behaviour of intact (Test BE4) and reconstituted (Test T1) lodgement till

5.5 Soil Suction.

5.5.1 Filter Paper Measurement of Soil Suction.

The mean suction measured, using the filter paper method described in Sections 4.5.2 and A.3, was about 1·9 kNm^{-2} for the unsaturated till (Test S1) and 3·7 kNm^{-2} for the saturated lodgement till (Test S2), which are very low values compared to the in situ effective stresses. However, these low values are considered to be in error, particularly in the case of Test S2 on the lodgement till, as low suction measurements of this kind are normally associated with silts and sands and result in the soil crumbling and falling apart; this was only observed in the deformation till (Test S1). (Silts and sands are not cohesive because the pore water between the soil particles cannot develop high meniscal tension.)

In contrast, Fig. **5.5.1** shows theoretical suction stresses that can develop in particulate materials (Sloan (1994) and Doran et al. (1995)); notice that the stresses increase substantially (to a value in excess of 500 kNm^{-2}) for materials composed of particles below clay size (less than 0·002 mm)[1]. The SEM study (see Section 5.6.3) showed that the till contains abundant rock flour particles considerably less than clay size and, hence, it would be expected that very high suction stresses would develop in Dublin boulder clay, which would also be more consistent with the intact strength of samples of the lodgement till[2].

5.5.2 Soil Suction Paradox.

It was observed that, during the course of this research, samples of the unsaturated deformation till (obtained from 0 – 1 m BTL) crumbled easily, consistent with a soil that is unable to sustain

---

[1] These high suctions are caused by the very small voids between the soil particles, resulting in pore water meniscii of very small radius, r, (see Fig. **2.8.2**) and thus very high suction (see Ridley and Wray (1995) for the theory of soil suction).

[2] It is considered, therefore, that the filter paper method is unsuitable for measuring suction in Dublin boulder clay. The filter paper method may be only be suitable for high plasticity homogeneous clays, which the calibrations are based upon. Furthermore, Bishop et al. (1965) suggested that the swelling pressure of a soil, p_k', corresponded to the suction stress (see Section 2.4.2). However, several isotropic consolidation tests were conducted, in which the lodgement till was found to consolidate at a stress much lower than in situ. Hence, this method also cannot be recommended.

matric suction. However, samples of the lodgement till were, conversely, relatively strong and intact. This presents something of a paradox. A possible source of the strength may be cementation; however, a large reconstituted sample (Test T1, which was consolidated to 150 kNm^{-2}) possessed a considerable intactness. Thus, the origin of the strength of the lodgement till samples, vis-à-vis the deformation till, can not be ascribed to natural cementation.

Instead, the difference between the lodgement till and the deformation till is considered to be due to differences in the soil density. The lodgement till has a very closed structure, as reflected in a very low void ratio of about 0·26, a natural water content close to optimum and a naturally high Skempton B-value. In contrast, the deformation till possesses a more open structure, reflected in a higher void ratio/lower density and a water content of about twice that of the lodgement till (see Sections 3.3 and 3.4). Jacobsen's (1970) suction tests (see Fig. **2.8.3**), described in Section 2.8 of the literature review, indicate low suction in the region of 20 kNm^{-2}. This is possibly because the tests were conducted in the top of the till layer, i.e. the deformation till. As a result, the contribution of suction to the engineering properties of the unsaturated till, i.e. in situ stiffness and strength, is considered to be limited.

5.5.3 Importance of Cohesive Forces (other than Clay Mineral Aggregation).

The boulder clay has been observed by the author and others (Hartford (1987) and Clarke (2002)) to be highly stable at the maximum slope angle of 90°, which is about 50° higher than the effective friction angle of the till[3]. This angle is a reflection of the combination of the very high suction stresses that develop and possibly diagenesis (see Section 5.6.4), which lend the soil an extra rigidity above that due purely to particle friction. Deformation tills above the water table stand at a lower angle of about 45°; this is because this soil does not sustain the capillary attraction stresses, as discussed above. Nevertheless, the 45° angle is high and is, possibly, an indication of cementation.

[3] The natural slopes referred to by the authors included a river embankment and a sea cliff; hence, it is possible that the erosion of the boulder clay continually generates suction pressures in the till, which take a long time to dissipate, thus allowing the slopes to stand at the high angles observed.

Sloan (1994) reported that, in the absence of substantial clay mineral aggregation, rock flour capillary attraction in clay till proved an invaluable source of apparent cohesion in the construction of the cross-passages of the Storebaelt tunnel. This capillary attraction is lost, however, when water is added to the soil. In effect, the addition of water contributes to a quick condition (i.e. a dramatic loss in strength) because there is insufficient clay mineral aggregation to bind the soil together[4]. As vertical cuts are subject to less incident rainfall than slopes at an angle, this may explain the observations that vertical cuts are more stable long-term than cuts at an angle and that very high slope angles are found in nature (see Section 2.10.2.1). The Dublin black boulder clay is also of very low permeability and is generally not fissured; hence, water does not easily percolate through the soil. Cracks induced by machinery and slope modification, however, may allow water to percolate deep into the soil.

[4] The simplest way of demonstrating this is the way in which the boulder clay disassociates in water, reducing to stones in muddy water, with few adhering particles.

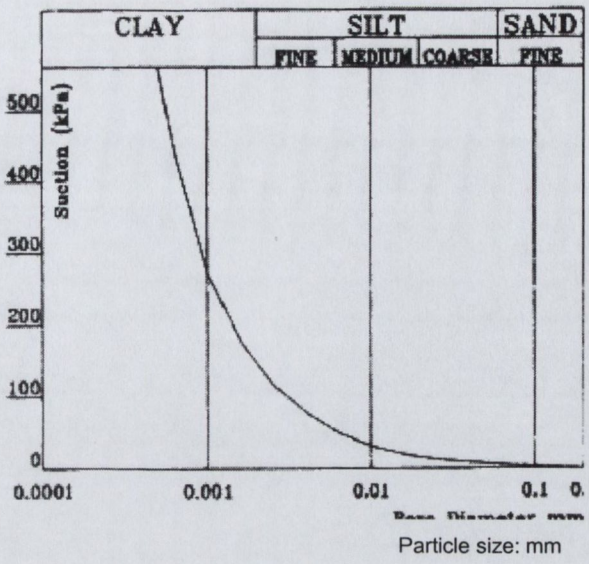

Fig. 5.5.1. Theoretical capillary attraction stresses in soils, after Doran et al. (1995)

5.6 Mineralogical and Microscopic Soil Studies.

5.6.1 Introduction.

The mineralogy of a soil, particularly that of the clay fraction, has a deterministic effect on many of the properties of interest to the soil engineer. Qualitative and quantitative X-ray diffraction tests and scanning electron microscope tests, which are discussed in this section, were conducted for this study. These tests showed that the black boulder clay is different in mineralogy and structure to the upper metre of the brown boulder clay. In contrast, the black boulder clay is similar in these respects to the lower metre of the brown boulder clay, except for some evidence of weathering in the latter. The black lodgement till is characterised by particle disorder, angular rock flakes and few/no clay minerals and, the lower metres of the brown boulder clay, by similar particle disorder and rock flour, but with more clay plates and also calcite recrystallisation. The upper metre of the brown till, however, is characterised by relative particle order, relative homogeneity and expandable clay minerals.

5.6.2 Qualitative X-Ray Diffraction (XRD).

Qualitative XRD tests (called XRD tests) were conducted on the soils shown in the photograph of Fig. **2.2.7**. The photograph shows a two-layer stratigraphy, which is typical of the Dublin Port Tunnel (Whitehall) area at depth. The upper till (Test XRD1) is very stiff grey black lodgement till and the lower till is a very stiff grey brown silty lodgement till (Test XRD2). However, the latter till has fewer gravel particles and, unusually for the Dublin boulder clay, contains fissures. It was of interest, therefore, to determine the origin of the lower till. The diffraction traces are shown in Figs. **A.4.1** (XRD1) and **A.4.2** (XRD2).

The mineral content of the two soils are very similar and are, in turn, very similar to the black and brown boulder clay XRD traces given by Farrell et al. (1995b). Hence, the lower, grey till is not greatly different mineralogically to the overlying black till and it can be concluded that the soils are of the same origin. The main features of the traces are:

(a) Swelling chlorite ($2\theta = 6°$) is present in XRD1 and XRD2. However, it is more significant in XRD2, the lower grey brown unit, which may explain the fissuring observed only in this till in situ (see Fig. **2.2.7**).

(b) There are significant illite peaks, although these may be indistinguishable from (or are masking) mica peaks. Furthermore, kaolinite can be masked by chlorite.

5.6.3 SEM.

5.6.3.1 Introduction.

The micrographs discussed below were calibrated against those presented by Smart and Tovey (1981). In distinguishing between rock flour, silt, recrystallised calcite and clay, in micrographs of boulder clay, the following has been found by the author to be a reasonable guide:

(a) Rock flour: wide range of particle sizes, some very small, angular, flakes or flour.
(b) Silt: range of particle sizes, blocks with mechanical erosion features.
(c) Recrystallised calcite: blocks (when desiccated) but not mechanically eroded, occasionally form arcuate shapes, amorphous material at low magnification.
(d) Clay: angular and wave-like plates, depending on mineral.

5.6.3.2 Mottled Brown Lodgement Till.

A wide range of very small particle sizes can be seen in micrograph **A.4.3**. This is rock flour and represents severe mechanical erosion. As Fig. **A.4.3** is also a very high magnification micrograph (2 μm dot-to-dot), it shows the very small diameters of rock flour, the smallest being orders of magnitude less than clay size (very much less than 2 microns).

The stacked unit clay plates that are visible in Fig. **A.4.4** are illite (see Smart and Tovey, their Figs. 2.7 and 2.8). This is because the plates are planar, relatively thin (compared to kaolinite) and angular with sharp edges. Immediately above the clay plates in the figure are rock flour particles. An amorphous coating of material is evident throughout this micrograph. This material is possibly cementateous and can also be seen in the bottom left of Fig. **A.4.5**. The

layering could be the amorphous iron oxides that result from the oxidation of ferrous-rich clay minerals, although it is considered that this would not be visible. Instead, the general indistinctness of individual particles and amorphous arrangement suggests a layer of cementateous material (see Smart & Tovey, their Fig. 11.21) and not a coating of clay, for example.

The particles outlined in Fig. **A.4.6**, resemble the chlorite crystal blocks of the sample shown in Fig. 11.10 of Smart and Tovey. These are distinct from the rock flour particles visible in the same micrograph and are possible evidence of recrystallised calcite.

Sand grains that are (partially) visible are largely sub-angular, compared to the very angular grains of newly deposited glacial grains (see Figs 14.1 and 14.2 in Smart and Tovey). This is in keeping with previous micrography of individual soil grains, as shown in Fig. **2.2.4**.

The arcuate structure of micrograph Fig. **A.4.6** and the amorphous material in Fig. **A.4.5** are reminiscent of the material shown in the micrograph of Knudsen et al. (1995) (Fig. **A.4.7**[1]), in which calcite crystals/cementation were identified. (Kavvadas (1998) also describes calcite precipitation in hard soils in terms of amorphous material.) Knudsen et al. (cited) found that the amount of cementateous material increases as the pore space decreases but that crystal size decreases as pore space decreases. Furthermore, the authors noted that "coarse" cement causes greater strength than "fine" cement. (The strength increase may be due to the increase in friction available.) As calcite is one of the predominant minerals in Dublin boulder clay (see Section 5.6.4), it is considered that the material identified in the above micrographs is recrystallised calcite. The recrystallisation is possibly due to this till being unsaturated. This calcite, also identified elsewhere[2], would have the effect of binding the soil particles together. However, the cement is brittle and would, therefore, not show up as a c′ component at failure.

---

[1] Note that these micrographs are of similar magnification and can, therefore, be compared. Note also that the base material shown in Fig. **A.4.7** is limestone; hence, the amount of calcite cement is relatively very high.

[2] Recrystallised calcite was also identified in samples of till, taken from exposed natural slopes in Howth, Co. Dublin, in the SEM studies of Kilkenny (1990). However, the extent of the effects of weathering on these samples is unknown.

5.6.3.3 Brown Deformation Till.

A very interesting feature of micrograph Fig. **A.4.8** (the firm brown soil in the upper metre of the till) is the orientation of the particles in one plane, which is indicated on the figure. This orientated fabric is in contrast to the highly non-orientated fabric of the lodgement till and supports the belief that the upper metres represent a zone of soil that has been sheared by the overlying glacier[3].

The micrographs in Test EM2 show homogeneity in all areas of the sample. Figs. **A.4.9**, **A.4.10**, **A.4.11** and **A.4.12** are (almost) concentric micrographs at increasing magnifications and generally show silt particles in a clay mass. Homogeneity of this nature suggests a highly weathered soil, not unlike top soil (see Smart and Tovey, their Fig. 12·2 (a)). This is good evidence of the biological weathering theory of Gleeson (2000). Fig. **A.4.13** shows evidence of numerous clay plates, which are stacked and orientated (in the indicated area). This elementary clay mineral domain is due to the large numbers of clay particles, which allows van der Waal's forces to become significant and form the assemblages shown. Many more clay plates are visible relative to the soil at 1·5 m depth. Note from Fig. **A.4.13** that there is evidence of non-illite clay plates. (The relative non-angularity compared to the illite of Fig. **A.4.4** and curled/wave-like plate edges suggests montmorillonite (see Fig. 2.5 in Smart and Tovey).) This is further evidence of biological weathering of this soil, as these minerals, which were also identified in quantitative XRD analyses given in the next section, were not found in the deeper till.

It can be concluded that the soil of Test EM2 has a medium to high plasticity as a result of relatively large amounts of 'true' clay minerals. Furthermore, the soil was more vividly brown than the mottled brown soil at 1·5 m, reflecting the difference in the amount of iron-rich clay minerals present. The crushing and breakdown of the soil relative to the boulder clay beneath was reflected in the PSD, which consisted of fewer coarse gravel and larger particles relative to the lodgement till.

[3] See geology chapter, Section 3.3.

5.6.3.4 Black Boulder Clay.

Many elongated, angular particles are in evidence in Test EM3 (e.g. Fig. **A.4.14**), which were not present in the upper/sheared/weathered zone. Hence, the black boulder clay has not been noticeably weathered. There are less, near spherical, rock flour-type particles than in the upper metres, the clay/fine silt fraction having a majority fraction of angular rock flakes (e.g. Fig. **A.4.15**). This angularity gives rise to a large degree of interlocking when sheared and hence a very high strength. On close inspection, (Fig. **A.4.14** and very close in Fig. **A.4.16**[4]) the particles are not clay minerals. In contrast to the deformation till (Fig. **A.4.8**), there is evidently a high degree of particle disorder and, unlike the unsaturated till (EM1), calcite cement was not evident in these micrographs. This latter finding is consistent with the black till being saturated, thereby preventing recrystallisation of the calcite present in the till.

The Au coated test (EM4) did not provide any improved resolution over the undisturbed tests at very high magnification. (It is considered that the rough surface of the air-dried sample hindered the plating stage.) The Au test instead gave very similar micrographs to the undisturbed test (e.g. Fig. **A.4.17**).

5.6.4 Quantitative XRD.

The primary minerals that have been identified in qualitative X-ray diffraction analyses on Dublin boulder clay (see Figs. **2.2.2**, **A.4.1** and **A.4.2** and Hartford (1987)) are grouped as follows:

Phyllosilicates;

Chlorite, illite, kaolinite, smectite (montmorillonite), mica (non-clay phyllosilicate).

Non-phyllosilicate minerals;

Calcite, the quartz (silica) group, the feldspar group.

The quantitaive X-ray diffraction (QXRD) analyses conducted for this thesis also show plagioclase (similar to K-spar), dolomite (very similar to calcite), geothite and pyrite. It is

[4] This micrograph is of very low resolution but shows that the flakes the are not clay plates.

interesting to note, however, that K-spar and dolomite are only found in the black boulder clay (QXRD1 and QXRD3) and not in the deformation till (QXRD2). The converse is true of geothite.

The primary rocks that have contributed to Dublin boulder clay, i.e. the Palaeozoic shales, mudrocks and, particularly, Carboniferous limestones all contain clay minerals, particularly illite. However, it is evident from Table **A.4.2(a)** that igneous rocks have also contributed significantly to the Dublin boulder clay. This is shown by the presence of abundant quartz and also K-spar, both of which are derived from igneous rock; metamorphic rock also contributes in the form of chlorite (Table **A.4.2(b)**). The QXRD, sub-2 micron, mineralogical tests (Table **A.4.2(b)**), however, show that illite is the predominant clay mineral in Dublin black boulder clay. Illite sheets were also observed in the scanning electron microscope in Test EM1.

Generally, illite (sometimes referred to as white mica) and mica are indistinguishable. Although similar in structure to the smectite (montmorillonite) group, the illite group has a low cation exchange capacity (CEC); hence, the electrical or 'chemical-electrical' bonds referred to by Jacobsen (1970) and Kavvadas (1998), amongst others, are probably not a significant source of soil structural strength to the Dublin boulder clay. Furthermore, the illite group minerals are not expandable; hence, swelling and heave of the soil should be limited. The group has a ferrous component which, along with chlorite (also ferric), reacts with water and air to produce iron oxides. Hence, the boulder clay will rust above the water table.

The predominant minerals in the Dublin boulder clay are calcite[5] and quartz, both of which are non-phyllosilicates. As a result, even for a very high illite component (the majority clay mineral in the lodgement till), the plasticity index remains low, particularly when combined with quartz, as shown by Moon (1978) (see Fig. **A.4.18**). It may be concluded, therefore, that clay mineral aggregation is not a major contributing factor to the cohesion of the black boulder clay, which

[5] It is noted, in relation to Table **A.4.2(a)**, Test QXRD3, that the absolute value for calcite is considerably lower than for QXRD1, also black boulder clay. Since these QXRD tests were conducted, however, Hillier (2003) has obtained X-ray fluorescence data on the same samples and concluded that the calcite variation is possibly due to local variability in the Carboniferous Limestone. This view is supported by the discussions of the author with Dr. David Doff (2001) on the subject of the variability of mineral content of boulder clay depending on local variations in the bedrock over which the glacier is passing.

is reflected in the till's low plasticity index. (When air-dried samples are mixed in (distilled) water, there are very few adhering particles, indicative of low clay mineral aggregation.)

The Dublin till evidently is composed of a wide range of minerals (see Table **A.4.2(a)**), the individual effects of which on the soil behaviour is largely unknown[6]. The results of tests on reconstituted till (see Section 5.3.3), when compared to lodgement till, suggest, however, that the diagensesis of the saturated lodgement till since the Ice Age has sufficiently advanced that there is a cementation component to the soil. Furthermore, recrystallised calcite, a cementateous material, is evident from the electron microscope examinations of the unsaturated till. A result of this diagenesis is that the yield point of the lodgement till is not as distinct as it is for high plasticity clays and for rocks, both of which possess 'true' inter-particle bonding. Hence, estimating the yield stress of the tills is difficult, as was demonstrated in Section 5.3.1.1.

The near-surface deformation till is somewhat different to the lodgement till in that the majority of the clay minerals are highly active expandables, mainly smectite (montmorillonite) (see Table **A.4.2(b)**). (Smectite stacks were also identified in scanning electron micrographs of the deformation till.) Significantly, the 'true clay minerals' form a high percentage of the total clay fraction. Hence, the deformation till would be expected to swell[7], be of higher plasticity than the black boulder clay (see Fig. **2.2.3** and Table **4.1.1**) and have a cohesion, c′, through clay mineral aggregation.

---

[6] For example, white precipitates have been identified in boulder clay in the Dublin Port area (Milligan, 2003). These could be indicative of white minerals, e.g. K-spar, calcite or dolomite.

[7] Evidence for this can be interpreted from the excavation of Treacy (1995). The 14-day settlements, plotted on Fig. **2.10.6(a)**, were taken after saturation of the ground surface with a water bowzer and show clear evidence of heave of the ground as a result of this.

5.7 In Situ Soil Testing: Pressuremeter and Seismic Tests.

5.7.1 Pressuremeter.

5.7.1.1 In Situ Stresses (K_0).

The pressuremeter estimates of K_0 compare well with the laboratory and theoretical predictions shown in Fig. **5.4.9**. As can be seen from that figure, the 3 No. tests that had a distinct take-off point all lie close to the elastic prediction, whereas the tests with less distinct yield points show more scatter. The very good pressuremeter test conducted in the brown till, indicated on Fig. **A.5.1**, was used to back-analyse the apparent yield stress of the deformation till, based on Equation [2.4.5], with an interpreted K_0 value of 3 for this soil. In this way, the apparent yield stress of the deformation till was found to be about 400 kNm^{-2}. This compares reasonably well with the theoretical value of 500 kNm^{-2} suggested by Boulton and Paul (1976)[1].

5.7.1.2 Stiffness.

The shear stiffness determined in the pressuremeter is important because it can be compared with the shear stiffness measured in the laboratory to determine stiffness anisotropy. This is because the pressuremeter measures the horizontal shear modulus. Figs. **A.5.3(a)** and **A.5.3(b)** show[2] that, at sufficient pressure (in the region of 1500 kNm^{-2}), the shear stiffness versus cavity strain curves become independent of the mean stress and strain levels over which the loops were conducted. The initial stiffness of these latter curves (Fig. **A.5.3(b)**), compare favourably with the very small strain shear modulus measured in the static and dynamic tests[3]. It follows that the horizontal soil stiffness is about equal to the vertical stiffness. This result is consistent with the mode of deposition of the lodgement till, which produces a highly mixed till sheet[4].

---

[1] See Section 3.3.

[2] These stiffness-strain curves are not the same as the stiffness-strain curves associated with the S-shape curve. This is because the soil stiffness does not degrade as rapidly with strain as it does on primary loading, owing to the effects of strain hardening, which was demonstrated in Section 5.4.1.

[3] See Fig. **5.4.6**.

[4] See Section 2.2.4.

Owing to this stiffness isotropy, a single modulus will approximately represent the stiffness under both vertical and horizontal loading conditions.

5.7.1.3 Strength.

The test in the top 2 m of the till yielded an undrained shear strength value of about 200 kNm^{-2}. This was a very good test and hence this strength is considered to be a good approximation of the strength of the deformation till[5].

5.7.2 Seismic.

The results of the seismic tests, shown in Fig. **A.5.5**, compare favourably with laboratory measured very small strain stiffness. It is reasonable to conclude, therefore, that the soil samples are representative of the field (e.g. absence of fissuring). Furthermore, the results show that the black, and mottled brown tills, approximately lie on a straight line on the double logarithmic, stiffness against confining stress, plot and, therefore, have the same reference stiffness, E_0^{ref}. In contrast, the top metre of till is about five times less stiff. The black and mottled brown tills are therefore lodgement tills and the upper till is the deformation till. With this value for the in situ stiffness of the deformation till, other important stiffness parameters were derived based on the relationships derived for the lodgement till, as follows:

$$E_0^{ref} \approx 20E_{50}^{ref} \qquad [5.7.1]$$

$$E_{ur}^{ref} \approx 4E_{50}^{ref} \qquad [5.7.2]$$

These correlations give $E_{50}^{ref} \approx 10$ MNm^{-2} and $E_{ur}^{ref} \approx 40$ MNm^{-2} for the deformation till.

[5] Note that no laboratory strength tests are available on the deformation till, hence the importance attached to this result.

CHAPTER 6

NUMERICAL MODELLING

CHAPTER 6

NUMERICAL METHODS

6.1 Introduction.

The finite element (FE) approach involves applying an external load, which causes an internal load at nodes in a FE mesh, which, in turn, causes nodal displacements, u. The system can be represented by the following equation:

$$K.\Delta u = \Delta f_{ext} - \Delta f_{int} \qquad [6.1.1]$$

where Δ represents infinitesimal increments (called rates), K is the global stiffness matrix, which is taken as the elastic (Hooke's) matrix, $\overset{4}{D}$, f_{ext} is the global load vector, which is the applied load, and f_{int} is the global reaction vector, which is the internal load. σ^1, the stress at the end of an increment, is calculated from the stress at the start of an increment, σ^0, by:

$$\sigma^1 = \sigma^0 + \Delta\sigma,\ \Delta\sigma = \overset{4}{D}.\Delta\varepsilon_e = \overset{4}{D}(\Delta\varepsilon - \Delta\varepsilon_p) = \overset{4}{D}(\Delta\varepsilon - \Delta\Lambda.\partial g/\partial\sigma) \qquad [6.1.2]$$

where ε is total strain, ε_e is elastic strain, ε_p is plastic strain, Λ is a plastic multiplier that is equal to zero for elasticity and is greater than zero for plasticity and g is a plastic potential function. If g is equal to the yield function, f, this is called associated plasticity, where f determines the (elastic or plastic) state of an element. (The derivative of f or g with respect to stress is a vector perpendicular to f or g.) If g is an independent function it is called non-associated plasticity.

The above equations clearly allow for constitutive equations that have been derived to represent observed soil behaviour. A set of these equations within the FE method is a soil model. Recent advances, which have improved the understanding of soil behaviour, have assisted in the development of a number of such models, which have been generally based on complex soil behaviour. The most efficient place to observe this behaviour is in the laboratory; hence, the parameters that control the models are generally measured in laboratory tests.

This chapter presents an assessment of the ability of the FE method to predict the response of the very stiff lodgement till under different loading conditions. This lodgement till has presented particular difficulties in the past due, for example, to its marked non-linearity and stress dependency (Lehane and Simpson, 2000). However, the Dublin till, unlike tills elsewhere (e.g. the tills of Northern England (Hughes et al., 1998)), has been found, in this study, to possess certain features which make computer modelling of the soil feasible, including a single till sheet, infrequent boulders and lack of fissuring. Furthermore, the isotropy of the soil, owing to its mode of deposition, in terms of strength, stiffness and permeability, simplifies the problem and thus allows greater freedom in FE modelling of complex soil behaviour.

Typical laboratory tests, including the oedometer and triaxial tests, were used to validate the essential aspects of two soil models, namely Hardening Soil (Schanz (1998) and Schanz et al. (1999)) and the elastic-perfectly plastic soil model, against actual soil behaviour. The FE predictions are then compared with field measurements of pile settlement and pile load distribution, ground movement measurements taken behind a vertical cut and also with the settlement of a footing. The results of this FE modelling are compared with the simple design methods described in the literature review (Section 2.10) in the concluding chapter of this thesis to determine if any real advantage accrues from the considerable extra effort involved.

6.2 Hardening Soil.

6.2.1 Hardening Soil Formulation.

The Hardening Soil model (HS), as described by Schanz et al. (cited) and Schanz (cited), includes many aspects of the behaviour of the stiff lodgement till observed in the laboratory tests described in the previous chapters. This soil model is included in the Plaxis (1998) FE code for rock and soil analyses. The HS model incorporates the non-linear stress-strain behaviour of soils and the stress dependency of the stiffness on the stress-state. It also distinguishes between two types of hardening, namely shear hardening and compression hardening, and incorporates soil dilatancy and a yield cap. The Mohr–Coulomb criterion is used to define the failure condition. The Plaxis (cited) program includes a load-step algorithm (van Langan and Vermeer, 1990), which was applied in all of the

predictions[1] detailed below. The reader is referred to the discussion chapter (Chapter 5) in relation to statements made in this chapter[2].

In the HS model, the post-yield (plastic) part of the shearing phase is modelled using the hyperbolic model of Duncan and Chang (1970), which in turn was a development of the non-linear (hyperbolic) stress-strain model of Konder (1963) (see Section 2.9.1).

Thus, on initial (primary) drained triaxial shearing, the axial strain is given by:

$$\varepsilon_a = (1/2E_{50})(q/(1-q/q_a) - q/E_{ur}, \text{ for } q < q_f \qquad [6.2.1]$$

where q is the deviator stress and q_a is the asymptotic value of the shear strength and $q_f = R_f q_a$

E_{50} is the secant effective Young's modulus at 50% strength in the triaxial, isotropically consolidated drained triaxial passive compression (CID) test. R_f is a ratio that ensures failure at finite levels of strain, which is back-analysed from CID measurements of q_f and failure strain and Equation [6.2.1]. E_{50} and R_f are determined directly from tests that give hyperbolic stress-strain curves. Essentially hyperbolic curves are obtained from standard CID tests; i.e. tests isotropically consolidated direct to an effective confining stress and sheared. It is noted that the geometry of the hyperbolic curve implies that the initial modulus is twice E_{50}. Thus the hyperbolic model by itself would not be expected to represent the stiffness at very small strain level, as the initial modulus is significantly higher than $2E_{50}$.

The model is elasto-plastic in that it distinguishes between shear loading and unloading/reloading, in which the soil behaves essentially elastically and some strain is recovered. The unload-reload modulus, E_{ur}^{ref}, has been found to be a constant under a range of testing conditions, including the

---

[1] Without an automatic step-size scheme, the load steps would have to be applied manually. However, the appropriate step-sizes are unpredictable (van Langan and Vermeer, cited). The iterative step-size scheme used in Plaxis is based entirely on information obtained from the current (load) step (i.e. it does not use information from previous steps), which allows analysis of non-associated plasticity problems without a high degree of non-normality creeping in.

[2] For example, for "The elasto-plastic behaviour of Dublin boulder clay has been shown," the reader is referred to Section 5.4.1.

oedometer test and the triaxial test[3]. The elasto-plastic behaviour of Dublin boulder clay has been shown.

In the HS model, the stress dependency of the stiffness is given by:

$$E_{50} = E_{50}^{ref}((c'.\cot\phi' + \sigma_3')/(c'.\cot\phi' + p_{ref}))^m \qquad [6.2.2]$$

where m is the power index that controls the amount of stress dependency of stiffness. As a c′ value of about zero was measured in the tests on the black boulder clay, this stress dependency equation reduces further. The stress dependency of the unload/reload modulus, E_{ur} and the tangent oedometer modulus, E_{oed}, are also given by Equation [6.2.2]. Below the yield stress, the soil is assumed to behave elastically with the stiffness given by E_{ur}[4].

The HS model includes soil dilatancy, dilatancy cut-off and plastic yield surfaces. The Mohr-Coulomb failure criterion is adopted for soil yielding perfectly-plastically. A tension cut-off option is included but, because c′ was taken as zero[5] in the analyses of the black boulder clay, it was not necessary to include this failure condition for the black boulder clay. (For the deformation till, which had a c′ component, the no-tension cut-off was used.)

Plastic strains can originate both from shear hardening and one-dimensional compression surfaces. The shear hardening yield surface has a non-associated flow rule (allowing dilatancy due to shearing to be incorporated) and the compression hardening yield surface (called a cap) has an associated flow rule. E_{50} is related to the plastic strain originating from the shear yield surface but E_{oed} is needed to describe the plastic strains originating from the compression yield surface, which is an elliptical cap to the shear yield surface that expands up to the Mohr- Coulomb cone (in principal stress space). The total yield contour of the HS model in principal stress space (for c′ = 0 kNm^{-2}) is shown in Fig. **6.2.1**.

---

[3] Note that E_{ur}^{ref} is determined in the triaxial test from the q-ε_a curve and in the oedometer from the σ_1'-ε_a curve.

[4] The value of E_{ur} that is determined from the part of the oedometer stress-strain curve below σ_{vy}' is approximately equal to that obtained from the triaxial tests.

[5] In fact, for numerical modelling reasons, a small c′ of 1 kNm^{-2} is required (van Langan and Vermeer, 1990).

For triaxial conditions, the following yield function, f, describes the shear hardening locus corresponding to plastic yielding:

$$f = f^* - \gamma_p \qquad [6.2.3]$$

where:

$$f^* = (2/E_{50})q/(1-q/q_a) - 2q/E_{ur} \qquad [6.2.4]$$

and γ_p is the shear hardening parameter.

The plastic volumetric strain increments, $\delta\varepsilon_{vp}$, and plastic shear strain increment, $\delta\varepsilon_{sp}$, are defined by the Mohr's circle of strain:

$$\delta\varepsilon_{vp} = \delta\varepsilon_{sp}.\sin\psi_m \qquad [6.2.5]$$

where $\delta\varepsilon_{sp}$ is the plastic shear strain increment and ψ_m is the mobilised angle of dilation. Rowe's (1962) stress-dilatancy theory is incorporated as the ϕ'-ψ flow rule to give ψ_m. Rowe's rule defines ψ_m as[6]:

$$\sin\psi_m = (\sin\phi_m' - \sin\phi_{cv}')/(1 - \sin\phi_m'.\sin\phi_{cv}') \qquad [6.2.6]$$

where:

$$\sin\phi_m' = (\sigma_1' - \sigma_3')(\sigma_1' + \sigma_3' - 2c'\cot\phi_p') \qquad [6.2.7]$$

and $\delta\varepsilon_{sp}$ is given by Equation [6.2.3][7].

Rowe's stress-dilatancy theory has been found, by experiment, to give a reasonable approximation of the dilatancy characteristics of Dublin boulder clay. Dilatancy cut-off is

---

[6] Schanz and Vermeer (1996) explain this formulation.
[7] $\delta\varepsilon_{sp}$ corresponds to γ_p.

reached when the soil, with an initial void ratio of e_0, reaches constant volume, at the critical void ratio, e_{cv}. At this point, volumetric strain ceases.

6.2.2 Soil Model Parameters.

The model requires input of stiffness related parameters (E_{50}, E_{oed}, E_{ur}, m, and p_{ref}), strength and dilatancy parameters (ϕ_p', ϕ_{cv}', ψ, c', and R_f), stress history and in situ stress-state parameters (γ, σ_{vy}', K_0, and K_0^{nc}) and some auxiliary parameters (k_x, k_y, e_0, $e_{max.}$, and ν'). The values of these parameters, derived from the laboratory and field tests discussed in the preceding chapters, are given in Tables **6.2.1** and **6.2.2**, for the lodgement and deformation tills, respectively. Tables **6.2.3(a)** to **6.2.3(d)** give a summary of how the parameters were obtained.

Table 6.2.1. Lodgement till soil model parameters for use in the HS model

Stiffness		Strength/dilation		Stress-state		Auxiliary	
E_{50}^{ref} (MPa)	50	ϕ_p' (deg.)	40	σ_{vy}' (kNm^{-2})	1500	k (ms^{-1})	10^{-11}
E_{oed}^{ref} (MPa)	33	ϕ_{cv}' (deg.)	32	K_0	Varies	e_o	0·26
E_{ur}^{ref} (MPa)	200	ψ (deg.)	10	K_0^{nc}	0·47	e_{max}	0·31
m	0·5	c' (kNm^{-2})	1	γ (kNm^{-3})	22·5	ν'	0·2
p_{ref} (kNm^{-2})	100	R_f	0·8				

Table 6.2.2. Deformation till soil model parameters for use in the HS model

Stiffness		Strength/dilation		Stress-state		Auxiliary	
E_{50}^{ref} (MPa)	10	ϕ_p' (deg.)	32	σ_{vy}' (kNm^{-2})	500	k (ms^{-1})	10^{-10}
E_{oed}^{ref} (MPa)	10	ϕ_{cv}' (deg.)	32	K_0	Varies	e_o	0·31
E_{ur}^{ref} (MPa)	40	ψ (deg.)	0	K_0^{nc}	0·47	e_{max}	0·31
m	0·5	c' (kNm^{-2})	5	γ (kNm^{-3})	21·5	ν'	0·2
p_{ref} (kNm^{-2})	100	R_f	0·9				

Table 6.2.3(a). Summary of how stiffness related parameters were obtained[8]

Parameter	
E_{50}^{ref}	Hyperbolic q-ε_a curve at 50% strength in 5 No. CD tests
E_{oed}^{ref}	σ_1'-ε_a curve in special oedometer tests
E_{ur}^{ref}	Unload-reload curves in oedometer (σ_1'-ε_a) and triaxial (q-ε_a) tests
m	The slope of the lines through the data in Fig. **5.4.6**
p_{ref}	Arbitrarily taken as atmospheric pressure

Table 6.2.3(b). Summary of how strength and dilation parameters were obtained

Parameter	
ϕ_p'	CIU tests at peak stress ratio, CD tests and large shear box test at failure
ϕ_{cv}'	CIU tests shearing at constant volume
ψ	Direct from CD tests and from Rowe's (1962) flow-rule
c′	CIU tests at peak stress ratio and CD and large shear box tests at failure[9]
R_f	Back-analysed from q-ε_a curve in 5 No. CD tests

Table 6.2.3(c). Summary of how stress-history and in situ stress-state parameters were obtained

Parameter	
σ_{vy}'	Measured in special oedometer tests
K_0	Measured in in situ pressuremeter tests and in laboratory K_0 tests. Compared favourably with the K_0 implied by elasticity and Schmidt's (1966) power law
K_0^{nc}	Measured in laboratory K_0 test on reconstituted soil. Compared favourably with Jaky's (1944) equation: $K_0^{nc} = 1 - \sin\phi_{cv}'$
γ	Measured in routine laboratory tests

[8] The in situ stiffness of the brown boulder clay was found from seismic tests, which have been found to compare favourably with laboratory stiffness when account is taken of the ground pressures. The remaining stiffness parameters were found from high pressure dilatometer tests and relationships derived for the black boulder clay (see Section 5.7.1.2).

[9] The c′ component was used for the soil above the water table to take account of the increased shear strength due to suction.

Table 6.2.3(d). Summary of how auxiliary parameters were obtained

Parameter	
k	Measured from c_v and m_v values in special oedometer tests and Equation [2.5.5]
E_o	Taken from the measurements made by Farrell et al. (1995b)
E_{cv}	The void ratio of the upper till was assumed equal to the constant volume void ratio of the till
ν'	Interpreted from laboratory and field dynamic tests and from Farrell et al. (1988)

6.2.3 Modelling In Situ Soil Stresses.

The stress history of the soil, as reflected by the initial at rest stresses, has a major influence on the response of the numerical model to loading or unloading conditions; i.e. the soil stiffness and the soil response are partly governed by these initial stresses. The initial stresses in the soil were modelled within the Plaxis (cited) code by applying a previous overburden pressure, which, for the lodgement till, would be the yield stress determined in the oedometer test, namely 1500 kNm^{-2}.

In the program, the yield stress is applied followed by unloading and the horizontal and vertical effective stresses are determined from elasticity. It has been found that the K_o-OCR relationship generated with the measured yield stress is in reasonable agreement with measurements of K_o. K_o has an upper limit, the passive (Rankine) limit, K_p, defined by the Mohr-Coulomb condition (see Fig. **5.4.9** and Equation [2.4.10]).

6.2.4 Validation of the HS Model.

The essential features of the HS model are illustrated in Fig. **6.2.2**[10]. The stress-paths shown are for triaxial and oedometer tests. This figure shows the hardening yield surface, the cap yield surface and the Mohr-Coulomb failure surface[11]. The HS model predicted the stress-paths and the yield surfaces shown were generated by the author, using the constitutive equations given above.

[10] The points and stress-paths on the figure refer to the analysis in this section.

[11] There is a fourth surface that takes account of the resistance of the soil to tensile stresses. With $c' = 0$ kNm^{-2}, this surface is not applicable. However, as the deformation till has $c' > 0$ kNm^{-2}, the surface is applicable; it was assumed that the soil could not sustain tensile stresses.

6.2.4.1 Drained Tests.

A triaxial test was modelled in axisymmetry using 15-noded triangular finite elements. Loads, boundary conditions and mesh are shown in Fig. **6.2.3**.

Fig. **6.2.4** shows the prediction of a CK_0RD triaxial test (see Section A.2.2), where the soil's stress-history was K_0 reconstructed to a vertical effective stress close to, but not exceeding, σ_{vy}' (thereby reconstructing the in situ stress-state). The soil was then sheared very slowly (drained) at the effective confining stress of 250 kNm^{-2}. The consolidation and swelling stage left a deviator stress in the sample prior to shearing, which was included in the prediction by an anisotropic consolidation stage prior to shearing.

Figs. **6.2.4** and **6.2.2** show that the response is elastic until the yield surface is reached (at A) whereupon it hardens until failure occurs at the Mohr-Coulomb failure surface (at B), defined by the value of ϕ_p' measured in the test. This is the three-stage behaviour that was measured in the soil tests described in Section 5.4.1; i.e. elastic, non-elastic and perfectly plastic. Hence, it is shown that the HS model models the fundamental behaviour of the boulder clay. However, the HS model does not include the very small strain yield surface referred to in Section 5.4.1. Thus it would be expected that the HS model would not model the behaviour of cases where the very small strain stiffness is relevant.

An important point concerning the prediction shown in Fig. **6.2.4**, is that the HS model, like the Cam-clay yield surface, predicts elastic behaviour for stresses below the yield surface. Hence, for a soil with a very high yield stress, the extent of the elastic region is very large and, therefore, elasticity predominates in most analyses. However, this is what is observed in tests on the till.

The HS yield surface is a 'hard' yield surface, in that there is a very sudden transition from elastic to non-elastic behaviour. This very brittle behaviour has been found to be typical of reconstituted Dublin boulder clay in triaxial and oedometer tests. In contrast, the intact soil has been found to have a structural strength that contributes to resisting yield and, thus, the till is less brittle than the reconstituted soil and less brittle than that predicted by a 'hard' yield surface. Nevertheless, the HS model predicts the intact behaviour in the triaxial test, as shown in Fig. **6.2.4**, because the post-

yield strains are predicted with a hyperbolic stress-strain curve, which appears to give a reasonable representation of the more gradual yield of the intact soil. However, the predicted failure strain level remains somewhat less than that measured.

An oedometer test (Test E) that included unload-reload, with stress history reconstruction (K_0R test), was modelled. The oedometer test was modelled in axisymmetry using 15-noded triangular finite elements. Loads, boundary conditions and mesh are shown in Fig. **6.2.5**. The test curve, plotted as an e - logσ_v' curve on Fig. **5.3.2**, is compared to the HS prediction as vertical effective stress against volumetric strain in Fig. **6.2.6** and as a stress-path plot in Fig. **6.2.2**. These graphs show that the soil is essentially elastic, until the cap yield surface (at C) is reached, at which stage the soil deforms plastically.

6.2.4.2 Undrained Tests.

It was necessary to validate the undrained model behaviour because, owing to the low permeability of Dublin boulder clay, most construction is initially undrained. Although the input parameters are effective parameters, it is possible to take account of the undrained response, as follows. The program incorporates a modified stiffness of the soil skeleton to take account of pore water and the development of pore water pressure by incorporating the following set of equations:

$$\Delta p' = K'\Delta\varepsilon_v \qquad [6.2.8]$$

and

$$\Delta p_w = K_w.\Delta\varepsilon_v/n \qquad [6.2.9]$$

where $\Delta p'$ is an increment of mean effective stress, n is the soil porosity, K_w is the bulk modulus of the pore fluid and $\Delta\varepsilon_v$ is an increment of volumetric strain. The bulk modulus of the soil skeleton is found from elasticity:

$$K' = E/3(1 - 2\nu) \qquad [6.2.10]$$

The undrained Poisson's ratio, ν_u, is taken as 0·495 (and not 0·5), for numerical reasons.

The values of the pore pressure parameters, A and B, are considered to be fundamental undrained parameters. Schweiger (2002a) showed that the values of the parameters predicted with the HS model in Plaxis are consistent with Skempton's parameters, e.g. A = 1/3 and B = 1 in the elastic, fully saturated case and negative values at failure in the case of dense (dilatant) soils.

A CIU test, consolidated to 250 kNm^{-2} and sheared undrained, was modelled. The mesh etc were as for the drained triaxial test. The peak effective friction angle and ψ determined from the CIU test was inputted and all other parameters were as in Table **6.2.1**. The prediction is compared with the measurements in Fig. **6.2.7(a)**, as deviator stress against mean effective stress. In Fig. **6.2.7(b)**, the prediction is compared with measurements of excess pore water pressure against axial strain[12]. The results show that the model predicts the excess pore water pressures of this test very well.

Although the laboratory tests are reasonably well predicted, they represent a limited number of stress paths and this must be considered when assessing the parameters in specific design situations. This is discussed in detail in the following section.

[12] The results are not shown in deviator stress-axial strain axes because the undrained tests generally do not have a failure point, even at very large strain, owing to the continuing dilatancy and associated decrease in excess pore water pressure. For this reason, the model prediction was terminated at the rupture deviator stress measured in the test.

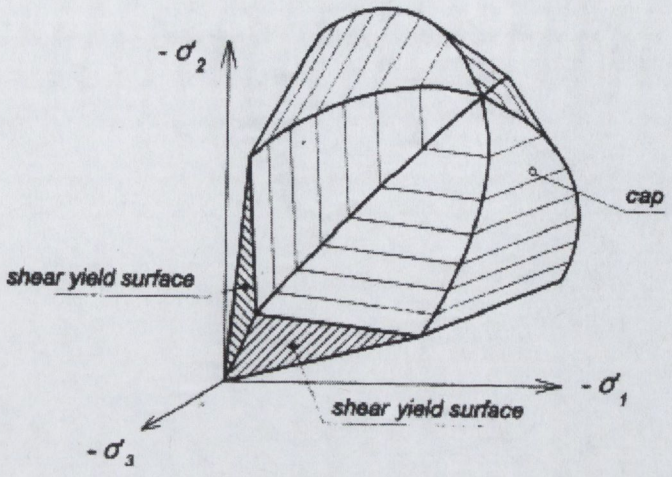

Fig. 6.2.1. Total yield contour of HS model

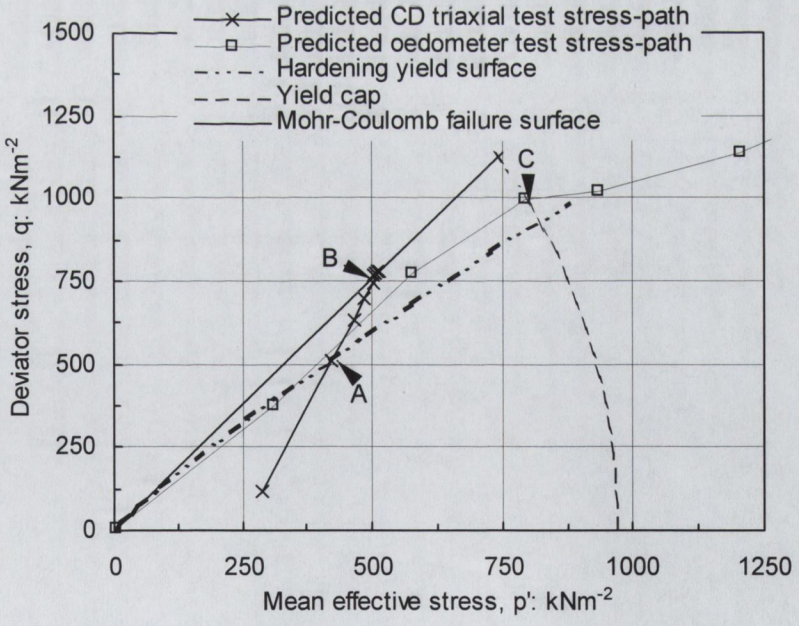

Fig. 6.2.2. Essential features of the HS model in q-p′ space

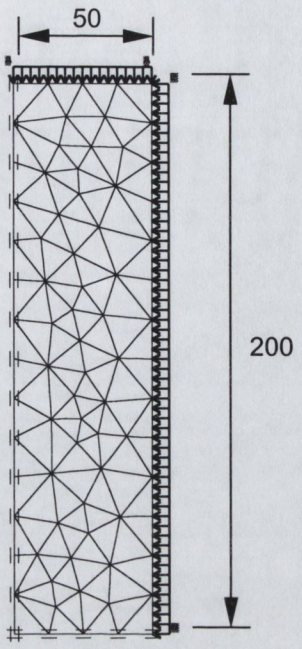

Fig. 6.2.3. FE mesh, loads and boundary conditions for triaxial test prediction

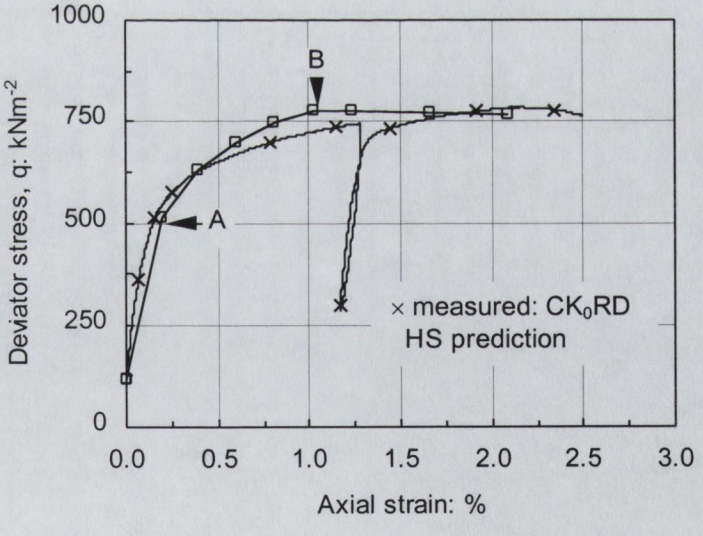

Fig. 6.2.4. Comparison of predicted (HS) and measured (Test BE4) triaxial tests

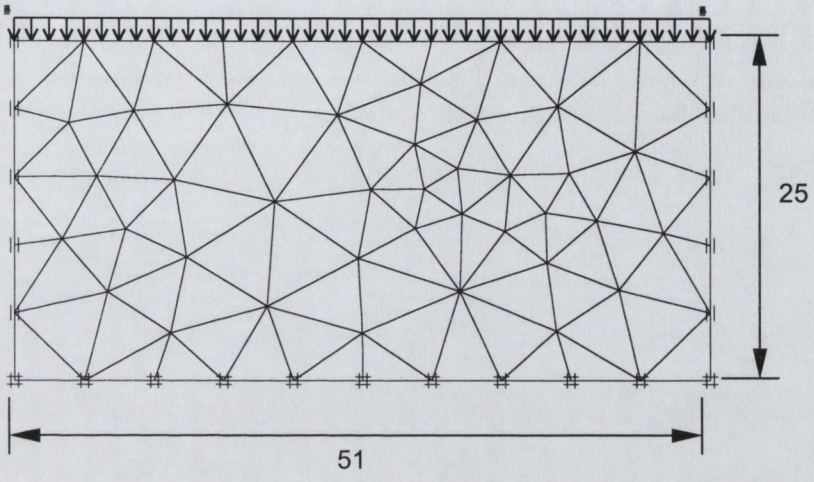

Fig. 6.2.5. FE mesh, loads and boundary conditions for oedometer test prediction

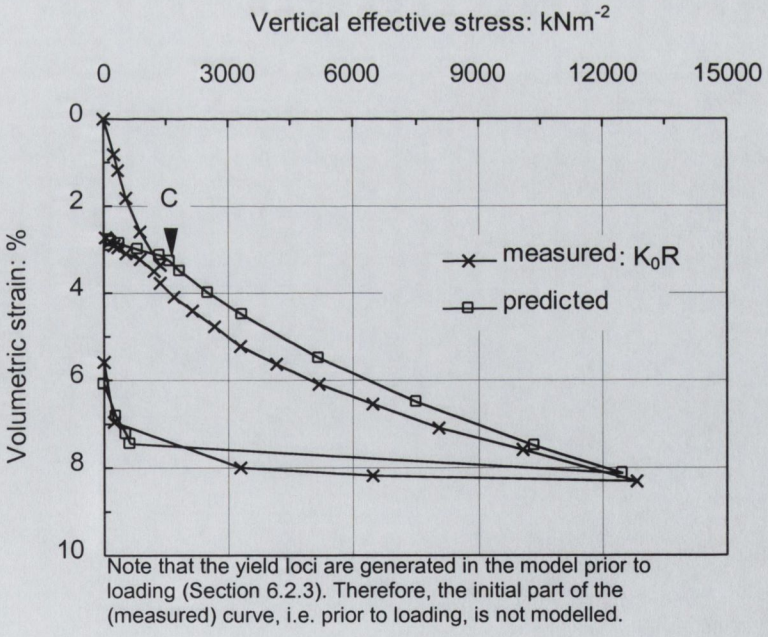

Fig. 6.2.6. Comparison of predicted and measured (Test E) oedometer tests

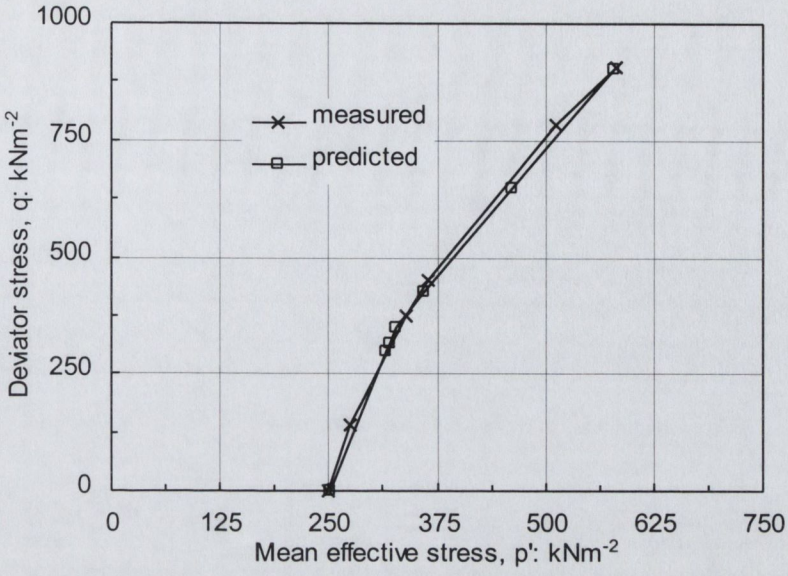

Fig. 6.2.7(a). Comparison of predicted and measured CIU triaxial test stress paths

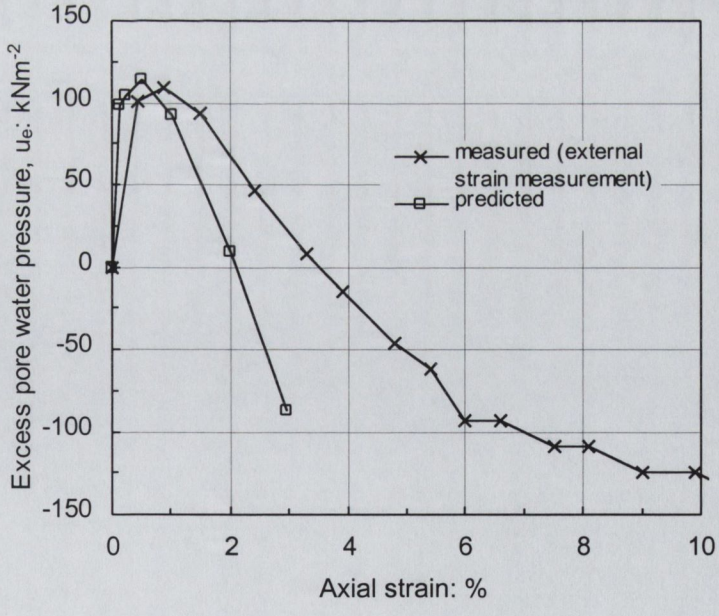

Fig. 6.2.7(b). Comparison of predicted and measured CIU triaxial test excess pore water pressure against axial strain

6.3 Predictions of Field Trials with the HS Model.

6.3.1 Footing.

The footing test summarised in the literature review (see Fig. **2.5.3**) was modelled. The initial deformation under the concrete pad and under the loading frame could not be recorded because of site restrictions. Consequently, the initial loading stage must be excluded when comparing the computer predictions with the actual measured values.

The loading was drained and the unloading was undrained. The square footing was modelled as an equivalent axisymmetric plate of radius 0·86 m. The plate element requires input of the normal stiffness, EA, flexural stiffness, EI and Poisson's ratio. These were calculated as $5{\cdot}25\times10^7$ kN/m^2, $1{\cdot}337\times10^7$ kN/m^2/m and 0·15, respectively. The water table was taken at ground level, as was observed on site. The mesh was refined, particularly in the vicinity of the corner point of the footing for numerical reasons[1], and 15-noded triangular finite elements utilised. Loads, boundary conditions and mesh are shown in Fig. **6.3.1**[2].

The stress history of the lodgement till was initially reproduced numerically by applying σ_{vy}' of 1500 kNm^{-2} to the level ground prior to construction of the footing. This resulted in very high lateral pressures near surface due to very high OCR so that, prior to the construction of the footing, the soil was in a state of passive failure near the surface of the soil. The load was then applied to the footing and drained conditions only were modelled.

The ground under the footing was loaded in compression to a stress level beyond the yield stress and into the plastic range in some zones. E_{ur} would govern the initial deformations, below the yield stresses, whereas those in the plastic zone would be governed by E_{50} and E_{oed}, and by perfect-

---

[1] The numerical problems were due to the large difference in the stiffness of the footing and soil, which causes problems in resolving the stiffness matrix.

[2] Rampello et al. (1998) and Schweiger (2002b) have shown the importance of boundary conditions in FE analysis. Essentially, problems arise, particularly in deformation prediction, if the extent of the mesh is insufficient, such that boundary effects become significant. Hence, for the analyses in this thesis, wide meshes were used and the depth of the mesh was taken, *a priori*, to be the depth of the till layer at the site.

plasticity for elements that have reached the Mohr-Coulomb surface. The values of E_{ur}, E_{50} and E_{oed} would be dependent on the initial stresses and by subsequent stress increases due to loading.

The bearing pressure – foundation settlement curve computed for this test, using the parameters given on Table **6.2.1**, compares favourably with that observed on site, as shown on Fig. **6.3.2**. This indicates that the parameters, measured in the laboratory and field test series and subsequently inputted into the HS model, give a reasonable representation of the ground response.

The load-settlement curve from this test is close to a straight line and hence, pragmatically, this result can be approximated by assuming a linear elastic or hyperbolic soil model (see Equations [2.9.1] and [2.9.22], respectively). However, the use of such simplified models could only be justified for similar load situations. For example, the use of the E′ value, back-analysed from the footing, underestimates the ground modulus in the case of piles (see Section 2.10.4.2).

The footing was then loaded to the ultimate condition to assess the capability of the model at large strains. The prediction is shown on Fig. **6.3.3**. As the predominant stress-path beneath the foundation is considered to be triaxial passive compression (Lehane and Simpson, 2000) then, based on the results of the CK_oRD triaxial test prediction, shown in Fig. **6.2.4**, it is considered that the settlement of the foundation at failure may be underestimated. However, the predicted ultimate bearing pressure, q_u, is close to the value of 1300 kNm^{-2} measured in the Edmonton till (see literature review, Section 2.10.3).

6.3.2 Trial Excavation.

The excavation of Treacy (1995), summarised in Section 2.10.2.2, was modelled. The stratification exposed in the face of the excavation was 1·5 m of brown boulder clay over black boulder clay. The simplified stratigraphy, shown in Fig. **3.5.2(b)**, of deformation till over lodgement till separated by the water table is applicable to this earthwork. However, at approximately 2 m from the surface, a 100 mm thick, water saturated sand lens (see Section 2.2.5 for typical properties) was exposed in the face, which resulted in some water seepage into the excavation for about 48 hours, at which stage it ceased.

The recorded ground deformations behind the excavated face were very small, being a maximum of about 0·5 mm vertical and 0·75 mm horizontal, increasing to 3 mm vertical and 4 mm horizontal after 14 days - see Figs. **2.10.6(a)** and **2.10.6(b)**[3]. The increased movement over time represents dissipation of pore water pressures; hence, the initial excavation was modelled undrained, followed by consolidation. In Plaxis (cited), the soil mass is modelled by setting up the mesh, boundary conditions, loads and in situ effective stresses. Then, to simulate an excavation, soil elements and water pressures are removed, the latter by revising the water table. The consolidation phase was then conducted to obtain an appreciation of the possible ground movements that may be expected due to pore pressure changes. The consolidation program is a 3-d version of Darcy's law. This program does not include creep, although this is not considered to be a severe limitation in the case of Dublin boulder clay. The input is the soil horizontal and vertical permeability and the consolidation time.

It was not possible to include the boundary effects of the sand layer/lens noted in the face[4] and, therefore, the field condition is not truly represented by the standard analysis. To solve this, the following approach was taken. The sand lens will have the effect of reducing the overall mass permeability of the ground. To replicate this, k can be increased or, alternatively, k of the soil kept constant and t increased. Therefore, the permeability was set as a constant and the consolidation phase run for the length of time at which the measurements were taken (14 days) and for an arbitrary length of time, the latter to determine the result of further dissipation of suction pressures.

The floor of the excavation was 3 m wide, with a 2·5 m high step opposite the cut where the readings were taken. This step was included in the analyses below; although, when not included in the geometry, the effect of the step on the instrumented face was found to be negligible. The excavation was modelled in plane strain, for geometrical reasons, using 15-noded triangular elements. Mesh and boundary conditions are shown in Fig. **6.3.4**.

This excavation represents an unloading of the soil; hence, the deformations will be mainly governed by the unload/reload modulus, E_{ur}. The ground movements computed using the value of

---

[3] The extent of the ground movements was limited to a distance of about 3 to 4 m from the face. Therefore, differential settlement may be substantial despite the very small ground movements. It is important, therefore, that this behaviour is correctly modelled.

[4] This was due to a lack of exact information on the position and extent of the lens.

E_{ur} determined from the laboratory tests overestimates both the immediate and 14 days vertical and horizontal movements, as can be seen from Figs. **6.3.5(a)** and **6.3.5(b)**. The predicted immediate vertical movement (nearest the face), of 5 mm, compares unfavourably with the measured movement of about 0·5 mm; the predicted immediate horizontal movement, of 10 mm, also compares unfavourably with the measured value, of about 0·75 mm. Furthermore, the computer model predicts movements, both for the immediate and 14 days situations, at a considerable distance from the excavation, which incorrectly suggests very small differential settlement.

Two factors give rise to this overestimation of deformations and, in particular, to the prediction of movements at distance from the excavation. These are the very high stiffness at small strains for this highly non-linear material and the dependence of the stiffness on stress-path direction. An appreciation of the very high stiffness of the soil on unload can be shown by including the effect of the high stiffness at low strains in the model; i.e. by using the stiffness determined from the bender element and seismic tests, E_0', in place of E_{ur}^{ref}. The *a posteriori* method predictions are plotted on Figs. **6.3.6(a)** and **6.3.6(b)**. This modification, although technically not advisable, greatly improves the predicted displacement curves over the *a priori* method[5]. Note that more realistic differential settlements are predicted with E_0' than with E_{ur}. This is because, in the top corner of the excavation face, which has elements which have yielded (see points A, B and C on Figs. **6.2.4** and **6.2.6**), E_{50}, E_{oed} and/or perfect plasticity is/are mobilised; hence, the differential settlement, shown in Fig. **6.3.6(a)**, is the result of a greater difference between E_0' and E_{50}/E_{oed} as compared to the smaller difference between E_{ur} and E_{50}/E_{oed}.

6.3.3 Pile Tests.

6.3.3.1 CFA Pile FE Model.

Continuous Flight Auger (CFA) pile tests were conducted during the course of this study, the results of which are given in Appendix B. One of these tests (Pile 600) is used here for modelling

[5] The difference in the stiffness of the ground that remains between the predicted and measured curves may, in part, be due to the increased stresses above the water table, owing to some soil suction in the deformation till. However, when these stresses were approximately included (according to Equation [2.8.3]), it was found that there was a negligible effect on the prediction.

purposes. The CFA pile has certain characteristics which ensure that it a relatively easy pile to model, compared to, for example, the complex installation processes involved in diaphragm wall installation (Rampello et al., 1998). Firstly, the borehole wall is supported at all times, being restrained by the soil filled auger flights and by fluid concrete as the auger is extracted. Hence, the modelling does not need to take into account the movement of an unsupported bore. Secondly, the soil-pile contact is close to perfect because the fluid concrete is placed under pressure, thereby filling any cavities in the borehole wall. Finally, loose debris at the base of the auger-drilled hole is transported away at the start of the concrete process, i.e. with the auger concrete injector in place at the base of the auger-drilled hole, by an initial injection of concrete (Fleming, 1995). Hence, the base of the pile can be taken to be undisturbed. The installation effects of the auger on the soil remain, however. (The reader is referred to Section B.1.2.1 for more details on CFA piles.)

The pile was modelled as a Mohr-Coulomb material. The compressive strength of the concrete was 35 Nmm^{-2}, which was inputted instead of c′ (with ϕ' set equal to zero). The Young's modulus (24 GNm^{-2}) was obtained from a cylinder load test on the pile concrete. The problem was modelled in axisymmetry and 15-noded triangular elements were used. The model stratigraphy was as in Fig. **3.5.2(b)**[6]. Mesh, loads and boundary conditions are shown in Fig. **6.3.7**. The maintained load (ML) test produces settlements that are less than fully drained (see Appendix B.1); however, if the creep settlements are removed, the undrained settlement of the pile is obtained. Hence, the pile was loaded in an undrained analysis for comparison.

Initially the piles were wished-into-place; i.e. no account was taken of installation effects on the soil surrounding the pile. The maximum load in the test was then applied to the pile (4·5 MN). The computed and predicted results are shown as pile head load, P, against pile head deflection, δ, in Fig. **6.3.8**. As can be seen, the predicted pile settlements are underestimated.

It is considered that the pile deflection is underestimated because the model pile was wished-into-place. This assumes that the pile-soil interface is perfect, which is not the case. For example, a major influence on the mobilised shaft friction (and therefore the pile resistance to load) is the initial pressure distribution of the pile concrete on the borehole wall. This pressure limits the radial

[6] The site stratigraphy included about 2 m of made ground. Although the properties of this fill were unknown, this ground contributed a small proportion of the total shaft friction resistance in the pile test (see Fig. **B.2.7(b)**); it was, therefore, not included in the analysis.

effective stress (see Equation [2.10.2]) and hence limits the available shaft friction. This was modelled in the FE analysis by applying a reduced value of K_0 to a thin strip of soil placed immediately adjacent to the pile shaft. (This approach is considered preferable to adding an interface along the pile length and assigning a strength reduction factor, α[7].)

The appropriate value of K_0 for the pile-soil interface was found by assuming that the concrete pressure distribution on the borehole wall is hydrostatic[8]. This gives the K_0 values for the pile-soil interface shown in Fig. **6.3.9**. The K_0 value is about constant with depth; therefore, a value of K_0 for the interface of 1·5 was taken. All the remaining HS parameters for the pile-soil interface were as for the surrounding soil[9].

The predicted pile head load versus pile head settlement, including construction effects, is shown in Fig. **6.3.10**. The prediction is now encouragingly closer to the measured load-deflection curve, than the wished-into-place prediction. The predicted load distribution and load distribution development in the pile is shown in Fig. **6.3.11**. As can be seen from this figure, the load distribution in the pile at different loads is well modelled because of the accurate prediction that the load would be largely taken in shaft friction, and not end bearing. The very good agreement between the measured and predicted load-settlement curves is, therefore, due to the correct prediction of the load in the pile; hence, the model of the pile behaviour is realistic.

6.3.3.2 Pile Design by the FE Method.

The above FE model could be utilised in the design of piles, as follows. Within the FE method it is possible to prescribe displacements instead of loads. This aspect of the FE method could

---

[7] This is because the interface elements are elastic-perfectly plastic and, hence, the soil adjacent to the pile shaft is not modelled by the HS model. Moreover, as it is the strength of the soil that governs failure, the α value should be 1.

[8] Although the actual pressure distribution may be distorted (see Rodin (1952) and Civil Engineering and Public Works Review (1965)).

[9] It is possible that the shearing effect of the auger mobilises some of the available dilatancy of the soil, in effect producing a modified zone of soil along the pile-soil interface. Houlsby (1991) has demonstrated that the angle of soil dilation plays a particularly important role in piles due to the high degree of soil shearing. However, the effect of augering would require a parametric study. Instead, including the hydrostatic pressure of concrete, takes account of construction effects by automatically modifying the shear strength, stiffness and dilatant capacity of the soil (which can be seen in the stress dependency of the constitutive equations of the model - see Section 6.2).

conceivably be used to prescribe the allowable building settlement/differential settlement to the top of a foundation. Following a prescribed displacement, it is then possible to check that the load in the pile(s) is less than the known working load. If it is found that the resulting loads are conservative, then the pile dimensions could be iteratively optimised, while maintaining the allowable building differential settlement within serviceability limits, to obtain a more economical design[10].

Alternatively, the FE model could be used to determine if the bearing pressure could be increased over the conservative initial estimates, for example those based on BS 8004, while maintaining the building differential settlements within known serviceability limits[11]. Following the initial estimate, if it is found that for a given bearing pressure the settlement/differential settlement of a building is well within serviceability limits, the bearing pressure could be increased/the pile dimensions optimised.

Both of these approaches require an initial estimate of the pile dimensions. Suitable methods for this in Dublin boulder clay conditions are the α, Eurocode 7 and Chin (1972) methods (see Section 2.10.4.1).

[10] The procedure was validated by the author by prescribing the maximum settlement, predicted by the HS model (shown in Fig. **6.3.10**), to the pile head and comparing the load distribution generated in the pile, by this procedure, with the load distribution in the pile, generated by applying a head load. The result, given in Fig. **6.3.12**, shows that the load distributions are identical.

[11] Note that the same design procedures can be applied to the design of footings.

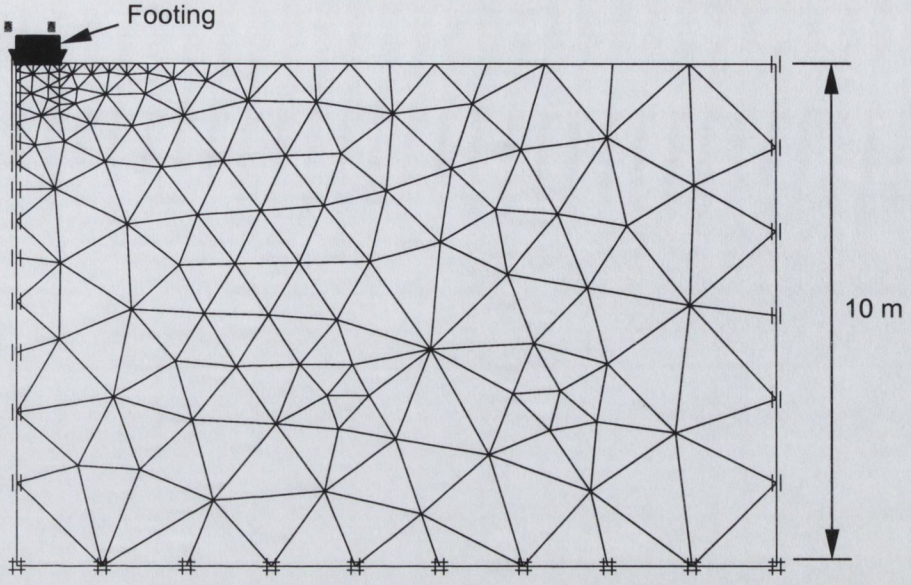

Fig. 6.3.1. FE mesh, loads and boundary conditions for footing prediction

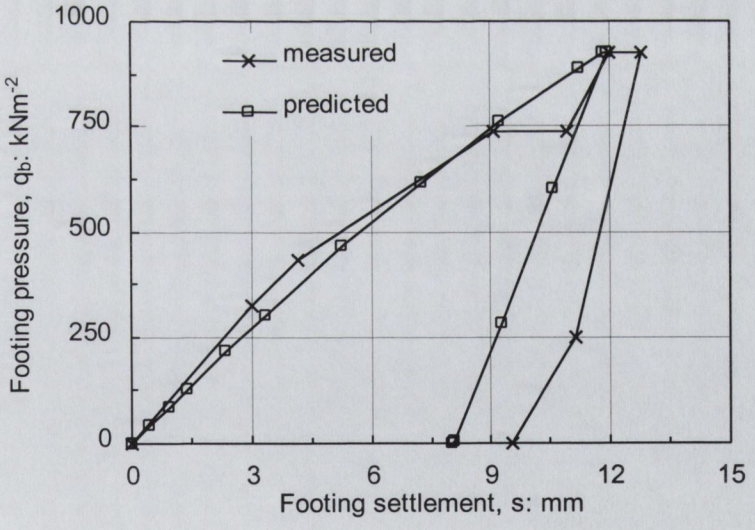

Fig. 6.3.2. Comparison of predicted (HS) and measured footing settlement

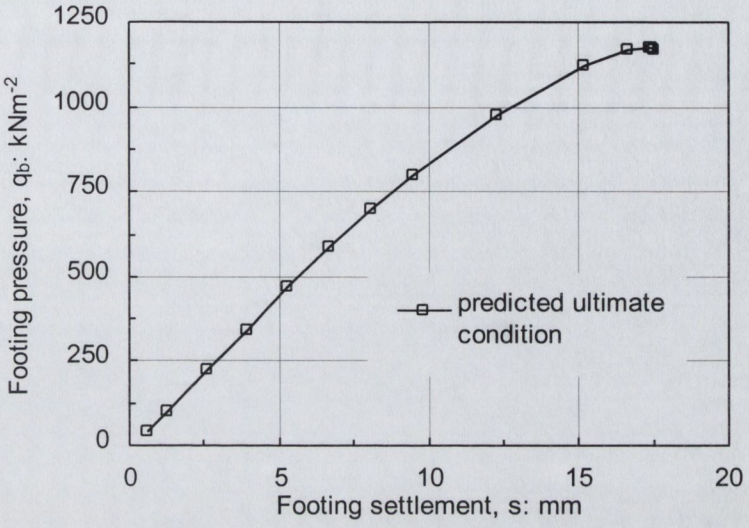

Fig. 6.3.3. HS prediction of the ultimate footing bearing stress and settlement condition

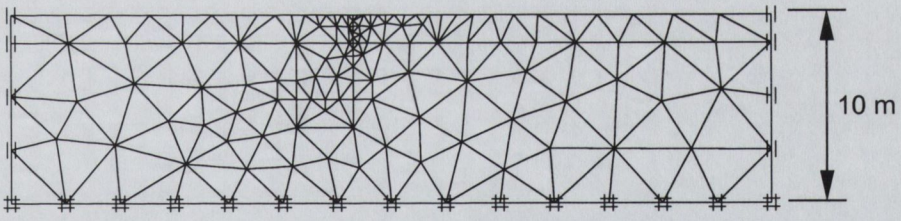

Fig. 6.3.4. FE mesh, loads and boundary conditions for excavation prediction

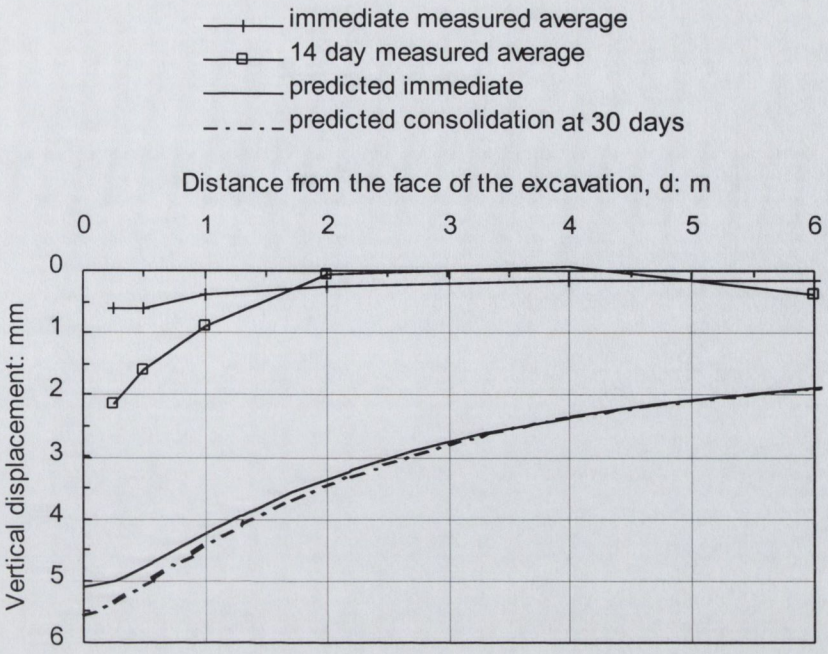

Fig. 6.3.5(a). Comparison of predicted (HS) and measured vertical ground movement of soil adjacent to an excavation

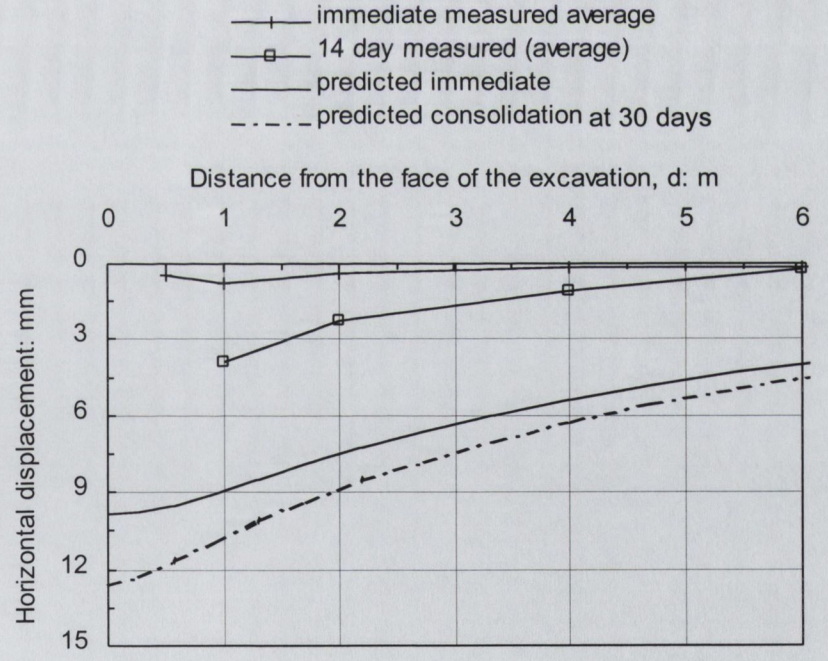

Fig. 6.3.5(b). Comparison of predicted (HS) and measured horizontal ground movement of soil adjacent to an excavation

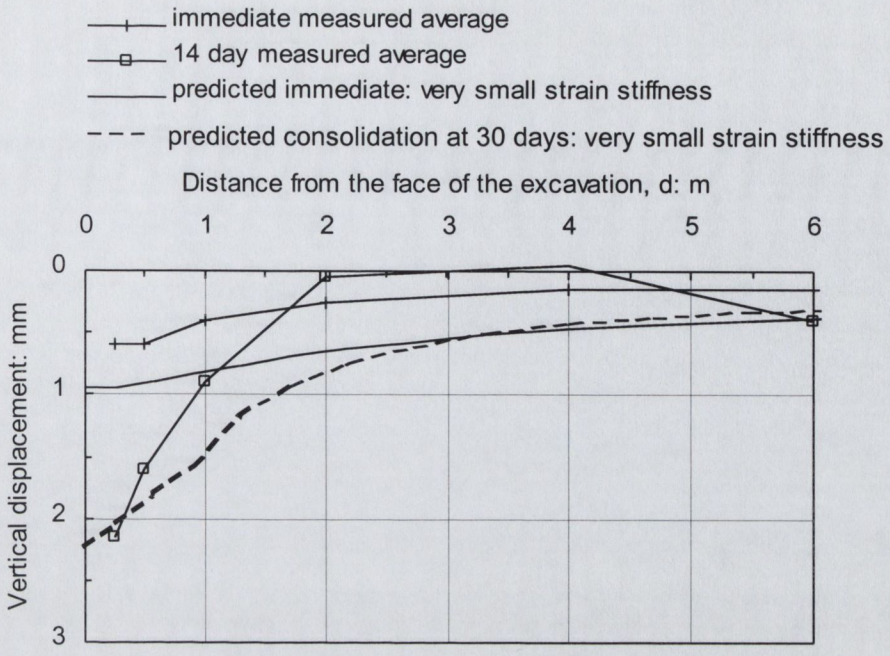

Fig. 6.3.6(a). Comparison of measured vertical ground movements with the movements predicted with very small strain stiffness

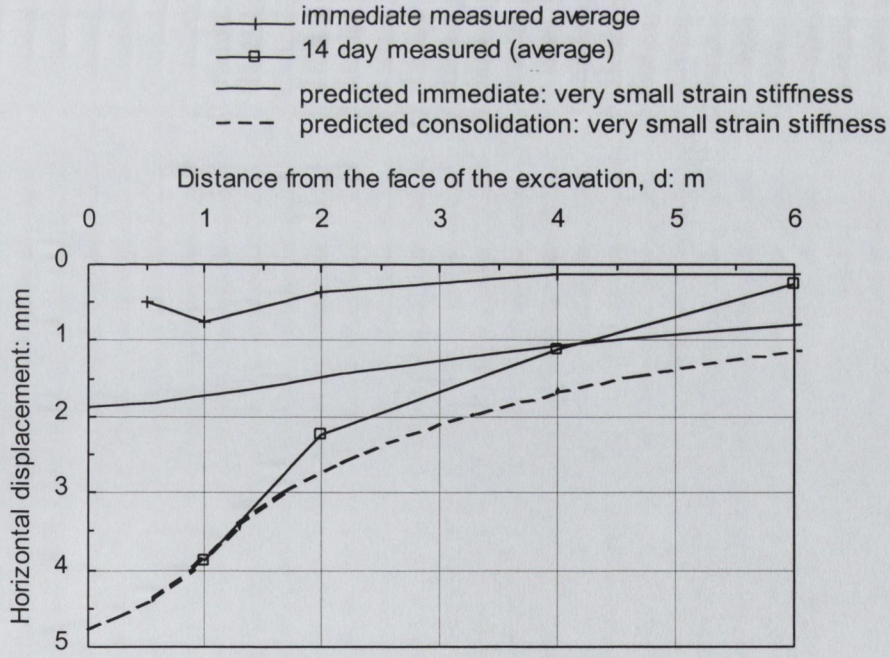

Fig. 6.3.6(b). Comparison of measured horizontal ground movements with the movements predicted with the double-stiffness HS model

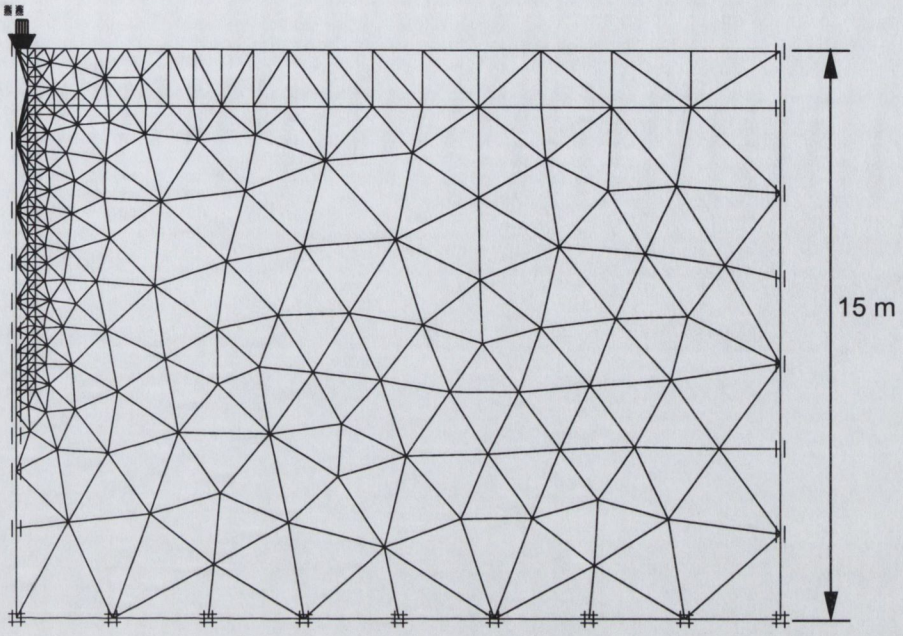

Fig. 6.3.7. FE mesh, loads and boundary conditions for pile prediction

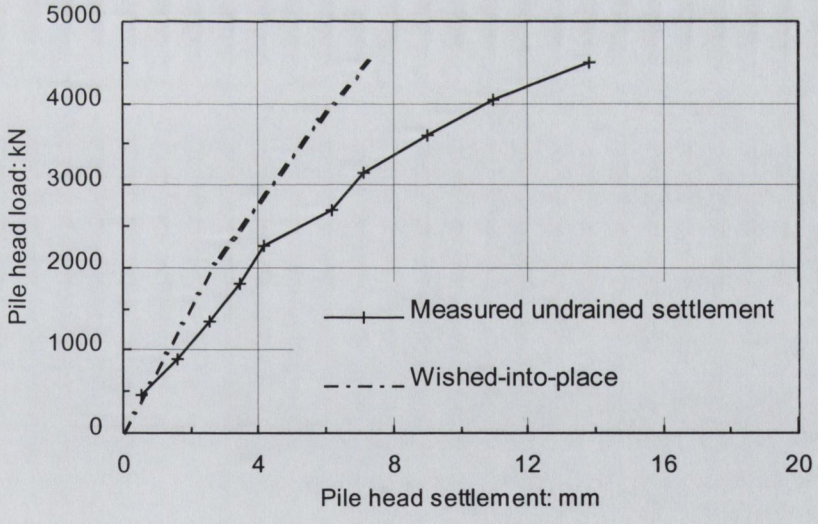

Fig. 6.3.8. Comparison of predicted and measured (Pile 600) pile head load against pile head settlement

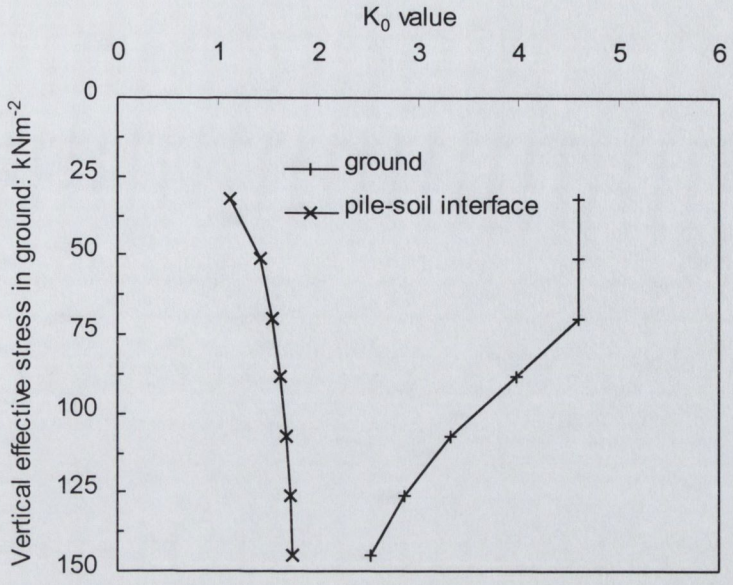

Fig. 6.3.9. Comparison of K_0 at the pile-soil interface and K_0 in the soil

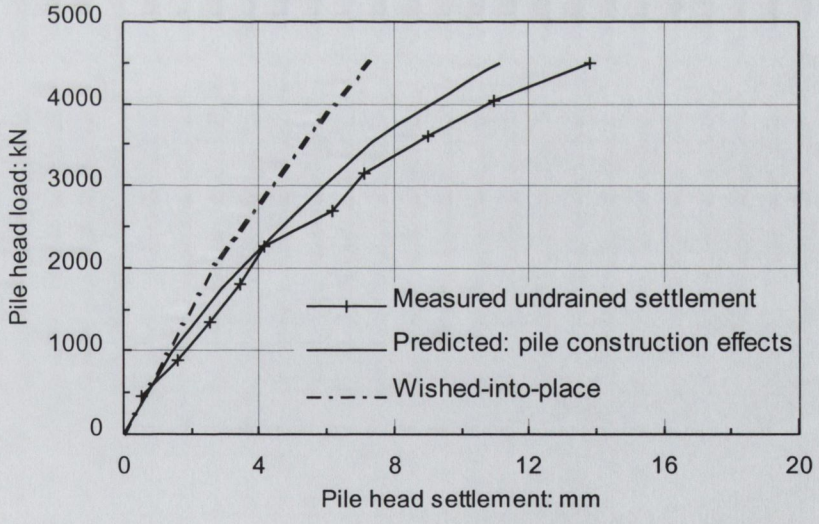

Fig. 6.3.10. Comparison of predicted and measured (Pile 600) pile head load against pile head settlement

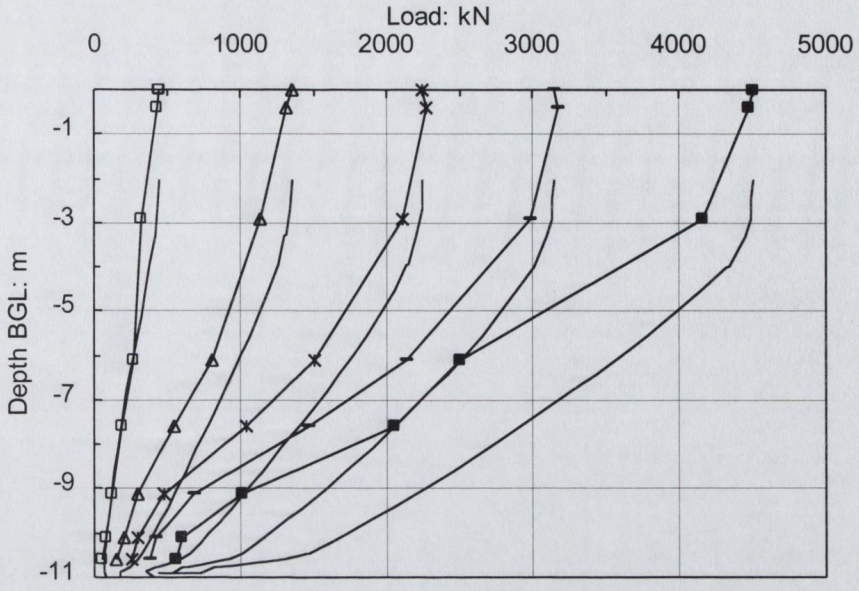

Fig. 6.3.11. Comparison of predicted and measured load distribution and the development of load distribution in Pile 600, including installation effects (note that lines without symbols are the predictions)

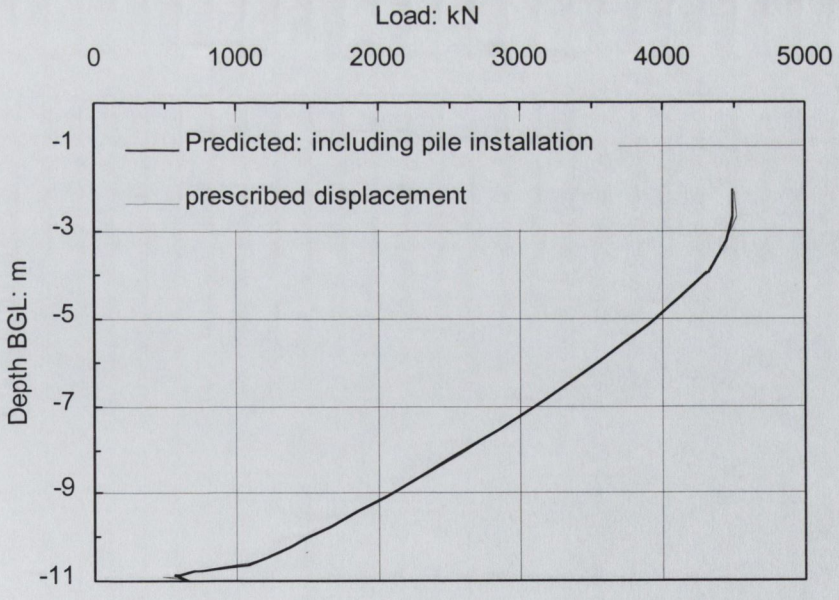

Fig. 6.3.12. Pile design procedure validation (note that the curves overlap)

6.4 Elastic-Perfectly Plastic Soil Model.

6.4.1 Introduction.

In this section, the soil parameters relating to the elastic-perfectly plastic model, the theory of which was explained in Section 2.9.1.2, are derived. The model is then validated, in like manner to the Hardening Soil model in Section 6.2.4, by predicting the same laboratory tests and ground deformations that were discussed in that section.

6.4.2 Elastic-Perfectly Plastic Predictions.

6.4.2.1 Selection of Parameters.

The Mohr-Coulomb model requires an elastic stiffness, E′, and Poisson's ratio, the strength parameters ϕ' and c′, the peak angle of soil dilation, and the in situ stress-state, the last of these represented by K_0, the coefficient of lateral earth pressure and γ, the unit weight of the soil.

The assumption that the stress-strain behaviour of soil was linear and constant with depth in the ground was, for practical purposes, commonplace practice for many years. It is now known that soil stiffness is highly non-linear, varying with strain level, confining stress level, stress-history and direction of loading (see Section 2.5.3). However, the parameters in the elastic-perfectly plastic model are constants and must, therefore, be carefully selected as being most relevant to the strain level, stress level and predominant direction of loading/unloading, of interest. Atkinson (2000) showed a graph (Fig. **2.5.9**) of the various strain levels at which typical field structures operate. The figure shows that, due to stiffness non-linearity, the stiffness of the ground around an excavation is higher than it is for foundations.

Owing to the unloading of the soil, a 'θ' value of 180°, as defined in Fig. **2.5.10**, is relevant to excavations in glacial till. Hence, the maximum shear modulus of the ground, G_{max}, is relevant (see Sections 2.5.3 and 2.10.2.2). G_{max}, which can be easily converted to the very small strain Young's modulus, E_0', by elastic theory with an effective Poisson's ratio, ν', of 0·2 for the till,

was measured in the bender element tests in the laboratory and seismic tests in the field. E_0' was found to vary approximately with stress level according to the power law Equation [5.4.2].

In the Mohr-Coulomb model, however, the stress dependency of stiffness is not taken into account. Assuming no stress-dependency, i.e. m = 0, typical values are found to be $E_0' = 1$ GNm^{-2} for the lodgement till and 200 MNm^{-2} for the deformation till. These values of stiffness are comparable with the apparent ground modulus, which can be ascertained from the ratio $E_u/c_u = 1000$, back analysed from excavations in stiff clay (see Section 2.10.2.2), where E_u and c_u are the undrained Young's modulus and undrained shear strength, respectively. It is evident from the ratio that the stiffness E_u is potentially very high in very stiff boulder clay, for which c_u is typically of the order of 500 kNm^{-2}. Several other authors (e.g. Jardine et al. (1986) and Simpson (1992)) have also given evidence that excavations in stiff clay generally operate initially at very small strain and are of this very high stiffness.

In the case of foundations, it can be seen, from Figure **2.5.9**, that the region of shear strain of 0·1% or more is relevant. Furthermore, the stress-path in the ground beneath a footing is predominantly loading in shear (triaxial compression) (see Section 2.9.2). Hence, it would be expected that the secant stiffness at small strain, E_s', derived from the triaxial compression test would be relevant. Furthermore, the value of E_s' derived from the triaxial tests, namely 200 MNm^{-2}, is similar to the pressuremeter stiffness measured by DeJong and Morgenstern (1973), which was found to give accurate estimates of the elastic behaviour of stiff till (see Section 2.5.5.1).

The angles of shearing resistance interpreted from the triaxial tests were, for peak stress ratio, $\phi_p' = 40°$ and, for constant volume shearing, $\phi_{cv}' = 32°$. Furthermore, a cohesion intercept, c', of zero was interpreted from Fig. **A.2.6**. The glacial remoulding of the upper metre of till, discussed in Section 3.3, will have caused constant volume conditions; therefore, the peak angle of friction of the deformation till is considered to be the constant volume angle of the lodgement till. It is evident, from a comparison of ϕ_p' and ϕ_{cv}', that the friction angle, ϕ', of the soil peaks and reduces as the strain level increases. Therefore, the value of ϕ' most suitable to the particular case must be chosen, which, at the (small) strain levels typically encountered in the ground, is ϕ_p', as has been discussed in Section 5.4.3.

To complement the peak angle of friction, the peak angle of dilation, ψ, is taken. Rowe's (1962) model of soil dilation was found by experiment, in Section 5.4.5, to give a reasonable estimate of the stress-dilatancy behaviour of the lodgement till. The flow rule gives a peak angle of soil dilation of 10°. A suitable value of ψ for the deformation till is 0° due to glacial remoulding.

The generation of the initial stresses in the ground requires an estimate of K_0, the coefficient of lateral earth pressure and a value for the unit weight of the soil, γ. Estimates of K_0, obtained from the triaxial tests and pressuremeter tests, have been shown in this thesis to be approximated by elasticity theory (see Fig. **5.4.9**). A value of OCR, the overconsolidation ratio, was estimated from the value of the yield stress of the lodgement till, namely 1500 kNm^{-2}, which was measured in the special oedometer tests; an average value is taken for the soil. $\sigma_{vy}' = 500$ kNm^{-2} was taken for the deformation till from the pressuremeter testing and Boulton & Paul (1976), as shown in this thesis (see Section 5.7.1.1 for details).

Tables **6.4.1(a)** and **6.4.1(b)**, for the lodgement till and deformation till, respectively, represent a summary of the parameters derived in this section for use in the Mohr-Coulomb model.

Table 6.4.1(a). Parameters used in the elastic-perfectly plastic prediction: lodgement till

γ: kNm^{-3}	E′: MNm^{-2}	ν'	ϕ': degrees	ψ: degrees	c′: kNm^{-2}	K_0	k: ms^{-1}
22·5	200: shear* 1000: very small strain* 125: 1-d†	0·2	40	10	1	2	10^{-11}

* See this section for derivation
† See Section 6.4.2.2 for derivation

Table 6.4.1(b). Parameters used in the elastic-perfectly plastic prediction: deformation till

γ: kNm^{-3}	E′: MNm^{-2}	ν'	ϕ': degrees	ψ: degrees	c′: kNm^{-2}	K_0	k: ms^{-1}
21·5	200: very small strain*	0·2	32	0	1‡	3	10^{-10}

‡ Note that it was not considered within the accuracy of this model to include the small c′ value, representing the contribution of suction to strength. (Remember that a small value of c′ is taken for numerical reasons.)

6.4.2.2 Laboratory Test Predictions.

The soil parameters used in the prediction of the laboratory triaxial test are given in Table **6.4.1(a)**, except for the friction and dilation angles, which were inputted as measured in the test being modelled. The relevant stiffness in this case is the 'shear' stiffness. Fig. **6.4.1** shows that the elastic-perfectly plastic prediction is, as expected, a bi-linear fit to the laboratory triaxial test curve (Test BE4). This prediction is also compared with that measured, in terms of stiffness degradation, in Fig. **6.4.2**. As can be seen, the model prediction of stiffness degradation is closer than may be suggested by the bi-linear stress-strain prediction. Nevertheless, the bi-linear model is much closer to the stress-strain behaviour of the reconstituted soil than to that of the intact soil (as is evident from Fig. **A.2.16**).

Next the oedometer test was modelled. The value of the oedometer modulus was shown, in Section 5.3.2, to vary considerably. However, a value of m_v of 0·008 m^2MN^{-1} was suggested, based on the results of consolidation tests in Section 5.3.2; this gives and approximate one-dimensional Young's modulus of 125 MNm^{-2}. This value was used in the prediction shown in Fig. **6.4.3**, which shows that the final settlement is well predicted, indicating that the stiffness modulus chosen is reasonable, but that the simple model does not predict the non-linear stress-strain response, as expected.

6.4.2.3 Footing.

The predominant stress-path associated with shallow footings is triaxial passive compression (Lehane and Simpson, 2000) and the strain level is small to intermediate; hence, the E_s' modulus was used. Fig. **6.4.4** shows that there is considerable application of the Mohr-Coulomb model to shallow footings. The ground under the footing was predicted to be loaded in compression to a stress level beyond the yield stress, defined by Equation [2.9.6]. E_s' would govern the deformations below the yield stress and perfect plasticity would govern elements that have reached the Mohr-Coulomb surface. It is interesting to note that this model may be applicable to typical construction practice, i.e. where the till is excavated and the foundations subsequently put down (see photograph Fig. **2.10.1**). This is because there is evidence to suggest that the stiffness modulus of the ground, at the base of an excavation in till, is about equal to the apparent stiffness of the ground, when

subsequently loaded (DeJong and Morgenstern, 1973). Hence, a typical construction sequence could be modelled with the E_s' modulus inputted in the elastic-perfectly plastic soil model.

6.4.2.4 Trial Excavation.

The appropriate stiffness, in the case of the excavation, is the very small strain stiffness. Figs. **6.4.5(a)** and **6.4.5(b)** show excellent agreement between the Mohr-Coulomb model and the field measurements of vertical and horizontal ground settlement, respectively. There are two reasons for this: one is that the near surface stiffness is not underestimated (as it is in the HS model, where the stiffness is stress-dependent and is, as a result, very low near surface – see Fig. **2.9.9**); therefore, the ground movements at distance from the excavation are not over-predicted. Secondly, the Mohr-Coulomb model has a sharp transition from elastic to plastic straining (with no smoothing of the transition) and, hence, greater plastic straining occurs, as compared to the HS model (which does incorporate an apparent smoothing of the transition). This greater plastic straining, in those areas that have yielded, produces the toppling effect of the soil in the direction of the excavation that was observed in reality. Note that the prediction at 30 days improves on the 14-day prediction, possibly because of the effect of the sand lens in increasing the overall permeability of the soil mass. It may be expected that, as the complexity of the excavation and support structure increases, and the number of stress-paths and variation in strain levels increase as a result, the Mohr-Coulomb model would become more difficult to implement. This was shown in the comparison of the triaxial and oedometer tests, which involve two different stress-paths/strain levels and, consequently, two different stiffness moduli.

6.4.2.5 Pile Tests.

The piles were modelled as for the HS model, including the effects of construction (i.e. $K_0 = 1{\cdot}5$ at the pile-soil interface), and the E_s' modulus was chosen for the elastic stiffness. Fig. **6.4.6** shows that the predicted pile settlement is in reasonable agreement with the measurements, but that the Mohr-Coulomb prediction is stiffer. This suggests that the elastic modulus of the ground around the pile is somewhat lower than E_s', which is consistent with the relatively high strain levels involved, when compared with footings[1].

[1] Note that the empirical formula Equation [2.10.3] over-predicts the pile modulus.

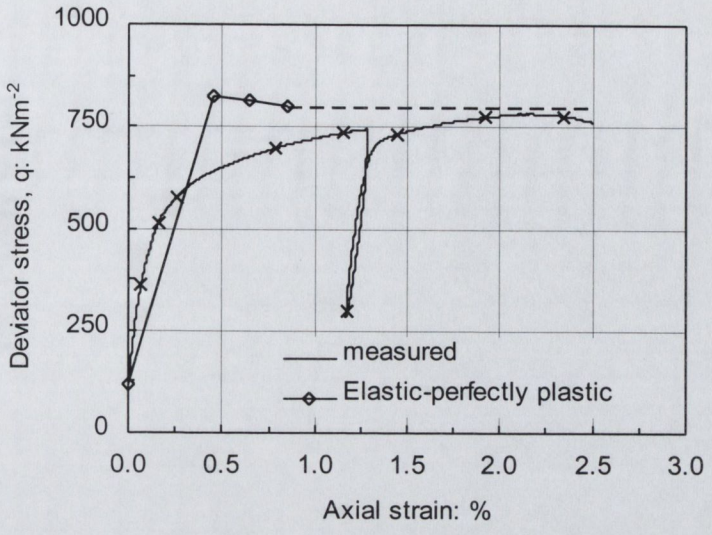

Fig. 6.4.1. Elastic-perfectly plastic prediction of CK_0RD test (Test BE4)

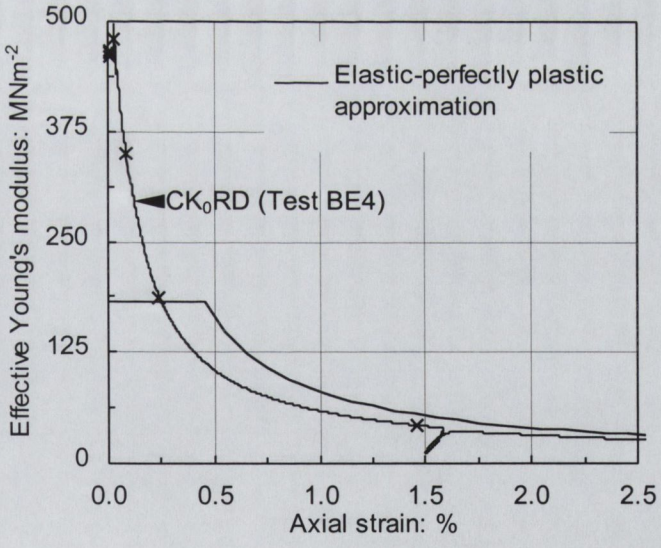

Fig. 6.4.2. Stiffness degradation prediction by elastic-perfectly plasticity

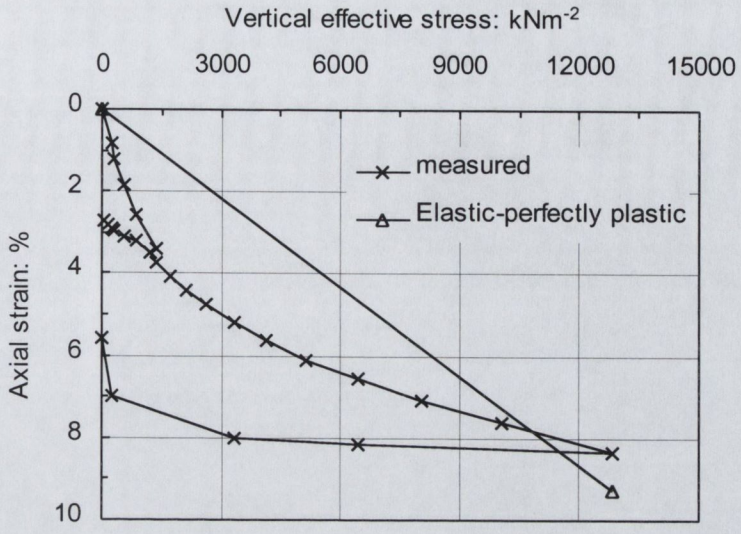

Fig. 6.4.3. Elastic-perfectly plastic prediction of oedometer test

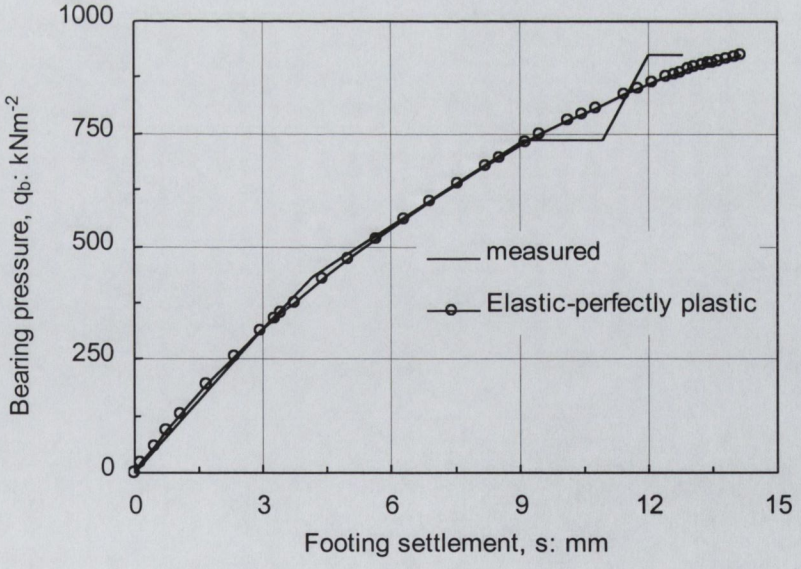

Fig. 6.4.4. Elastic-perfectly plastic prediction of footing settlement

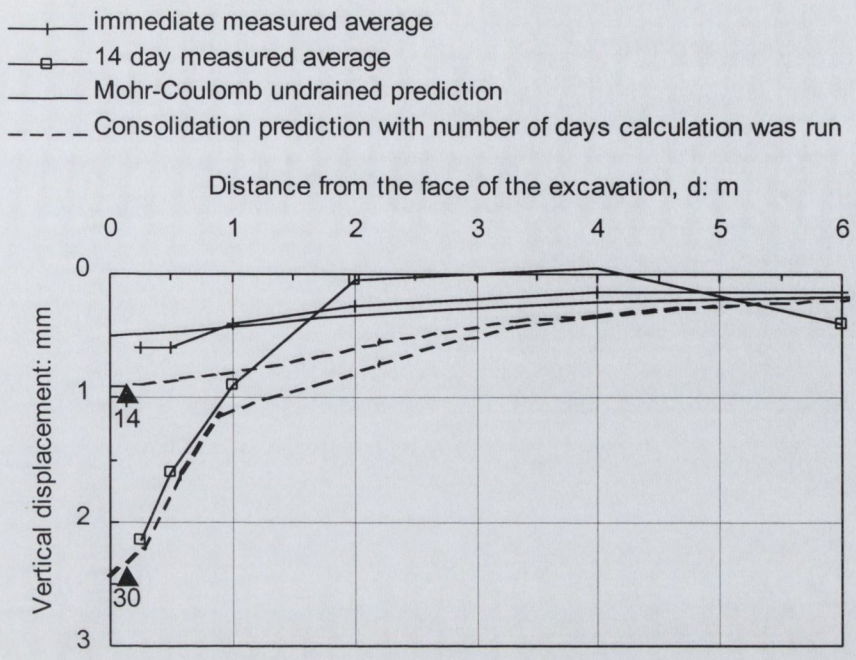

Fig. 6.4.5(a). Elastic-perfectly plastic prediction of the vertical deformation adjacent to an excavation

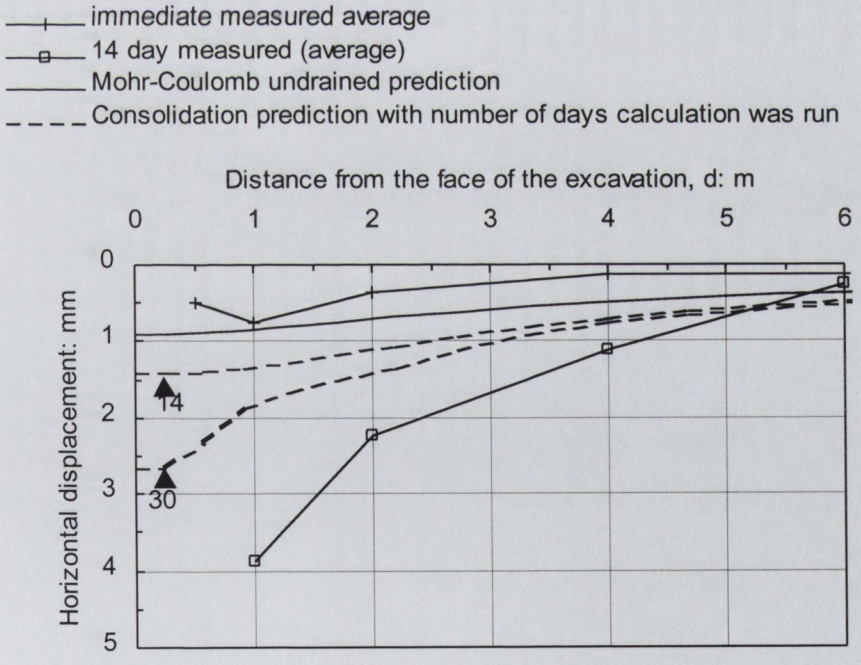

Fig. 6.4.5(b). Elastic-perfectly plastic prediction of the horizontal deformation of the ground adjacent to an excavation

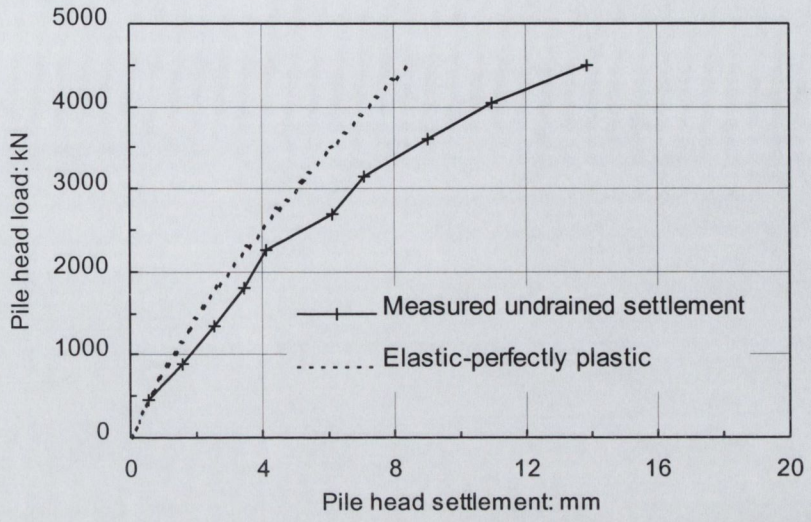

Fig. 6.4.6. Elastic-perfectly plastic prediction of Pile 600 head settlement

CHAPTER 7

CONCLUSIONS

CHAPTER 7

CONCLUSIONS

7.1 Introduction.

An experimental and research study has been conducted with the objective of numerically modelling accurately the deformations associated with construction in Dublin boulder clay. Soil models with potential commercial application were chosen and a programme of fundamental laboratory testing put in place. From these investigations, the decisive areas of the till behaviour were examined and essential soil parameters obtained. Special sampling techniques and apparatuses were developed to overcome the difficulties of sampling and testing intact specimens of the boulder clay. Fundamental tests on the properties and composition of the soil have been updated using state-of-the-art test equipment and methods. Reconstituted soil testing was included in the laboratory research programme, which aided greatly the understanding of the intact soil behaviour. These limited number of research tests were supplemented with a large number of laboratory and field experiments arising from investigations associated with the Dublin Port Tunnel works, with recent laboratory studies conducted at Trinity College and with data from lodgement tills in similar latitudes in Scandinavia, Canada and Britain. This chapter gives the main findings of the research.

7.2 Soil Modelling.

7.2.1 HS Model.

The behaviour of Dublin boulder clay, in the oedometer and triaxial laboratory tests, was found to correspond well with many of the features of the HS model. These were:

(a) Stress dependent stiffness according to a power law.

(b) Hyperbolic relationship between deviator stress and plastic strain.

(c) A pseudo-elastic plastic yield surface controlled by the yield stress, applicable to one-dimensional and triaxial stress-paths.

(d) Increased stiffness, E_{ur}, on unload-reload under triaxial, and oedometric, conditions.

(e) Strain hardening due to deviatoric loading.

(f) Significant plastic straining post-yield in one-dimensional compression and shearing.

(g) Failure according to the Mohr-Coulomb failure criterion.

(h) On shearing, compression-dilatancy characteristics approximately according to the Rowe stress-dilatancy theory.

(i) The automatic modification of the stiffness matrix to take account of pore water for undrained loading.

(j) Stiffness and strength isotropy.

Model input parameters were obtained from triaxial tests, with local strain measurement, from oedmeter tests, from bender element tests and in situ tests. The main results of the numerical modelling of the field trials were as follows.

The bearing pressure against settlement load-unload behaviour of a footing was very well predicted by the HS model. Although the number of stress-paths in the case of the footing was limited, the strain range was very wide, with elastic, non-elastic and perfectly plastic straining. However, the inadequacy of the model at very small strain was shown when the ground deformations, due to an excavation, were poorly predicted with the HS model, in terms of magnitude and distribution of ground deformation. The relevance of very small strain stiffness was shown by setting $E_{ur} = E_0$ in the model, which resulted in an improved prediction, including that of the important differential settlement.

A wished-into-place CFA pile, which does not take account of the installation effects of the pile on the surrounding ground, under-predicts pile settlement. When pile construction effects, based on the hydrostatic pressure of the fluid concrete in the bore, are included, however, a substantial improvement results, in the pile load-settlement prediction with the HS model. The good agreement thus found is partly attributable to the relatively straightforward CFA pile installation procedure.

A procedure for the design of piles and footings was suggested and validated. The procedure requires the input of the allowable foundation settlement/allowable bearing pressure and the forces/settlements generated in the foundation are then compared with the working load/allowable building differential settlement. The HS model could be reasonably used in

design, provided account is taken of the relevance of very small strain stiffness and the installation effects of piles on the stresses at the pile-soil interface is adopted. The Plaxis FE program proved to be a comprehensive environment for FE modelling.

7.2.2 Elastic-Perfectly Plastic Soil Model.

The elastic-perfectly plastic soil model in the Plaxis FE code has been shown to give accurate *a priori* predictions of relatively complex soil behaviour. The model potentially has considerable advantage over the use of more complex models, in that the parameters are relatively easily obtained and the predictions easily analysed, as has been shown.

Predictions of the settlements of a footing, an excavation and a CFA pile in Dublin boulder clay were made. The following are the main conclusions from these:

(a) The non-linear response of a footing bearing on Dublin black boulder clay was well-modelled using a comparable stiffness modulus, E_s' (or, alternatively, E_{ur}, which is equal to E_s'), which is a secant Young's modulus at small strain in the triaxial test.
(b) The observed, horizontal and vertical, surface ground movements adjacent to an excavation in Dublin boulder clay were well predicted by the elastic-perfectly plastic model using G_{max} measured in dynamic tests. The significance of the result is limited by the relatively simple nature of the problem compared to complex soil-structure interaction problems.
(c) Predicted pile settlement were in reasonable agreement with measurements using the E_s' modulus. However, unlike the footing test, the prediction was stiffer, suggesting that relatively high strain levels (lower stiffness), due to intense shearing, are involved.

7.2.3 Comparison of FE Methods with other Methods.

The HS model gave a very good representation of the settlement of a pad footing and generally outperformed other design methods. However, the differences between the advanced FE models and the simple elasticity and hyperbolic models, suggests that the use of the FE method is not justified in the case of shallow footings. Nevertheless, it would be expected that the FE method

would be relevant to combined foundations that involve substantial excavation or complex staged construction, the effects of which could be modelled in a FE analysis.

A commonly applied method of excavation design takes account of the difference in height of excavations to predict settlements. However, in addition to this, FE modelling of excavations has the ability to include the very large variety of support systems and construction sequences, common to actual construction situations. The potential savings involved in the application of the FE method are of particular significance in this respect. If complex construction sequences and support structures are required, an advanced soil model can approximately take account of the wide range of stress and strain levels induced in the ground. It is believed that the use of soil models, such as the HS model, in preliminary design will allow the widespread use of the observational method. Furthermore, the FE method has considerable potential over existing empirical methods and closed-form solutions for the design of piles.

7.3 Geology.

The findings of the study on the glacial successions were in general agreement with previous work, which identified multiple ice events. However, modern climate systems research shows that these were not separate events but instead represented ice oscillations of a Europe-wide ice sheet. This mechanism explains the single till sheet that underlies Dublin, which is inconsistent with traditional theories of glacial successions with long, inter-glacial periods.

Ice transport and deposition has produced a highly mixed, unlayered soil. The till would, therefore, not be expected to possess the anisotropy, in terms of stiffness, strength and permeability of layered, i.e. sedimentary, soils, evidence for which was found in this research.

Under a special combination of effective stress and glacial basal shear stress, the top of the lodgement till layer is remoulded. This remoulded zone is widespread because the conditions under which remoulding occurs, occur at the glacier margins on retreat. Direct evidence for shearing was found in the parallelism of the soil particles in samples of the till, when examined in the electron microscope. The depth of this shearing is about 1·5 m in Dublin, which is close to that identified in lodgement tills elsewhere. This section of the till is called deformation till, which has a lower frequency of large stones, than the lodgement till, due to crushing during

shearing. The strength and void ratio of the deformation till is, therefore, similar to the lodgement till at constant volume shearing. The stiffness of the till is also less than the lodgement till beneath. The deformation till has a theoretical apparent yield stress of 500 kNm^{-2} due to freezing of pore water, which is close to value interpreted from a pressuremeter test.

Above the water table, the till, which contains ferrous minerals, is subject to rusting. The brown boulder clay is largely made up of deformation till; however, beneath the deformation till, there is a mottled brown lodgement till that represents partial oxidation of the black till, owing to water table fluctuations. The deformation till, being near surface and of higher void ratio, is subject to biological weathering, which further breaks down the soil, producing a high plasticity. This is possibly because of the relatively high instance of highly active expandables, identified in quantitative X-ray diffraction analyses, which would be expected to result in the deformation till being liable to swell in situ.

In contrast, the black boulder clay largely shows evidence of particle disorder and angular rock flour. Quantitative XRD analysis on the black boulder clay showed that illite is the predominant clay mineral in this lodgement till. Illite sheets were observed in the scanning electron microscope in the, similar, brown lodgement till. The illite group minerals are not expandable; hence, swelling and heave of the soil, unlike the deformation till, should be limited. Clay mineral aggregation is not a major contributing factor to the cohesion of the black boulder clay and, therefore, the c′ component of the soil is negligible, especially when compared to the very high peak deviator stress. The till typically has a large calcite component (about 40% of the total minerals present in the soil). Calcite, and possibly other minerals present through diagenesis since the last Ice Age, may act as a type of soil cement. This would have the effect of binding the soil together and thus enhance the soil strength and stiffness above that due purely to inter-particle friction, which is what is observed in earthworks in the till.

As a result of this geological study, a simple ground model of deformation till overlying lodgement till, separated by the water table, overlying rock is suggested. However, in the region of the Dublin Port Tunnel (Whitehall/Griffith Ave.) the till sequence at depth is highly layered and the lower, grey brown/brown grey, till contains fissures. XRD tests were conducted on this till layer and it was found to contain more swelling chlorite than the

unfissured black boulder clay; this essential difference between the two provides a possible explanation for the fissuring observed in the lower till unit.

The glacial consolidation equation was derived based on the formulation for glacial consolidation proposed by Boulton et al. (1974), which in turn was based on actual observations of glacial lodgement in Iceland. The major mechanisms involved are: (a) the discharge of glacial melt-water into the till, (b) the pressure of ice and (c) the decrease in till permeability with applied pressure. The resulting differential equation was solved and the solution showed that the theoretical effective stress in lodgement till, due to the pressure of an overlying glacier, increases as the amount of gravel and large particles in the till increases. Hence, the preconsolidation stress of a well-graded, gravelly till would be expected to be greater than the preconsolidation stress of a till possessing a higher proportion of fines. This solution, which is backed up by laboratory and field evidence, coupled with *en masse* deposition of fingers of pre-glacial material, provides a mechanism to explain the presence of soils of low OCR lying beneath soils of high OCR, both in the Dublin Port Tunnel (Whitehall/Griffith Ave.) area and in similar glacial sequences found elsewhere, i.e. in Britain and Canada.

Sand lenses act as discontinuities in the till, causing block falls in tunnelling and may, also, affect the stability of slopes. However, the lenses possess a stiffness and strength similar to the lodgement till; hence, ground movements are not be adversely affected. However, the lenses could act as conduits for ground water flow, possibly affecting long-term ground movements.

7.4 Sampling.

The Geobor S method of till sampling was adopted. Importantly, it was found, this coring method, coupled with good handling and transport procedures, procured cylindrical soil samples of unfractured lodgement till. However, if the samples are to be stored, the soil cores should be extruded from the core liner (which is over-sized) and restrained from swelling.

7.5 Stress-History.

Laboratory measurements of the yield stress of the lodgement till, namely 1500 kNm^{-2}, compared favourably with previous estimates and with a solution derived from CSSM. This

yielding was found to be related to the soil strength and not solely the past maximum pressure. Interestingly, it was noted that the familiar bi-linear, e-logσ_v', plot for stiff clays was not applicable to Dublin boulder clay on primary loading. This is because, without a stress-history reconstruction, the soil behaviour is non-elastic, resulting in an inaccurate assessment of σ_{vy}' based on the Casagrande method. Instead, a comparison of the intact and reconstituted soil behaviour in one-dimensional compression validated the method of plotting (inverse) coefficient of volume compressibility against (the logarithm of) vertical effective stress to obtain σ_{vy}'.

The Marsland and Randolph (1977) analysis, of pressuremeter tests with a distinct yield point, gave values of in situ stresses that corresponded well with estimates, particularly those based on elasticity using the value of σ_{vy}' measured independently in the oedometer. The results also compared favourably with K_0 interpreted from the laboratory K_0 consolidation tests on intact till, in which an accuracy of about 0·002% radial strain was obtained in the triaxial apparatus. Laboratory measurements of K_0^{nc} compared favourably with the prediction of Jaky (1944). The reconstituted till was found to be unable to sustain the high K_0 values of the intact soil, possibly due to the absence of structural strength from this soil.

Important information on the in situ stress-state and strength of the deformation till was obtained from a pressuremeter test in the soil. A K_0 value was obtained, corresponding to a yield stress close to the theoretical value given by Boulton and Paul (1974), namely 500 kNm^{-2}.

7.6 Stiffness and Stress-Strain.

Loading of the soil near to the value of the yield stress, followed by unloading, i.e. a K_0 stress-history-reconstruction (K_0R test), induces in the soil sample an anisotropic stress-state close to that in situ and reconstructs the boundary surfaces that separate elastic from non-elastic behaviour. On reloading from this stress-state, a stiffness comparable to that in the field was obtained in the oedometer, for example, and realistic stress-strain and dilatancy characteristics were obtained in the oedometer and triaxial apparatuses, respectively, as follows.

In the triaxial apparatus, the CK_0RD test, once the threshold point was reached, separating elastic from non-elastic behaviour, exhibited classical, compression followed by dilation,

behaviour, whereas the CID and CIRD tests dilated, almost from the start of shearing. The latter results in largely hyperbolic stress-strain behaviour, which represents post-yield, non-elastic, straining. In the oedometer, K_0R tests resulted in the classical bi-linear consolidation curve, whereas primary loading gave large, non-elastic, strains from the start of loading.

The stress-strain characteristics of the, realistic, CK_0RD tests are highly non-linear, with elastic, pseudo-elastic and plastic sections. This behaviour is directly linked to the relative movement of the soil particles, resistance to yield due to the structural strength of the till and the development of soil dilatancy. The CK_0RD tests are, as a result, more brittle than measured previously (in CID tests). The stiffness-strain behaviour is described reasonably well by the classical S-shape curve on the semi-logarithmic plot.

Although there is a substantial difference in boundary conditions between the oedometer and the triaxial tests, the stiffness obtained on an unload-reload loop, E_{ur}^{ref}, is the same in both tests. This is because of common yield surfaces, which are independent of boundary conditions. When normalised according to a power law, this stiffness is found to be a constant, i.e. $E_{ur}^{ref} = 200\ MNm^{-2}$. E_{ur}^{ref} is equivalent to the small strain secant stiffness, $E_s^{ref\prime}$, the latter being measured at the point of onset of the maximum rate of soil dilation. This modulus, and, therefore E_{ur}, is particularly suited to foundation settlement and excavation base heave prediction. In terms of void ratio, the value of C_s is about 0·01, which is very close to the recompression index, C_e, giving a single modulus for unload and reload, as before.

The threshold point, the point at which non-elastic behaviour commences, occurs at a shear strain in the region 0·006% - 0·01%, which is greater than the value of 0·001% common to many clays. As a result, the associated very small strain stiffness, G_{max}, is relevant to excavations in the soil. This relatively high resistance to yield is caused by the very great structural strength of the till.

The bender element method of stiffness measurement is a suitable test for the measurement of G_{max} and, when conducted on natural soil samples, is particularly important, as the effects of soil structure on stiffness are automatically included. The results of the BE tests compare favourably with those measured from the deviator stress against local strain curve, and with in

situ seismic tests, when account is taken of the effective confining pressures on the sample/in the ground. An empirical expression for G_{max} was also found to be remarkably accurate in this regard.

The in situ Young's modulus of the ground is given by a power law, where $E_0^{ref\prime} = 1\ GNm^{-2}$, with the power value, m, equal to 0·5 and a drained Poisson's ratio, ν', of 0·2. This power law covers a wide range of stiffnesses, namely E_0, E_{ur}, E_{50} and E_{oed}. The value of m is 0·5 for E_0 and E_{ur} but increases from 0·5 initially to about 0·6 at 50% strength in the triaxial CID test. Seismic tests confirmed the similar stiffness of the mottled brown lodgement till and black lodgement till and also gave the approximate stiffness of the deformation till, which was about five times less stiff than the lodgement till, i.e. $E_{0ref\prime} \approx 200\ MNm^{-2}$. The seismic measurements in the deformation till provided a basis for estimating the stiffnesses E_{ur}^{ref} and E_{oed}^{ref} of this unit, based on correlations developed for the lodgement till.

The stiffness determined from the primary loading curve in the oedometer, E_{oed}, greatly underestimates soil stiffness. However, E_{oed} was found to model the post-yield stiffness of the till in one-dimensional compression very well.

A typical value of m_v is 0·008 m^2MN^{-1}, found from the reload curve of the K_0R test. Related to m_v, c_v values of about 5 m^2/year were interpreted, which are consistent with the low values interpreted from field observations. A value of permeability, k, of about $1\times10^{-11}\ ms^{-1}$, can be interpreted from these c_v and m_v values. Furthermore, owing to the till being unlayered, it would be expected that this permeability value would be applicable to both the vertical and horizontal directions. The relationship between permeability and vertical effective stress was found to be exponential. However, the rate of reduction in permeability, with increasing vertical effective stress, was found to reduce as the gravel content of the soil sample increased.

External and local strain measurements are similar in both CID and CIRD tests above a shear strain of about 0·1%. However, in CK_0RD tests, bedding and seating errors are eliminated and hence external strain measurements tend to the local strain measurements.

The maximum shear stiffness measured from accurate pressuremeter unload-reload loops was about equal to the (equivalent) stiffness measured in the laboratory. As the pressuremeter stiffness represents the horizontal till stiffness, the in situ stiffness anisotropy of the lodgement till is not considered significant, at least within the experimental accuracy. The stiffness isotropy of the lodgement till, so determined, is consistent with the mode of deposition and with the ground movements measured in an open excavation in the soil.

7.7 Strength.

A value of $\phi_p' = 40°$ and $c' = 0$ kNm^{-2} was interpreted for the black boulder clay from a large number of triaxial, drained and undrained, compression tests. The variability of soil samples, and the very high deviator stresses associated with failure, may hide any c′ component the soil possesses. A ϕ_{cv}' of 32° was interpreted for the lodgement till, which is consistent with a low plasticity soil. The deformation till, by virtue of the shearing action of the glacier, would be expected to have a peak friction angle close to the constant volume angle of the lodgement till.

A number of indicators of structural strength have been found. For example, the high resistance of the intact soil to swelling relative to the reconstituted soil, prepared with the same particle sizes and stress-history and swelled from the same void ratio, and the resistance of intact till to yield (indicated by a high threshold point). Apart from these indicators, actual recrystallised calcite cement was observed in scanning electron micrographs of unsaturated lodgement till. The source of this structural strength is partly attributable to the diagenesis of the intact soil. In conjunction with very high capillary suction, caused by abundant, very small rock flour particles, the stability of vertical faces of Dublin boulder clay, and the very small ground movements associated with these earthworks, can be explained in this way. Furthermore, the rapid reduction in strength of the soil, with the addition of water, can be attributed to the dissipation of the rock flour capillary attraction.

The structural strength produces a relatively high resistance to yield, in both one-dimensional compression and shearing, when compared to the reconstituted soil. Hence, the soil is not as brittle as would be expected from a low plasticity soil. In this respect, the boulder clay falls between typical 'true' clay soils and hard rocks, both of which have true cohesion and, hence,

distinct yield points. Conversely, the lack of bonding in the reconstituted soil results in a brittle, elastic-perfectly plastic, response, which is a truer reflection of the low plasticity index. It follows that the applicability of reconstituted soil in testing is limited.

7.8 Dilatancy.

The variability in the angle of soil dilation with strain, strain rate, stress level and inter-particle friction necessitates a flow-rule estimation of this angle. Rowe's (1962) flow rule was shown to give a reasonable estimate of the dilatancy characteristics of the, realistic, CK_0RD tests, for both the peak and mobilised state. Thus, this rule is considered preferable to laboratory measurements of the peak angle of dilation, determined from CD tests, which are considered to be unrepresentative due to the very low rate of strain these tests require. Nevertheless, the dilatancy behaviour of realistic CK_0RD tests, observed on the ε_v-ε_s plot, is an excellent indicator of soil yield; i.e. the threshold point, and the onset of a shear band, can be easily identified, as the slope of the ε_v-ε_s curve is zero ($\psi = 0°$) at these points.

7.9 Soil Suction.

The filter paper method is unsuitable for measuring suction in Dublin boulder clay. Very low suctions were measured with this test, belying the high suctions that are known to develop in dense soils possessing an abundance of rock flour particles. These rock flour capillary stresses enhance the strength of the lodgement till, allowing excavations, for example, to stand at 90°; they were also utilised in the construction of the Storebaelt tunnel. The deformation till however possesses a more open structure and therefore can not sustain these high suction stresses.

7.10 Suggestions for Further Research.

It is considered that the research warrants a number of lines of investigation. These include:

(a) The HS model should be developed to include the very small strain stiffness. This could be conducted using a kinematic yield surface inside the current boundary surfaces. Furthermore, the stiffness non-linearity with strain prediction of the

hyperbolic model could be improved, by including the observed increase in the dependency of stiffness on stress level as strain level increases. (User defined input is possible in the next version (8) of Plaxis.) Further work could then be conducted on modelling the deformations associated with excavations in the till; for example: slopes, slopes with sand lenses, deep excavations, 3D tunnels (with dynamic analyses) and complex, soil-structure interaction cases. The model performance should then be compared with 'Brick' of Lehane and Simpson (2000) and the model for structured soils of Kavvadas and Amorosi (1998).

(b) A major field investigation into the long-term stability and deformation of excavations in Dublin boulder clay conditions should be undertaken. This work would include the effect of sand lenses on the stability of slopes, and on mass permeability, and in situ measurements of capillary suction, preferably with the Ridley and Burland (1993) device. Deep excavations should be included. In conjunction with this work, a fundamental research programme should be put in place to investigate the soil diagenesis and the effects that the individual minerals, that compose the till, have on the soil behaviour. The research thus conducted would yield fundamental information on structural strength and the effect of this on Dublin boulder clay, particularly the contribution of structural strength to the rigidity of earthworks.

(c) Further work is warranted on the initial conditions set-up on bored pile installation. For example, measurements should be made of the pressure distribution of the auger injected concrete on the borehole wall to determine if these are hydrostatic and of the effects of augering on the properties of the soil in the vicinity of the auger-drilled hole.

(d) The bender element in the base platen of the triaxial apparatus should be reinforced and the bender elements wired to act as extenders (see Lings and Greening (2001)).

(e) Owing to the potential variability of the glacial soil, further extensive laboratory, and in situ, testing is warranted on till from a very wide range of sites. This research should include tests on boulder clays of various mineral composition, taking into account variation in the base rock, tests on the deformation till, on the brown boulder clay, on sand lenses and, finally, on glacial gravel layers.

APPENDICES

APPENDICES

A Field and Laboratory Work - Experimental Results.

A.1 One-Dimensional Consolidation

A.1.1 Oedometer Test O.

A.1.1.1 Aim and Details.

The main objective of this test was to determine the yield stress, σ_{vy}', of the lodgement till. To measure σ_{vy}', the soil was loaded to a pressure of about an order of magnitude greater than σ_{vy}'.

Secondary objectives of the test were to obtain the oedometer compression and swelling indices (C_c and C_s, respectively), the tangent oedometer modulus, E_{oed}, the coefficient of volume compressibility, m_v, and the soil consolidation characteristics, i.e. the coefficient of consolidation, c_v, and the vertical permeability, k.

Soil location: Ballinteer Rd., Dundrum. From depth 9 m BGL. $\sigma_{v0}' = 132$ kNm^{-2}. Sample dimensions: $H_0 = 27$ mm, $D = 102$ mm.

A.1.1.2 Test Results.

The test is shown on the void ratio against the logarithm of vertical effective stress, e-logσ_v', plot in Fig. **A.1.1**.

The values of the oedometer compression, recompression and swelling indices, C_c, C_e and C_s, respectively, and the oedometer stiffness modulus, E_{oed}, are given in Table **A.1.1**; E_{oed}^{-1} is plotted on Fig. **A.1.2**, m_v is shown as $1/m_v$ versus logσ_v' on Fig. **A.1.3(c)**, c_v is given as c_v against vertical effective stress in Fig. **A.1.4** and k is plotted against σ_v' on Fig. **A.1.5**.

c_v and k were determined based on the measured time to the end of primary consolidation, s_{100} (obtained from the log-time plot). This was suitable for c_v and k; however, it was not always possible to determine s_{100} with accuracy, therefore the settlement at about 1000 minutes was taken throughout the tests for the determination of the void ratio, e. (From testing, it was found that primary settlement was finished by this time.) The small initial compression that occurs immediately as a load is applied to the soil was included in the deflections[2].

Fig. **A.1.6** shows some typical consolidation curves. These curves were transformed to the well-known root-time and log-time plots for graphical determination of c_v.

Table A.1.1. Oedometer compression, recompression and swelling indeces

	Test O – intact till	Test E – intact till	Test R – reconstituted till
C_c	0·087	0·069	0·112, 0·117*
C_s	0·012	0·008	0·023
C_e		0·007	
E_{oed} (MNm^{-2})	28·78	36·69	
E_{ur}^{ref}		210·1	

* indicates an intrinsic property as defined by Burland (1990). Note, from the e-logσ_v' curves, that the value of C_c is not constant, particularly at low effective stresses. However, it was possible to determine C_c with some accuracy from the readings at very high pressure, which is what is shown in this table.

A.1.2 Oedometer Test E.

A.1.2.1 Aim and Details.

The main objective of this test was to re-establish the in situ stress-state of the lodgement till prior to measuring the soil stiffness. This test was, therefore, a static unload-reload test. Secondary objectives were as for Test O. In addition, this, undisturbed, test was to be compared with the equivalent reconstituted test.

[1] E_{oed} is generally measured as a tangent to the primary curve at $\sigma_v' = 100\ kNm^{-2}$ (see Fig. **2.5.11**), which is below the minimum pressure applied in the tests. However, the tangent to the curve was found to extend over a wider range.

Soil location: Dublin Port tunnel access shaft. From depth 17 m BGL. $\sigma_{v0}' = 269$ kNm^{-2}.
Sample dimensions: $H_0 = 26{\cdot}5$ mm, D = 102 mm.

A.1.2.2 Test Results.

The test time was 58 days. The test results are plotted on the same figures and table as Test O. In addition, Fig. **A.1.7** shows the detail of the unload-reload loops on stress-strain axes.

A.1.3 Oedometer Test R.

A.1.3.1 Aim and Details.

The main objective of this test, which was a reconstituted soil test, was as a control to aid in the understanding of the behaviour of the intact till, measured previously. The test method was static unload-reload, as for Test E.

Soil location: Dublin Port tunnel access shaft. From depth 13·3 m BGL. $\sigma_{v0}' = 260$ kNm^{-2}.
Sample dimensions: $H_0 = 34$ mm, D = 102 mm.

A.1.3.2 Test Results.

The e-logσ_v' curve is plotted on Fig. **A.1.8**. Typical time-settlement plots are given in Fig. **A.1.9** and the remaining results are given in Table **A.1.1**.

[2] This is considered good practice in stiff glacial soils (Danish Geotechnical Institute - see Steenfelt (1997)).

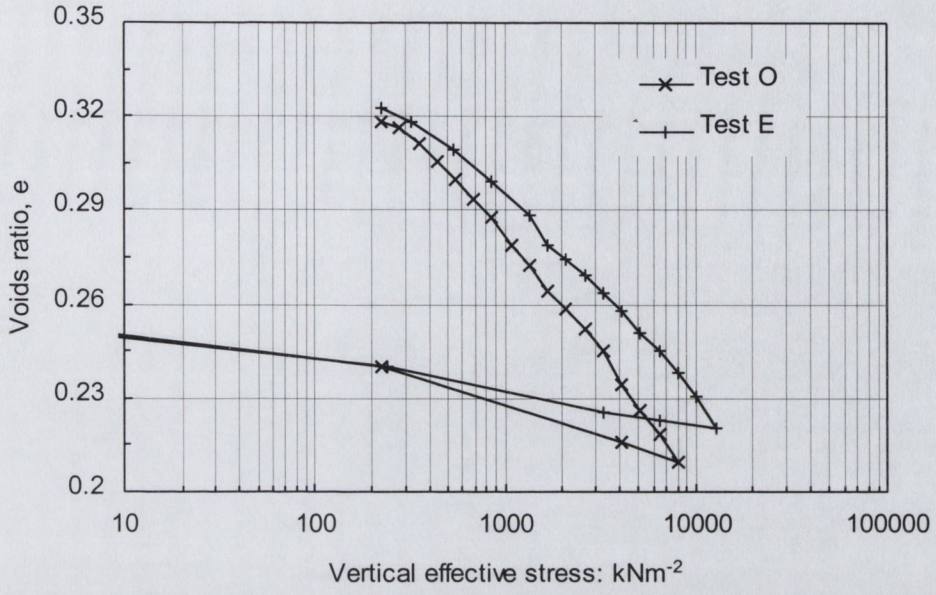

Fig. A.1.1. Consolidation curves of undisturbed oedometer tests (note that the unload-reload loops of Test E are not plotted)

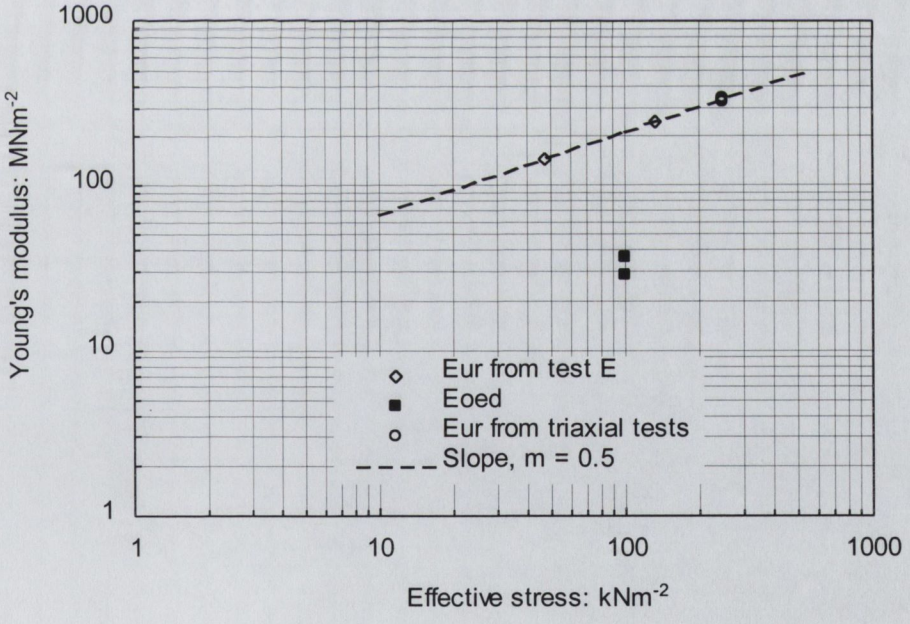

Fig. A.1.2. Stiffness parameters

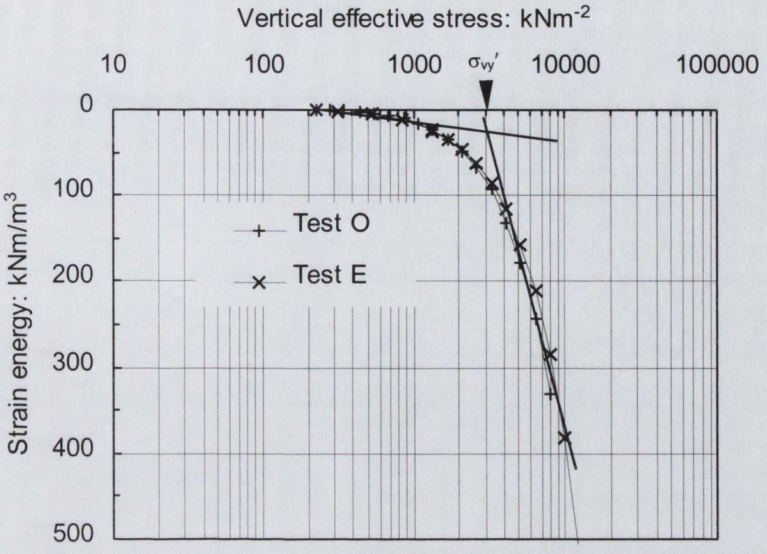

Fig. A.1.3(a). Methods of measuring σ_{vy}': (a) Tavenas et al. (1979)

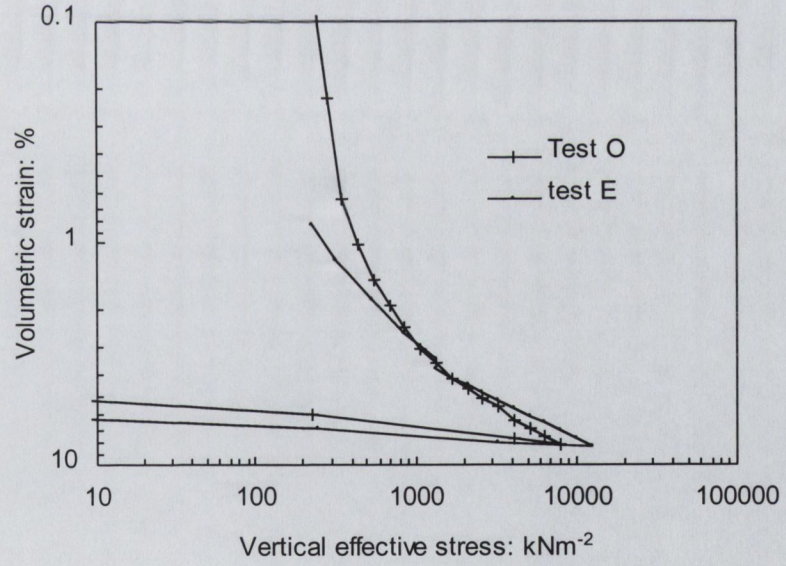

Fig. A.1.3(b). Methods of measuring σ_{vy}': (b) Butterfield (1979)

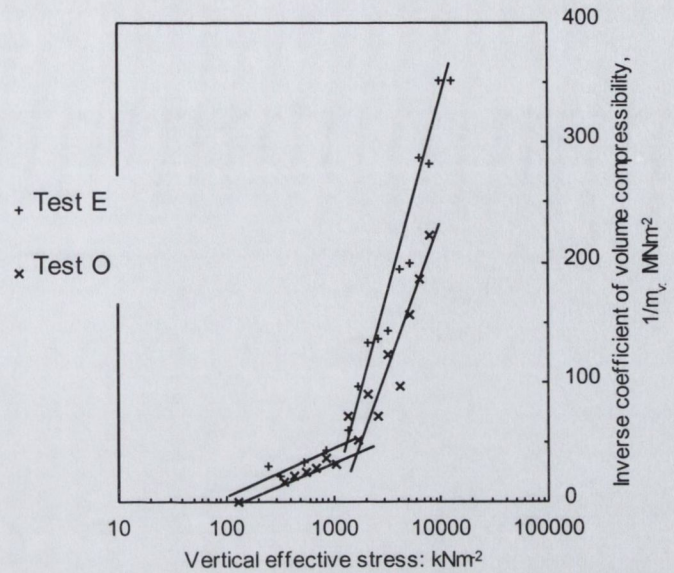

Fig. A.1.3(c). Methods of measuring σ_{vy}': (c) Janbu (1991)

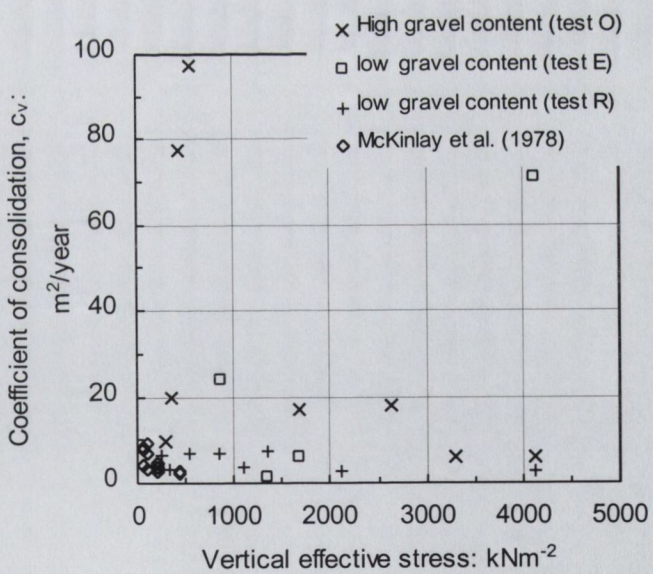

Fig. A.1.4. Coefficient of consolidation

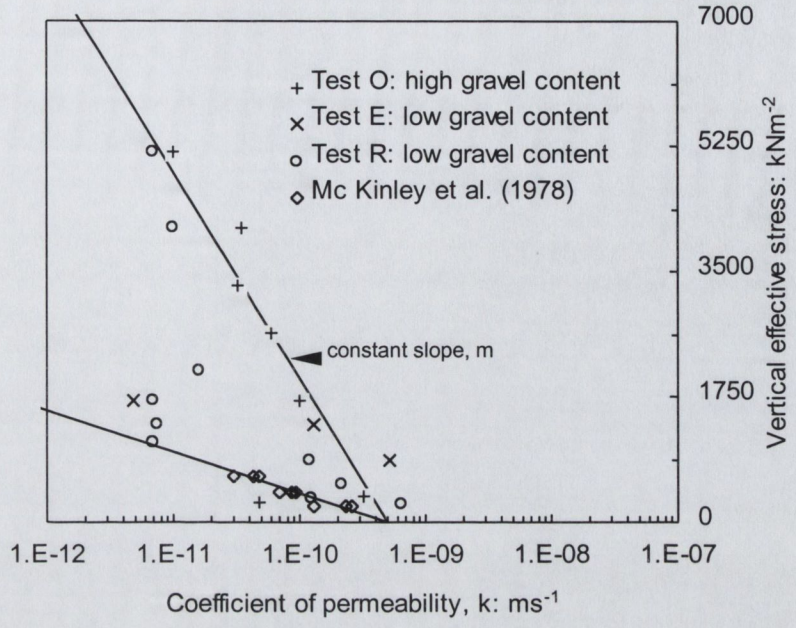

Fig. A.1.5. Coefficient of permeability change with vertical effective stress

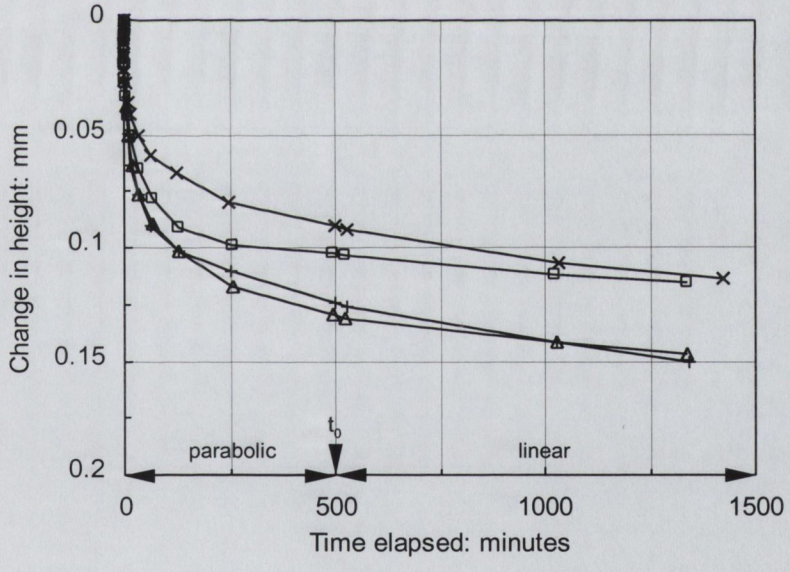

Fig. A.1.6. Typical time-settlement plots

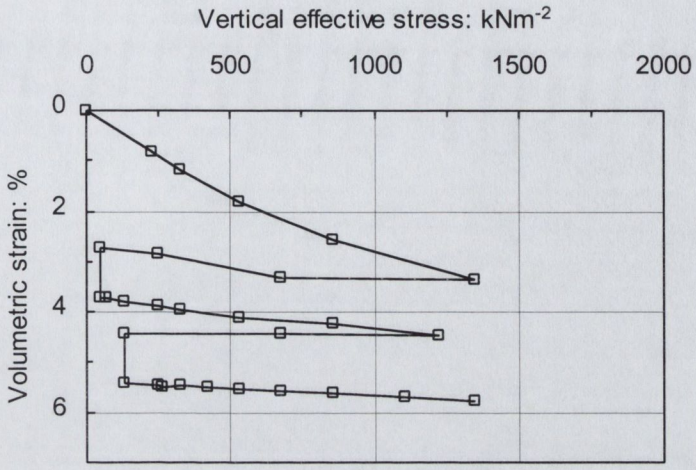

Fig. A.1.7. Detail of unload-reload curves of Test E (note that the loops have been separated out for clarity; i.e. the curves do not show creep settlement)

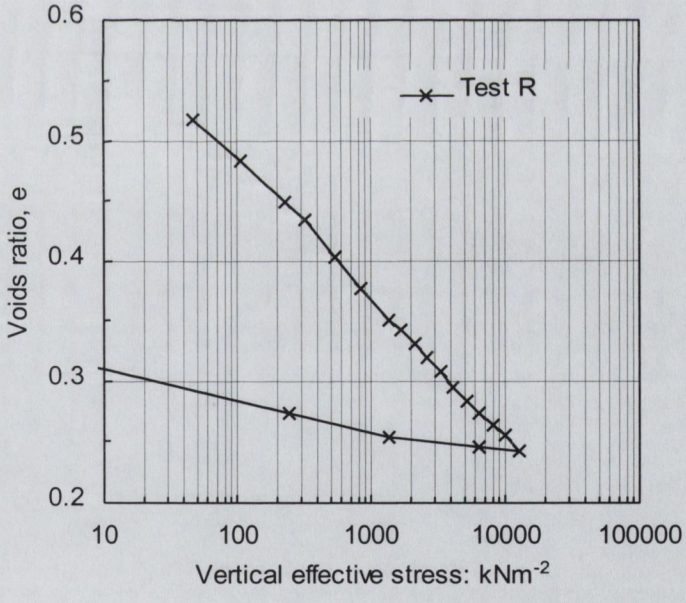

Fig. A.1.8. Reconstituted oedometer Test R (note that the unload-reload loops have been removed)

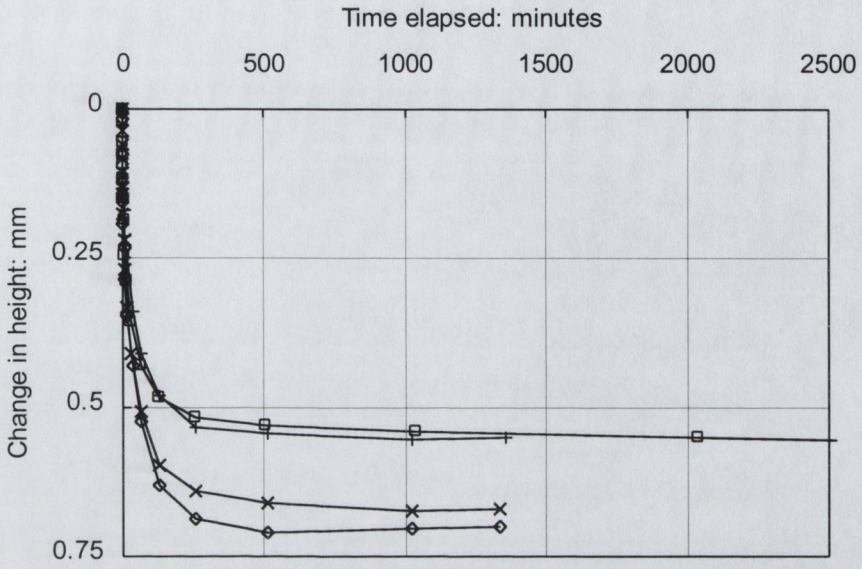

Fig. A.1.9. Typical time-settlement curves for reconstituted soil

A.2 Triaxial Testing.

A.2.1 Triaxial Test BE1 (CIRD).

A.2.1.1 Aim and Details.

The primary objective of the test was to determine the G_{max} variation for intact boulder clay, isotropically consolidated to a mean effective stress theoretically equivalent to R_p and swelled back to the in situ mean effective stress (CIRD test). Secondary objectives were to determine the stiffness, deformation and peak and residual strength properties of the lodgement till.

Soil location: Ballinteer Rd., Dundrum. From depth 8·1 m BGL. $\sigma_{v0}' = 120$ kNm^{-2}. Sample dimensions: $H_0 = 206{\cdot}2$ mm, $D_0 = 102$ mm.

A.2.1.2 Test Results.

A.2.1.2.1 Pre-Tests.

The B-test following saturation gave a Skempton factor, B, of 0·895, which was close to 100% saturation for very stiff soil (see Black and Lee (1973), as given by Head (1998)).

A.2.1.2.2 Bender Element Tests and Isotropic Consolidation.

The ends of the specimen were trimmed in a split-former, giving an exact initial height, H_0, of 206·2 mm and, therefore, an exact L_e. The soil was consolidated in 250 kNm^{-2} stages near to the estimated isotropic OCR, R_p (i.e. $p_{pc}' = 900$ kNm^{-2}). BE tests were conducted at the end of each stage to give the variation of G_{max} with stress level. The density used at each consolidation stage in the calculation of G_{max} was the saturated density, back-analysed from the final mass and the net volume change. Alternatively, the sample was weighed before the test and zero change in volume was assumed in the saturation stage and the density change was found from the volume change.

The results of the tests are shown, on Fig. **A.2.1**, as the logarithm of the maximum shear modulus, G_{max}, against the logarithm of effective cell pressure and Fig. **A.2.2** shows the specific against the logarithm of effective cell pressure, v-$\log_{10}p'$. The values of G_{max} shown were generally taken as an average of five to seven waves generated at each stress level. Linear regression was performed on the data shown in Fig. **A.2.1** thus: the slope of the lines, m, shown are 0·513 (load) and 0·436 (unload). The isotropic consolidation and swelling tests gave an isotropic compression index, λ, of 0·0326 and an isotropic swelling index, κ, of 0·0056.

BE tests were run at the start of shearing. Owing to the rapid decrease of stiffness at small strains, an arbitrary waveform, which included more than one waveform, was developed, of the form given in Table **4.4.1**.

A.2.1.2.3 Shearing.

In the absence of an extension top cap, the sample was manually brought into contact with the piston prior to shearing. It is noted that the water filled cell aided in the procedure (as opposed to opaque oil). Nevertheless, it was difficult to dock the sample without exceeding the docking point. The soil was subsequently sheared at a constant rate of 0·001%/min. Unload and reload stages were conducted at the same, slow, rate. Fig. **A.2.3** shows the test stress-strain curve, including the unload-reload loops.

A.2.1.2.4 Stiffness.

E_{ur} was determined from the unload-reload curves shown in Fig. **A.2.3**, based on the definition shown in Fig. **2.5.12**. (Note that the length of the loops were sufficient to allow E_{ur} to be well defined.) The results are plotted on the double logarithmic plot, of stiffness versus effective stress, in Fig. **A.2.4**. As the curve is essentially hyperbolic, E_{50} was found[1], which is plotted on Fig. **A.2.4**. E_0' was found from the linear initial section of the stress-strain curve, prior to the threshold strain, and is also plotted on Fig. **A.2.4**. The threshold axial strain was measured as 0·007%. The stiffness degradation curves for inferred local and external strain measurement are shown in Fig. **A.2.5**. Also shown on Fig. **A.2.5** are BE tests conducted at the start of shearing.

[1] See Section 2.9.1.3.

A.2.1.2.5 Strength and Dilatancy.

The failure condition is plotted in Fig. **A.2.6**, along with other triaxial data. The failure condition was $\phi' = 41{\cdot}7°$, $q_f = 960{\cdot}1$ kNm^{-2}, $p_f' = 570$ kNm^{-2} and $\varepsilon_{af} = 2{\cdot}91\%$. The test was continued to an axial strain of 6·4%, in an attempt to determine the residual condition, giving the effective residual angle, ϕ_r', of 32·6°. R_f was back-calculated as 0·835. The failure mode was in classical shear with some barrelling. The angle of the shear plane was measured at about 49°.

The dilatancy characteristics are plotted as a graph of volumetric strain against shear strain in Fig. **A.2.7**. (Note that the strain is entirely dilative.) The peak dilation angle, ψ, interpreted from the line of constant slope, was 3·3°.

A.2.2 Triaxial Test BE4 (CK_0RD).

A.2.2.1 Aim and Details.

The objective of the test was to determine the stress-strain, stiffness and strength characteristics of K_0 consolidated lodgement till, with a stress-history reconstruction based on the value of σ_{vy}' measured in the oedometer tests (CK_0RD test).

Soil location: Ballinteer Rd., Dundrum. From depth 6·32 m BGL. $\sigma_{v0}' = 102$ kNm^{-2}. Sample dimensions: $H_0 = 193{\cdot}2$ mm, $D_0 = 102$ mm.

A.2.2.2 Test Results.

A.2.2.2.1 Pre-Tests.

A filter paper leak occurred initially, which meant that the test had to be stopped and the filter paper carefully readjusted. This problem did not affect the test. The B-test, following saturation, gave a Skempton factor, B, of 0·95, for the cell pressure increment 100-200 kNm^{-2}, which is considered more accurate than the B-value of 0·87, obtained for the increment

5–100 kNm^{-2}. B = 0·95 is close to 100% saturation for very stiff soil (Black and Lee (cited), as given by Head (cited)).

A.2.2.2.2 Bender Element and Consolidation Tests.

The soil was consolidated in 50 kNm^{-2}, effective stress, increments up to 150 kNm^{-2}, followed by K_0 consolidation to an effective vertical stress of about 1400 kNm^{-2}. (although this is less than the estimated yield stress of the till, the unloading stage was actually started at $\sigma_v' \approx 1300$ kNm^{-2} but the, computer controlled, cell pressure continued to rise before reducing.) The soil was then K_0 unloaded to a mean effective stress equal to the effective confining stress, namely 250 kNm^{-2}. The test was stopped and the cell pressure and back pressure controllers were targeted to the effective confining stress (250 kNm^{-2}) for the subsequent shearing stage. (Note that little or no excess pore water pressure was generated by targeting the controllers.) The K_0 consolidation stage is shown in Fig. **A.2.8**. BE tests were conducted at the end of the isotropic stages and at intervals during the K_0 consolidation stage. The radial strains during the K_0 consolidation stage remained below 0·001%, as can be seen in Fig. **A.2.9**. The results of the BE tests are shown, on Fig. **A.2.10**, as the logarithm of the shear modulus, G_{max}, against the logarithm of the vertical effective stress, in K_0 consolidation and swelling stages.

A.2.2.2.3 Shearing.

No docking of the sample was necessary because of the vertical load on the soil at the end of the consolidation stage. The deviator stress in the sample prior to shearing was 115·5 kNm^{-2}. Only one unload-reload loop could be conducted between yield and failure.

A.2.2.2.4 Stiffness[2].

Fig. **A.2.11** shows the test stress-strain curve, including the unload-reload loop. E_{ur} was determined from this loop and the results are plotted on Fig. **A.2.4**[3]. The stiffness degradation curves, for inferred local and external strain measurement, are shown in Fig. **A.2.12**.

---

[2] E_{50} and R_f could not be determined from the curve because it is not hyperbolic: see Section 2.9.1.3.

[3] Note that E_{ur} is about identical to that measured in Test BE1.

A.2.2.2.5 Strength and Dilatancy.

The failure condition, plotted on Fig. **A.2.6**, was $\phi' = 37{\cdot}6°$, $q_f = 783$ kNm^{-2}, $p_f' = 511$ kNm^{-2} and $\varepsilon_{af} = 2{\cdot}2\%$. (The strength includes the deviator stress in the sample prior to shearing.)

The dilatancy characteristics are plotted as a graph of volumetric strain against shear strain in Fig. **A.2.13**. The peak dilation angle, ψ, interpreted from the line of constant slope, was 3·4°.

A.2.2.2.6 K_0.

The K_0-OCR relation measured in the test is shown in Fig. **A.2.14**, along with other test data.

A.2.3 Triaxial Test T1 (CK_0RD-reconstituted).

A.2.3.1 Aim and Details.

The objective of the test was to determine the stress-strain, stiffness and strength characteristics of K_0 consolidated reconstituted lodgement till (CK_0RD-reconstituted) for comparison with test BE4.

Soil location: Griffith Avenue, Marino (disturbed sample).

A.2.3.2 Test Results.

A.2.3.2.1 Pre-Tests.

The initial (prior to saturation) B-value of the soil was 0·96 (second increment – see Test BE4).

A.2.3.2.2 K_0 Consolidation.

The soil was K_0 consolidated from an effective confining stress of 5 kNm^{-2}. The vertical effective stress reached 1900 kNm^{-2} before the second stage was started. K_0^{nc} was measured,

from the slope of the line in Fig. **A.2.15**, as 0·47. The K_0 against OCR relation is shown in Fig. **A.2.14**. The remainder of the test was conducted in the same way as Test BE4. The radial strains during the K_0 consolidation stage did not exceed 0·003%.

A.2.3.2.3 Shearing.

The soil was sheared to large strain to determine the residual condition. Fig. **A.2.16** shows the test stress-strain curve.

A.2.3.2.4 Strength and Dilatancy.

The failure condition was $\phi' = 37{\cdot}8°$, $q_f = 791{\cdot}7$ kNm^{-2}, $p_f' = 513{\cdot}9$ kNm^{-2} and $\varepsilon_{af} = 0{\cdot}491\%$. The residual condition was: $q_{cv} \approx 750$ kNm^{-2}, $\phi_{cv}' = 36{\cdot}8°$.

The dilatancy characteristics are plotted as a graph of volumetric strain versus shear strain in Fig. **A.2.17**. The peak dilation angle, ψ, interpreted from the line of constant slope, was 1·3°.

A.2.4 Triaxial Test SS1 (CK_0RD).

A.2.4.1 Aim and Detials.

This test, conducted on lodgement till, a CK_0RD compression test with local axial (LVDT) strain measurement, was intended both for comparison with Test BE4 and to obtain very accurate small strain data.

Soil location: Ballinteer Rd., Dundrum. From depth 8·95 m BGL. $\sigma_{v0}' = 130$ kNm^{-2}. Sample dimensions: $H_0 = 175$ mm, $D_0 = 102$ mm.

A.2.4.2 Test Results.

A.2.4.2.1 Pre-Tests.

The till had a very low initial Skempton B-value of 0·62. The soil was then saturated under a back pressure of 170 kNm^{-2}, giving a B-value of 0·87. The soil was further saturated under a back pressure of 280 kNm^{-2}, giving a final B-value of 0·95. (Note that in the K_0 consolidation stage, the cell pressure can be very high, close to the capacity of the cell. Therefore, it was necessary to keep the back pressure as low as possible in the saturation stage.)

A.2.4.2.2 K_0 Consolidation.

The rate of stress in the K_0 stage was 0·167 kNm^{-2}/min to ensure fully drained K_0 loading/unloading, as the sample was draining from the end platen and not the sides. The maximum vertical effective stress applied in the test was 1075 kNm^{-2}, which was lower than Test BE4, to test for the effect of the magnitude of the consolidation stress on the subsequent shearing characteristics.

A.2.4.2.3 Shearing.

The deviator stress in the sample immediately before shearing was 247 kNm^{-2}. The test stress-strain curve is shown in Fig. **A.2.18**.

A.2.4.2.4 Stiffness[4].

The stiffness degradation curves for measured local, inferred local and external strain measurements are shown in Fig. **A.2.19**.

A.2.4.2.5 Strength and Dilatancy.

The failure condition, plotted on Fig. **A.2.6**, was $\phi' = 36°$, $q_f = 712{\cdot}8$ kNm^{-2}, $p_f' = 660{\cdot}3$ kNm^{-2} and $\varepsilon_{af} = 4{\cdot}09\%$. (The strength includes the deviator stress in the sample before shearing.)

The dilatancy characteristics are plotted as a graph of volumetric strain against shear strain in Fig. **A.2.20**. The peak dilation angle, ψ, was $1{\cdot}6°$.

[4] E_{50} and R_f could not be determined from the curve because it is not hyperbolic: see Section 2.9.1.3.

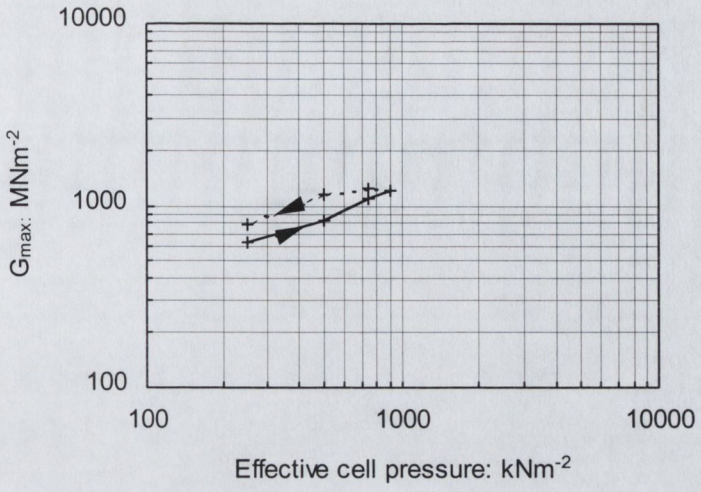

Fig. A.2.1. G_{max} versus isotropic effective stress: Test BE1

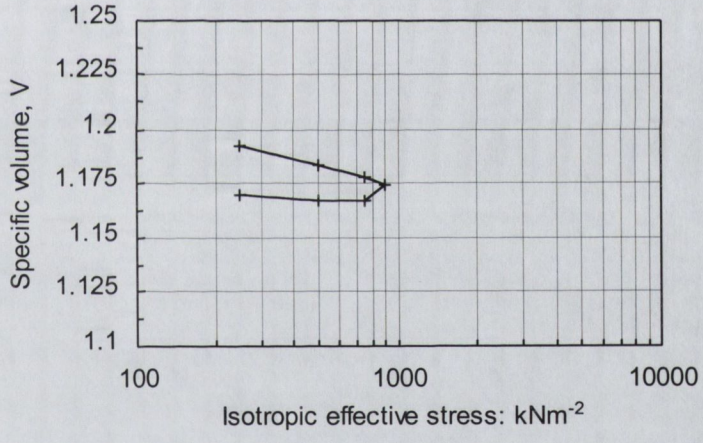

Fig. A.2.2. Isotropic consolidation: Test BE1

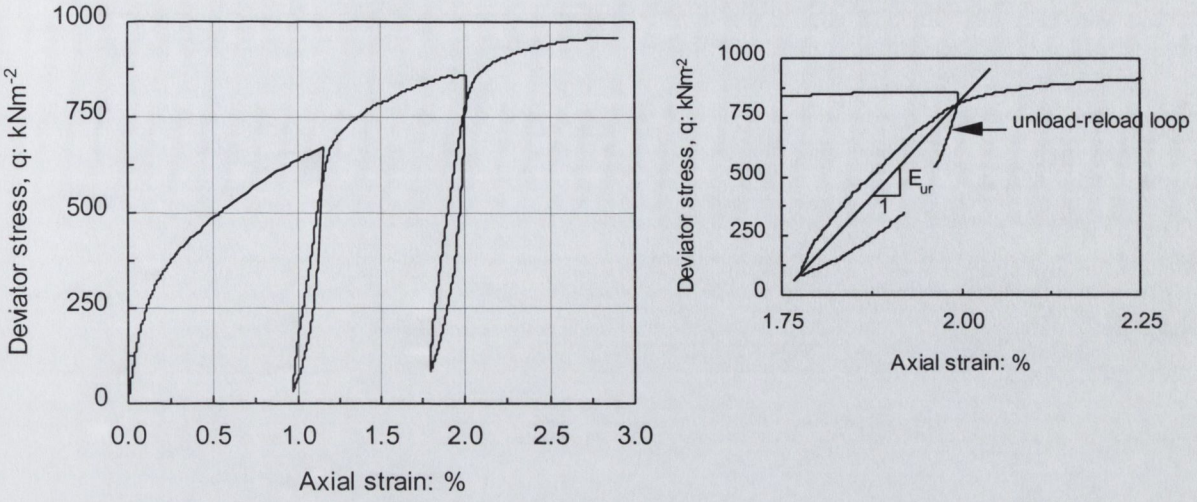

Fig. A.2.3. Deviator stress against axial strain for Test BE1

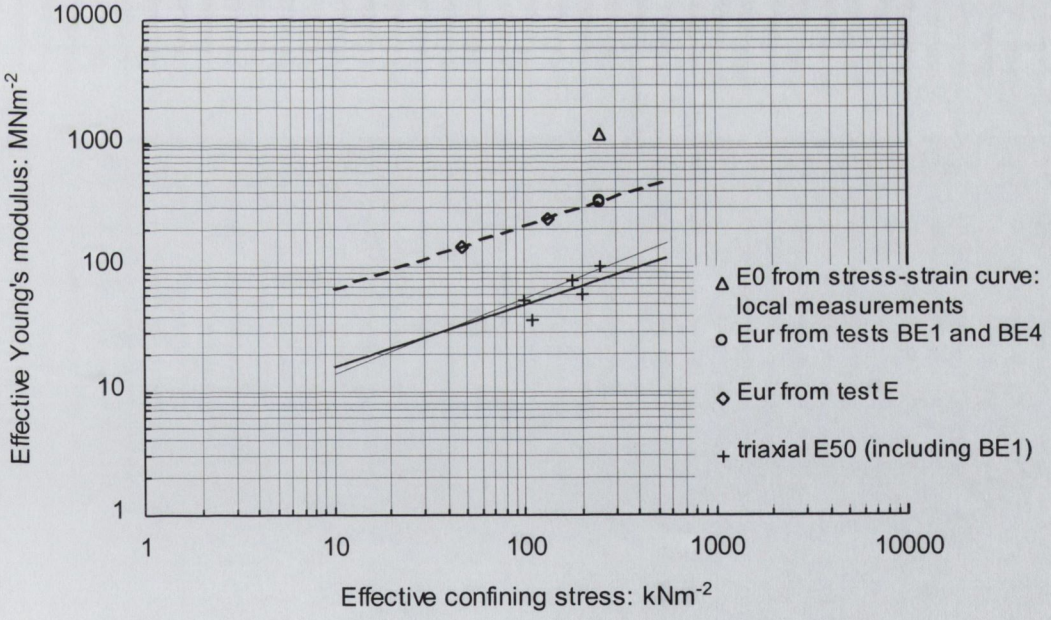

Fig. A.2.4. Stiffness data from triaxial Test BE1

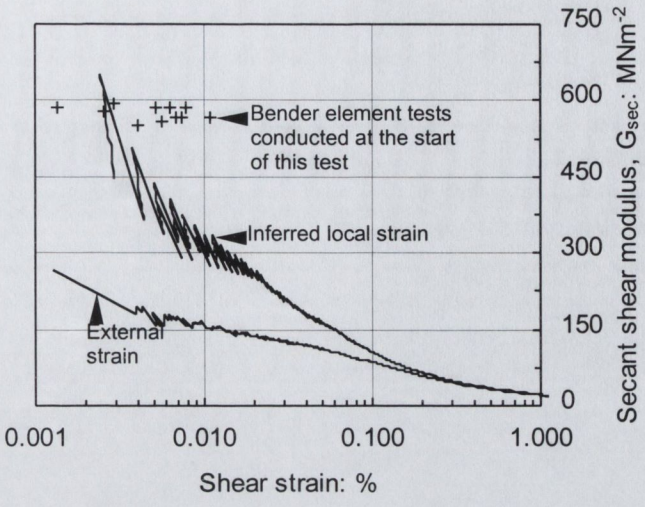

Fig. A.2.5. Stiffness data and stiffness degradation for Test BE1

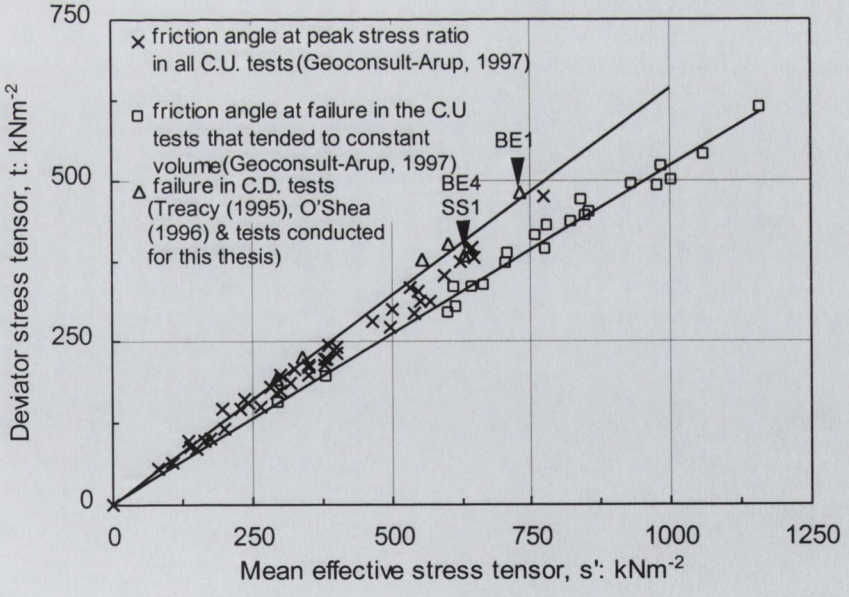

Fig. A.2.6. Shear strength data

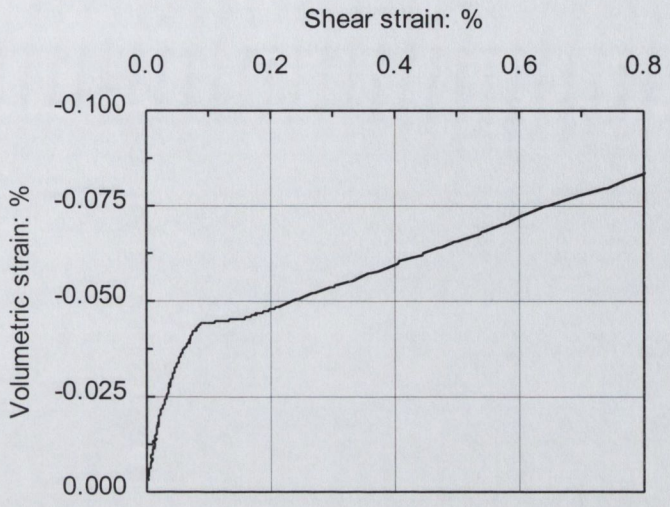

Fig. A.2.7. Volumetric strain (dilative) against shear strain for Test BE1

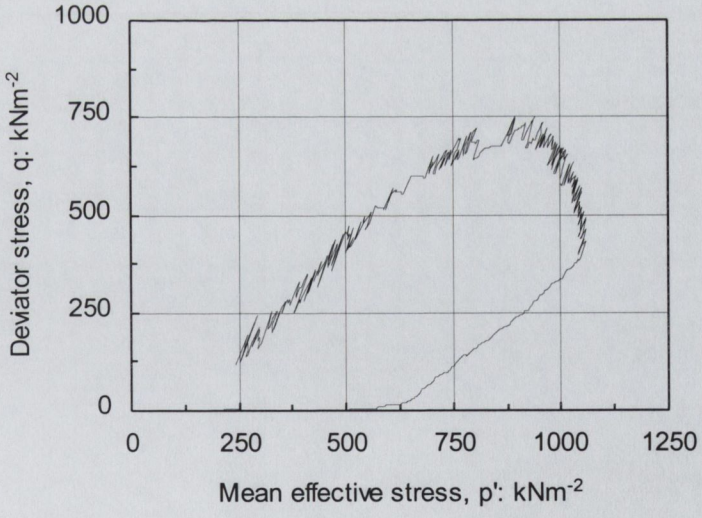

Fig. A.2.8. K_0 consolidation stress-path in Test BE4

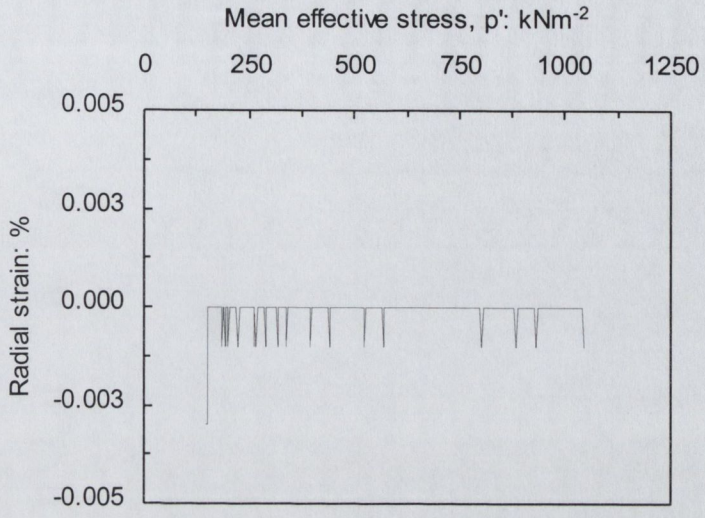

Fig. A.2.9. Radial strain measured in K_0 consolidation stage of Test BE4

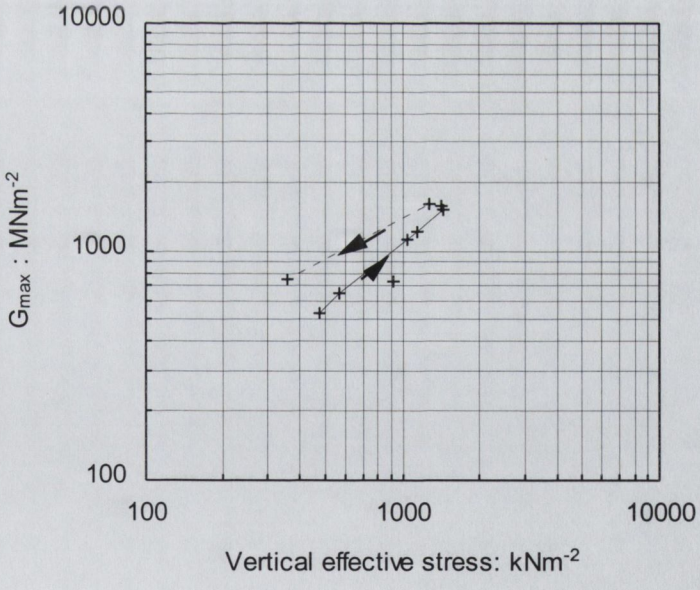

Fig. A.2.10. G_{max} against vertical effective stress in K_0 consolidation/swelling stage: Test BE4

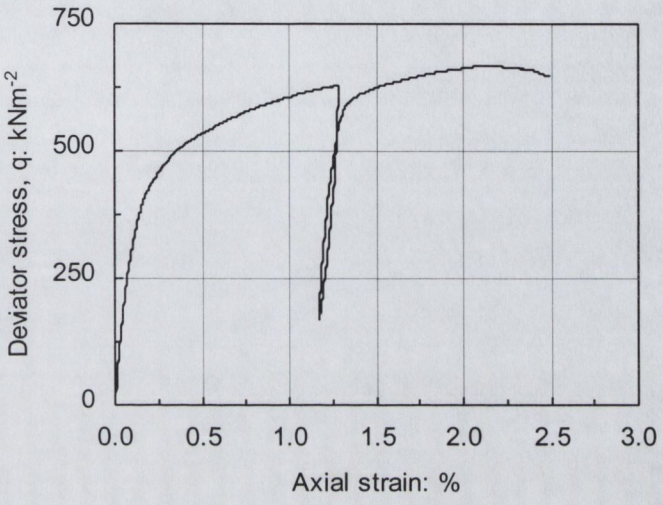

Fig. A.2.11. Deviator stress against axial strain curve of Test BE4

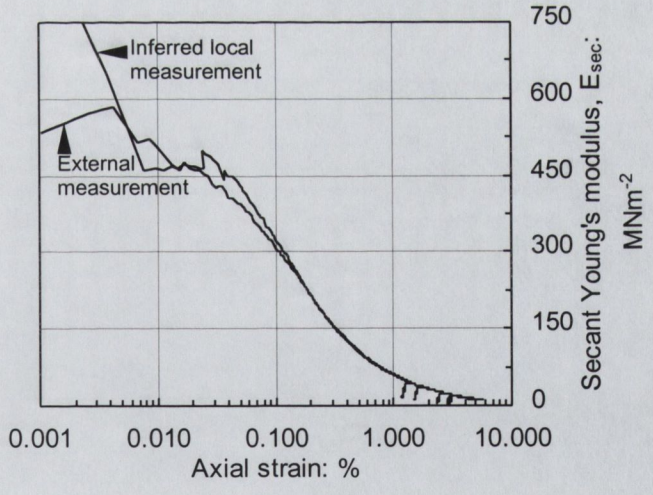

Fig. A.2.12. Stiffness degradation curves for Test BE4

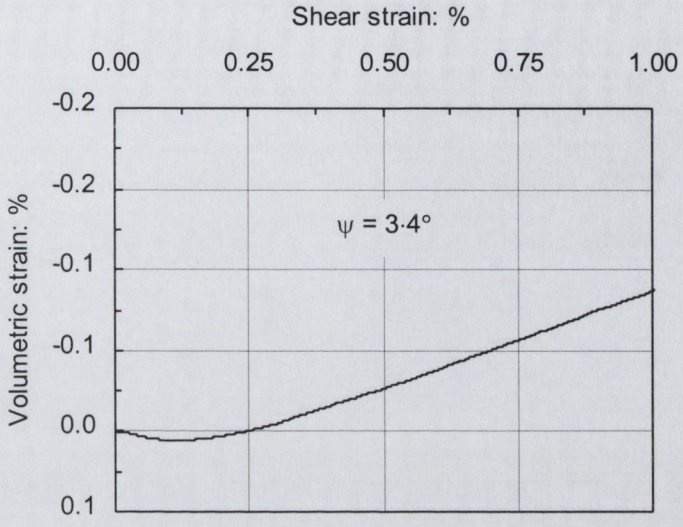

Fig. A.2.13. Shear strain against volumetric strain for Test BE4

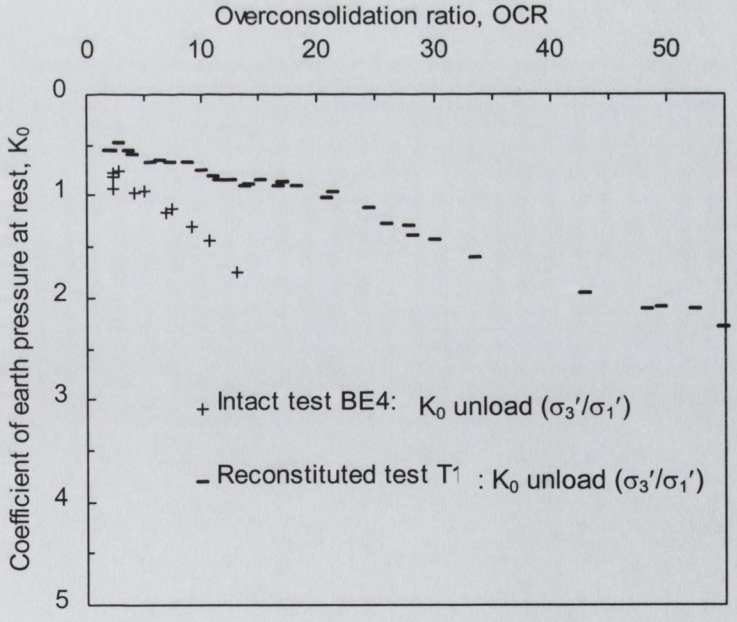

Fig. A.2.14. K_0 data measured in the triaxial tests

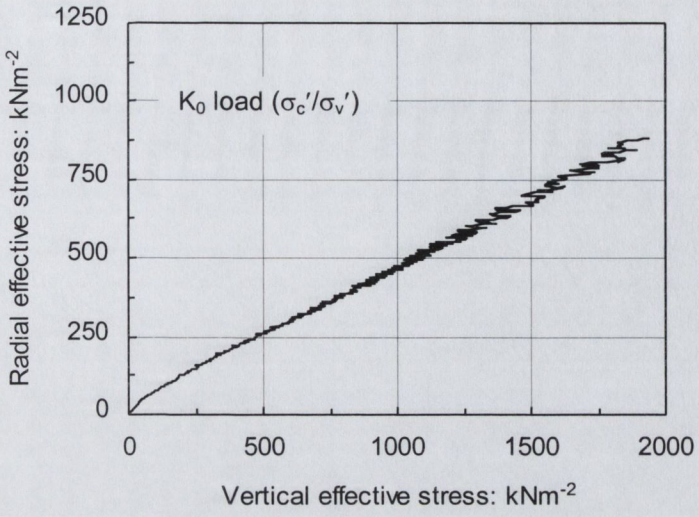

Fig. A.2.15. Radial effective stress against vertical effective stress for K_0 load stage of reconstituted Test T1

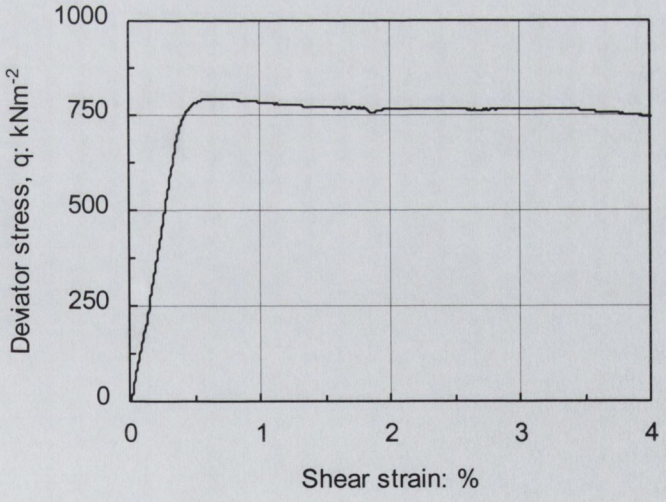

Fig. A.2.16. Stress-strain curve of reconstituted Test T1

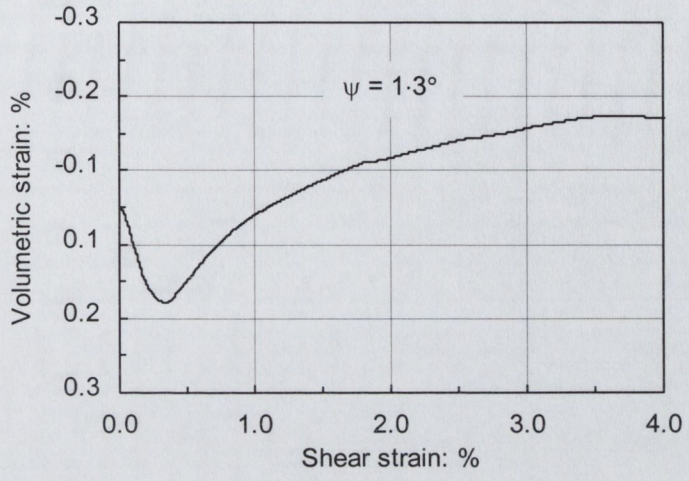

Fig. A.2.17. Shear strain against volumetric strain for Test T1

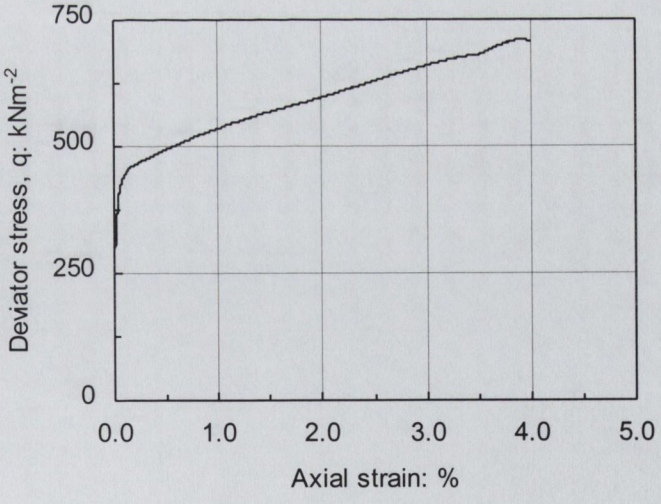

Fig. A.2.18. Stress-strain curve of Test SS1

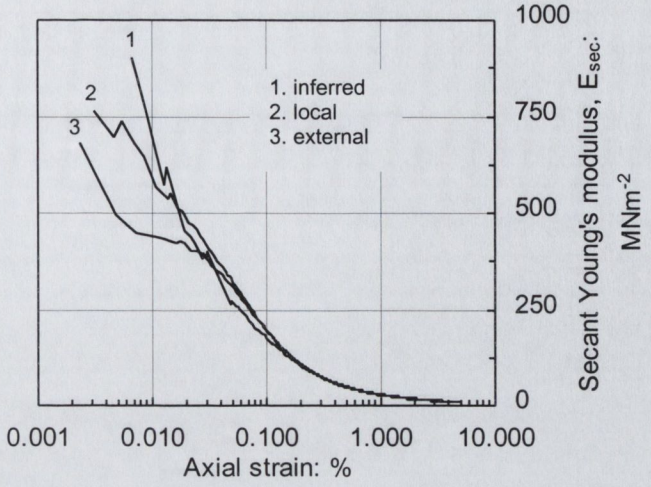

Fig. A.2.19. Comparison of methods of strain measurement in the triaxial test (Test SS1)

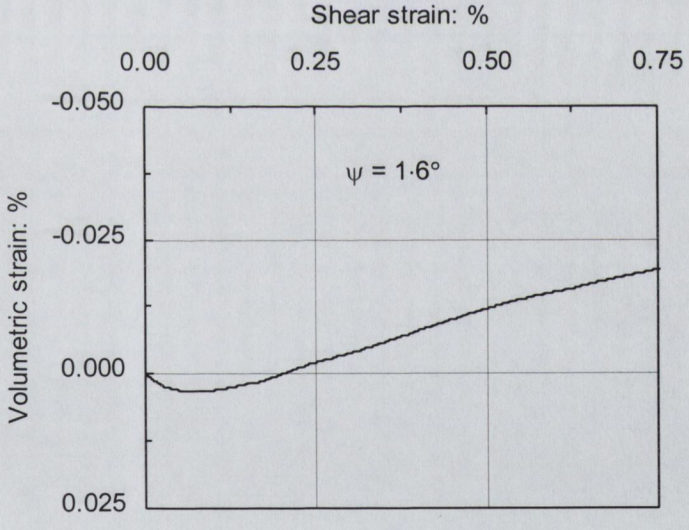

Fig. A.2.20. Compression-dilation characteristics measured in Test SS1

A.3 Soil Suction.

A.3.1 Test S1.

A.3.1.1 Test Details.

Test reference: S1. Soil description: Oxidised boulder clay from above the water table. Soil location: Donnybrook. From depth 1·3 m BGL. Sample dimensions: irregular. 3 No. cut papers in an irregular sized block of trimmed soil. Contact time: 7 days. Temperature fluctuation: 19·5 ± 1·5 °C.

A.3.1.2 Test Results.

Table A.3.1. Suction test results: unsaturated till

Paper	M_b (g)	M_{bw} (g)	M_{bd} (g)	M_b (g)	M_d (g)	w_p (%)	p_k (kNm^{-2})
1	3.0763	3.6201	3.3418	3.0787	0.2655	204.8211	2.0787
2	2.9870	3.7961	3.3710	2.9910	0.3840	210.7031	1.9377
3	3.0233	3.5987	3.2915	3.0275	0.2682	214.5414	1.8529

Mean 1·956 kNm^{-2}

M is mass; subscripts: b – bag, bw – bag and wet paper, bd – bag and dry paper, d – dry paper; w_p is the filter paper water content; p_k is the suction stress.

A.3.2 Test S2.

A.3.2.1 Test Details.

Test reference: S2. Soil description: Lodgement till from below the water table. Soil location: Ballinteer Rd., Dundrum. From depth 7·2 - 7·6 m BGL. Sample dimensions: 101·6 mm soil cylinder. 3 No. cut papers in trimmed soil. Contact time: 7 days. Temperature fluctuation: 18·5 ± 2·5 °C.

A.3.2.2 Test Results.

Table A.3.2. Suction test results: lodgement till

Paper	M_b (g)	M_{bw} (g)	M_{bd} (g)	M_b (g)	M_d (g)	w_p (%)	p_k (kNm^{-2})
1	3.2842	4.5547	4.0793	3.2832	0.7951	159.7912	3.8476
2	2.7894	3.4317	3.2012	2.7887	0.4118	155.9738	4.0854
3	2.8738	3.2680	3.1005	2.8733	0.2267	173.8862	3.1199

Mean 3·684 kNm^{-2}.

A.4 Microscopic and Mineralogical Soil Studies.

A.4.1 Qualitative XRD.

Qualitative XRD diffraction traces of lodgement till are shown in Figs. **A.4.1** and **A.4.2**, as intensity versus 2θ. The soils tested are described in Table **A.4.1** below. The reader is referred to Section 4.1 for a description of the soils.

Table A.4.1. Soils tested in XRD analysis

Test type	Test reference	Soil location	Soil description
Qualitative	XRD1	Griffith Avenue	Stiff black till
Qualitative	XRD2	Griffith Avenue	Grey brown stiff fissured till
Quantitative	QXRD1	Griffith Avenue	Stiff black till
Quantitative	QXRD2	UCD - 0·25 m BTL	Firm brown till
Quantitative	QXRD3	Dublin Port Tunnel	Stiff black till

A.4.2 Scanning Electron Microscope.

The SEM micrographs are shown in Figs. **A.4.3** thru' **A.4.17**. All the micrographs that were taken are shown, except those of very poor resolution and those that would be repetitious. The soils tested are described below.

A.4.2.1 Test EM1.

Test reference: EM1. Soil description: mottled brown unsaturated lodgement till. Soil location: UCD. From depth: 1·5 m BTL. Sample dimensions: irregular. Undisturbed lump. No coating.

A.4.2.2 Test EM2.

Test reference: EM2. Soil description: reddish brown deformation till. Soil location: UCD. From depth: 0·25 m BTL. Sample dimensions: irregular. Undisturbed lump. No coating.

A.4.2.3 Test EM3.

Test reference: EM3. Soil description: black lodgement till. Soil location: Dublin Port Tunnel. From depth: 13·3 m BGL. Sample dimensions: irregular. Undisturbed lump. No coating.

A.4.2.4 Test EM4.

Test reference: EM4. Soil description: black lodgement till. Soil location: Dublin Port Tunnel. From depth: 13·3 m BGL. Sample dimensions: irregular. Undisturbed lump. Au coating.

A.4.3 Quantitative XRD.

The results of the QXRD tests are given in Tables **A.4.2(a)** and **A.4.2(b)** (see Table **A.4.1** for description of soils), for the bulk sample and relative percentage of clay minerals present, respectively.

Table A.4.2(a). Results of quantitative analyses (percentage of mineral by weight) using the RIR method (Hillier, 2002)

Test	Quartz	Calcite	Illite	Kaolin	Expand-ables	K-feldspar	Plagio-clase	Dolo-mite	Geo-thite	Pyrite
QXRD 1	37·6	35·5	7·6	1	4·4	2·9	4·2	1·3	-	0·8
QXRD 2	33·9	45·4	8·2	-	5·2	-	2·5	-	1·5	-
QXRD 3	40·1	17·3*	11·7	4	4·3	3·6	5·2	1·4	-	-

* See Footnote 5 in Section 5.6.4.

Table A.4.2(b). Relative percentage of clay minerals in the sub-2 micron fraction

Test	Illite	Chlorite	Kaolin	Expandables
QXRD1	64	21	4	11
QXRD2	38	3	3	56
QXRD3	51	12	3	34

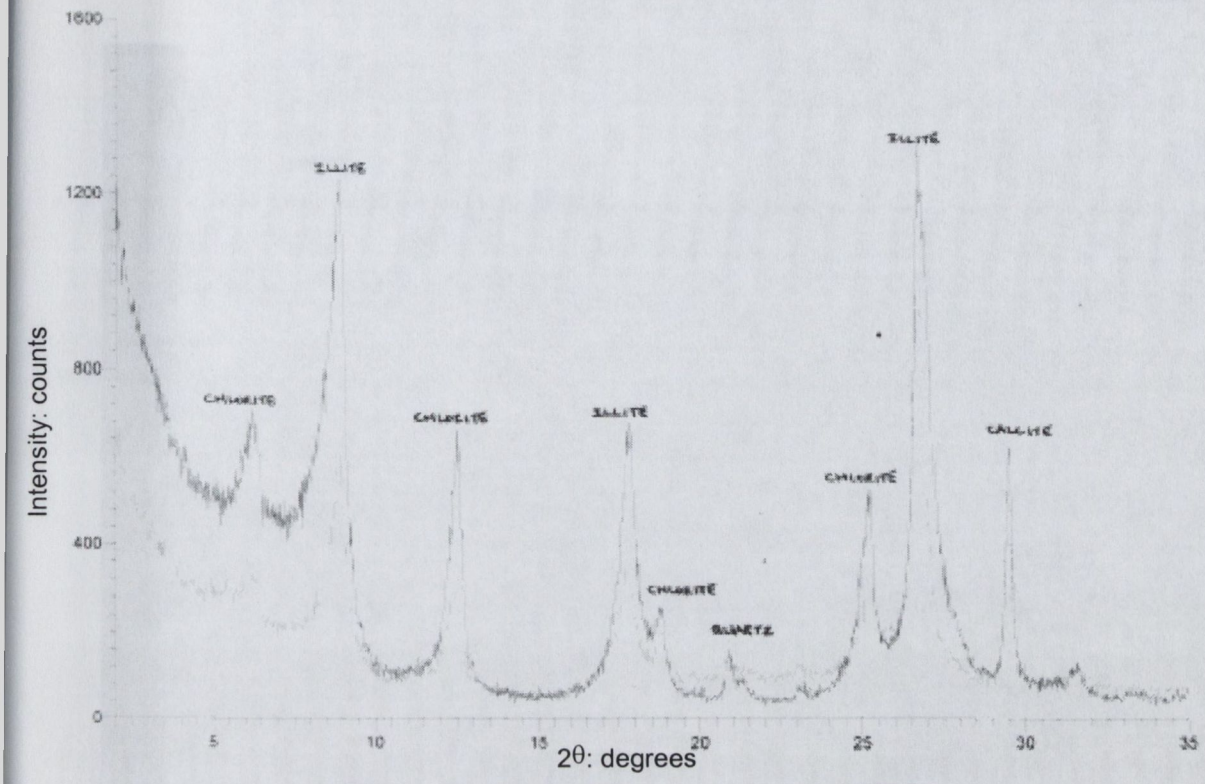

Fig. A.4.1. X-ray diffraction trace, Test XRD1

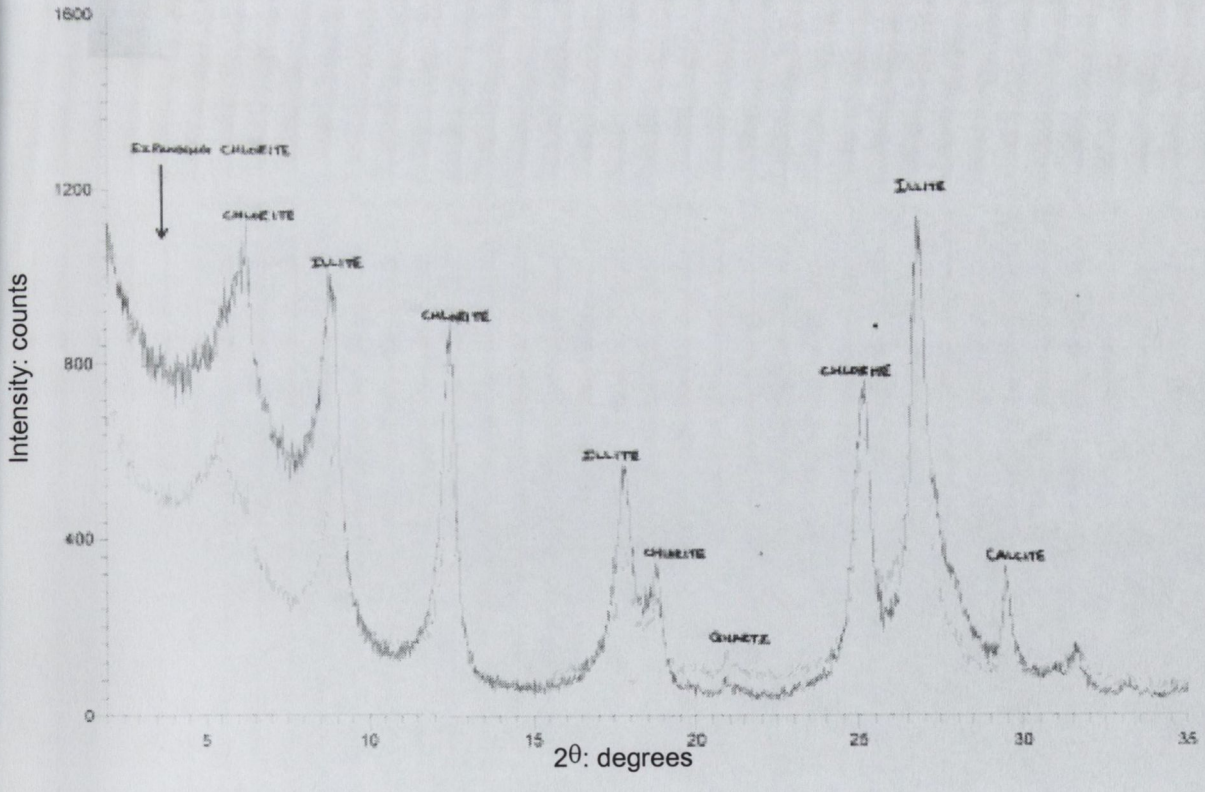

Fig. A.4.2. X-ray diffraction trace, Test XRD2

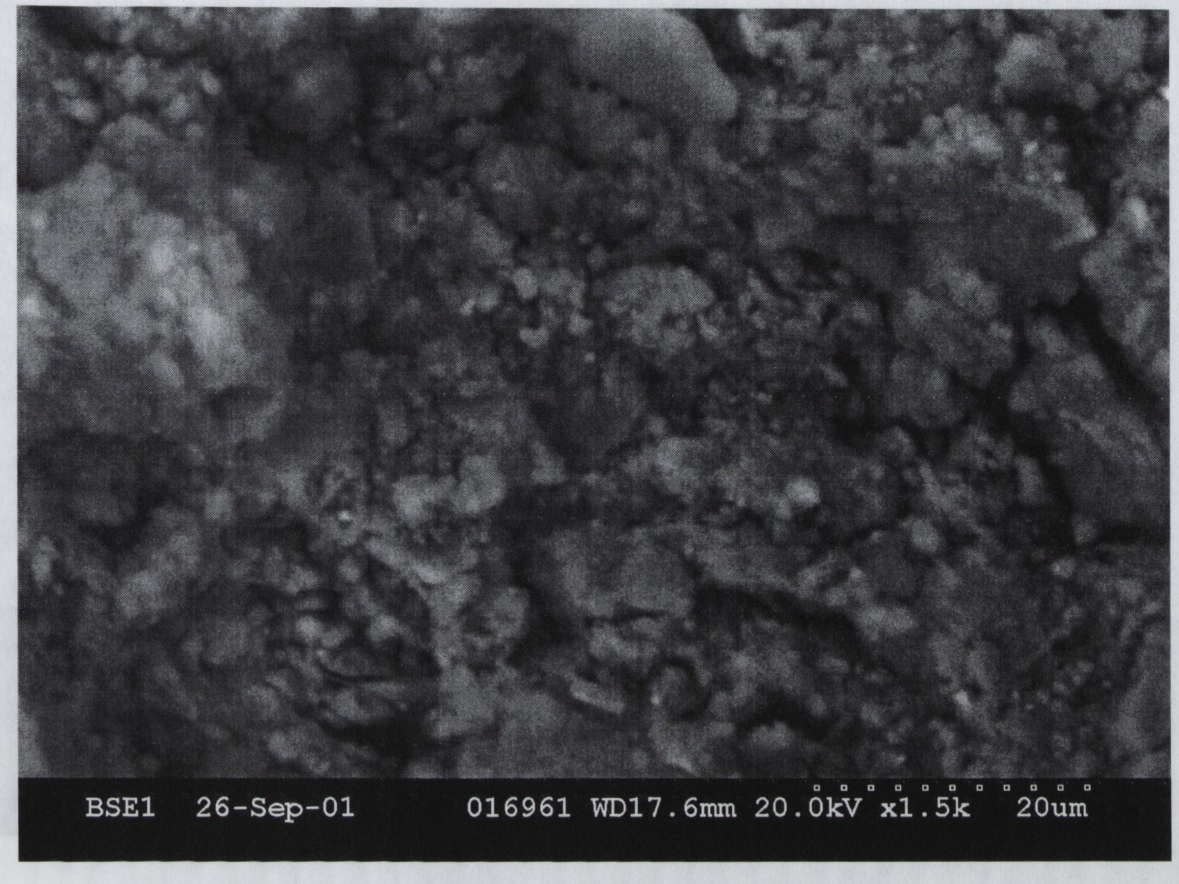

Fig. A.4.3. EM1: stiff mottled brown till

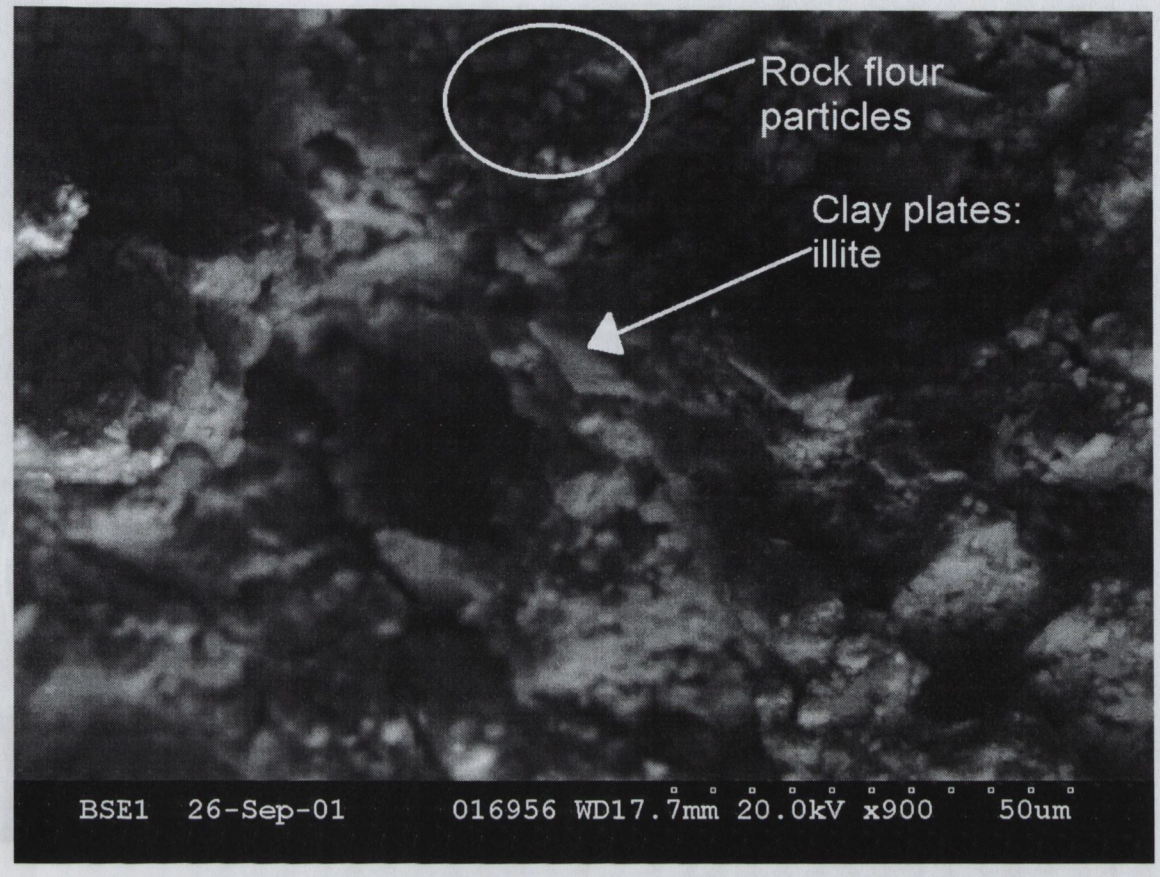

Fig. A.4.4. EM1: stiff mottled brown till

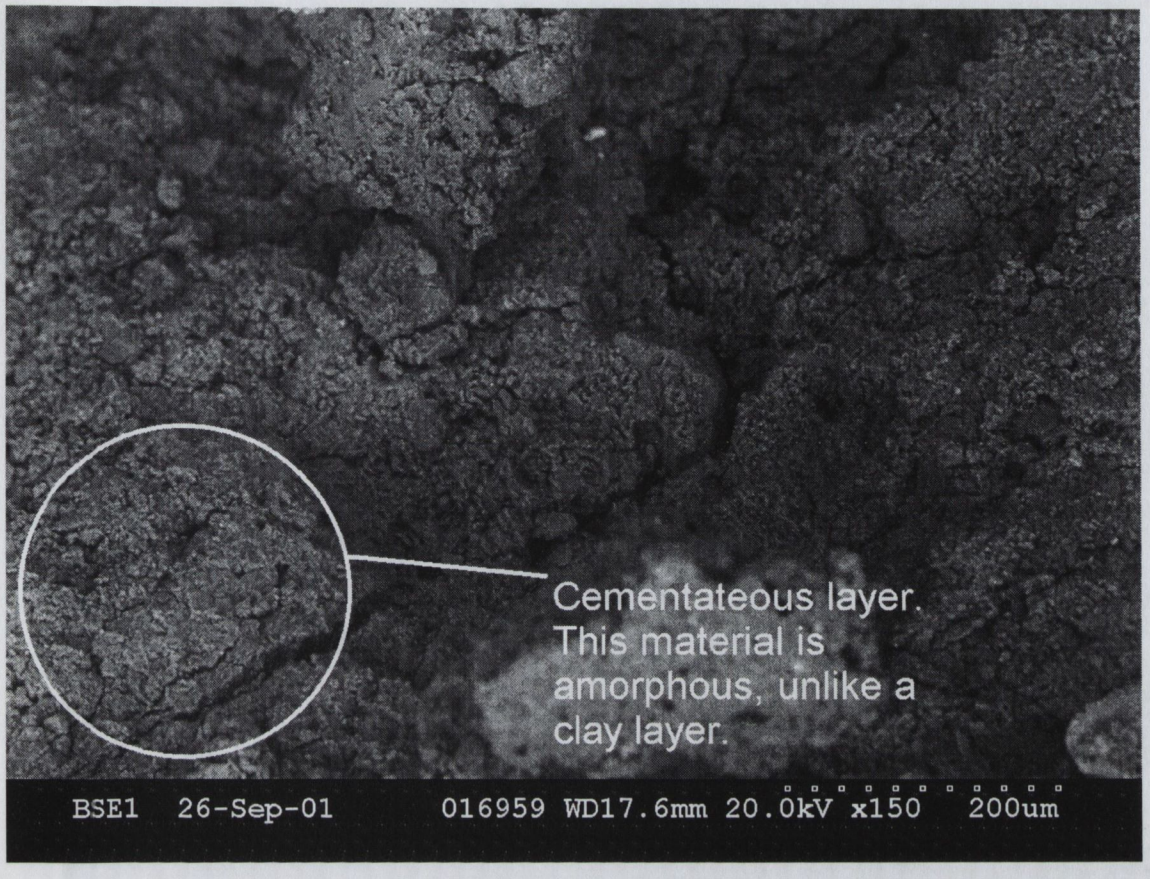

Fig. A.4.5. EM1: stiff mottled brown till

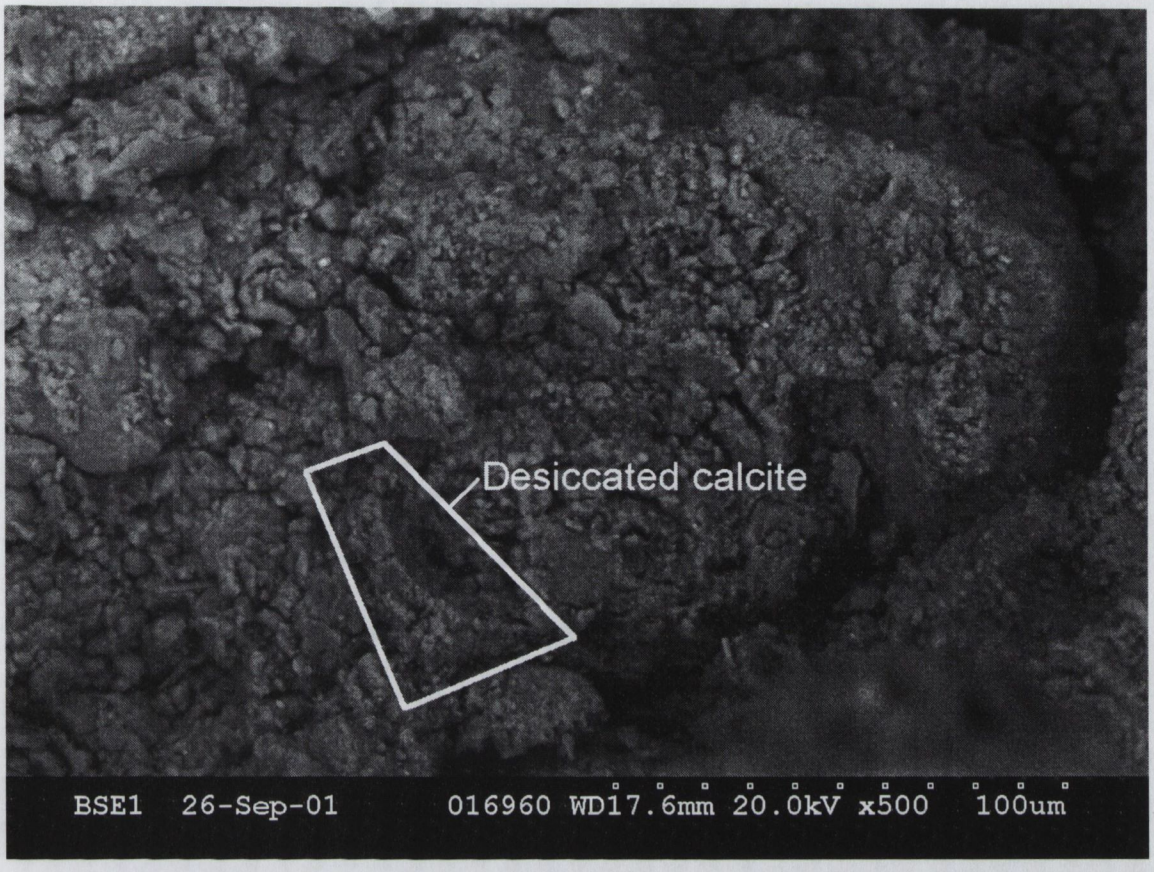

Fig. A.4.6. EM1: stiff mottled brown till

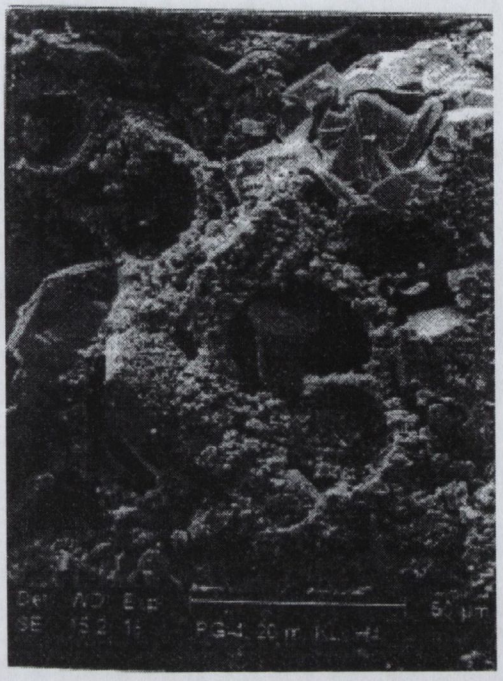

Fig. A.4.7. Calcite cementation, after Knudsen et al. (1995)

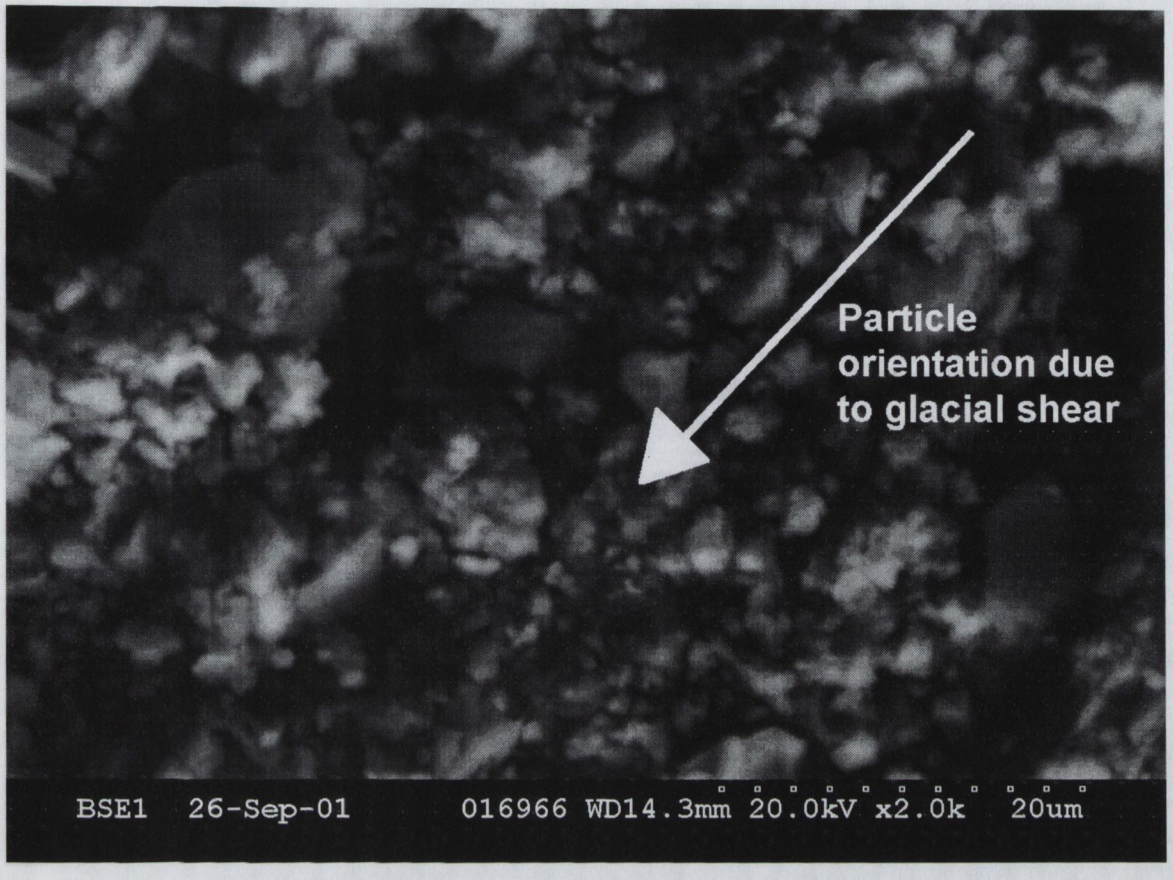

Fig. A.4.8. EM2: firm brown till

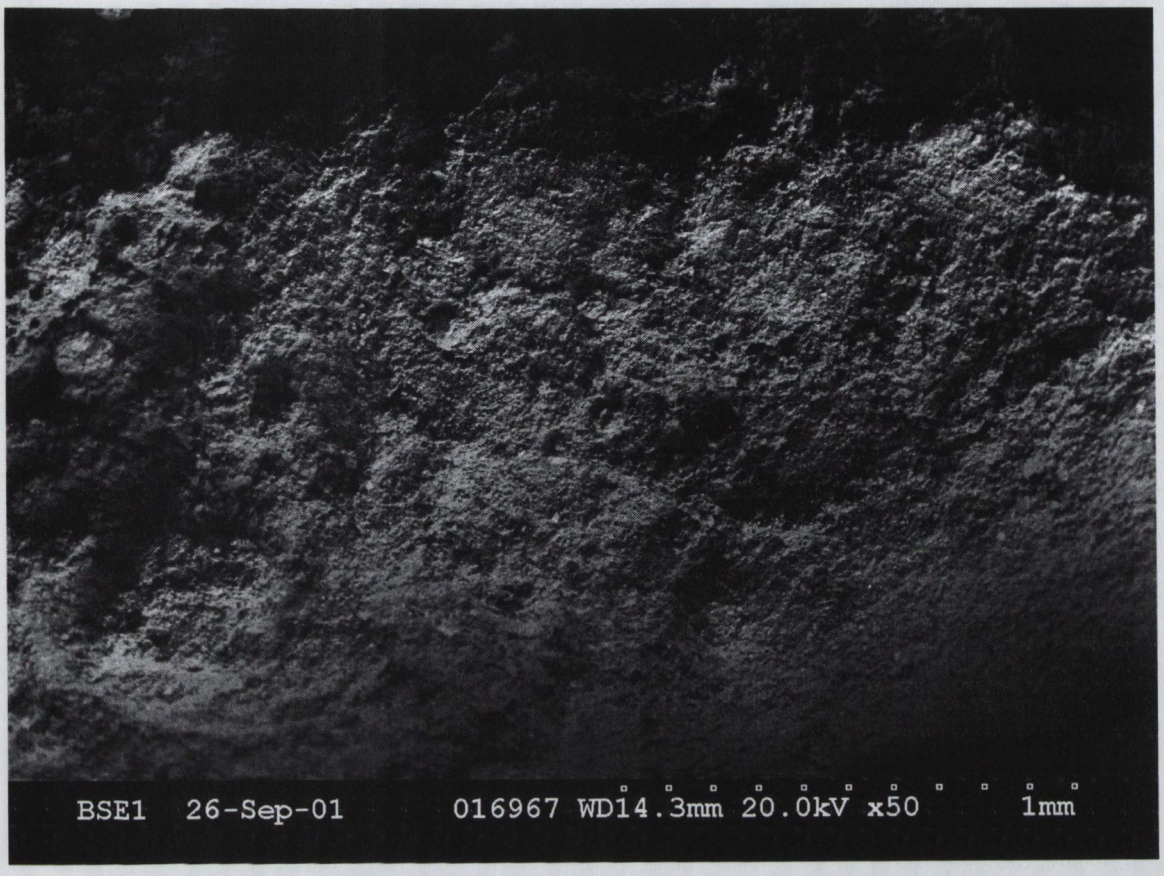

Fig. A.4.9. EM2: firm brown till

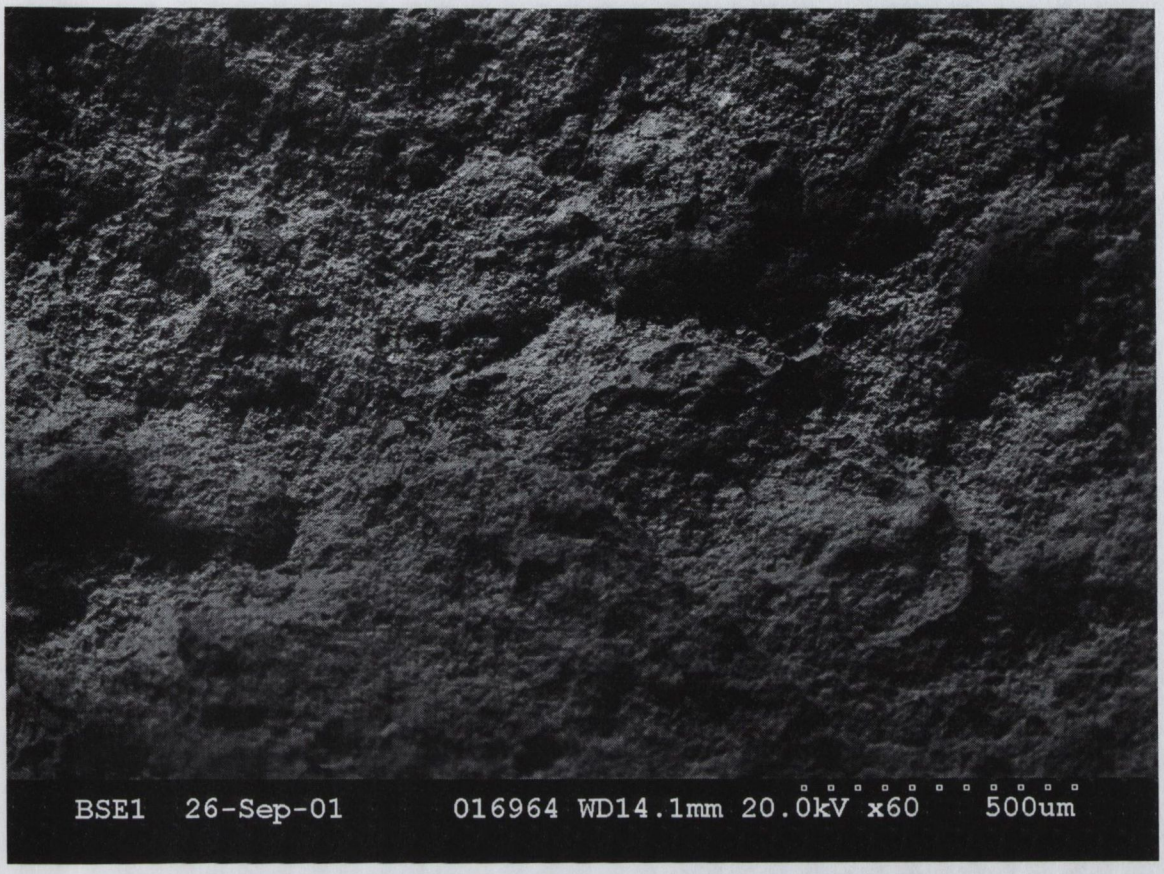

Fig. A.4.10. EM2: firm brown till

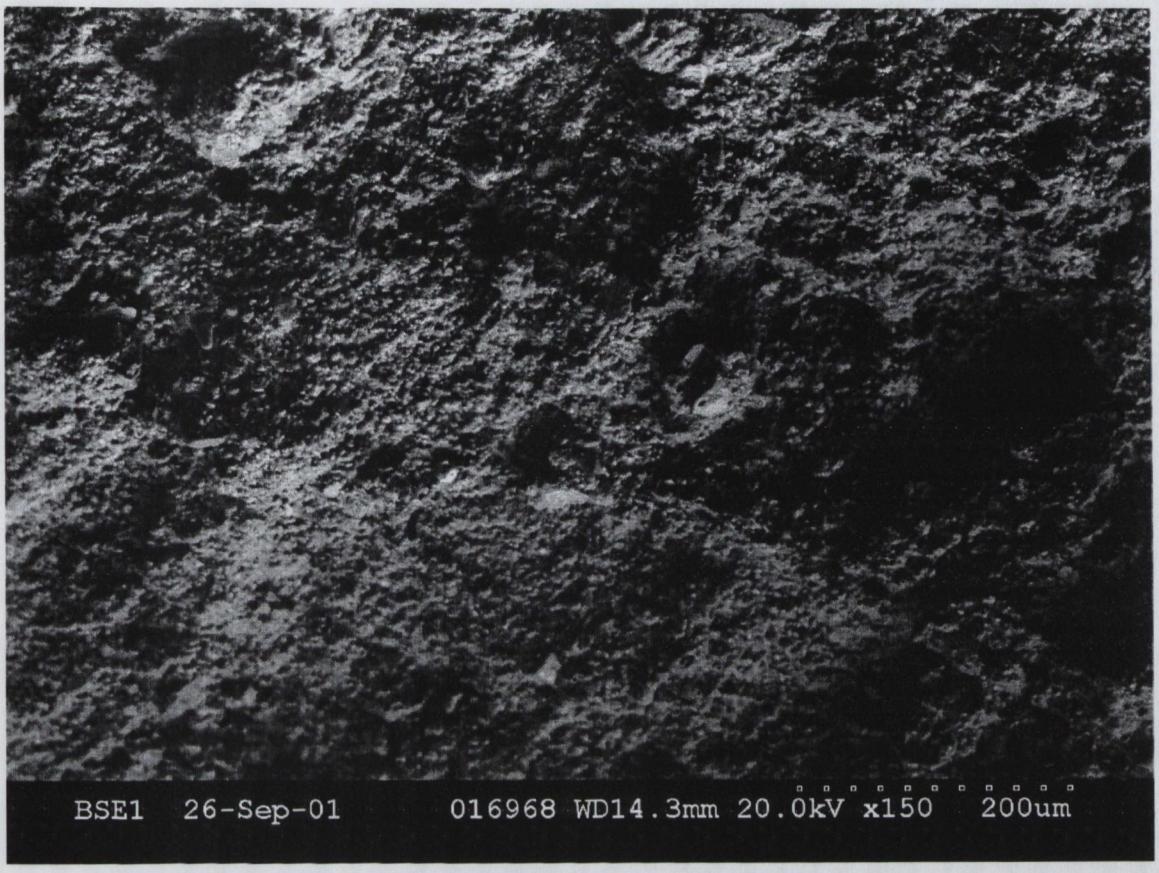

Fig. A.4.11. EM2: firm brown till

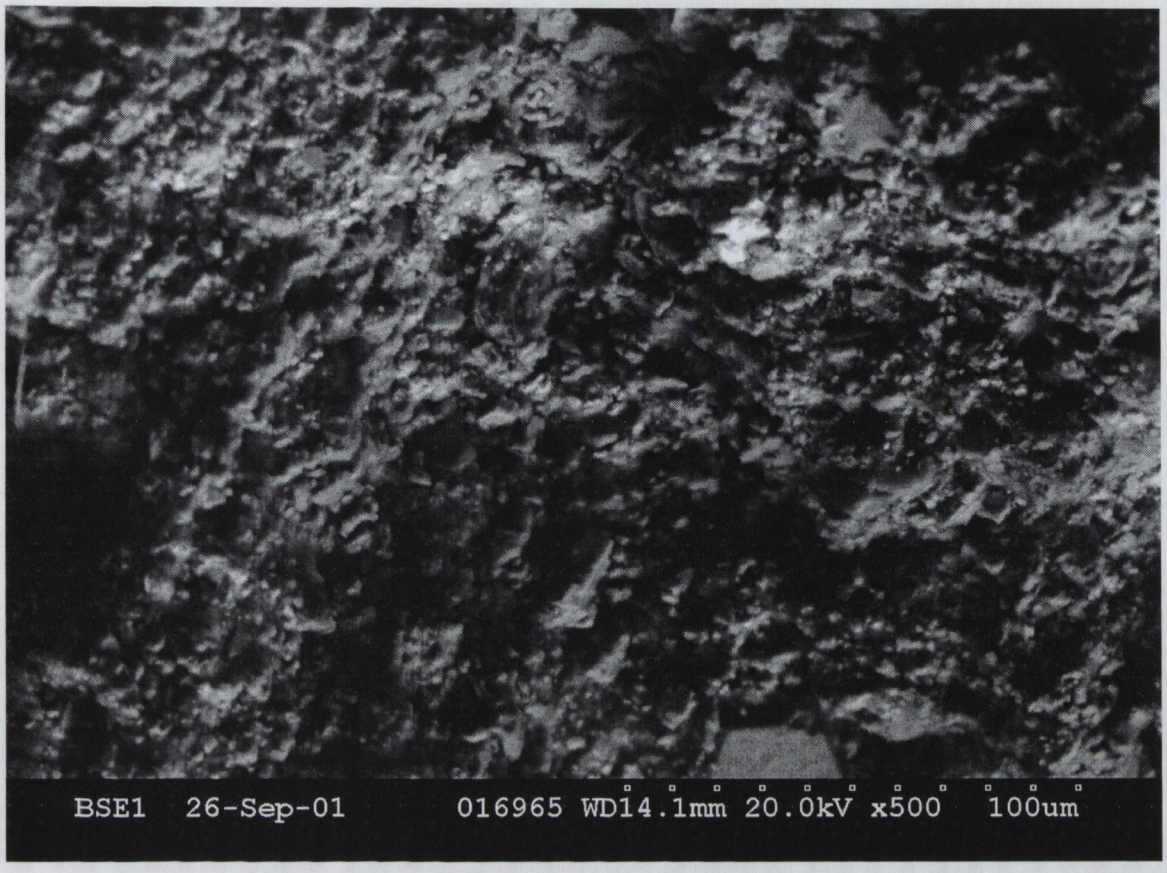

Fig. A.4.12. EM2: firm brown till



Fig. A.4.13. EM2: firm brown till

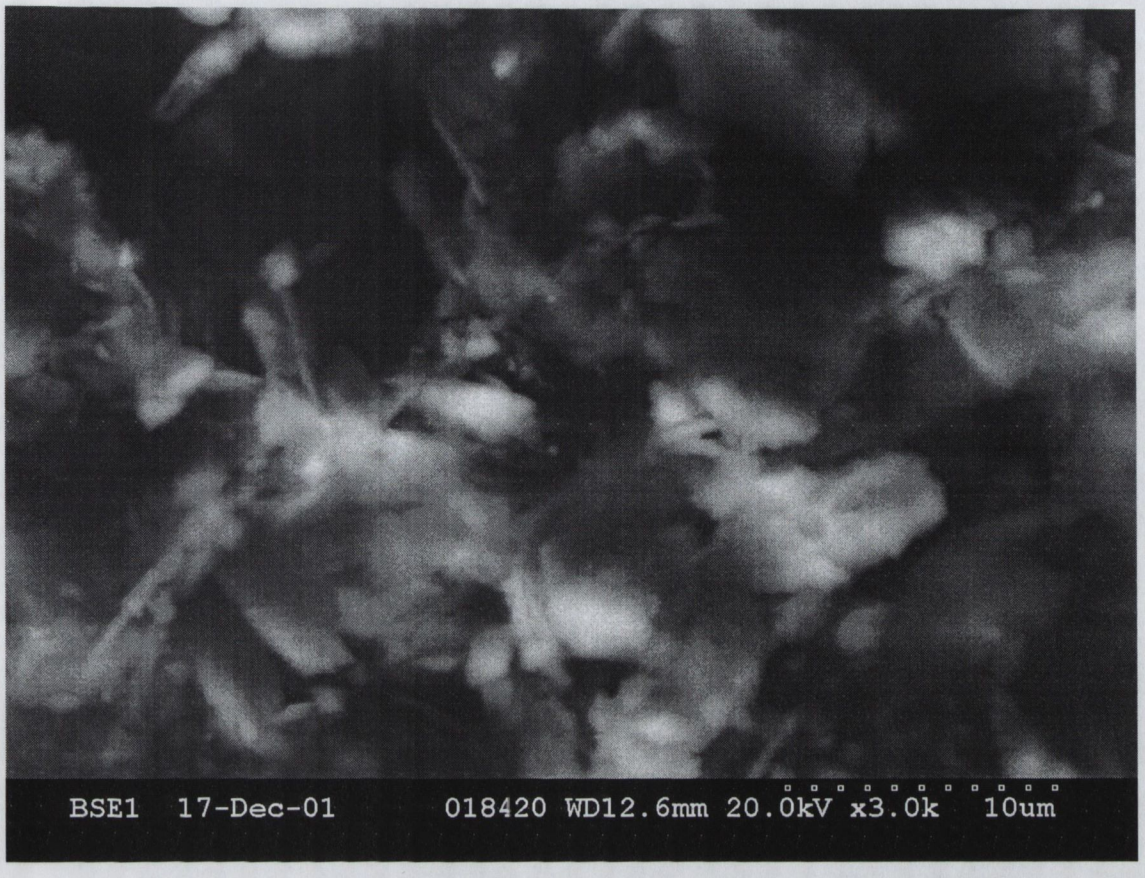

Fig. A.4.14. EM3: stiff black till

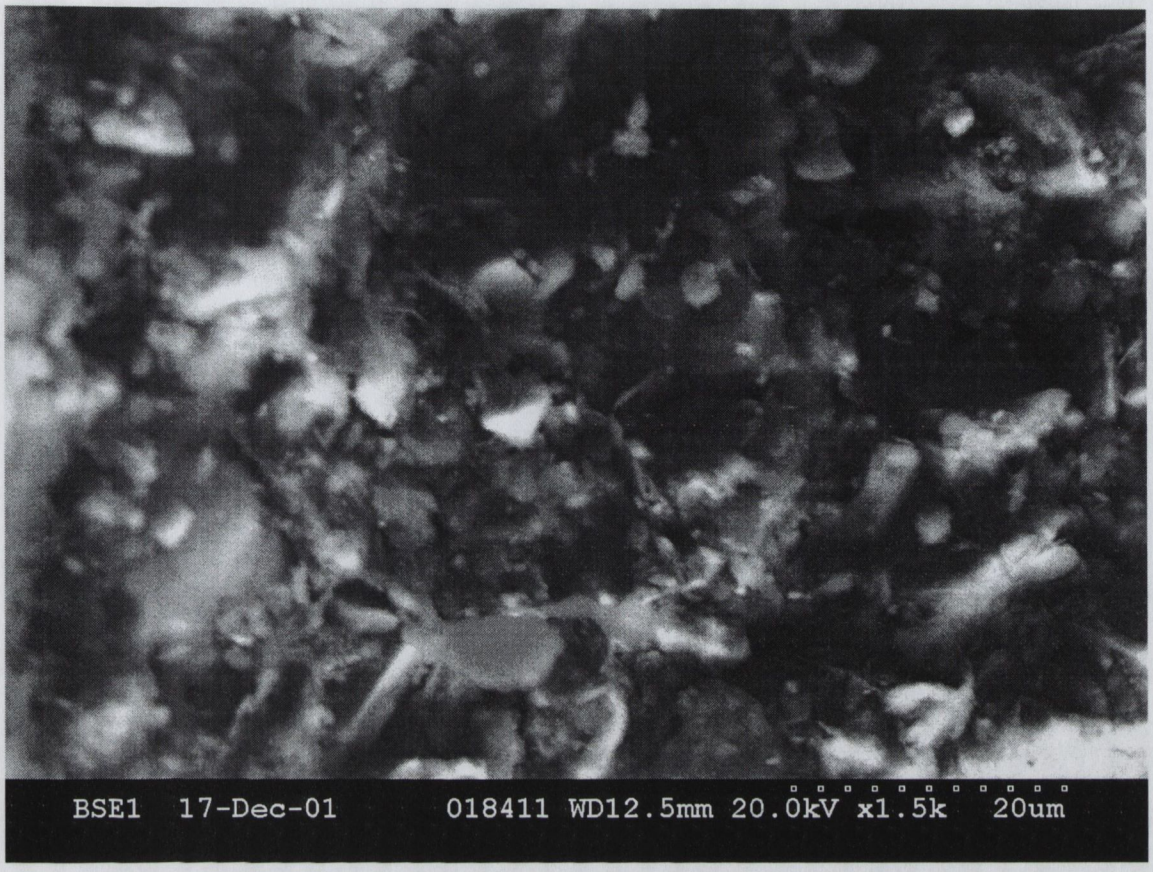

Fig. A.4.15. EM3: stiff black till

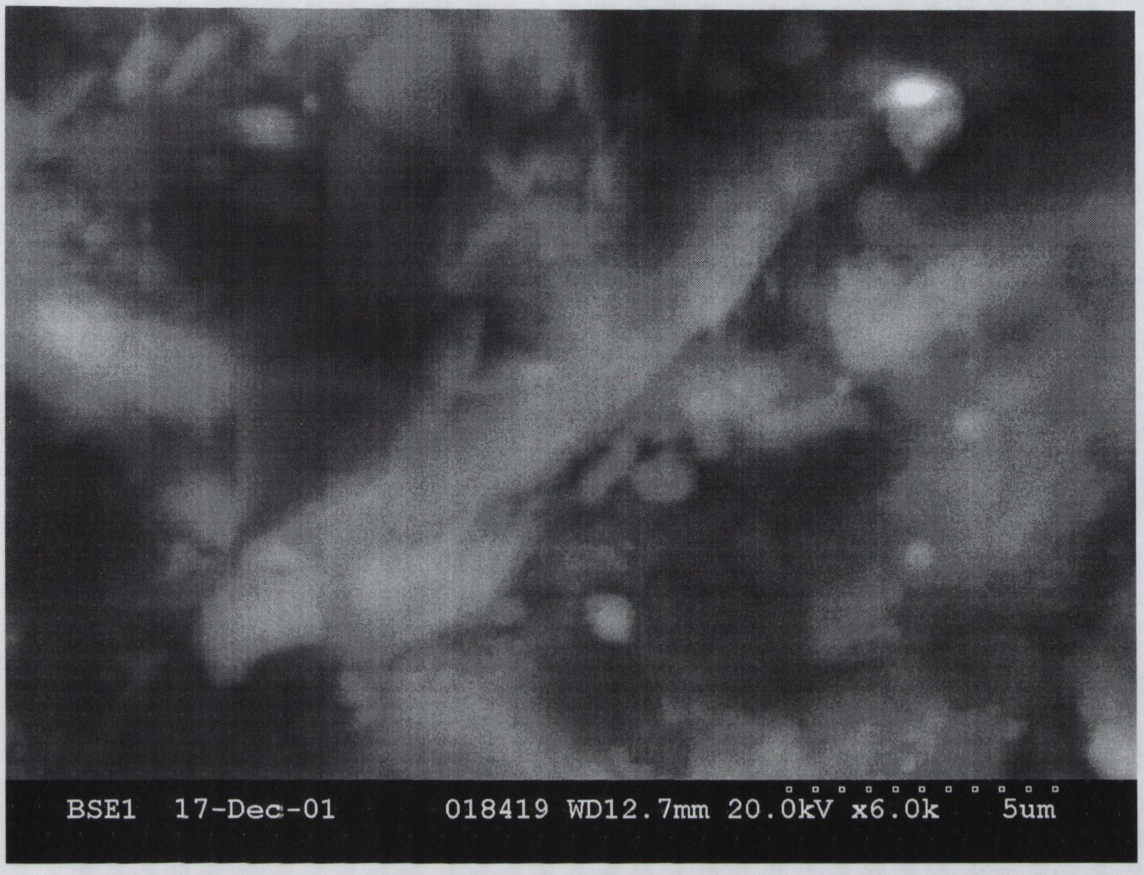

Fig. A.4.16. EM3: stiff black till

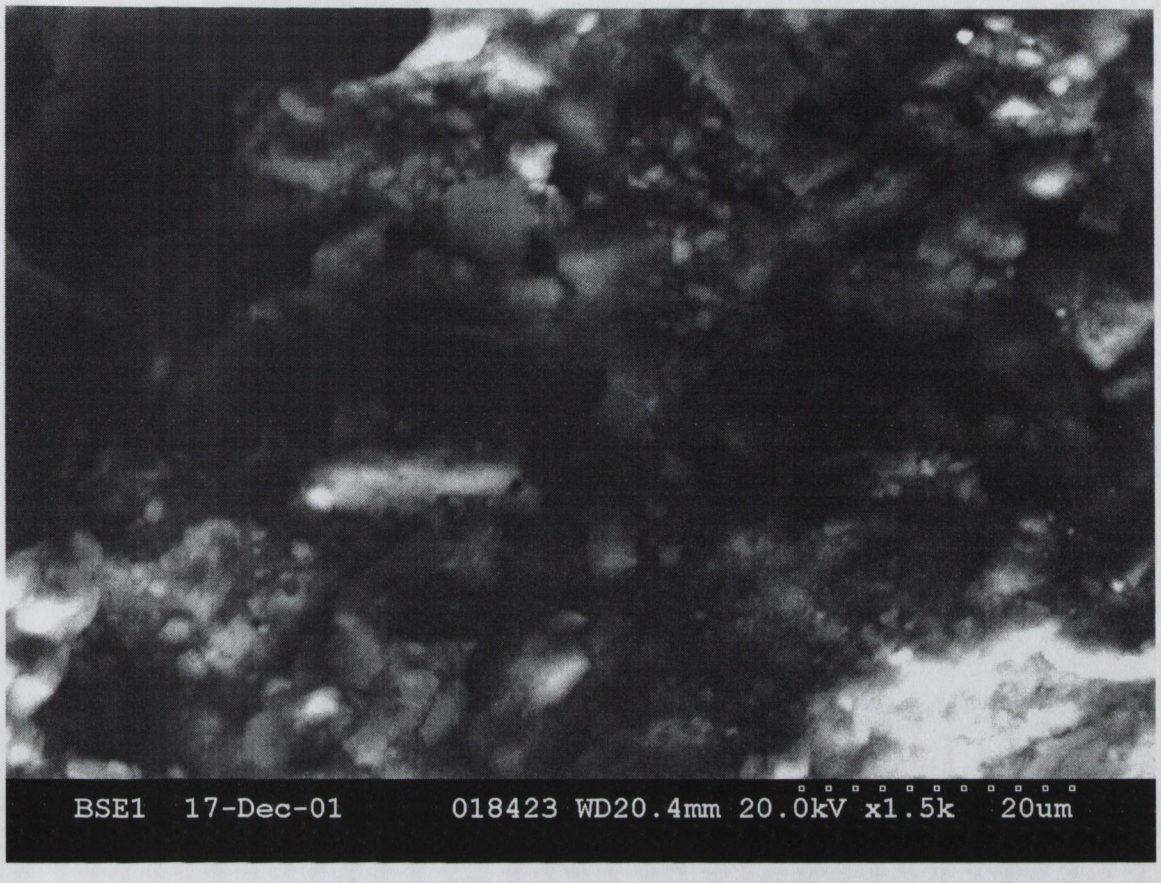

Fig. A.4.17. EM4: stiff black till

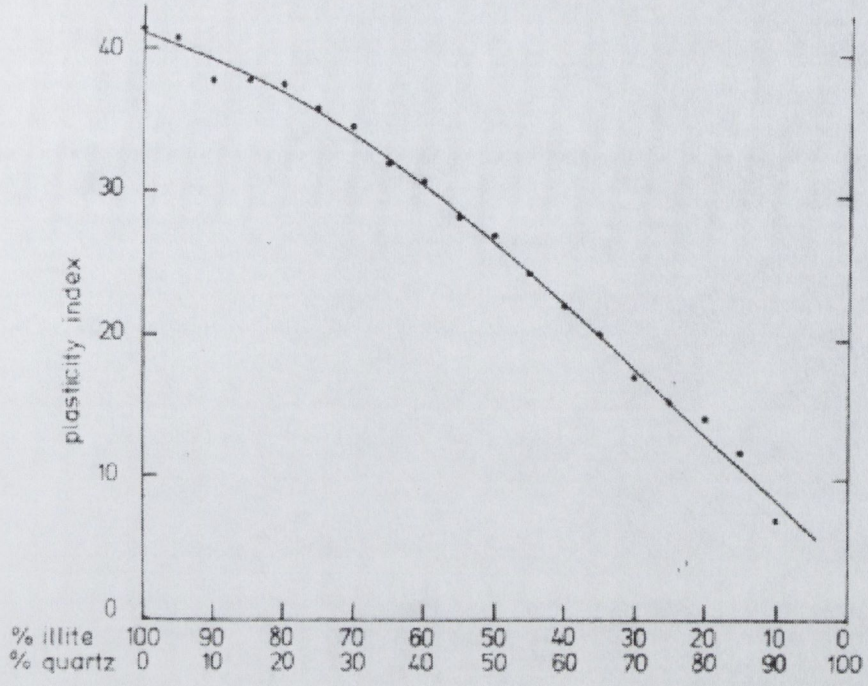

Fig. A.4.18. Influence of inactive minerals on the plasticity of a soil, after Moon (1978)

A.5 In Situ Soil Testing: Pressuremeter and Seismic Tests.

A.5.1 Pressuremeter.

All of the tests of interest, bar one, were conducted in the very stiff black boulder clay. The p-ε_v response, showing a linear phase and a distinct yield point, in one of the boulder clay pressuremeter tests, is shown in Fig. **A.5.1**. The in situ stress-states determined from the tests are shown, in Fig. **A.5.2**, with open symbols for cases where visual inspection of yielding was relatively indistinct, when compared to the distinct yielding of the closed symbol cases. Note that these K_0 values are based on total stresses and are, therefore, lower than the in situ effective stress values.

Horizontal shear stiffness, G_h, determined from two good unload-reload loops in the black lodgement till are shown in Figs. **A.5.3(a)** and **A.5.3(b)**, as G_h versus cavity strain.

The undrained shear strength of the brown boulder clay (2 m depth) was determined from the Marsland and Randolph analysis (see Section 4.7.1) as 207 kNm^{-2}. It has been assumed, based on the depth, that this test was conducted in the deformation till.

A.5.2 Seismic.

The seismic refraction data, detailed in Table **A.5.1**, gave the stiffnesses of specific units within the till layer, as identified by the boreholes. The borehole records in the vicinity of the seismic tests are given in Figs. **A.5.4(a)** and **A.5.4(b)**. By comparing the seismic data and the borehole logs, it was found that there was specific stiffness data for firm brown till, stiff brown till and very stiff black till. The seismic data are summarised in the mean stiffnesses, plotted on Fig. **A.5.5**, against estimated mean effective confining stresses in the ground, σ_c'. Note that each data point represents the mean of a number of tests[1]. (Also shown on the plot are the dynamic stiffnesses measured in the laboratory for comparison.) σ_c' requires an estimate of the vertical effective stress, σ_{v0}', in the ground and K_0. σ_{v0}' was calculated at mid-layer from the borehole

[1] The mean stiffness at the site of the Dublin Port Tunnel was 2083 MNm^{-2} (SD = 315 MNm^{-2}) and 507 MNm^{-2} (SD = 205 MNm^{-2}) for the stiff black till and stiff brown till, respectively. The standard deviations, SD, about the mean were low, suggesting that the results are accurate.

records, in the location of the seismic spreads. The equivalent K_0 values were then found from the K_0 measurements. The K_0 values were close to 2, for the stiff black till, and 3, for the stiff brown and firm brown tills. These K_0 values are considered to be suitable average values for the boulder clay units.

Table A.5.1. Seismic test data

Location	Till	V_p: ms^{-1}	V_s: ms^{-1}	Density: kgm^{-3}	Poisson's ratio	G_{max}: MNm^{-2}	E_0': MNm^{-2}
Scholarstown	D*	550	200	2150	0·42	86	206
	B†	1050	400	2250	0·42	360	864
	BL‡	2030	500	2250	0·47	563	1350
DPT L1/L1S	B	800	250	2150	0·45	134	323
	BL	2000	600	2250	0·45	810	1944
DPT L2/L2S	B	1000	350	2150	0·43	263	632
	BL	2200	700	2250	0·44	1103	2646
	B	400	250	2150	~~0·18~~	134	323
	BL	2300	600	2250	0·46	810	1944
	B	650	300	2150	0·37	193·5	464
	BL	1750	600	2250	0·43	810	1944
	B	1972	392	2150	0·48	330	793
	BL	1972	599	2250	0·45	807	1938

* Deformation till
† Brown lodgement till
‡ Black lodgement till

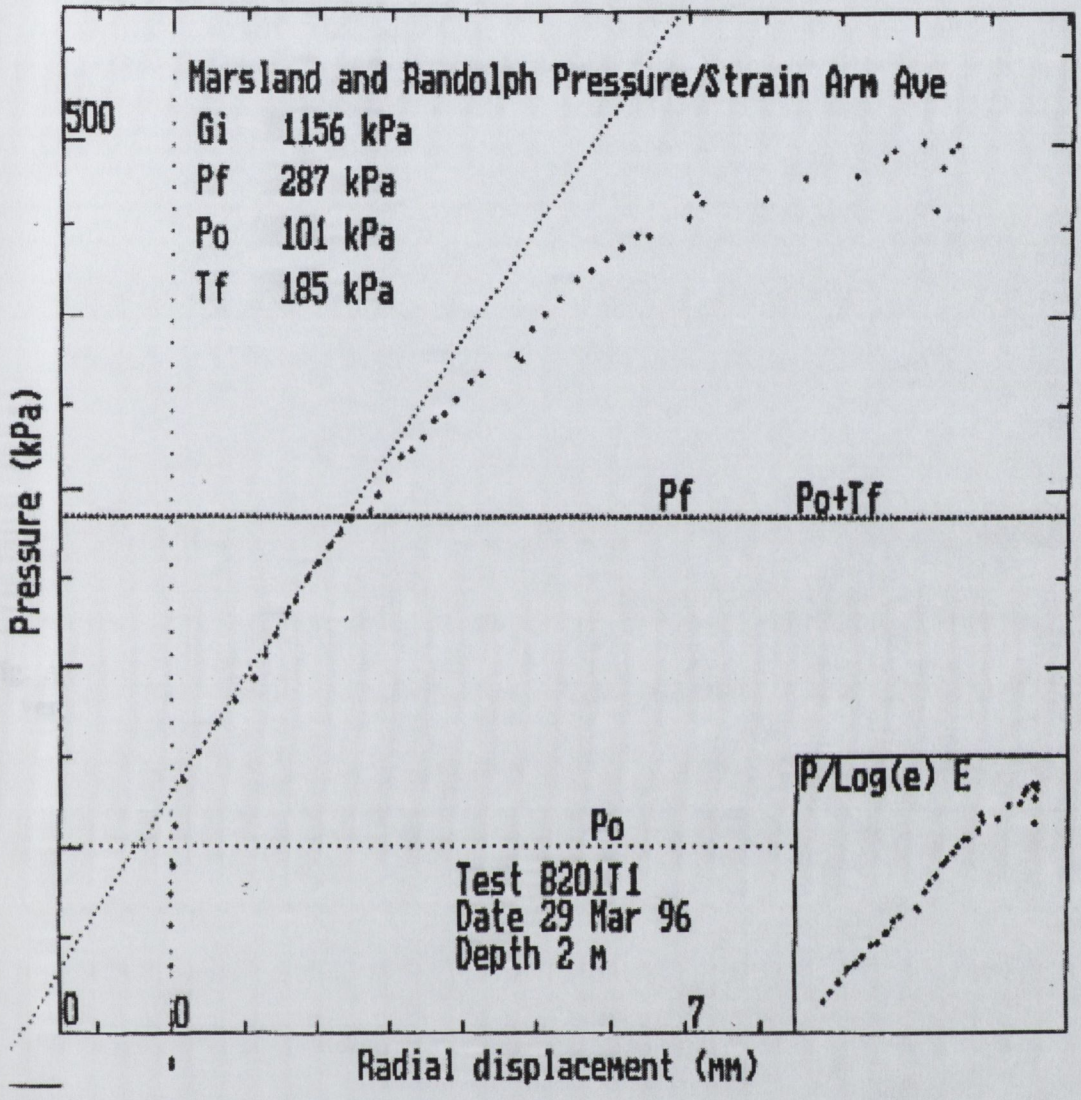

Fig. A.5.1. A good pressuremeter test in the boulder clay, after Geoconsult-Arup (1997)

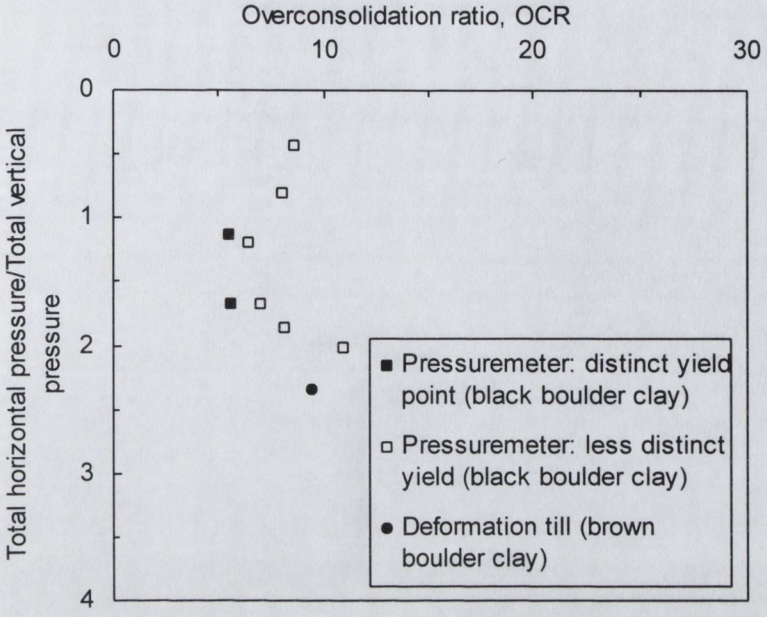

Fig. A.5.2. K_0 determined from the pressuremeter tests (closed symbols indicate tests with very distinct yield points and open symbols indicate that the yield point was less well defined)

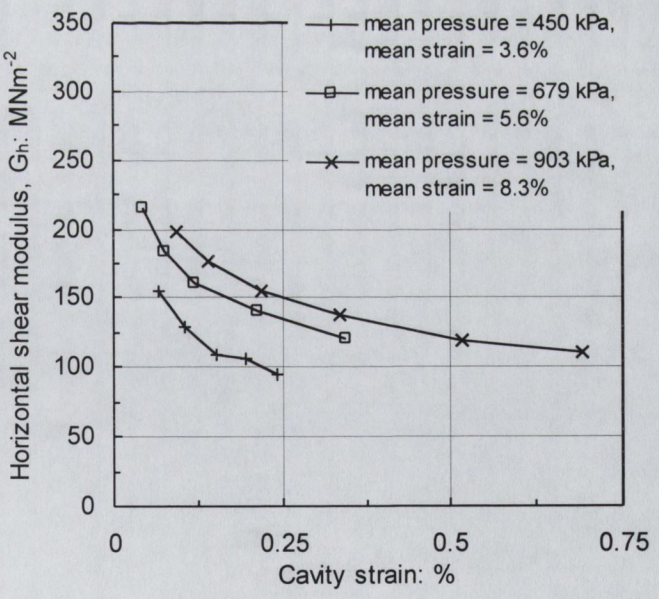

Fig. A.5.3(a). Secant stiffness measured on reload in pressuremeter test loop

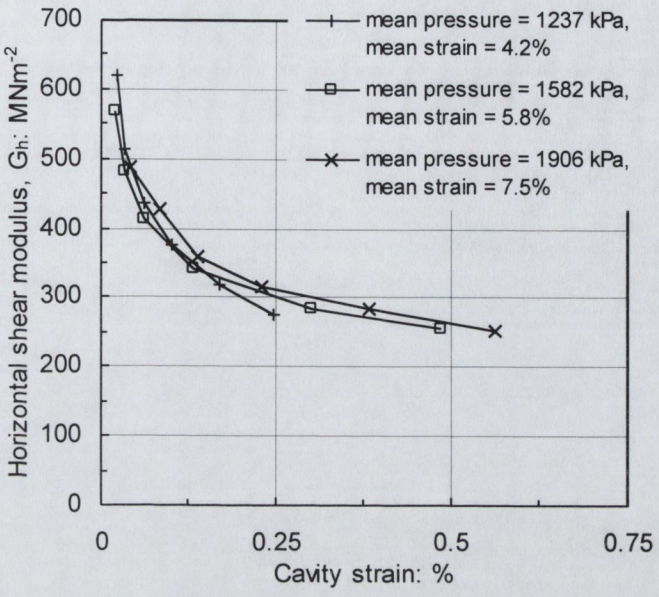

Fig. A.5.3(b). Secant stiffness measured on reload in pressuremeter test loop

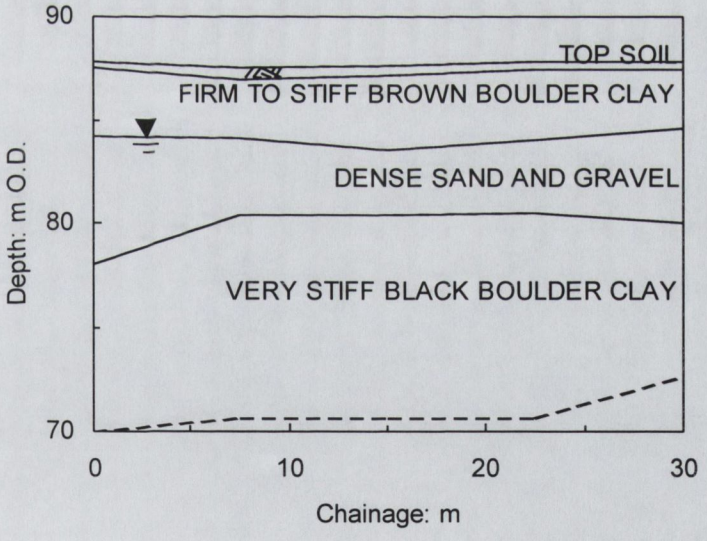

Fig. A.5.4(a). Borehole records in the vicinity of the Scholarstown seismic refraction study

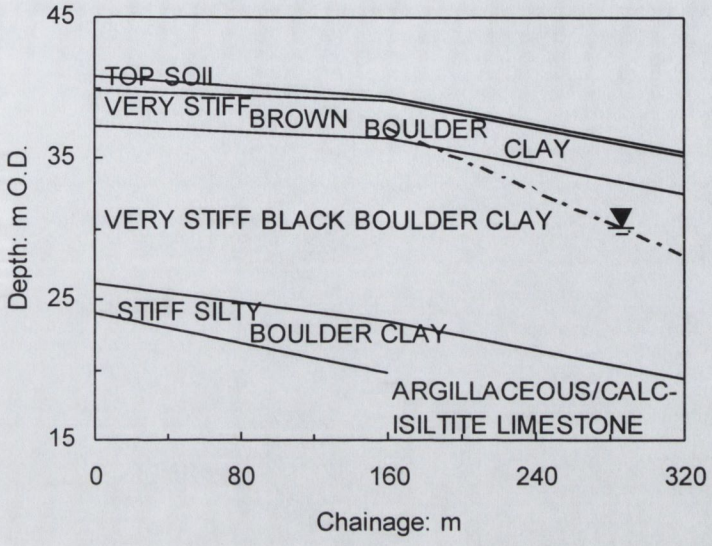

Fig. A.5.4(b). Borehole records in the vicinity of the Dublin Port seismic refraction study

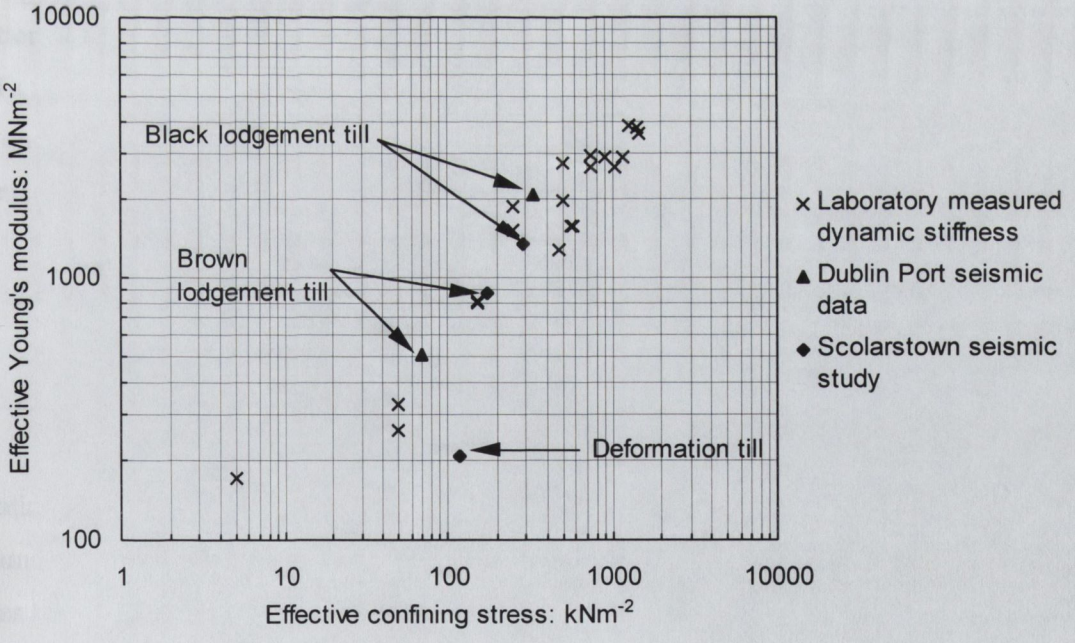

Fig. A.5.5. Comparison of stiffness measured in situ and in the laboratory dynamic tests

B Pile Tests.

B.1 Materials and Methods.

B.1.1 Ground Conditions at Site of Pile Tests.

The site of the test piles was a brown field site at Saint James's St., about 1 mile from the city centre. The ground conditions at the site have been classified in a number of previous site investigations (Fairhurst Garland and Partners (1978), Thomas Garland and Partners (1996), TJ O'Connor and Associates (1997) and LRT (1997)). A further borehole was sunk next to one of the test piles for this project. Based on these, site stratigraphies relevant to the locations of the pile tests are shown in Figs. **B.1.1(a)** and **B.1.1(b)**. The reader is referred to the soils section for typical soil properties. In general, ground investigation shows 2 m of made ground/silty clay overlying 2 m of brown, gravelly clays overlying black, gravelly clays. The water table corresponded with the top of the lodgement till at 2·5 m to 2·9 m BGL.

A graph of SPT N_{60} against depth, based on all available site data, is given in Fig. **B.1.2**. There is a definitive progression of N_{60} with depth; however, as is expected, there is considerable scatter at any given depth. The results also contained a large number of refusals. One of the SPTs was conducted within 1 m of the 450 mm pile and deliberately carried to blows well beyond what would be considered refusal due to boulders. The very high blow counts are well in excess of the rest of the site.

B.1.2 CFA Pile Testing.

B.1.2.1 Introduction.

Continuous Flight Auger (CFA) piles are formed by drilling a continuous flight auger into the ground. The CFA piling rig is shown in Fig. **C.9**. The sides of the hole are supported at all times by the soil-filled auger, eliminating the need for temporary casing or bentonite slurry. When the auger has reached the required depth, the temporary plug, which prevents soil from entering the hollow stem, is ejected by an auger lift and subsequent concrete pressure. At this

stage, efforts should be taken to avoid 'decompression' of the shaft, which is a loss of stiffness and strength due to the concrete pressure.

When the concrete head has been established, extraction is commenced at a rate consistent with concrete supply to maintain a head of concrete and, hence, a shaft fully supported by either the soil filled auger flights or concrete. 'Positive rotation' of the auger is necessary to retain the drilling spoil and to ensure that the concrete fills the entire pile cross section. The concrete pressure and extraction rate must be balanced, which is conducted with rig-based instrumentation; otherwise, drilling spoil can contaminate the pile shaft.

The reinforcement is installed after the auger has been withdrawn, i.e. while the concrete is fluid. The placement of a long reinforcement cage into the hole can be cumbersome, in which case vibration is used. Furthermore, the cage can cause contamination of the concrete shaft with eroded soil. Therefore, it is important that the cage is stiff or, alternatively, precautions taken to ensure concentric placement.

Two CFA piles, of 450 mm and 600 mm diameters, were instrumented. The piles are sketched in Figs. **B.1.3(a)** and **B.1.3(b)**.

B.1.2.2 Pile Instrumentation.

Seven Gage Technique vibrating wire strain (embedment) gauges (VWSGs) were fitted along the longitudinal rebar over the pile lengths. A further seven were fitted diametrically opposite, for study of opposite sides of the piles and for measuring any load eccentricity. The large number of instruments also acted as insurance in the case of breakage. The readings were converted to strains with the VWSG gauge equation:

$$\text{microstrain} = K(1/T_i^2 - 1/T^2)\times 10^{14} \qquad [B.1]$$

where K is the gauge stiffness and T_i and T are the initial and current frequency readings, respectively.

No gauges were placed near the (1 m length) overlap of the rebars, to avoid an overestimation of the load bearing capacity. The spot welded gauges were sealed with a plastic housing and filled with polyurethene potting compound, to avoid damage to the gauges. Spacers were added along the lengths of the piles to ensure concentric placement of the reinforcement in the concrete filled shaft.

In addition to VWSGs, K-type thermocouples were placed, at two instrument levels, in the 450 mm pile, to determine the effects of heat of hydration on the VWSGs[1]. The pile head was instrumented with a load cell and four LVDTs mounted on two reference beams supported by steel posts at a distance on either side of the pile. The test arrangement and instrumentation are shown in Figs. **C.7, C.8, C.9** and **C.11**.

B.1.2.3 Calibration.

The calibration was conducted in situ and with a 450 mm diameter, 1 m length, laboratory dummy pile. (The calibration was based on the average of the dummy pile gauges and the average of the top level of VWSGs in the test piles.) The top level of VWSGs in the test piles were very shallow in fill; therefore, no load was taken in shaft friction. Hence, the full applied pile head load could be taken in conjunction with the measurements of the pile head deflection (the latter measurements were recorded continuously by PMC Ltd.). The stiffnesses of the VWSGs were assumed equal to those at the top level and the gauges were zeroed based on the reading immediately prior to loading of the pile.

B.1.2.4 Test Piles.

Two CFA piles were tested: a 450 mm diameter, 12·3 m length pile (Pile 450) and a 600 mm diameter, 11 m length pile (Pile 600). The piles were constructed with a, May Gurney Ltd., heavy rig of high torque capacity (15-20 Tm) (see photographs). The augers were bored to the required depth and 35 Newton concrete was pumped under pressures exceeding hydrostatic and the auger gradually withdrawn. The full-length reinforcement cages with spacers, the VWSGs and the thermocouples attached to the reinforcement bars, were then inserted into the fluid

[1] The EMF versus temperature graph is linear, where 1 mV = 1 °C.

concrete. (This concrete possesses a very high slump, of about 175 mm.) Pile 450 was vibrated in and Pile 600 was pushed in the last few metres with the bucket of a mechanical digger. A pile cap was then cast. At the same time as the piles were being cast, concrete cylinder samples of the pile concrete were taken for subsequent compression testing in the laboratory.

B.1.2.5 Pile Loading.

Load was applied to the piles with a reaction frame of 5 MN capacity. The anchor piles contained 4 No., 26 mm, Dywidag rebars of 568 kN ultimate strength each. The placing of the anchor piles was in accordance with the recommendations of Whitaker (1976); i.e. to avoid interaction between the test pile and anchor piles[2]. Pile head displacement was measured automatically every 5 minutes by four displacement gauges at 90° offsets mounted on two reference beams supported by steel posts on either side.

The piles were loaded in a maintained load (ML) test to Specification for Piling and Embedded Retaining Walls (1996). For each applied load increment, the load is held at the value for not less than that specified: (a) the rate of settlement in a period of 30 minutes is less than 0·5% of the current cumulative settlement which has occurred or (b) the rate of settlement is 0·05 mm per 30 minutes, which ever is the higher. Pile 450 was tested about 3 days after installation and Pile 600 was tested 5 days after installation.

B.1.2.6 Pile Test Results Interpretation.

Fig. **B.1.4** is a sketch of a pile section indicating forces and critical dimensions. The following calculations were used:

(a) The strain at the top of the pile, ε:

$$\varepsilon = P/A \qquad [B.2]$$

[2] Whitaker (1976) recommended a distance of at least three pile diameters between the test pile and the anchor piles and not less than 1·5 m.

(b) The shaft friction over length l, τ_s:

$$\tau_s = (P_1 - P_2)/\pi Dl \qquad [B.3]$$

(c) Mid-level deflection, Δ:

$$\Delta = (\Delta_1 + \Delta_2)/2 \qquad [B.4]$$

(d) Mid-level depth, d:

$$d = d_1 + (d_2 - d_1)/2 \qquad [B.5]$$

where the symbols are as on Fig. **B.1.4**.

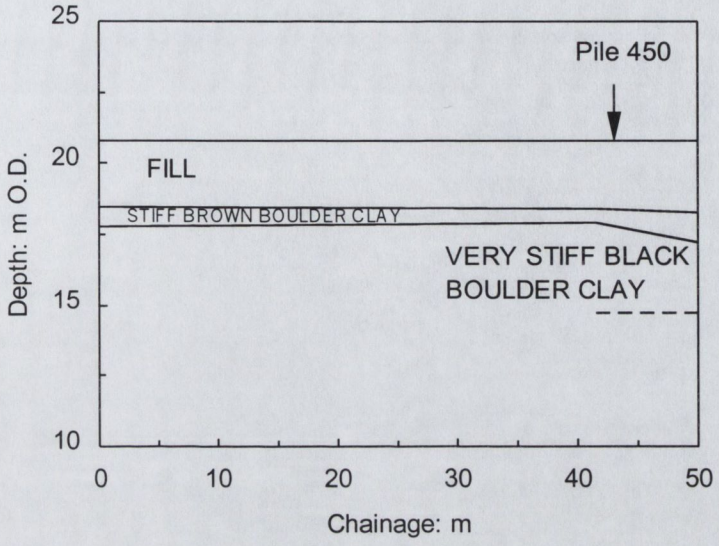

Fig. B.1.1(a). Stratigraphy relevant to Pile 450

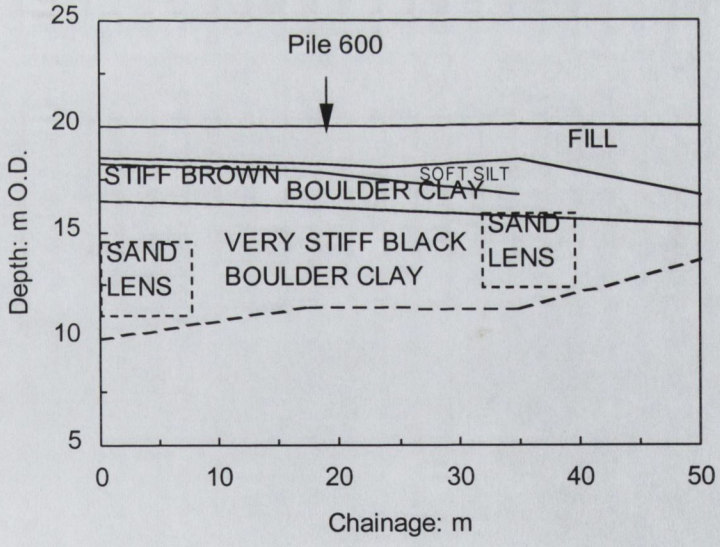

Fig. B.1.1(b). Stratigraphy relevant to Pile 600

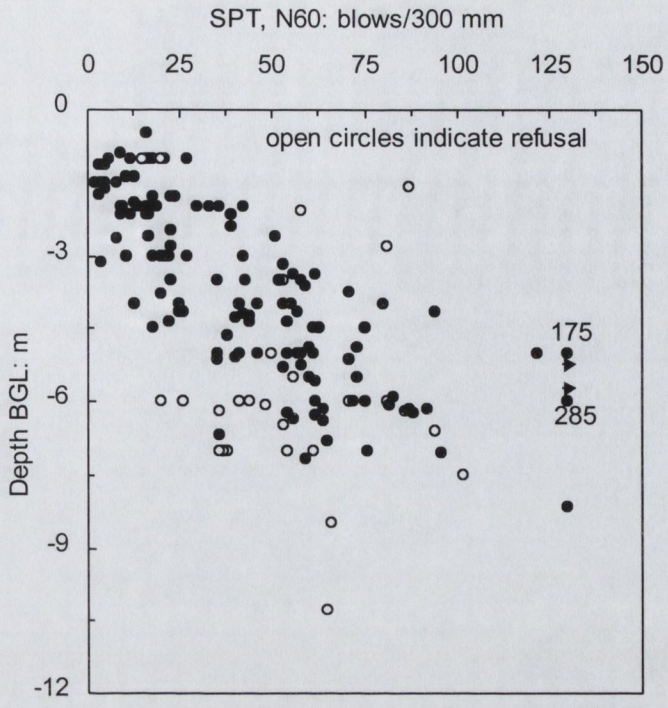

Fig. B.1.2. Standard Penetration Test results at Saint James's St.

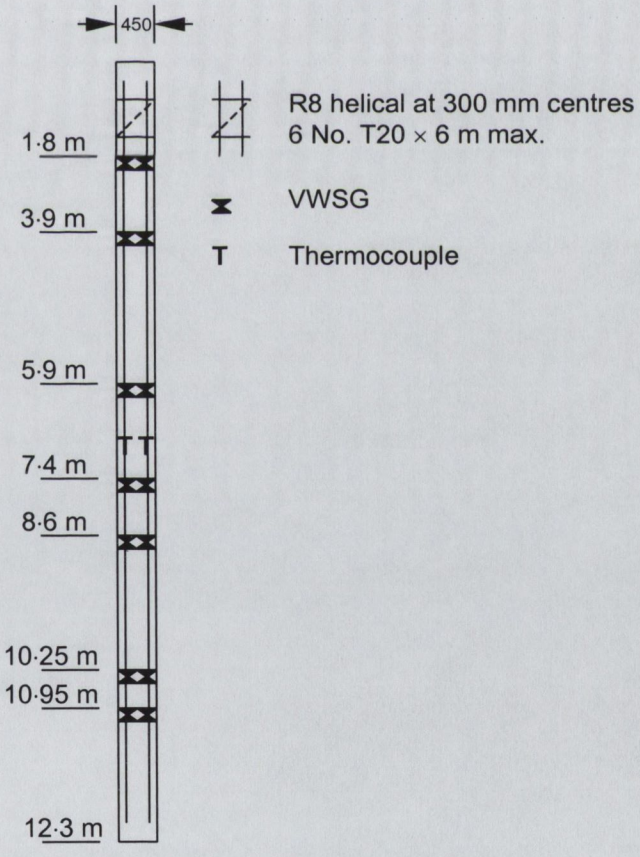

Fig. B.1.3(a). Pile 450 dimensions and instrumentation

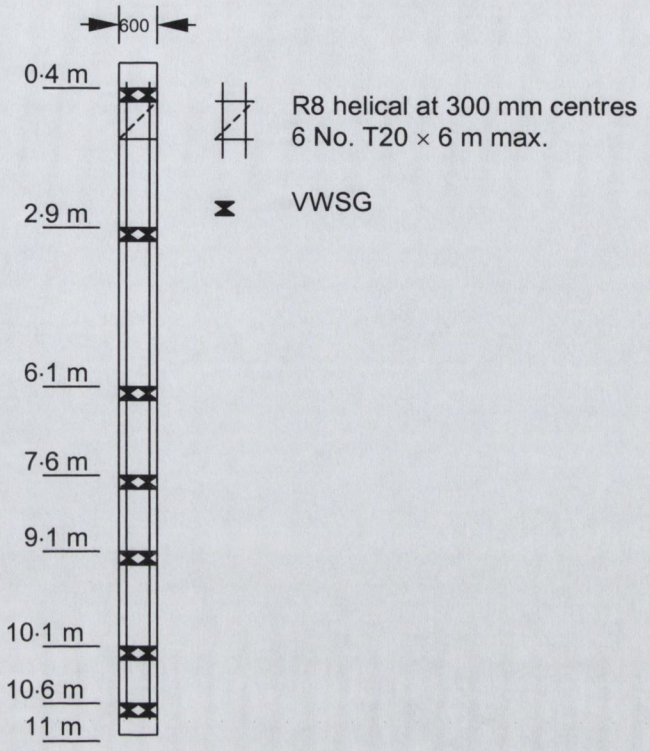

Fig. B.1.3(b). Pile 600 dimensions and instrumentation

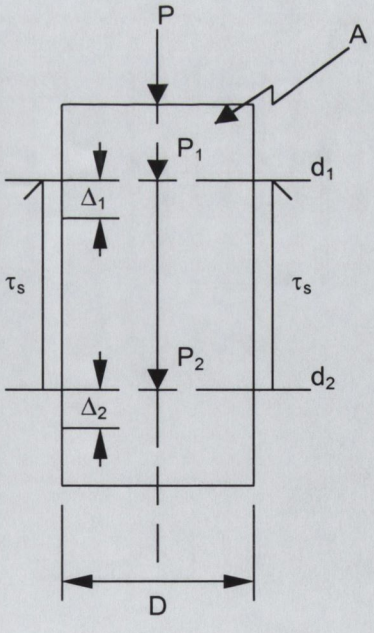

Fig. B.1.4. Pile section indicating forces and dimensions for load and strain calculations

B.2 Results.

B.2.1 Pile Instrumentation.

Gauge working rate was found to be about 80% at the end of the load tests. Significant zero drift was recorded for about the first 2 days of concrete curing, after which it ceased.

B.2.2 Calibration.

The calibrations are shown in Figs. **B.2.1(a)** and **B.2.1(b)**[1].

B.2.3 Pile Loading.

The Pile 450 pile cap fractured at 3·15 MN applied head load (P). Pile 600 was loaded, as close as safety allowed, to the capacity of the test frame (5 MN). A test summary is given in Table **B.2.1**.

Table B.2.1. Pile test summary

	Date cast	Date tested	Design load (MN)	Maximum load applied (MN)	Maximum settlement (mm)
Pile 600	31/7/98	5/8/98	1·8	4·5	29·4
Pile 450	17/7/98	21/7/98	1·4	3·15	10·7

[1] These are also pile head load against pile head deflection curves.

B.2.4 Strain Distribution.

The strain distribution diagrams, of microstrain against depth, are given in Figs. **B.2.2(a)** and **B.2.2(b)**. The strains developed during curing of the concrete are shown against depth in Fig. **B.2.3**, at about 1 day and 2 days after maximum concrete temperature.

B.2.5 Thermocouple Readings.

The temperature variation with time is shown in Fig. **B.2.4**.

B.2.6 Load Distribution.

Load against depth diagrams are shown in Figs. **B.2.5(a)** and **B.2.5(b)**, from which the end bearing can be obtained

B.2.7 Load-Settlement.

Load against settlement diagrams are shown in Figs. **B.2.6(a)** and **B.2.6(b)**. These graphs show the load and deflection at a given level in the pile.

B.2.8 Shaft Friction-Depth.

Shaft friction against depth graphs are shown in Figs. **B.2.7(a)** and **B.2.7(b)**.

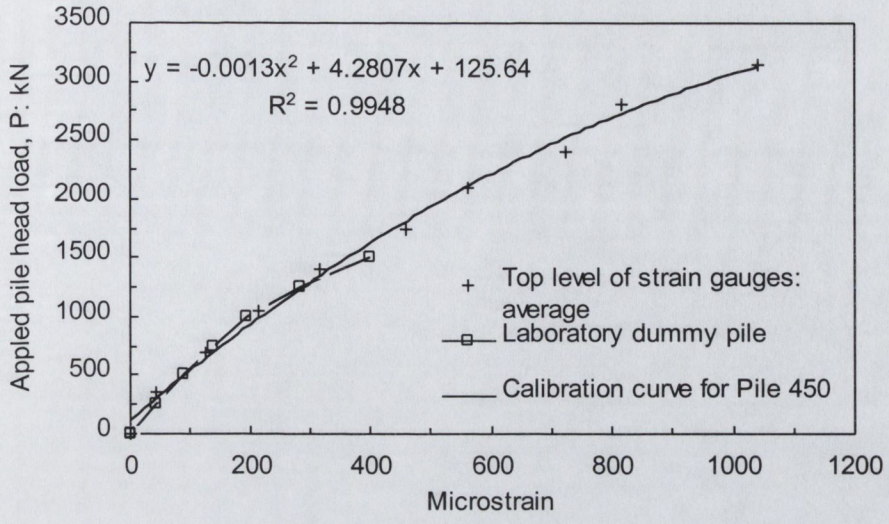

Fig. B.2.1(a). Pile 450 calibration curve

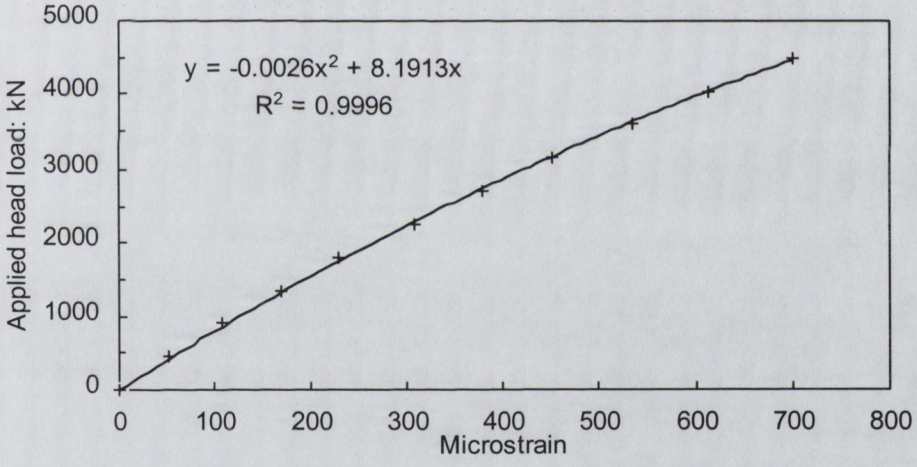

Fig. B.2.1(b). Pile 600 calibration curve

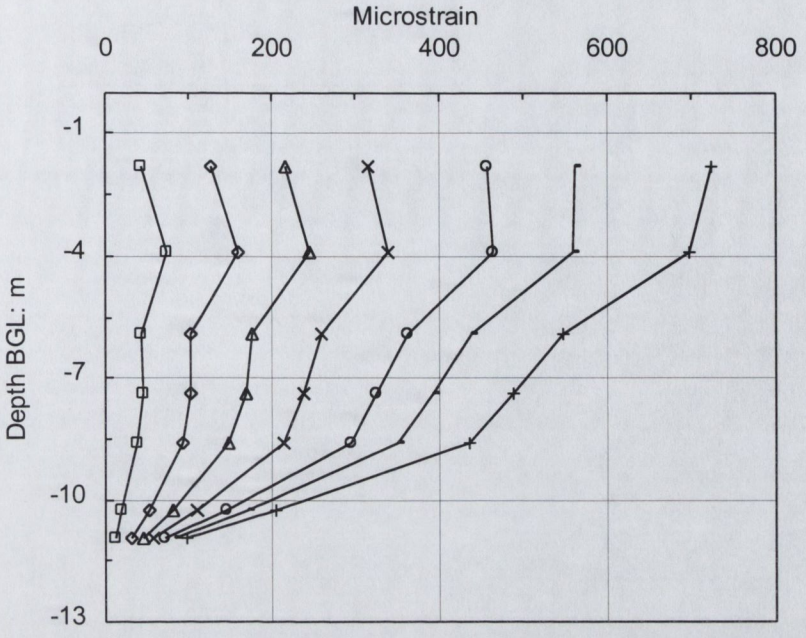

Fig. B.2.2(a). Strain distribution against depth for Pile 450

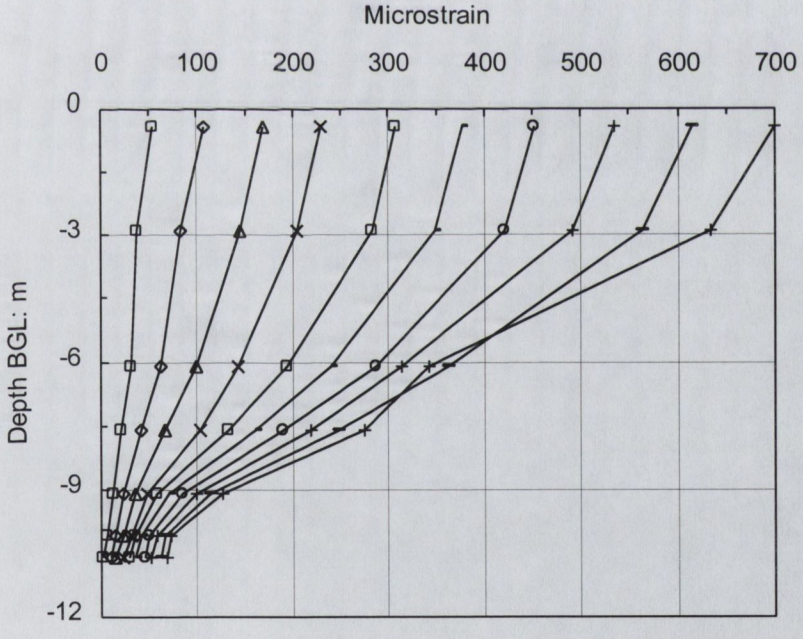

Fig. B.2.2(b). Strain distribution against depth for Pile 600

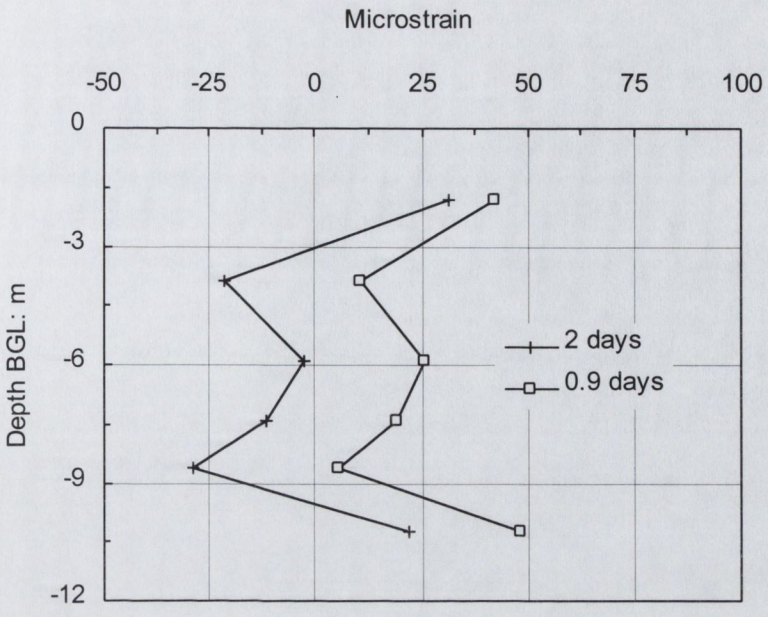

Fig. B.2.3. Strains in Pile 450 due to curing

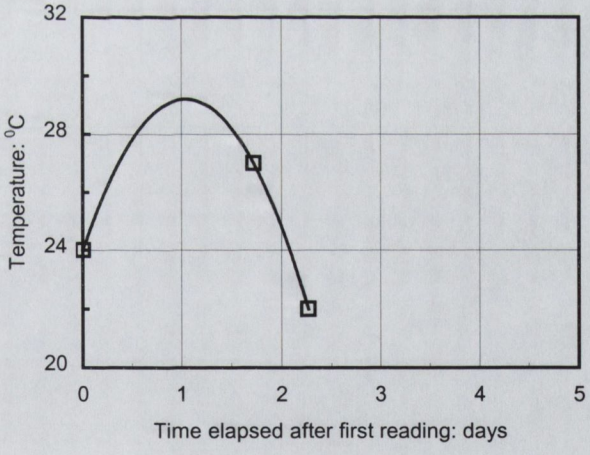

Fig. B.2.4. Temperature variation in Pile 450 due to curing

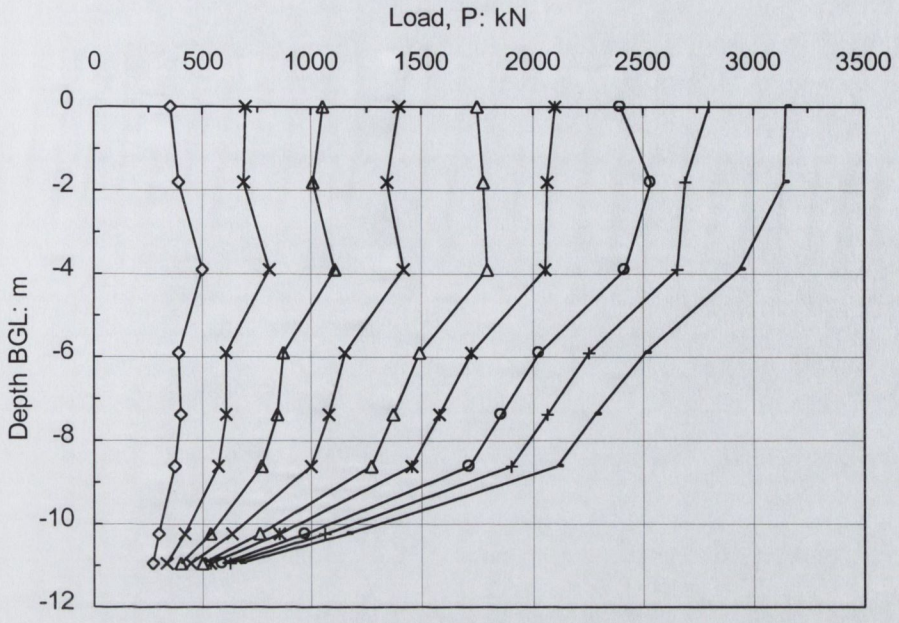

Fig. B.2.5(a). Load distribution in Pile 450

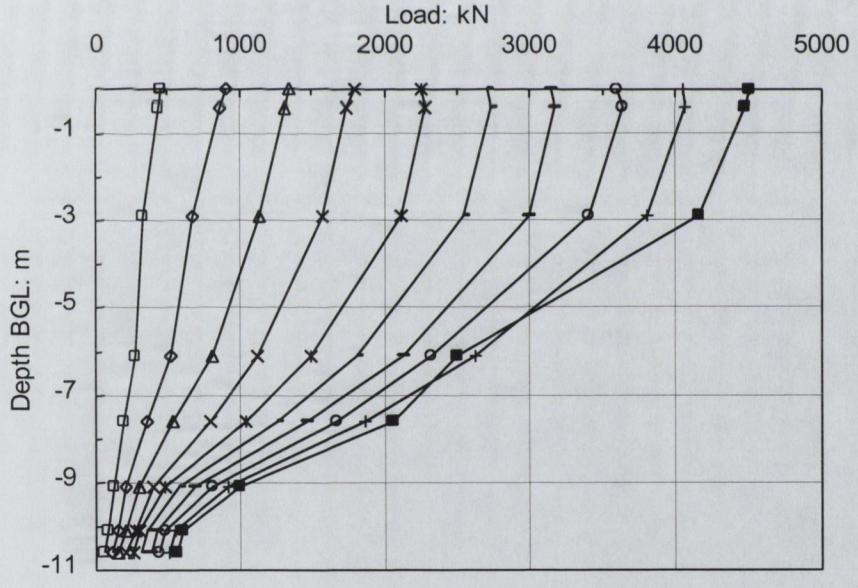

Fig. B.2.5(b). Load distribution in Pile 600

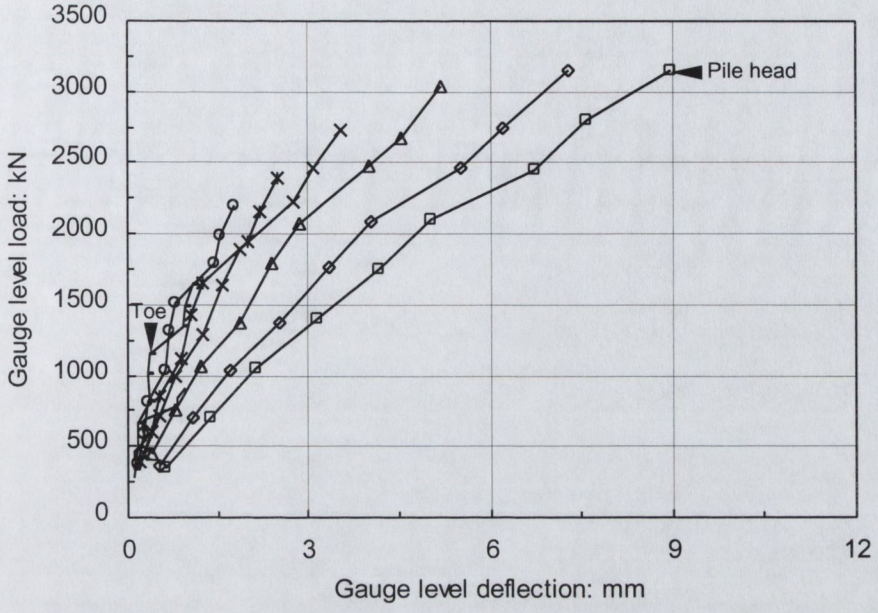

Fig. B.2.6(a). Gauge level load against gauge level deflection in Pile 450

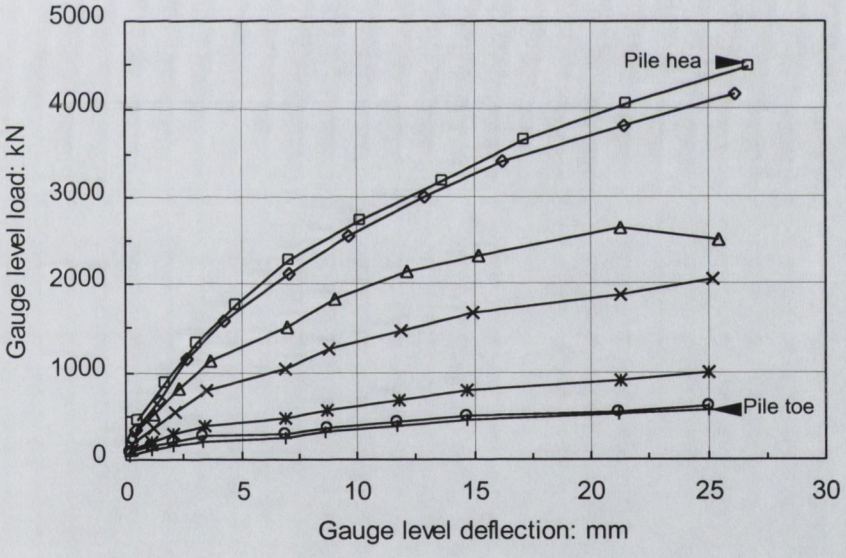

Fig. B.2.6(b). Gauge level load against gauge level deflection for Pile 600

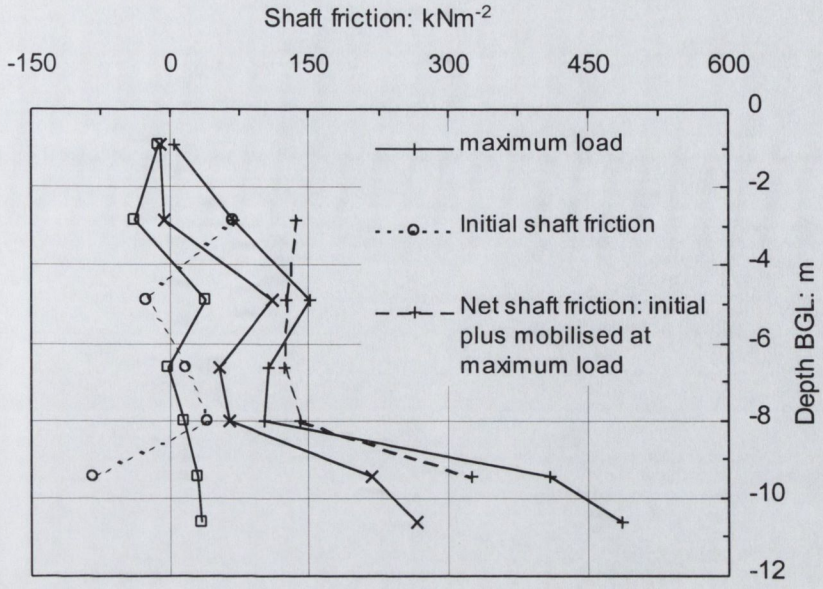

Fig. B.2.7(a). Shaft friction distribution/mobilisation in Pile 450

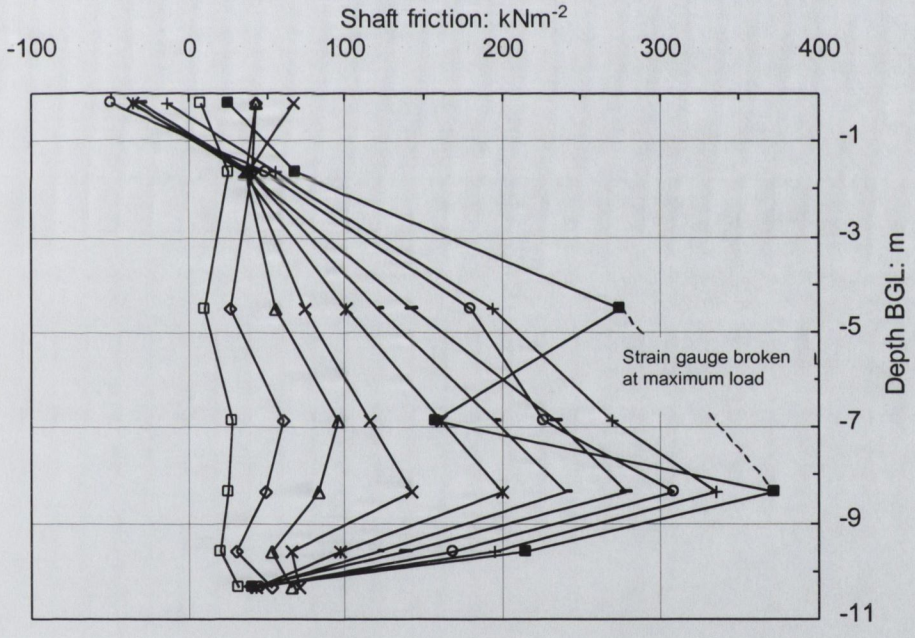

Fig. B.2.7(b). Shaft friction distribution/mobilisation in Pile 600

C Apparatus Design Drawings and Photographs.

C.1 Oedometer Design Drawings and Photographs.

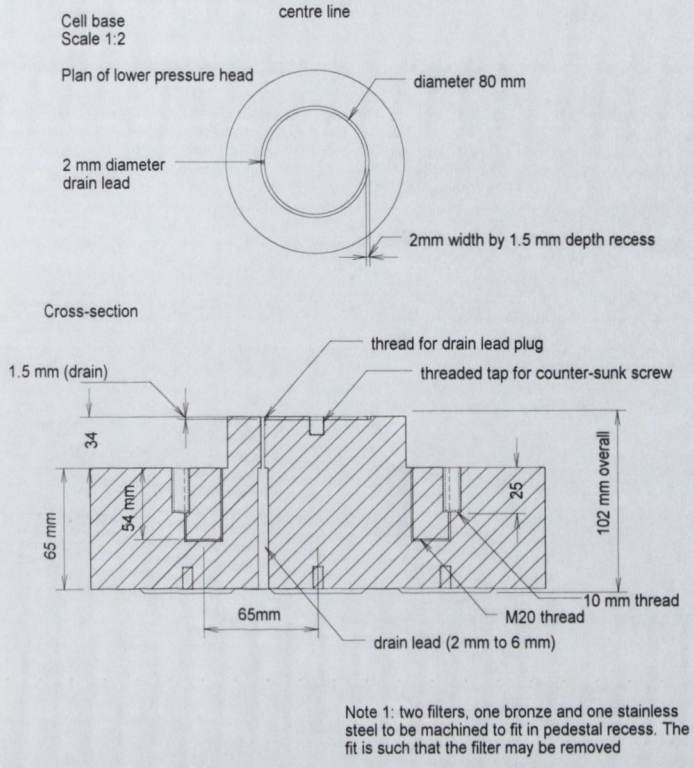

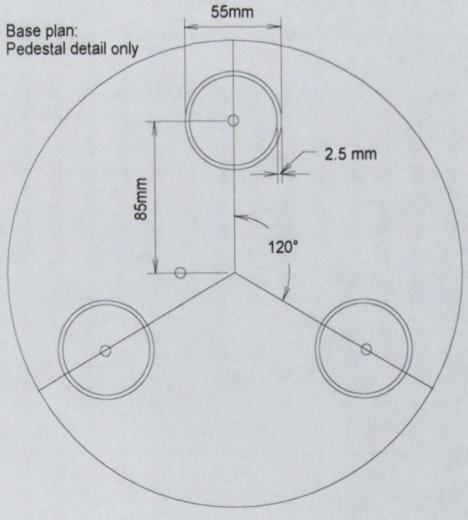

Fig. C.1. Special oedometer design drawings

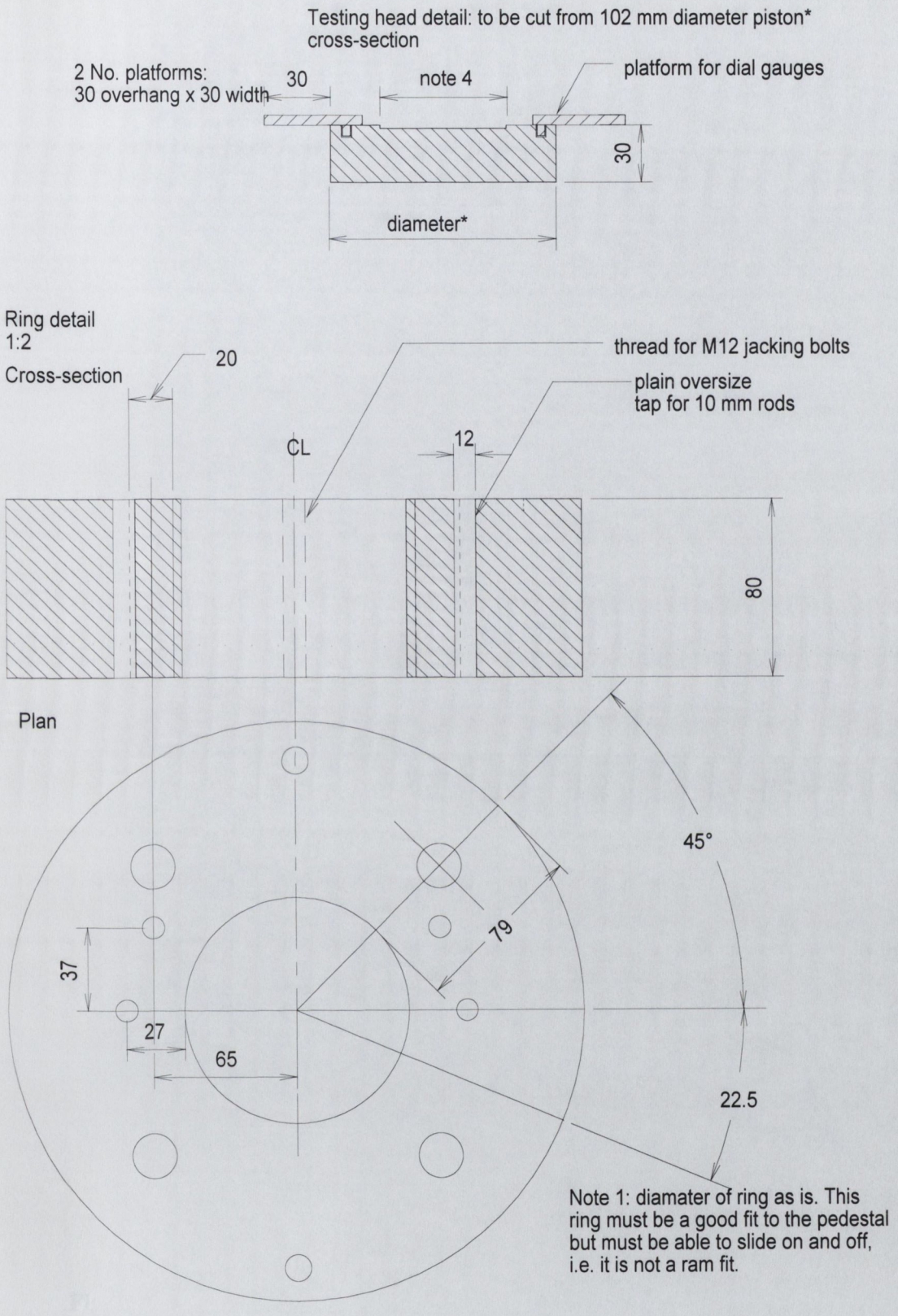

Fig. C.1. cont'd... Special oedometer design drawings

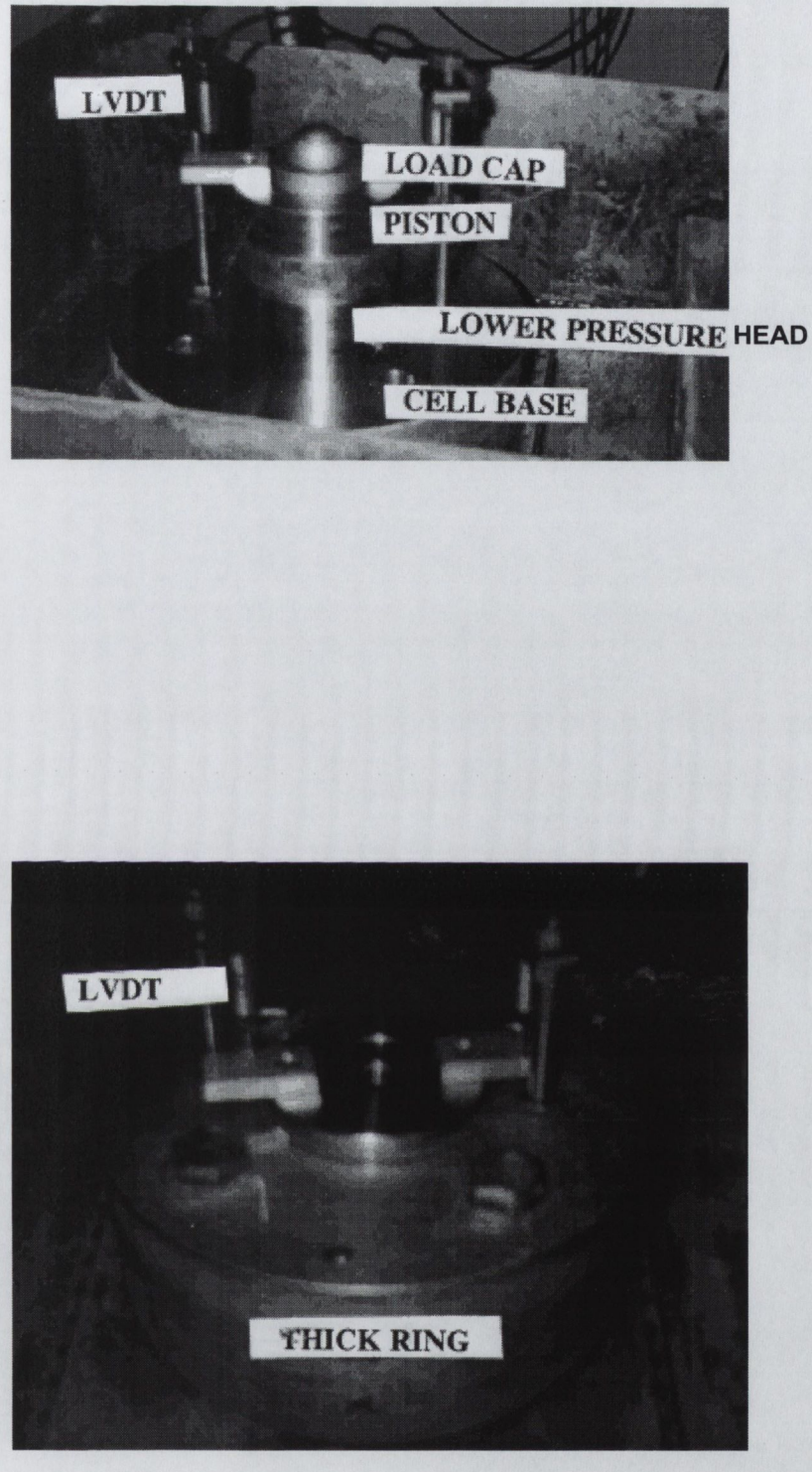

Fig. C.2. Special oedometer: cell, load cap and LVDTs: with and without ring

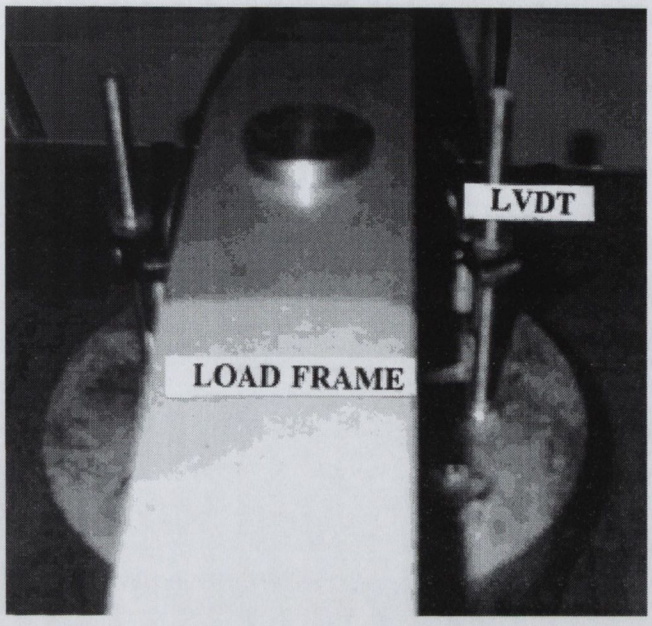

Fig. C.2 cont'd.... Oedometer load frame

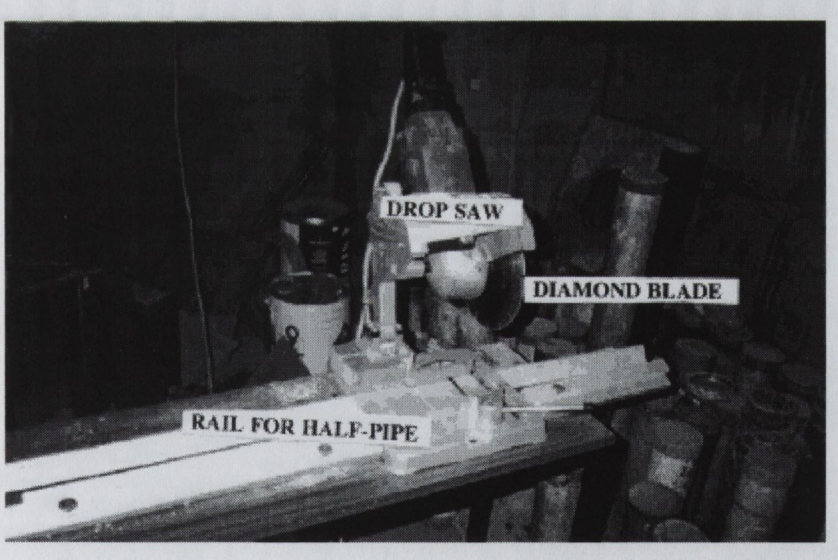

Fig. C.3. Diamond bladed drop saw used for slicing oedometer specimens

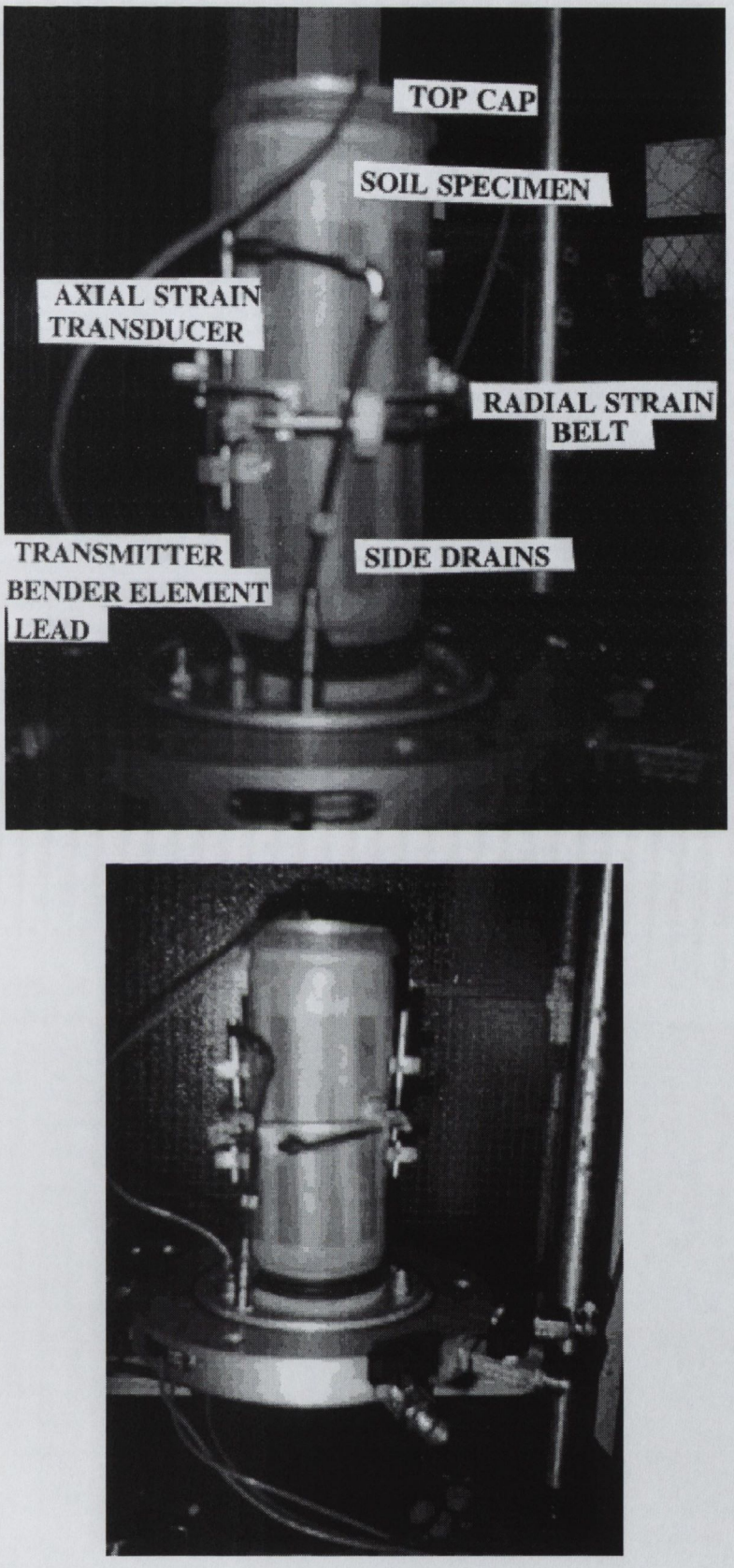

Fig. C.4 Triaxial test set-up: bender element top cap and radial and axial LVDTs

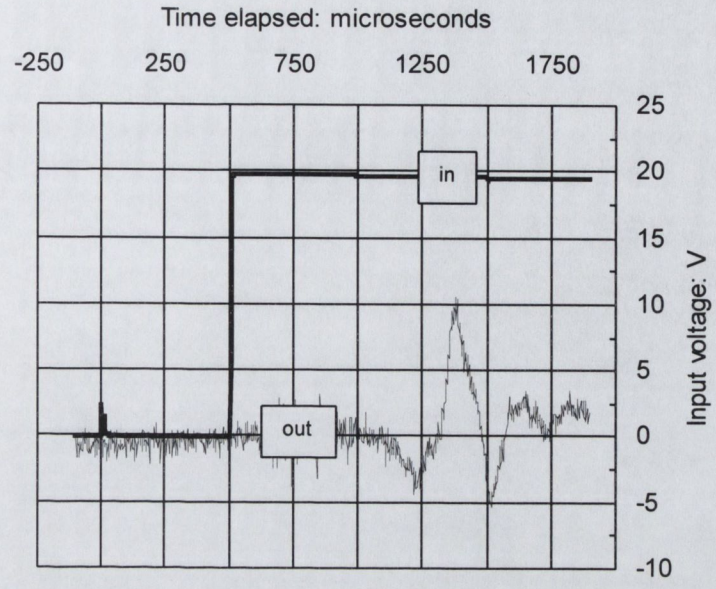

(a)

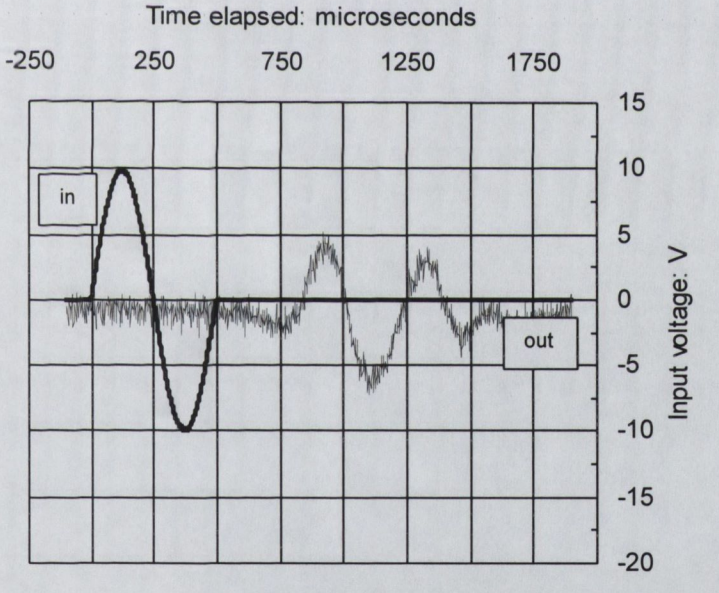

(b)

Fig. C.5. (a) Typical square wave; (b) typical sine wave (note near field effect)

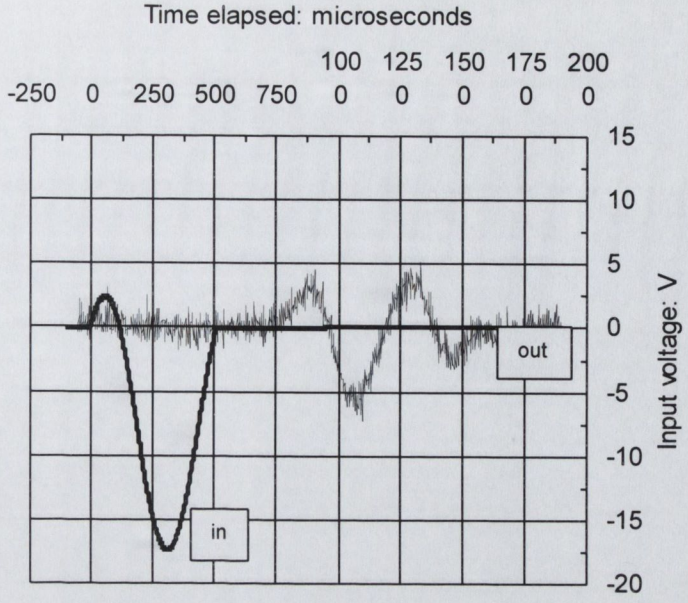

(c)

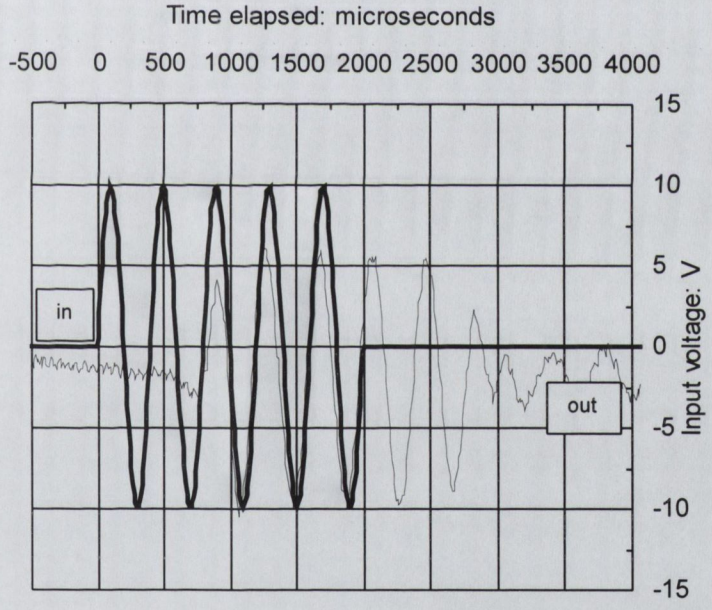

(d)

Fig. C.5 cont'd.... (c) arbitrary sine wave (near-field effect removed – see Fig. D.2(b)); (d) typical resonance test (note that the instability, evident in the previous traces, is resolved)



Fig. C.6. Geobor S rig, wire-line and polymer gel flush

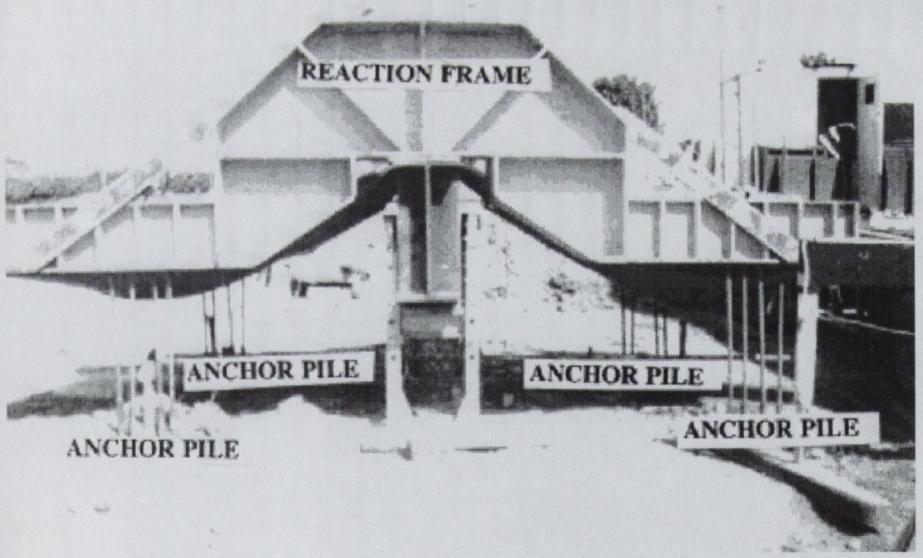

Fig. C.7. Pile testing equipment: Pile test reaction frame

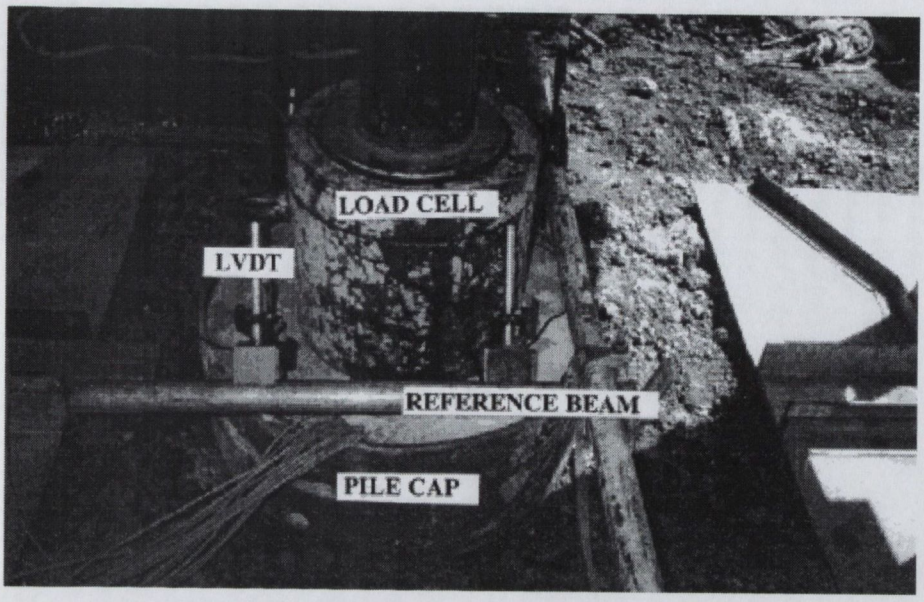

Fig. C.8. Pile testing equipment: load cell, displacement transducers and pile cap

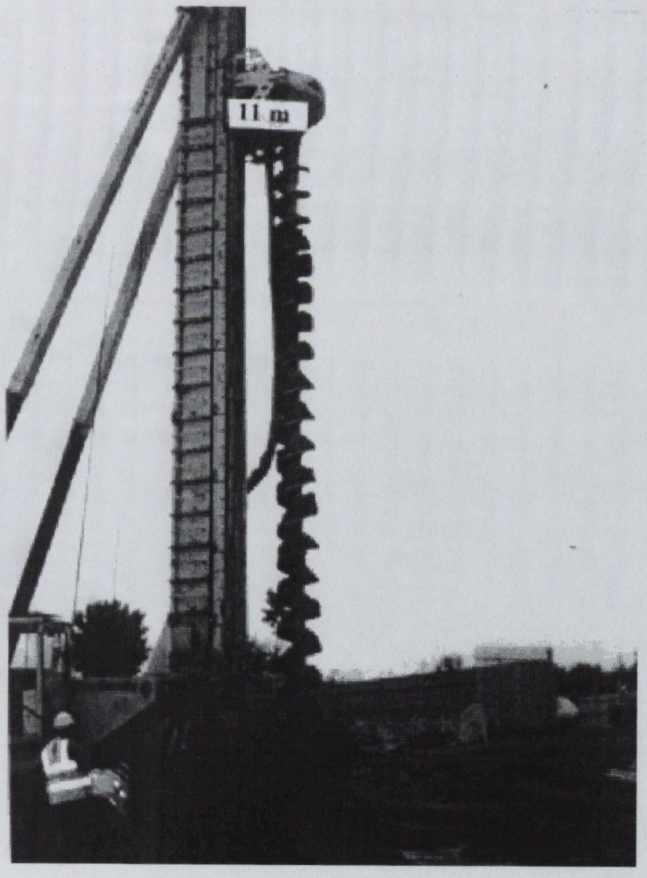

Fig. C.9. Pile testing equipment: CFA rig immediately prior to construction of 11 m length Pile 600

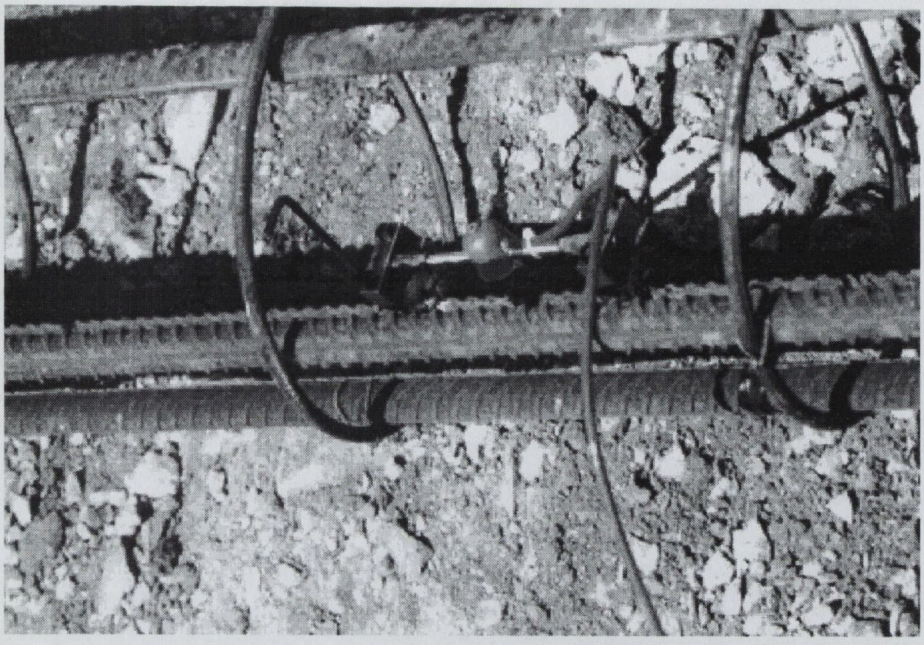

Fig. C.10. Pile testing equipment: VWSG spot-welded to rebar

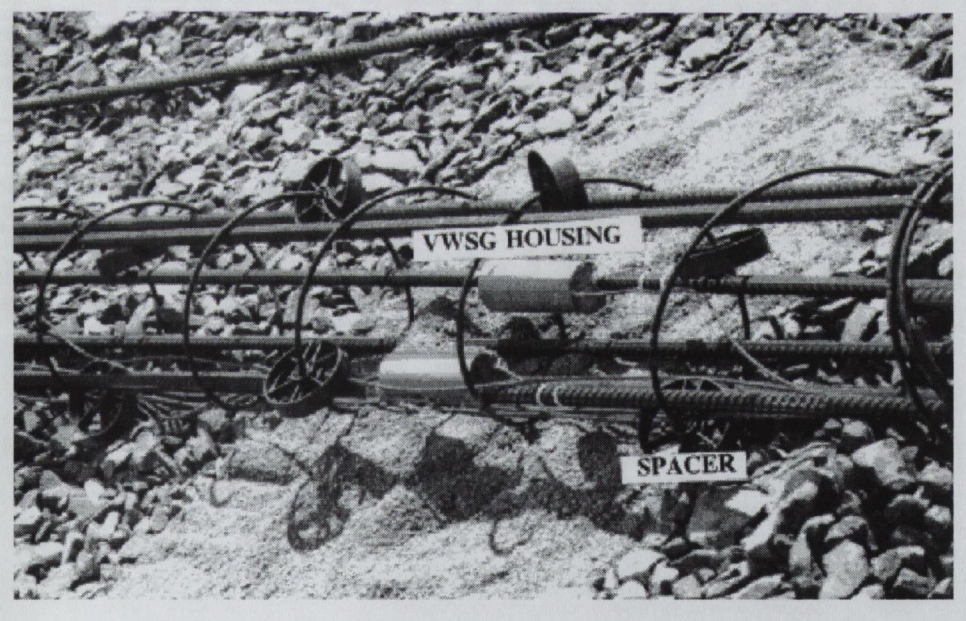

Fig. C.11. Pile testing equipment: Diametrically opposite VWSGs in housing, pile cage and spacers

REFERENCES

REFERENCES

Books: Author's surname, Initials, Title of book, Publisher, Place of Publication, year.

Periodicals: Author's surname, Initials, Title of article, *Title of periodical* year, **volume**, month or part, first - last page number. (Earliest - latest paper.)

Conference Proceedings: Author's surname, Initials, Title of paper, Title of conference proceedings, Place of Conference, date, year, first - last page number. (Earliest - latest paper.)

Anderson, W.F. & McKinlay, D.G.,Tests to find the modulus of deformation of till, The Engineering Behaviour of Glacial Materials (Proceedngs of the Symposium held at the University of Birmingham, 21-23rd April, 1975, revised and reprinted), Geo Abstracts, Norwich, 1978, 129-137.

Arman, A. & McManis, K. L., Effects of storage and extrusion on sample properties, *ASTM Sp. Tech. Pub.* 1976, **599**, 66-87.

ASTM, Standard test method for measurement of soil potential (suction) using filter paper, *An. Bk. ASTM Stds.* 1992 (**D 5298 - 92**), 1312-1317.

Atkinson, J.H., A note on modelling small strain stiffness in Cam clay, Predictive Soil mechanics, Thomas Telford, London, 1993, 111-120.

Atkinson, J.H., Non-linear soil stiffness in routine design, *Geotechnique* 2000, **50**, No. 5, 487-508.

Atkinson, J.H. & Evans, J.S., The measurement of soil stiffness in the triaxial apparatus; discussion and reply, *Geotechnique* 1985, **35**, No. 3, 378-382.

Atkinson, J.H. & Sallfors, G., Experimental determination of stress-strain-time characteristics in laboratory and in situ tests, *Proc. X Euro. Conf. Soil Mech. Found. Engng.*, Firenze 1991, Vol. III, 915-956.

Baker, C.L., Lahti, L.R. & Roumbanis, D.C., Urban geology of Toronto and surrounding area, *Special Paper Geol. Assoc. Can.*, **Vol. 42**, 1998, 323-352.

Bernardi, R., Influence of non-linear behaviour of soils on the performance of bored piles, Proc. Deep Founds. Bored Auger. Piles, AA Balkema, Rotterdam, 1998, 369-376.

Bevan, O.M. & Parkes, D.B., Tunnelling in glacial materials in the British Isles, The Engineering Behaviour of Glacial Materials (Proceedngs of the Symposium held at the University of Birmingham, 21-23rd April, 1975, revised and reprinted), Geo Abstracts, Norwich, 1978, 235-243.

Bishop, A.W., Test requirements for measuring the coefficient of earth pressure at rest, *Proc. Conf. Earth Pr. Probs.*, 1958, Vol. 1, 2-14.

Bishop, A.W., Webb, D.L. & Lewin, P.I., Undisturbed samples of London Clay from the Ashford Common shaft: strength effective stress relationships, *Geotechnique* 1965, **15**, No. 1, 1-31.

Black, D.K. & Lee, K.L., Saturating laboratory specimens by back-pressure, *J. Soil Mech. Found. Div. A.S.C.E.* 1973, **99**, No. SM1, 75-93 (cited by Head, 1998).

BMA, Unpublished seismic survey and site investigation report at Scholarstown, 1995.

Bodare, A. & Massarsch, K., Determination of shear wave velocity by different cross-hole methods, *Proc. VIII World Conf. Earthquake Engng.* 1984, Vol. 3, 39-45.

Bolton, M.D., The strength and dilatancy of sands, *Geotechnique* 1986, **36**, No. 1, 65-78.

Boulton, G.S., Modern Arctic glaciers as depositional models for former ice sheets, *J. Geo. Soc. Lon.* 1972, **128**, 361-393.

Boulton, G.S., Processes and patterns of subglacial sedimentation: a theoretical approach, Ice Ages Ancient and Modern: *Proc. XXI Inter-Uni. Geolog. Cong.*, University of Birmingham 1975, 7-42.

Boulton, G.S., The genesis of glacial tills – a framework for geotechnical interpretation, The Engineering Behaviour of Glacial Materials (Proceedngs of the Symposium held at the University of Birmingham, 21-23rd April, 1975, revised and reprinted), Geo Abstracts, Norwich, 1978, 52-59.

Boulton, G.S., The origin of till sequences by subglacial sediment deformation beneath mid-latitude ice sheets, *An. of Glaciology* 1996, **22**, 75-84.

Boulton, G.S. & Paul, M.A., The influence of genetic processes on some geotechnical properties of glacial tills, *Quart. J. Engng. Geol.* 1976, **9**, No. 3, 159-194.

Boulton, G.S., Dent, D L. & Morris, E.M., Subglacial shearing and crushing, and the role of water pressures in till from south-east Iceland, *Geografiska Annaler* 1974, **56**, A, 135-145.

Bowen, D.Q., Time and space in the glacial sediment systems of the British Isles, Glacial Deposits in Great Britain and Ireland, AA Balkema, Rotterdam, Brookfield, 1991, 3-12.

Bowen, D.Q., The Pleistocene of north west Europe, *Sci. Progr.* 1992, **76**, 209-223.

Boyer, L., Bensoussen, A., Durand, M., Grice, R.H. & Bernard, J., Geology of Montreal, Province of Quebec, Canada, *Bull. Assoc. Engng. Geols.* 1985, **22**, No. 4, 329-394.

Brignoli, E.G.M., Gotti, M. & Stokoe, K.H., Measurement of shear waves in laboratory specimens by means of piezoelectric transducers, *A.S.T.M. Geo. Test. J.* 1996, **19**, No. 4, 384-397.

Brooker, E.W. & Ireland, H.O., Earth pressures at rest related to stress history, *Can. Geo. J.* 1965, **II**, No. 1, 1-15.

BS, 8110: 1985, **2**, Sec. 3.

Burghignoli, A., Payne, V. & Cavalera, L., Modelling stress-strain-time behaviour of natural soils: monotonic loading, *Proc. X Euro. Conf. Soil Mech. Found. Engng.*, Firenze 1991, Vol. III, 961-980.

Burland J.B., Small is beautiful – the stiffness of soils at small strains, *Can. Geo. J.* 1989, **26**, No. 4, 499-516.

Burland, J.B., On the compressibility and shear strength of natural clays, *Geotechnique* 1990, **40**, No. 3, 329-378.

Butler, F.G., Heavily over-consolidated clays, *Proc. Conf. Settlement Structs.*, Cambridge 1975, Session III, review paper (cited by Simpson et al. (1979)).

Butterfield, R., A natural compression law for soils (an advance on e-log p′), *Geotechnique* 1979, **29**, No. 4, 469-480.

Chandler, R.J., Clay sediments in depositional basins: the geotechnical cycle, *Quart. J. Engng. Geol.* 2000, **33**, 7-39.

Chandler, R.J., Crilly, M.S. & Montgomery-Smith, G., A low-cost method of assessing clay desiccation for low-rise buildings, *Proc. Instn. Civ. Engng., Civ. Engng.*, 1992a, **92**, May, 82-89.

Chandler, R.J., Harwood, A.H. & Skinner, R.J., Sample disturbance in London Clay, *Geotechnique* 1992b, **42**, No. 4, 577-585.

Charlesworth, J.K., The glacial retreat from central and southern Ireland, *Quart. J. Geol.Soc. Lon.* 1928, **84**, 293-342 (cited by Hoare, 1991c).

Chin, F., The inverse slope as a prediction of (the) ultimate bearing capacity of piles, *Proc. III S.E. As. Conf. Soil Engng.*, 1972, 83-91.

Civil Engineering and Public Work Review, Recent research into the pressure of concrete on formwork, *Civ. Engng. Pub. Wrks. Rev.* 1965, **Dec.**, 1779-1781.

Clarke, B.G., Pressuremeter testing in ground investigation Part II – interpretation, *Instn. Civ. Engrs.: Geo. Engnr.*, 1997, **125**, No. 1, 45-52.

Clarke, B.G., 2002, In a lecture to the GSI.

Clarke, B.G., Chen, C.-C. & Aflaki, E., Intrinsic compression and swelling properties of a glacial till, *Quart. J. Engng. Geol.*, 1998, **31**, 235-246.

Cotechhia, F. & Chandler, R.J., One-dimensional compression of a natural clay: structural changes and mechanical effects, The Geotechnics of Hard Soils - Soft Rocks Vol. I (conf. in print), Balkema, Rotterdam, 1998, 103-114.

Cour, F.R., Inflection point method for computing c_v, *J. Soil Mech. Founds. Div. A.S.C.E.* 1971, **97**, No. SM5, 827-831.

Crilly, M.S. & Chandler, R.J., A method of determining the state of desiccation in clay soils, *Build. Res. Estab. Info. Pap.* 1993, IP 4/93, pp 4.

Culleton, E.B., Characterisation of glacial deposits in South Wexford, *Proc. Roy. Ir. Acad.* 1986, **LXXVIII, B**, 293-308 (cited by Warren, 1991b).

Davies, G.L.H. & Stephens, N., Ireland [by], Methuen, London, 1978, p 250.

Davis, A.M. & Schultheiss, P.J., Seismic signal processing in engineering site investigation; a case history, *Grd. Engng.* 1980, **13**, No. 4, 44-48.

DeJong, J., Foundation displacements of multi-storey structures, Ph.D. thesis, University of Alberta, Edmonton, Edmonton, Alberta, unpublished (cited by DeJong and Harris, 1971).

DeJong, J. & Harris, M.C., Settlements of two multistory buildings in Edmonton, *Can. Geo. J.* 1971, **8**, 217-235.

DeJong, J. & Morgenstern, N.R., Heave and settlement of two tall building foundations in Edmonton, Alberta, *Can. Geo. J.* 1973, **10**, 261-281.

De Moor, E.K., An analysis of bored pile/diaphragm wall installation effects, *Geotechnique* 1994, **44**, No. 2, 341-347.

Derbyshire, E., Distribution of glacial soils in Great Britain, The Engineering Behaviour of Glacial Materials (Proceedngs of the Symposium held at the University of Birmingham, 21-23rd April, 1975, revised and reprinted), Geo Abstracts, Norwich, 1978, 6-17.

Doff, D., Dept. of Geochemistry, Trinity College, 2001. Personal communication.

Donath, A.D., Untersuchungen ueber den Erddruck auf Stuetzwaende, Zeitschrift fuer Bauwesen, Berlin, 1891 (cited by Hendron, 1963).

Doran, S.R., Kofoed, N., Hartwell, D.J. & Warren, S., Design and implementation of cross-passages ground treatment, *Proc. XI Euro. Conf. Soil Mech. Found. Engng.*, Copenhagen 1995, Vol. 5, 83-102.

Drucker, D.C. & Prager, W., Soil mechanics and plastic analysis in limit state design, *Quart. J. App. Math.* 1952, **10**, 157-165 (unseen).

Duncan, J.M. & Chang, C., Nonlinear analysis of stress and strain in soils, *J. Soil Mech. Founds. Div. Proc. A.S.C.E.* 1970, **96**, No. SM5, 1629-1653.

Dyvik, R. & Madshus, C., Laboratory measurements of G_{max} using bender elements, *Meet. Advs. Art Test. Soils Under Cyc. Conds.*, Detroit 1985 (cited by Brignoli et al., 1996).

Dyvik, R., Lacasse, S. & Martin, R., Coefficient of lateral stress from [an] oedometer cell, *XI Int. Conf. Soil Mech. Founds. Engng.*, California 1985, 1003-1006.

Ehlers, J., Gibbard, P. & Rose, J., Glacial deposits of Britain and Europe; general overview, Glacial Deposits in Great Britain and Ireland, AA Balkema, Rotterdam, Brookfield, 1991, 493-501.

Eisenstein, Z. & Morrison, N.A., Prediction of foundation deformations in Edmonton using an in situ pressure probe, *Can. Geo. J.* 1973, **10**, 193-210.

Eisenstein, Z. & Thomson, S., Geotechnical performance of a tunnel in till, *Can. Geo. J.* 1978, **15**, 332-345.

Eisenstein, Z. & Medeiros, L.V., A deep retaining structure in till and sand. Part II: Performance and analysis, *Can. Geo. J.* 1983, **20**, 131-140.

Eyles, N. & McCabe, A.M., Glaciomarine facies within subglacial tunnel valleys: the sedimentary record of glacio-isostatic downwarping in the Irish Sea Basin, *Sedimentology* 1989, **36**, 431-448 (cited by, inter alios, Elyes and McCabe, 1991).

Eyles, N. & McCabe, A.M., Glaciomarine deposits of the Irish Sea Basin: the role of glacio-isostatic disequilibrium, Glacial Deposits in Great Britain and Ireland, AA Balkema, Rotterdam, Brookfield, 1991, 311-332.

Fahey, M. & Carter, J.P., A finite element study of the pressuremeter test in sand using a nonlinear elastic plastic model, *Can. Geo. J.* 1993, **30**, 348-362.

Faillace, G.A. & Silver, M.L., Effect of sampling on the dynamic stress-strain properties of till, The Engineering Behaviour of Glacial Materials (Proceedngs of the Symposium held at the University of Birmingham, 21-23rd April, 1975, revised and reprinted), Geo Abstracts, Norwich, 1978, 141-148.

Fairhurst Garland and Partners, Unpublished Saint James's St. site-investigation report, 1978.

Farrell, E.R., Settlement parameters of Dublin black boulder clay, *Grd .Engng.* 1989, **22**, No. 5, 33-35.

Farrell, E.R. & Wall, D., Soils of Dublin, *Trans. Inst. Engngs. Ir.* 1990, 44-96.

Farrell, E.R. & Lawler, M., Estimating ground movements in a very stiff lodgement till, *Proc. XIV SEAGC*, Hong Kong, 2001, 309-314.

Farrell, E.R., Bunni, N. & Mulligan, J., The bearing capacity of Dublin Black Boulder Clay, *Trans. Instn. Engrs. Ireland* 1988, **112**, 77-104.

Farrell, E.R., Lehane, B. & Looby, M., An instrumented driven pile in Dublin boulder clay, *Proc. Instn. Civ. Engrs., Geotechnical Engineering* 1998, **131** No. 4.

Farrell, E.R., Lawler, M. & Treacy, P., Modelling ground movements in stiff glacial soil, to be published in *Geotechnique* 2003.

Farrell, E.R., Orr, T., Lehane, B. & O'Brien, S., Stiffness of Dublin black boulder clay, *Proc. XI ECSMFE*, Copenhagen, 1995a, pp 6.

Farrell, E., Coxon, P., Doff,.D. & Pried'homme, L., Genesis of brown boulder clay in Dublin, *Quart. J. Engng. Geol.* 1995b, **28**, 143-152.

Farrington, A., The pre-glacial topography of the Liffey Basin, *Proc. Roy. Ir. Acad.* 1929, **XXXVIII, B, 9** (cited by Farrell and Wall, 1990).

Farrington, A., The glacial drift near Brittas, on the border between Co. Dublin and Co. Wicklow, *Proc. Roy. Ir. Acad.* 1942, **XXXXVIII, B**, 279-291 (cited by Warren, 1991b)

Farrington, A., The glacial drifts of the district around Eniskerry, Co. Wicklow, *Proc. Roy. Ir. Acad.* 1944, **L, B.**, 133-157 (cited by Hoare, 1991c)

Faulkner, A., Application to Irish conditions of new field and laboratory geotechnical testing techniques, M.Sc. thesis, University of Dublin, Trinity College, 1998.

Fleming, W.G.K., A new method for single pile settlement prediction and analysis, *Geotechnique* 1992, **42**, No. 3, 411-425.

Fleming, W.G.K., The understanding of continuous flight auger piling, its monitoring and control, *Proc. Instn. Civ. Engng., Geo. Engng.* 1995, **113**, No. 3, 157-165.

Francis, E.A., On the classification of glacial sediments, Quaternary in Britain, Pergamon, Oxford, 1983, 237-247 (cited by Paul and Little, 1991).

Fredlund, D.G., Rahardjo, H., Leong, E.C. & Ng, C.W.W., Suggestions and recommendations for the interpretation of soil-water characteristic curves, *Proc. XIV S. E. As. Geo. Conf.*, Hong Kong 2001, Vol. 1, 503-508.

Foged, N., Larsen, G., Larsen, B. & Thomsen, E., An overview on engineering geological conditions at Storebaelt, *Proc. XI Euro. Conf. Soil Mech. Found. Engng.*, Vol. 5, Copenhagen 1995, 1-6.

Fookes, P.G., Gordon, D.L. & Higginbottom, I.E., Glacial landforms, their deposits and engineering characteristics, The Engineering Behaviour of Glacial Materials (Proceedngs of the Symposium held at the University of Birmingham, 21-23rd April, 1975, revised and reprinted), Geo Abstracts, Norwich, 1978, 18-49.

Gage Technique Ltd., 1998.

GDS, Geotechnical Digital Systems Ltd.

Geoconsult-Arup Consortium, Unpublished Dublin Port Tunnel reports: site investigation, laboratory testing & field testing, 1997.

Germaine, J.T., Mass. Inst. Tech. 2002. Personal communication.

Gibson, R.E. & Anderson, W.F., In-situ measurement of soil properties with the pressuremeter, *Civ. Engng. Pub. Wrks. Rev.* 1961, **56**, No. 5, 615-620 (cited by Eisenstein and Morrison, 1973).

Gleeson, T., Kinsealy (Dublin) Land Research Institute, 2000. Personal communication.

Hanrahan, E.T., Irish glacial till: origin and characteristics, Special Pub. of Forbairt, **No. 1**, 1977.

Hartford, D.N.D., Some aspects of the engineering behaviour of well graded soils, Ph.D. thesis, University of Dublin, Trinity College, 1987.

Head, K.H. Manual of soil laboratory testing (Vol. 3), John Wiley & Sons, Chichester, 1998.

Hendron, A.J., The behaviour of sand in one-dimensional compression, Ph.D. thesis, University of Illinois, 1963.

Hight, D.W., Gens, A. & Jardine, R.J., Discussion on: The reaction of clays to sampling stress relief, *Geotechnique* 1985, **35**, No. 1, 86-89.

Hillier, S., Accurate quantitative analysis of clay and other minerals in sandstones by XRD; comparison of a Rietveld and a reference intensity ratio (RIR) method, and the importance of sample preparation, *Clay Minerals* 2000, **35**, 295-306 (cited by Hillier, 2002).

Hillier, S., McCaulay Land Use Research Institute, 2002. Personal communication.

Hillier, S., McCaulay Land Use Research Institute, 2003. Personal communication.

Hird, C.C. & Pierpont, N.D., Stiffness determination and deformation analysis for a trial excavation in Oxford clay, *Pre-failure deformation behaviour of geomaterials*, Geotechnique Sym. in Print, Thomas Telford, London, 1998, 279-306.

Hird, C.C. & Moseley, V. J., Model study of seepage in smear zones around vertical drains in layered soil, *Geotechnique* 2000, **50**, No. 1, 89-97.

Hoare, P.G., The pattern of glaciation of Co. Dublin, *Proc. Roy. Ir. Acad.* 1975, **75B**, 207-224 (cited by Farrell and Wall, 1990).

Hoare, P.G., Pre-Midlandian glacial deposits in Ireland, Glacial Deposits in Great Britain and Ireland, AA Balkema, Rotterdam, Brookfield, 1991a, 37-45.

Hoare, P.G., Late-Midlandian glacial deposits and glaciation in Ireland and the adjacent offshore region, Glacial Deposits in Great Britain and Ireland, AA Balkema, Rotterdam, Brookfield, 1991b, 69-78.

Hoare, P.G., The glacial stratigraphy and deposits of eastern Ireland, Glacial Deposits in Great Britain and Ireland, AA Balkema, Rotterdam, Brookfield, 1991c, 367-378.

Houlsby, G.T., How the dilatancy of soils affects their behaviour, *Proc. X Euro. Conf. Soil Mech. Found. Engng.*, Firenze 1991, Vol. IV, 1189-1202.

Hughes, D.B., Clarke, B.G. & Money, M.S., The lowland tills of Northern England, *Quart. J. Engng. Geo.*, 1998, **31**, 211-234.

I.G.S.L., Unpublished site investigation report, Sandymount Strand, 1992.

Izumi, K., Ogihara, M. & Kameya, H., Displacements of bridge foundations on sedimentary soft rock, *Pre-failure deformation behaviour of geomaterials*, Geotechnique Sym. in Print, Thomas Telford, London, 1998, 233-246.

Jacobsen, M., Bulletin of the D.G.I., 1970, **No. 27**, pp 60.

Jaky, J., A nyugalmi nyomas tenyezoje, *J. for Soc. of Hungarian Architects and Engnrs.* 1944, **October**, 355-358.

Janbu, N., Soil compressibility as determined by oedometer and triaxial tests, *Proc. Euro. Conf. Soil Mech. Found. Engng.*, Wiesbaden 1963, 19-25 (cited by Duncan and Chang (1970) and Schanz and Vermeer (1998)).

Janbu, N., Stress-strain-time behaviour of porous media: A case history based review, *Proc. 10th Euro. Conf. Soil Mech. Found. Engng.*, Firenze 1991, 1417-1433.

Jardine, R.J., Saint John, H.D., Hight, D.W. & Potts, D.M., Some practical applications of a non-linear ground model, *Proc. X Euro. Conf. Soil Mech. Found. Engng.*, Firenze 1991, Vol. I.

Jardine, R.J., Potts, D.M., Fourie, A.B. & Burland, J.B., Studies of the influence of non-linear stress-strain characteristics in soil-structure interaction, *Geotechnique* 1986, **36**, No. 3, 377-396.

Jeffries, H., The Earth: the origin, history, and physical constitution (3rd edn.), Cambridge University press, 1952, 282.

Johansson, H.G., Moraine ridges and till stratigraphy in Vasterbotten, northern Sweden, *Sveriges Geologiska Undersoekning*, Serie c, **673**, pp 50 (cited by May and Thomson, 1978).

Jonsson, A., Andersson, B. & von Storkirch, C., A method study of Geobor S, Master of science thesis, Dept. of Engng. Geol., Lund Uni., 1995.

Jovicic, V., Coop, M.R. and Simic, M., Objective criteria for determining G_{max} from bender element tests, *Geotechnique* 1996, **46**, No. 2, 357-362.

Kamb, W.B. & LaChapelle, E.R., Direct observation of the mechanism of glacier sliding over bedrock, *J. Glaciol.* 1964, **5**, No. 38, 159-172 (cited by Weertman, 1964).

Kavvadas, M.J., General report: modelling the soil behaviour - selection of soil parameters, The Geotechnics of Hard Soils - Soft Rocks Vol. III (conf. in print), Balkema, Rotterdam, 1998, 1441 - 1482.

Kavvadas, M.J. & Amorosi, A., A plasticity model for the mechanical behaviour of structured soils, The Geotechnics of Hard Soils - Soft Rocks Vol. II (conf. in print), Balkema, Rotterdam, 1998, 603-613.

Kilkenny, B., Investigation of the long-term stability of the steep slopes at Strawberry Beds, Co. Dublin, Ireland, M.Sc. thesis, Imperial College London, 1990.

Kirkpatrick, W. M. & Khan, A. J., The reaction of clays to sampling stress relief, *Geotechnique* 1984, **34**, No. 1, 29-42.

Knudsen, C., Andersen, C., Foged, N., Jakobsen, P.R. & Larsen, B., Stratigraphy and engineering geology of Kobenhavn limestone, *Proc. XI Euro. Conf. Soil Mech. Found. Engng.*, Copenhagen 1995, Vol. 5, 117-126.

Konder R.L., Hyperbolic stress-strain response: cohesive soils, *J. Soil Mech. Founds. Engng, Div. A.S.C.E.* 1963, **89**, 115-143.

Kriegel, H.J. & Weisner, H.H., Problems of stress-strain conditions in subsoil, *Proc. XIII Int. Conf. Soil Mech Found. Engng.*, Moscow 1973, Vol. 1 133-144 (cited by Burghignoli, A., Pane, V. & Cavalera, L., Modelling stress-strain-time behaviour of natural soils: monotonic loading, *Proc. X Euro. Conf. Soil Mech. Found. Engng.*, Firenze 1991, Vol. 3, p 963).

Kristensen, P.S., Regtop, J. & Balstrup, T., Predicted and observed settlements and tilts of offshore bridge piers, *Proc. XI Euro. Conf. Soil Mech. Found. Engng.*, Copenhagen 1995, Vol. 5, 43-52.

Kulhawy, F.H., Some thoughts on the evaluation of undrained shear strength for design, Predictive Soil mechanics, Thomas Telford, London, 1993, 394-403.

Ladd, C.C. & Foott, R., New design procedure for stability of soft clays, *J. Geo. Engng. Div. A.S.C.E.* 1974, **100**, No. GT7, 763-786.

Lawler, M. & Farrell, E., Predicting the behaviour of C.F.A. piles in stiff till, to be submitted to the *Proc. Instn. Civ. Engng., Geo. Engng.* 2003.

Lawler, M., A geological study of Dublin for F.E. methods, to be submitted to *Quart. J. Engng. Geol.*, 2003.

Lehane, B. M. and Farrell, E.R., A serviceability limit state design approach for footings. *Procs. 14th Int. Conf. Soil Mech. Found. Engng.*, Hamburg 1997, 359-362.

Lehane, B. M. and Simpson, B., Modelling glacial till under triaxial conditions using a Brick soil model. *Can. Geotech. J.* 2000, **37**, 1078 – 1088.

Leroueil, S., Samson, L. & Bozozuk, M., Laboratory and field determination of preconsolidation pressures at Gloucester, *Can. Geo. J.* 1983, **20**, No. 3, 477-490.

Lings, M.L. & Greening, P.D., A novel bender/extender element for soil testing, *Geotechnique* 2001, **LI**, No. 8, 713-718.

Lings, M.L., Pennington, D.S. & Nash, D.F.T., Anisotropic stiffness parameters and their measurement in a stiff natural clay, *Geotechnique* 2000, **50**, No. 2, 109-125 (cited by Atkinson, 2000).

Long M., Design and construction of deep basements in Dublin, Ireland, *Proc. XIV Int. Conf. Soil Mech. Found. Engng.*, 1997, Vol. 2, 1377-1380.

Looby, M. Investigation of the behaviour of driven piles in overconsolidated clay, M.Sc. thesis, University of Dublin, Trinity College, 1996.

LRT, Unpublished Luas Light Rail site-investigation report, 1997.

Mancuso, C., Simonelli, A.L. & Vinale, F., Numerical analysis of in situ S-wave measurements, *Proc. XII Int. Conf. Soil Mech.* 1989, Rio de Janeiro, Vol. 3, 277-280.

Mancuso, C., Rampicco, C. & Vinale, F., Influence of matric suction on stiffness (sic.) of a compacted silty sand, The Geotechnics of Hard Soils - Soft Rocks Vol. II (conf. in print), Balkema, Rotterdam, 1998, 669-674.

Marsland, A. & Randolph, M.F., Comparison of the results from pressuremeter tests and large in situ plate tests in London Clay, *Geotechnique* 1977, **27**, No. 2, 217-243.

Martin, R., Ardaman Geotechnical (Assoc.) 2001, Personal communication.

Matheson, D.S., A tunnel roof failure in till, *Can. Geo. J.* 1970, **7**, 313-317.

Matthews, M.C., Clayton, C.R.I. & Own, Y., The use of field geophysical techniques to determine geotechnical stiffness parameters, *Proc. Inst. Civ. Engnrs. Geo. Engng.* 2000, **143**, 31-42.

May, R.W. & Thomson, S., The geology and geotechnical properties of till and related deposits in the Edmonton, Alberta, area, *Can. Geo. J.* 1978, **15**, 362-370.

Mayne, P.W., Determining OCR in clays from laboratory strength, *J. Geo. Engng.* 1988, **114**, No. 1, 76-92.

Mayne, P.W. & Kulhawy, F.H., K_o-OCR relationships in soil, *J. Geo. Engng. Div. A.S.C.E.* 1982, **108**, No. GT6, 851-872.

McCabe, A.M., Quaternary deposits and glacial stratigraphy in Ireland, *Quart. Sci. Rev.* 1987, **6**, 259-299 (cited by Farrell et al., 1995b).

McCabe, A.M., Dating and rhythmicity from the last deglacial cycle in the British Isles, *J. Geol. Soc.* 1996, **153**, No. 4, 499-502.

McCabe, A.M., Knight, J. & McCarron, G., Ice-flow stages and glacial bedforms in north central Ireland: a record of rapid environmental change during the last glacial termination, *J. Geo. Soc.* 1999, **156**, 63-72.

McKinlay, D.G., McGown, A., Radwan, A. M. & Hossain, D., Representative sampling and testing in fissured lodgement tills, The Engineering Behaviour of Glacial Materials (Proceedngs of the Symposium held at the University of Birmingham, 21-23rd April, 1975, revised and reprinted), Geo Abstracts, Norwich, 1978, 129-137.

Menard, L., Rules for the calculation and design of foundation elements on the basis of pressuremeter investigations in the ground, *Proc. XI Int. Conf. Soil Mech. Found. Engng.*, Vol. 2, 1965, 295-299 (cited by Eisenstein and Morrison, 1973).

Milligan, G., University of Oxford/Geotechnical Consulting Group, 2003. Personal communication.

Mitchell, F., The Shell guide to reading the Irish landscape, Wild Ireland library, County house, Dublin, 1986.

Moon, C.F., The failure mechanism of quickclay soils – a model approach, The Engineering Behaviour of Glacial Materials (Proceedngs of the Symposium held at the University of Birmingham, 21-23rd April, 1975, revised and reprinted), Geo Abstracts, Norwich, 1978, 75-80.

Muir Wood, D., Soil behaviour and critical state soil mechanics, Cambridge University Press, Cambridge, 1990.

Naylor, D., Pleistocene and post-pleistocene sediments in Dublin Bay, Dept. Geology, Trinity College, 1965, pp 14.

Nye, J.F., The flow of glaciers and ice-sheets as a problem in plasticity, *Proc. Roy. Soc.* 1951, **A**, Vol. 207, 554-572.

O'Riordan, N.J., The mobilisation of shaft adhesion down a bored, cast-in-situ pile in the Woolwich and Reading Beds, *Grd. Engng.* 1982, **April**, 17-26.

O'Rourke, T.D., Ground movements caused by braced excavations, *J. Geo. Engng. Div. A.S.C.E.* 1981, **107**, No. GT9.

Orr, T. & Farrell, E., Geotechnical design to Eurocode 7, Springer, London, 1999.

O'Shea, B., Stress path tests to determine the strength and deformation properties of Dublin boulder clay, M.Sc. thesis, University of Dublin, Trinity College, 1996.

Paul, M.A. & Little, J.A., Geotechnical properties of glacial deposits in lowland Britain, Glacial Deposits in Great Britain and Ireland, AA Balkema, Rotterdam, Brookfield, 1991, 389-404.

Pico, *PicoScope Manual (version 1.0)*, 2001.

Plaxis, *Plaxis Manual (version 7)*, A.A. Balkema, Rotterdam, 1998.

Pennington, D.S., Cracked? Exploring post-construction evidence in the interpretation of trial pile data, *Proc. Instn. Civ. Engng., Geo. Engng.* 1995, **113**, No. 3, 132-143.

PMC Ltd., Precision Monitoring and Control Ltd..

Poulos, H.G. & Davis, E.H., Pile foundation analysis and design, John Wiley and Sons, 1980.

Rampello, S., Stallebrass, S.E. & Viggiani, G.M.B., Panel report: ground movements associated with excavations in stiff clays; current prediction capability, The Geotechnics of Hard Soils - Soft Rocks Vol. III (conf. in print), Balkema, Rotterdam, 1998, 1527-1540.

Randolph, M.F. & Wroth, C.P., Analysis of deformation of vertically loaded piles, *J. Geo. Engng. Div. A.S.C.E.* 1978, **104**, No. GT12, 1465-1488.

Ridley, A.M. & Burland, J.B., A new instrument for the measurement of soil moisture suction, *Geotechnique* 1993, **43**, No. 2, 321-324.

Ridley, A.M. & Wray, W.K., Suction measurement: a review of current theory and practices, *Proc. 1st Int. Conf. Unsat. Soil Mech.*, Paris 1995, 1293-1322.

Ritchie, A.G.B., The pressures developed by concrete on formwork, *Civ. Engng. & Public Works Rev.* 1962, 885-888.

Robertson, P.K. & Ferreira, R.S., Seismic and pressuremeter testing to determine soil modulus, Predictive Soil mechanics, Thomas Telford, London, 1993, 562-580.

Rodin, S., Pressure of concrete on formwork, *Proc. Inst. Civ. Engnrs.* 1952, **1**, No. I, N.5863.

Rowe, P.W., The stress-dilatancy relation for static equilibrium of an assembly of particles in contact, *Proc. R. Soc.* 1962, **A269**, 500-527.

Sanchez-Salinero, I., Roesset, J.M. & Stokoe II, K.H., Analytical studies of body wave propagation and attenuation, *Rep. GR86-15* 1986, University of Texas (cited by inter alios Mancuso et al., 1988).

Schanz, T., A constitutive model for hard soils, The Geotechnics of Hard Soils - Soft Rocks Vol. II (conf. in print), Balkema, Rotterdam, 1998, 861-868.

Schanz, T.& Vermeer P.A., Angles of friction and dilatancy of sand. *Geotechnique* 1996, **46**, No. 1, 145-151.

Schanz T. & Vermeer P.A., On the stiffness of sands, *Pre-failure deformation behaviour of geomaterials*, Geotechnique Sym. in Print, Thomas Telford, London, 1998, 383-387.

Schanz, T., Vermeer P.A. & Bonnier, P.G.. The hardening soil model: formulation and verification, *Beyond 2000 in Computation Geotechnics - 10 years of Plaxis*, Balkema, Rotterdam, 1999. (To be published in *Int. J. An. Num. Mets. Geomech.*.)

Schmidt, B., Lateral stresses in uniaxial strain. *Can. Geo. J.* 1966, **3**, No. 4, 239-242.

Schweiger, H.F., Some remarks on pore pressure parameters A & B in undrained analyses with the Hardening Soil model, *Bull. Plaxis Users Assoc. (NL)* 2002a, **12**, 6-8.

Schweiger, H.F., Plaxis benchmark No. 1: shield tunnel 1 – results, *Bull. Plaxis Users Assoc. (NL)* 2002b, **12**, 9-12.

Shirley, D.J. & Hampton L.D., Shear-wave measurements in laboratory sediments, *J. Acoust. Soc. Am.* 1977, **63**, No. 2, 607-613.

Simons, N., Discussion, *Proc. Conf. Earth. Pr. Probs.*, Brussels 1958, Vol. III, 50-53 (cited by Hendron, 1963 and Schmidt, 1966).

Simpson, B., Retaining structures: displacement and design, *Geotechnique* 1992, **42**, No. 4, 541-576.

Simpson, B, Calabresi, G., Sommer, H. & Wallays, M., Design parameters for stiff clays, *Proc. VII Eur. Conf. Soil Mech. Found. Engng.*, Vol. 5, 1979, 91-127.

Skempton, A.W., Long-term stability of clay slopes, *In* Milestones in soil mechanics, Thomas Telford, Edinburgh, 1975.

Sloan, A., Storebaelt tunnels: ground treatment of cross passages, *Grd. Engng.* 1994, **August**, 20-22.

Smart, P. & Tovey, N.K., Electron microscopy of soils and sediments (2 vols.), Clarendon Press, Oxford, 1981.

Specification for Piling and Embedded Retaining Walls, Thomas Telford, London, 1996, 55-64.

Steenfelt, J.S., Type A prediction of settlements for railway box culvert in road embankment on clay till, *Proc. ICSMFE XIV*, vol. 2, 1997, 1037-1044.

Steenfelt, J.S., C.O.W.I. Ltd., 2001. Personal communication.

Stroud, M.A. & Butler, F.G., The standard penetration test and the engineering properties of glacial materials, (Proceedngs of the Symposium held at the University of Birmingham, 21-23rd April, 1975, revised and reprinted), Geo Abstracts, Norwich, 1978, 129-137.

Synge, F.M., The coasts of Leinster (Ireland), The Quarternary History of the Irish Sea, Seal House Press, Liverpool, 1977, 199-222 (cited by Hoare, 1991c)

Synge, F.M., Quaternary glaciation in Ireland, *Quarternary Newsletter*, **28**, 1979, 1-18 (cited by Hoare, 1991c)

Synge, F.M., Quaternary glaciation and changes in the sea level in the south of Ireland, *Geologie en Mijnbouw* 1981, **60**, 305-315.

Synge, F.M., In an interview with D.N.D. Hartford, *Some aspects of the engineering behaviour of well graded soils*, Vol. 1, Ph.D. thesis, University of Dublin, Trinity College, 1987, 89-90.

Tavenas, F., Des Rosiers, J.-P., Leroueil, P., La Rochelle, P. & Roy, M., The use of strain energy as a yield and creep criterion for highly overconsolidated clays, *Geotechnique* 1979, **29**, No. 3, 285-303.

Taylor, D.W., Research on consolidation of clays, *Pubs. Dept. Civ. & Sanitary Engng. M.I.T.* 1942, **No. 82** (cited by Hendron, 1963).

Terzaghi, K., Large retaining wall tests, *Engng. News Rec.* 1934, **Feb. 1**, 136-140 (cited by Hendron, 1963).

Thomas Garland and Partners, Unpublished site investigation report, Saint James's St., 1996.

Thomson, S., Evaluation of pile load tests in the Edmonton area, *Can. Geo. J.* 1981, **18**, 313-316.

Thomson, S. & Yacyshyn, R., Slope instability in the city of Edmonton, *Can. Geo. J.* 1977, **14**, No. 1, 1-16.

Thomson, S. & El-Nahhas, F., Field measurements in two tunnels in Edmonton, Alberta, *Can. Geo. J.* 1980, **17**, 20-23.

T.J. O'Connor and Assocs., Unpublished site investigation report, Saint James's St., 1997.

Thurston, C.W. & Deresiewicz, H., Analysis of a compression test of a face-centered cubic array of elastic spheres, *J. App. Mech.* 1959, Vol. **26**, 251-258 (cited by Hendron, 1963 and Schmidt, 1966).

Treacy, P., *Deformations around a deep excavation in boulder clay*. M.Sc. dissertation, University of Dublin, Trinity College, 1995.

van Langan, H. & Vermeer P.A. , Automatic step-size correction for non-associated plasticity problems, *Int. J. Num. Mets. Engng.* 1990, **29**, 579-598.

Vaughan, P.R., Chandler, R.J., Apted, J.M., Maguire, W.M. & Sandroni, S.S., Sampling disturbance with particular reference to its effect on stiff clays, Soil mechanics, Thomas Telford, London, 1993, 685-708.

Viggiani, G., Small strain stiffness of fine grained soils, Ph.D. thesis, City University, London, 1992 (cited by Viggiani and Atkinson (1995) and Atkinson (2000)).

Viggiani, G. & Atkinson, J.H., Interpretation of bender element tests, *Geotechnique* 1995, **46**, No. 1, 149-154.

Ward, W.H., Marsland, A. & Samuels, S.G., Properties of the London clay at the Ashford Common shaft: in situ and undrained strength tests, *Geotechnique* 1965, **15**, No. 4, 321-344.

Warren, W.P., Fenitian (Midlandian) glacial deposits and glaciation in Ireland and the adjacent offshore region, Glacial Deposits in Great Britain and Ireland, AA Balkema, Rotterdam, Brookfield, 1991a, 79-88.

Warren, W.P., Till lithology in Ireland, Glacial Deposits in Great Britain and Ireland, AA Balkema, Rotterdam, Brookfield, 1991b, 415-420.

Weertman, J., On the sliding of glaciers, *J. Glaciol.* 1957, **3**, 33-38.

Weertman, J., The theory of glacier sliding, *J. Glaciol.* 1964, **5**, 287-303.

Weltman, A.J. & Healy, P.R., Piling in 'boulder clay' and other glacial tills, 1978, Report No. **PG5**, CIRIA.

Whitaker, T., The design of piled foundations, Perganon Int. Lib. 1976, 135-156.

World of Mathematics, Wolfram Research (Mathematica) 2000, Web site based on 'Eric Weisstein's World of Mathematics'.

Wroth, C.P., The interpretation of in situ soil tests, *Geotechnique* 1984, **34**, No. 4, 449-489.

Yimsiri, S. & Soga, K., Anisotropy of highly overconsolidated clay at small and intermediate strain levels, *Proc. XIV S. E. As. Geo. Conf.*, Hong Kong 2001, Vol. 1, 599-604.